Downstream processing development of enveloped viruses for clinical applications

Innovative tools for rational process optimization

Tiago Manuel Ferreira da Silva Vicente

Supervisors:
Manuel J. T. Carrondo and Paula M. Alves

Dissertation presented to obtain a Ph.D. degree in Engineering and Technology Sciences, Biotechnology at the *Instituto de Tecnologia Química e Biológica*, *Universidade Nova de Lisboa*

Oeiras, September 2010

Downstream processing development of enveloped viruses for clinical applications

by Tiago Vicente

First edition, September 2010
Copyright number:

Cover:
Baculovirus particle schematic (an enveloped virus) (*Product*); surface plasmon resonance adsorption (*Measurement*); selectivity prediction based on electrostatics (*Modeling*); scanning electron microscopy (SEM) picture of porous *versus* bead matrices (*Optimization*). Artwork by the author except SEM micrograph obtained from www.sartorius-stedim.com.

ITQB-UNL/IBET, Animal Cell Technology Unit
Instituto de Tecnologia Química e Biológica,
Universidade Nova de Lisboa
Apartado 12, 2781-901 Oeiras, Portugal
Phone: +351 214469362; Fax: +351 214421161
http://www.itqb.unl.pt
http://www.ibet.pt
http://tca.itqb.unl.pt

A meus pais

BRIEF CONTENTS

CONTENTS

Foreword

This thesis represents four years of research undertaken at the Animal Cell Technology Unit of the *Instituto de Tecnologia Química e Biológica* from the *Universidade Nova de Lisboa / Instituto de Biologia Experimental e Tecnológica* under the supervision of Dr. Paula Alves and Professor Manuel Carrondo.

The work presented in this dissertation intended to create fundamental knowledge in the downstream processing of complex biopharmaceuticals, in particular, of enveloped viral vectors that constitute a relevant system for application in gene therapy and vaccination. The use of rational, sound analytical tools combined with state-of-the-art unit operation principles contributed to build a more solid and cost-effective strategy for the development of the current purification processes for these complex biologicals.

Tiago Vicente
Oeiras, Portugal

Acknowledgements

I would like to express my sincere gratitude to the people that contributed in any way to this thesis; without them I would not be able to write this document.

To Prof. Manuel Carrondo, my co-supervisor, for the rigor, the guidance and the confidence from the very first day, for allowing me the freedom and opportunities to evolve in this very exciting area. I remember when we first met and you and Paula launched me to the DSP: it was a damned good shot; thank you so much!

To Dr. Paula Alves, my co-supervisor, for being the boss she is at the helm of the ACTU, for the peculiar and sharp view of science and technology, for letting and pushing me to do my very best.

To Dr. Cristina Peixoto, my mentor and "sister in arms" at the downstream processing lab of the ACTU, for the everlasting support, for the illuminating discussions, for sharing with me her deepest experience. I owe you a lot and this thesis as well.

To Dr. Paulo Mota, my other mentor, for conveying me his enthusiasm and encouragement and the bright ways of translating what one sees from an experiment into a sensible mathematical description and the proper means to explain it.

To David Tomaz and Rimenys Carvalho, for allowing me to learn how to teach what I know best, for technical support during their internships at the ACTU. To Nita Clemente, for her highly skilled and accurate analytical support: this work belongs to you also, wherever you are. To Ana Alves for analytical support during the baculovirus work.

To Dr. Pedro Cruz, for very enlightening and relieving discussions, opening new perspectives to solve the omnipresent issues of complex biological systems. And, of course, for the great laughs!

To the Baculogenes guys at IBET, Dr. Vicente Bernal, Nuno Carinhas and Dr. António Roldão for the fruitful discussions, companionship and all the fun.

To Dr. Uwe Gottschalk and Sartorius Stedim Biotech, for providing very promptly materials, support and advice, for the opportunities to join the stimulating Downstream Technology Forums at Sartorius College in Göttingen. To Dr. René Fáber, for providing the membrane prototypes and sharing his best knowledge in the development of new materials for purification of biologicals.

To Dr. Otto-W. Merten, for the support throughout the Baculogenes consortium, for providing bulk material for DSP testing and for guidance and criticisms during the project. To Dr. Kari Airenne, for sending the baculovirus vectors used in this thesis and for sharing his so thorough knowledge in the baculovirus biology. To Emilia Makkonen for taking care of me during my stays in Kuopio.

To Dr. John Auniņš, for the advice and criticisms since the very early days and during his visits at the ACTU. To Dr. John Konz, for the criticisms and very insightful suggestions during the VLP work.

To Dr. Teresa Rodrigues and Dr. Marlene Carmo, for their friendly and prompt support and for introducing me to the nightmare of working with enveloped viruses—their retros—even though I eventually went on working with baculos.

To Dr. António Lopes, for the support in DLS and electrokinetic fundamentals. To Dr. Gonçalo Costa and Dr. Ana Barbas, for the support and advice with our Biacore and SPR.

To Carmen Valle and Cristina Alvarez from GE Healthcare for the support on materials, equipment and opportunities to attend their seminars.

To Marcos Sousa, for the expertise and support at the upstream processing. To Ana Rodrigues, for the support on the cholesterol assays for envelope content determination.

A Cláudia, Rita, Sofia e Liliana, pela amizade especial que criámos nestes anos, por estarem sempre lá quando precisava, pelas gargalhadas, as cervejas ou caipirinhas... Muito obrigado!

A todos os actuais e anteriores membros da UTCA, em especial Helena, Paulo, Francisca, Guida, Carina Silva, Ana Teixeira, Ana Sofia, Gonçalo, pela boa disposição, companheirismo e excelente ambiente de trabalho.

A meus amigos de mais longa data, em especial JP, Rui, Carolina, Filipa, André, Rita, Andreia pelo apoio e amizade.

A meus pais: é por vossa "culpa" que cheguei até aqui; obrigado pelo vosso interminável e incondicional apoio e carinho! A meu irmão pelo fio condutor que me incutiu desde muito, muito cedo. A minha família próxima e a minha avó Júlia por tratar sempre de mim.

A Ivette, especialmente nesta última etapa da tese, por aquele apoio muito especial que faz com que tudo faça realmente mais sentido na vida.

To the funding from the European Commission (Baculogenes, LSHB-2006-037541 and Clinigene – Network of Excellence, LSHB-2006-018933) and the Portuguese *Fundação para a Ciência e a Tecnologia* (PTDC/EQU-EQU/71645/2006 and SFRH/BD/31257/2006), essential for the development of the work presented in this dissertation.

FCT Fundação para a Ciência e a Tecnologia
MINISTÉRIO DA CIÊNCIA, TECNOLOGIA E ENSINO SUPERIOR Portugal

Jury

Dr. Uwe Gottschalk, Group Vice President Purification Technologies at Sartorius Stedim Biotech, Göttingen, Germany.

Dr. John G. Auniņš, Executive Scientific Director at Merck Research Labs, West Point PA, USA and Visiting Professor at ITQB-UNL, Oeiras, Portugal.

Prof. Alírio E. Rodrigues, Professor of Chemical Engineering at the *Faculdade de Engenharia da Universidade do Porto*, Porto, Portugal.

Dr. José P. B. Mota, Associate Professor at the *Faculdade de Ciências e Tecnologia da Universidade Nova de Lisboa*, Caparica, Portugal.

Dr. Cristina C. Peixoto, Investigator at the Animal Cell Technology Unit, ITQB-UNL/IBET, Oeiras, Portugal.

Dr. Paula M. Alves, Principal Investigator at the Animal Cell Technology Unit, ITQB-UNL/IBET, Oeiras, Portugal.

Prof. Manuel J. T. Carrondo, Professor of Chemical and Biochemical Engineering at the *Faculdade de Ciências e Tecnologia da Universidade Nova de Lisboa*, Caparica, Portugal and CEO of IBET, Oeiras, Portugal.

Thesis publications

1. **Vicente T**, Sousa MQ, Peixoto C, Mota JPB, Alves PM, Carrondo MJT. Anion exchange membrane chromatography for purification of rotavirus-like particles. *Journal of Membrane Science* 2008; 311:270–283.

2. **Vicente T**, Peixoto C, Carrondo MJT, Alves PM. Virus production for clinical gene therapy. *Methods in Molecular Biology* 2009; 542:447–470.

3. **Vicente T** and Peixoto C, Carrondo MJT, Alves PM. Purification of recombinant baculoviruses for gene therapy using membrane processes. *Gene Therapy* 2009; 16:766–775.

4. **Vicente T**, Mota JPB, Peixoto C, Alves PM, Carrondo MJT. Modeling protein binding and elution over a chromatographic surface probed by surface plasmon resonance. *Journal of Chromatography A* 2010; 1217:2032–2041.

5. **Vicente T**, Peixoto C, Alves PM, Carrondo MJT. Modeling electrostatic interactions of baculovirus vectors for ion-exchange process development. *Journal of Chromatography A* 2010; 1217:3754–3764.

6. **Vicente T**, Mota JPB, Peixoto C, Alves PM, Carrondo MJT. Analysis of adsorption of a baculovirus bioreaction bulk on an ion-exchange surface by surface plasmon resonance. *Journal of Biotechnology* 2010; 148:171–181.

7. **Vicente T**, Mota JPB, Peixoto C, Alves PM, Carrondo MJT. Rational design and optimization of downstream processes of viral particles for biopharmaceutical applications: current advances. *Biotechnology Advances*; submitted.

8. **Vicente T**, Fáber R, Alves PM, Carrondo MJT, Mota JPB. Impact of ligand density on the optimization of ion-exchange membrane chromatography for viral vector purification. In final preparation (see Chapter 7).

Additional publication

1. Lesch HP, Laitinen A, Peixoto C,**Vicente T**, Makkonen K.-E., Laitinen L, Pikkarainen JT, Samaranayake H, Alves PM, Carrondo MJT, Ylä-Herttuala S, Airenne KJ. Production and purification of lentiviral vectors generated in 293T suspension cells with baculoviral vectors. *Gene Therapy*; submitted.

Summary

Viral vectors and virus-like particles hold a tremendous potential in various clinical applications in the areas of gene therapy and/or vaccination, drawing the attention of biotechnology and pharmaceutical companies. The majority of these products are manufactured in animal cell cultures, inherently making the process costly. A great deal of effort is taking place to generate optimized biological and engineering strategies to find scalable and cost-effective processes, easily transferable to cGMP facilities. However, the implementation of robust downstream processes generating this type of biopharmaceuticals in the amounts required for pre-clinical and clinical trials is still lacking and lagging. By including a labile lipid membrane layer harboring glycoproteins (often critical for infection) over the viral capsid, enveloped viruses bring extra challenges in terms of their bioprocessing particularly downstream. The work developed during this thesis aimed at improving the state-of-the-art purification processes for these types of viral particles. The rationale was to integrate process understanding with product characterization, still scarce in such biological systems.

An introduction in **Chapter 1** reviews the current advances in the development of the purification processes for these types of complex biopharmaceuticals. A focus is given to the development of rational approaches in detriment of an empirical-based process development. As starting points, the better known principles and solutions provided by more mature systems as mAbs and recombinant proteins were utilized.

The first part of this thesis, **Part I**, deals with a somewhat simpler system – a virus-like particle from Rotavirus (RLP). **Chapter 2** describes on the integration of an anion-exchange chromatographic step into the DSP of this RLP vaccine candidate. Ion-exchange chromatography is a separation process of choice, if not the most used, for the recovery/purification of biologicals. The objective of this study was to gain preliminary theoretical and predictive knowledge on this chromatographic process when employed for such a VLP. Membrane chromatography has been studied for the adsorption of these RLPs. Screening studies provided evidence on the sensitive effect of the ionic strength and the pH of the equilibration buffer on final product recovery. We could implement a steric mass action (SMA) model for the prediction of the elution profile of purified RLP pulses and confirm that these VLPs can be purified to clinical grade at almost 50% global recovery yield, with close to 100% removal of host bulk DNA and 98% of host cell protein using the proposed DSP.

In **Part II**, we step further into complexity and take baculovirus as an enveloped

virus model. In **Chapter 3**, a scalable, cost-effective DSP is tested and proposed based on membrane processes. These viruses have recently been recognized as promising for human gene therapy or vaccination. A complete downstream process comprising three steps—depth filtration, ultra/diafiltration and membrane sorption—was established as a strong DSP backbone. Global recovery yields of clinical grade material reached 40% using technologies easy to scale under cGMP guidelines, constituting a major breakthrough over the yet much lower yield and non-scalable purification process based on ultracentrifugation density gradients.

Chapter 4 and **Chapter 5** report on the development of a scale-down approach based on surface plasmon resonance (SPR); an analytical "pseudo"-chromatographic tool for analyzing binding and elution of the viruses over a surface mimicking the ion-exchange matrix has been developed. **Chapter 4** describes the necessary theory implementation and testing of conditions using bovine serum albumin (BSA) as a model protein. A sorption rate model capable of quantitatively describing BSA binding and elution for protein titers from dilute to overloaded conditions and a broad range of salt concentrations was proposed. **Chapter 5** validates this tool for our baculovirus vector system. By separately studying the key component cuts of the baculovirus bioreaction bulk—the product (infective baculovirus), the main product-related impurities (damaged baculovirus particles), and the main process-related impurities (host cell protein, host cell dsDNA and endotoxins)—adsorption isotherms over a broad range of equilibrium conditions were obtained.

Chapter 6 describes a similar rationale as the one put forward in the previous two chapters, but here using dynamic light scattering (DLS) for the determination of the ζ(zeta)-potential (a measure of the electrostatic equilibria) of the different components of this baculovirus system. For this purpose, the main species, product (infective virus particle) and product-derived impurities (dsDNA-, glycoprotein-, and envelope-deprived baculovirus particles), were isolated and correspondent ζ-potentials were measured through DLS. A deterministic model based on the virus components, that are critical for their biological function, was fine-tuned accounting for the experimental data. The contribution of these viral components to the overall particle electrostatic interaction energy profile (calculated between the particle and a putative ion-exchange surface) was evaluated allowing to distinguish the electrostatic properties of the infective virus particle from the major virus-related impurities. A prediction of the operating conditions promoting process selectivity was achieved based on such an approach. Such knowledge has serious impact at the final targeted clinical application as the quality/potency of the virus preparation is improved

by decreasing the total to infective virus particle ratio (TP/IP) as intended.

Chapter 7 works out as a proof of concept study of the developed scaled-down, fundamental-based tools. From preliminary tests resorting to the insights gained in **Chapters 5** and **6**, a more straightforward testing of membrane prototypes for anion-exchange chromatography was performed. Such study allowed to draw important conclusions regarding the effect of ligand density in overall process performance in terms of recovery yields and purity. Lowering ligand density was shown to be beneficial for baculovirus particle purification, decreasing host cell protein, host cell dsDNA and non-infective baculoviruses, increasing overall yields by over 20% as compared to the current process. The previously implemented SMA model provided, for this enveloped virus system, a useful predicting tool generating methodologies to help increase resolution/selectivity.

This thesis has contributed to the fields of gene therapy, vaccination and bioengineering of complex biopharmaceuticals by developing innovative analytical tools combined with *in silico* models grounded on fundamental knowledge. This was possible due to an in-depth study of both the product physico-chemical properties and the unit operations principles used, in particular ion-exchange chromatography. This work demonstrates how rational design and optimization can streamline process development of such challenging biological particles. We believe that the methodologies developed herein provide a new way of creating knowledge allowing for a more rational process design of these and potentially other viruses and VLPs.

Resumo

A indústria farmacêutica e de biotecnologia está a focar a sua atenção numa nova classe de produtos biológicos: biofármacos complexos. Vectores virais e partículas semelhantes a vírus (VLPs) representam dois tipos destes produtos com enorme potencial para aplicações clínicas nas áreas de terapia génica e vacinação. Estes biofármacos são na sua maioria produzidos por células animais, o que torna o seu processo de produção inerentemente complexo. Há actualmente um grande esforço na tentativa de obter as melhores estratégias, tanto ao nível biológico como ao nível de engenharia de processos, capazes de encontrar soluções que permitam aumento de escala economicamente viável, facilmente transferíveis e implementáveis em instalações com boas práticas de fabrico (cGMP). No entanto, o desenvolvimento de estratégias de purificação capazes de processar este tipo de material biológico nas quantidades necessárias em testes pré-clínicos e clínicos está ainda bem aquém do que seria desejável. Os vírus com envelope representam um dos tipos de biofármacos mais complexos: incluem não apenas cápside e genoma viral mas também uma membrana lipídica glicoproteica necessária para a sua função biológica, i.e. para a manutenção da sua infecciosidade. De facto, a fragilidade destes envelopes levanta sérias preocupações no que respeita ao *design* dos processos de purificação. O trabalho desenvolvido nesta dissertação teve o objectivo de melhorar o estado actual da arte ao nível dos processos de purificação deste tipo de partículas de elevada complexidade através do desenvolvimento de estratégias inovadoras, contribuindo para o conhecimento mais fundamental. A abordagem consistiu em alcançar um novo patamar de conhecimento, actualmente ainda muito escasso, ao nível da purificação e da caracterização deste tipo de partículas biológicas.

A introdução, apresentada no **Capítulo 1**, revê os actuais avanços no desenvolvimento dos processos de purificação destes biofármacos complexos. Dá-se especial ênfase ao desenvolvimento de abordagens mais racionais em detrimento do desenvolvimento de processos apenas baseado em conhecimento empírico. Existem já algumas abordagens relevantes na literatura focadas neste tipo de biofármacos, além de ser possível ter como base o conhecimento adquirido de outros sistemas mais bem caracterizados como é o caso de anticorpos monoclonais ou proteínas recombinantes.

O primeiro passo deste trabalho, aqui apresentado na **Parte I**, trata de um sistema biológico ligeiramente mais simples – uma partícula semelhante a vírus do Rotavírus (RLP) – como modelo biológico relevante. O **Capítulo 2** reporta a integração de um passo de cromatografia de troca aniónica no processo de purificação desta vacina de enorme potencial. A cromatografia de troca iónica é um dos processos de separação mais usados na

recolha/purificação de produtos biológicos. O objectivo deste estudo foi obter conhecimento teórico e predictivo preliminar neste processo cromatográfico quando implementado neste sistema. Para esse efeito, foi usada cromatografia de membranas para estudar a adsorção de RLPs. Estudos sistemáticos permitiram determinar o impacto da força iónica e pH do tampão na recolha final de produto. Foi possível implementar com sucesso um modelo estérico de acção mássica (SMA) para a predição do perfil de eluição de pulsos purificados de RLPs e confirmar que, usando este processo de purificação, este tipo de partículas semelhantes a vírus podem ser processados até elevada pureza com rendimentos globais de 46%, ∼100% de remoção de DNA celular e 98% de proteína celular.

Na **Parte II**, entramos num nível de complexidade superior usando baculovírus como modelo de vírus com envelope. No **Capítulo 3**, testa-se um processo de purificação escalável e económico baseado em processos de membranas. Estes vírus foram recentemente reconhecidos como altamente promissores em terapia génica humana ou para vacinação. Foi estabelecido um processo completo de purificação baseado em três passos: filtração por filtro de profundidade, ultra/diafiltração e sorção por membranas. Os rendimentos globais de purificação de virus a elevada pureza alcançaram os 40% usando tecnologias muito simples de transferir para escalas de produção em instalações operando com boas práticas de fabrico. Esta estratégia integrada de purificação representa um marco importante face ao procedimento clássico baseado em gradientes de densidade por ultracentrifugação tipicamente apresentando muito menores rendimentos e não passível de aumento de escala.

Os **Capítulos 4** e **5** desenvolvem um modelo para redução de escala de ensaio baseado em espectroscopia de *surface plasmon resonance* (SPR). Sendo a cromatografia de troca iónica um passo crucial neste processo e susceptível de melhoramento, foi implementada uma ferramenta "pseudo"-cromatográfica usando esta metodologia analítica com o fim de analisar a adsorção e eluição dos vírus numa superfície mimetizando uma matriz cromatográfica de troca iónica. O **Capítulo 4** descreve a teoria necessária para analisar convenientemente as condições de adsorção usando um modelo de proteína, albumina de soro bovino (BSA). Nesse sentido foi postulado um modelo de sorção capaz de descrever quantitativamente a adsorção e eluição de BSA desde concentrações muito diluídas a condições de saturação e numa larga janela de concentrações de sal. O **Capítulo 5** valida esta mesma ferramenta para o nosso sistema biológico relevante, baculovírus. Ao estudar de forma isolada os componentes chave de um caldo de biorreacção de baculovírus—o produto (baculovírus infeccioso), as principais impurezas relativas ao produto (partículas de baculovírus degradadas), e as principais impurezas relativas ao processo (proteína celu-

lar, dsDNA e endotoxinas)—, foram obtidas isotérmicas de adsorção numa gama larga de condições de equilíbrio. Não seria possível obter tal informação usando os mesmos recursos implementando os típicos ensaios de cromatografia por membranas em pequena escala.

O **Capítulo 6** descreve uma estratégia semelhante à utilizada nos dois capítulos anteriores, usando aqui a técnica de dispersão dinânima de luz (DLS) para a determinação do potencial-ζ(zeta) (uma medida do equilíbrio electrostático) dos diferentes componentes deste sistema de baculovírus. Neste sentido, as principais espécies, produto (baculovírus infeccioso) e principais impurezas relativas ao produto (baculovírus sem, respectivamente, genoma, glicoproteína, e envelope), foram isoladas e os seus potenciais-ζ foram avaliados. De acordo com os dados experimentais, adaptou-se um modelo determinístico baseado nos componentes virais críticos para a função biológica viral. Analisou-se a contribuição destes componentes virais no perfil de energia de interacção electrostática global (experimentado entre a partícula viral e uma superfície hipotética de troca iónica) permitindo distinguir as propriedades electrostáticas dos vírus infecciosos e das impurezas analisadas. Baseado nesta estratégia, conseguiu obter-se uma predição das condições operatórias óptimas para melhorar a selectividade do processo cromatográfico em questão. Tal conhecimento tem um forte impacto na desejada aplicação final dado que a qualidade/potência da preparação viral é melhorada ao reduzir significativamente a razão entre partículas virais totais e partículas virais infecciosas (TP/IP) como pretendido.

No **Capítulo 7** faz-se uma prova de conceito da importância e utilidade das ferramentas fundamentais aqui desenvolvidas. A partir de testes preliminares usando o conhecimento apreendido nos **Capítulos 5** e **6** foi possível realizar uma análise de protótipos de membranas cromatográficas muito mais rápida e eficiente. Este estudo permitiu tirar importantes conclusões acerca do efeito da densidade de ligando nos rendimentos globais do processo e performance em termos de remoção de impurezas. A utilização de densidades relativamente baixas de ligando mostrou ser vantajosa para aumentar (em mais de 20%) o rendimento de purificação de baculovírus, reduzindo a proteína celular, dsDNA celular e baculovírus não infecciosos no produto final. O modelo SMA previamente estabelecido serviu também neste sistema mais complexo como uma boa ferramenta para prever o comportamento do processo cromatográfico e gerar recomendações úteis para incrementar a resolução/selectividade do processo.

Em suma, esta tese gerou importantes contribuições para os campos da terapia génica, vacinologia, engenharia de biofármacos complexos e cromatografia. Criaram-se ferramentas analíticas inovadoras combinadas com modelos matemáticos *in silico* solidamente alicerça-

dos em conhecimento fundamental. Tal foi possível devido a um estudo em profundidade das propriedades fisico-químicas do produto e dos princípios das operações unitárias usadas, em particular, cromatografia de troca iónica. Este trabalho de investigação demonstra como o *design* e optimização racionais podem acelerar o desenvolvimento de processos para partículas biológicas complexas. Indubitavelmente, a tendência aqui desenvolvida e demonstrada irá servir no progresso desta área científica, conseguindo gerar e integrar conhecimento básico com potencial para aplicação a outro tipo de vectores virais com (ou sem) envelope ou VLPs.

Abbreviations

DEAE diethylaminoethyl

BEVS/IC baculovirus expression vector system / insect cells

dsDNA double-stranded DNA

DoE Design of Experiments

DSP downstream processing

HC DNA host cell DNA

HCP host cell protein

HTS high-throughput screening

IEX ion-exchange

MW molecular weight

PAT process analytical technology

pfu plaque forming units

QbD Quality by Design

rBV recombinant baculovirus

RLP Rotavirus like particle

SMA steric mass action

TP/IP total particles *versus* infective particles

VLP virus-like particle

Chapter 1

INTRODUCTION

Adapted from:

Vicente T, Mota JPB, Peixoto C, Alves PM, Carrondo MJT. Rational design and optimization of downstream processes of viral particles for biopharmaceutical applications: current advances. *Biotechnology Advances*; submitted.

Abstract

The advent of advanced therapies in the pharmaceutical industry has moved the spotlight into virus-like particles and viral vectors produced in cell culture holding great promise in a myriad of clinical targets, including cancer prophylaxis and treatment. Even though a couple of cases have reached the clinic, these products have yet to overcome a number of biological and technological challenges before broad utilization. Concerning the manufacturing processes, there is significant research focusing on the optimization of current cell culture systems and, more recently, on developing scalable downstream processes to generate material for pre-clinical and clinical trials. We review the current options for downstream processing of these complex biopharmaceuticals and underline current advances on knowledge-based toolboxes proposed for rational optimization of their processing. Rational tools developed to increase the yet scarce knowledge on the purification processes of complex biologicals are discussed as alternative to empirical, "black-boxed" based strategies classically used for process development. Innovative methodologies based on surface plasmon resonance, dynamic light scattering, scale-down high-throughput screening and mathematical modeling for supporting ion-exchange chromatography show great potential for a more efficient and cost-effective process design, optimization and equipment prototyping.

Contents

1.1 Introduction

Over the last 25 years, the pharmaceutical industry has been shifting a great deal of interest and resources into the development of novel pharmaceutical molecules based on biologicals: biopharmaceuticals (Crommelin et al., 2003). Beyond the exponential market growth on monoclonal antibodies (mAbs), there is today great promise for novel biopharmaceuticals based on virus particles, either for vaccination (e.g., virus-like particles (VLPs) (Buckland, 2005)) or for gene or cell therapies (e.g., recombinant viral vectors (Ferguson et al., 2010)). These products are not only far larger than mAbs—e.g., over 10^7 Da for an HPV-VLP (Hanslip et al., 2006) when compared to the average 1.5×10^5 Da molecular weight of an immunoglobulin G (IgG) (Shukla et al., 2007)—but are also required to contain a well assembled three-dimensional geometry, properly characterized with the necessary subunits in the proper place and ratio and with the proper post-translational modifications of the exposed proteins. The latter being critical for instance to elicit the desired immune responses (for vaccination purposes) or to allow efficient cell target internalization and ultimately transgene expression (for gene therapy purposes).

Moreover, viral vectors should remain infective, which in some systems, as retroviral vectors, means the presence of specific viral enzymes biologically active for completion of

the gene transfer process (Carmo et al., 2009). All this complexity raises both biological and technological challenges (Rodrigues et al., 2007a).

As far as the manufacturing process is concerned, there have been great achievements in the implementation of scalable systems using animal cells for improvement of product titer and quality. However, much less effort has been put to the essential downstream purification processes for the more complex biopharmaceutical particles thus constituting currently a major bottleneck.

Due to the intricate nature of these biological particles, there are critical implications on the downstream processing concerning purity, potency and quality of the final product. The regulatory authorities—US Food and Drug Administration (FDA) and the European Medicines Evaluation Agency (EMEA)—require the industry to define strict process and product guidelines. According to the desired final target: i) the process-derived impurities such as host cell protein (HCP) and host cell (HC) DNA contents must be below a certain limit—**purity**—; ii) the concentration (or titer) must be as high as possible so that the volume of the required dose is as reduced as possible—**potency**—; iii) the quantity of product-derived impurities, damaged, non-functional virus particles should be as low as possible compared to the functional virus particles—**quality**. The downstream processes should thus be designed to accommodate these requirements. Often, a sensible compromise must be made between cost, throughput, and purity to meet both the quality and potency aimed at in a given pre-clinical or clinical trial. It is the goal of the integrated manufacturing process to ideally deliver the product in large quantities (scalability), with high quality (purity) and in high titer (potency), and doing so in a cost-effective manner.

This chapter discusses the state of the art of the everlasting quest for the design of "the ideal" DSP for these complex biopharmaceuticals. The rising interest in the use of knowledgeable tools for process design and optimization over heuristics-based process development is discussed, addressing relevant case studies where process knowledge and/or product characterization had an impact on improving current recovery yields and productivities.

1.2 Current choices in DSP of complex biopharmaceuticals

The state of the art in the purification of complex biopharmaceuticals produced by animal cell culture has its ground on membrane and chromatographic processes (Przybycien et al.,

2004; Peixoto et al., 2007; Rodrigues et al., 2007a; Konz et al., 2008; Vicente et al., 2009a,b). These unit operations are part of some of the commonly named platform technologies for purification; prominent examples include monoclonal antibodies (mAbs) (Kelley et al., 2009; Li et al., 2009) and adenoviral vectors (Konz et al., 2008), where there is already considerable processing knowledge and maturity.

Hereby we overview the current choices for the three major steps of a general DSP for virus particles—clarification, concentration/purification and polishing (Lightfoot and Moscariello, 2004). For virus particles purification, the scientific community has long made an enormous effort to move away from the single ultracentrifugation, density gradient-based purification protocols that were and, in some cases, still are the standard purification step (Konz et al., 2008). The relevance of understanding/studying in-depth the product of interest—enveloped (or not) virus particle—product lability, the importance of working out the specific biological issues and translate these into process requirements are discussed herein. The statement "the process defines the product" dictated by the regulatory authorities, is, indeed, somewhat bidirectional in these systems.

Fig. 1.1 depicts the schematic of a general DSP flow diagram, encompassing the typical requirements/fed materials, the desired removal targets, i.e., the waste products coming out of each step, the typical unit operations employed, and the potential issues that can be encountered. The schematic is meant to be an outlined strategy for virus particles, to which process practitioners and developers can resort to.

Meanwhile, one should mention that, in the field of protein purification, unit operations alternative to chromatography-based processes are generating unique interest (Przybycien et al., 2004). For instance, in mAb manufacturing the overall downstream processing (DSP) can become prohibitively expensive due to the large cost of Protein A (or G) based affinity chromatography used as a capture step. Indeed, the increase in product titers has created a bottleneck downstream as the capacities cannot physically accommodate the economies of scale achieved upstream (Gottschalk, 2008). Aqueous-two or three phase partitioning, precipitation and crystallization have been revisited over the last years so that alternative production-scale DSP processes may become more cost-effective, whether removing totally or still integrating less chromatographic processes (Przybycien et al., 2004). Certain viruses withstand phase separations with polyethylene glycol (PEG) (Aboud et al., 1982; Lewis and Metcalf, 1988; Tsoka et al., 2000; Smith et al., 2008), ammonium sulphate (Maranga et al., 2002) or calcium phosphate (Morling and Russell, 1995). Nevertheless, the implementation of these alternative unit operations has yet to receive wider emphasis for virus purification;

this is likely due to the fact that these particles are generally more labile and prone to irreversible aggregation through flocculation or precipitation procedures.

1.2.1 Clarification

A suitable clarification step should efficiently remove cell debris and large aggregates, while maintaining and protecting the quality of the product in the flowthrough stream. Often, even before the clarification process, due to the presence of a reasonable content in host cell derived proteases (Gotoh et al., 2001), product preservatives may have to be added during bioreaction or while initiating DSP: e.g., in the baculovirus expression vector system (BEVS) using insect cell hosts, a protease inhibitor cocktail is routinely added for preservation of the virus-like particle produced, avoiding the degradation of the external glycoprotein layer essential for proper bioactivity upon final application (Vieira et al., 2005).

On the other hand, if the product of interest is not secreted to the extracellular medium, cell membrane disruption may be necessary to obtain significant productivities: examples include non-enveloped viruses as adenoviruses (Konz et al., 2008), where detergent is added to the bioreactor for cell membrane solubilization.

Clarification steps widely used in biopharmaceutical purification include the use of centrifugation for cell sedimentation (either continuous or batch). More recently, however, membrane processes appear as an attractive alternative: scalability is guaranteed as the membrane area is easily up-scaled either by using cartridges of larger membrane sheet area or stacking membrane units in parallel mounted in stainless steel holders. These processes either work in dead-end mode, eg., using disposable depth-filtration modules (Peixoto et al., 2007; Mellado et al., 2008; Vicente et al., 2009a,b) or in tangential flow mode, using membrane cassettes or hollow fiber units (Saha et al., 1994) with cut-offs within the micrometric order of magnitude. The use of depth filters makes the sieving and particulate retention process much more efficient because of the depth-dependent size separation factor; also, due to the charged nature of state-of-the-art depth-filter membranes and their three-dimensional arrangement (Prashad and Tarrach, 2006), a higher degree of coarser impurity accumulation is achieved, while still facilitating the passage of the finer particles, which include virus particles from the tens to the hundreds of nanometers size.

In line with the increasing interest in the use of cleaning- and validation-free disposable technologies, membrane processes represent a clear advantage over centrifugation as the former are very easily adaptable to disposable formats. Indeed, major manufacturers of

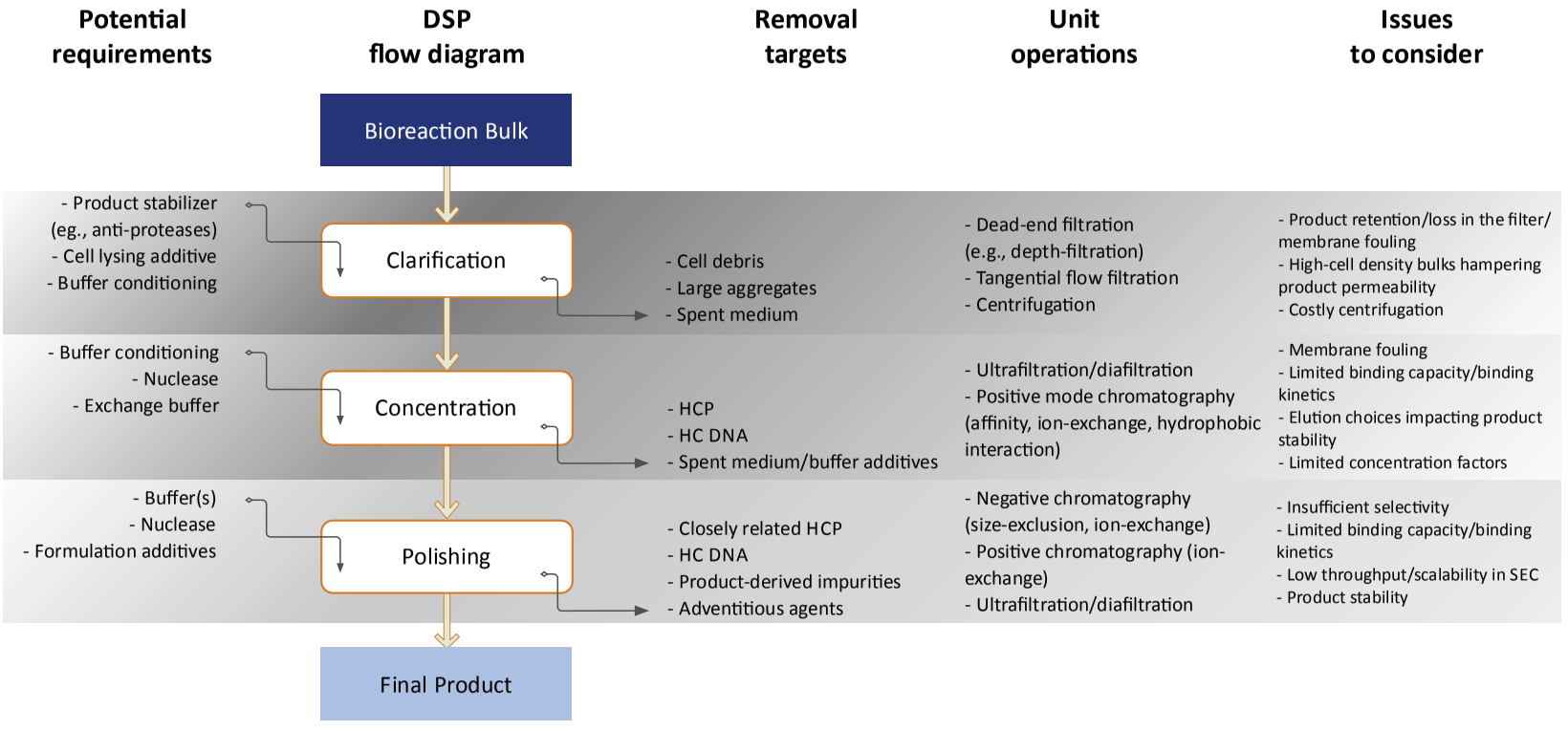

Figure 1.1: *Overview of DSP strategy for virus particles, potential requirements and removal targets, correspondent state-of-the-art unit operations and potential issues to be considered; HCP: host-cell protein; HC DNA: host-cell DNA; SEC: size exclusion chromatography.*

bioseparation equipment and consumables add every year to their portfolios innovative materials of this kind.

Other alternative for clarification step is expanded-bed chromatography (Hjorth, 1997) where process intensification is achieved by allowing clarification of the bioreaction bulk and capturing of the virus particles simultaneously. Adenovirus type 5 (Ad5) has been successfully processed by these means (Lusky, 2005; Peixoto et al., 2006). However, this unit operation is typically labour-consuming with some technical issues in terms of cleaning and regeneration, and necessary fluidized bed heights compromising robustness. Such drawbacks have failed expanded-bed chromatography when compared to what novel membrane technologies can bring in terms of ease of operation.

Concerning more rational process developments, little has been reported besides the implementation of fouling models to predict permeate flux decay over time (Shukla and Kandula, 2009). Process development normally relies on heuristics of critical operating conditions, such as fluxes through dead-end filters or recirculation flow rates, in order to find the best options minimizing membrane fouling in tangential flow filtration (TFF) (Grzenia et al., 2006). Important efforts are especially directed to controlling product stability at a very early stage in the purification train. Process development teams therefore invest in clarifying the product as quickly as possible (removing potential impairing agents in the bulk), preventing the virus particles to precipitate or aggregate irreversibly (Fig. 1.1). Nevertheless, important lessons should be learned from high-cell density process platforms where extremely high turbidities are achieved through perfusion cell cultures; a combination of flocculant addition, selective precipitation of particulates or even sedimentation can be rationally devised to improve the clarification step at reasonable throughputs and high recoveries (Shukla and Kandula, 2009). For the typical cell density used for viral productions, membrane processes perform fairly well with recovery yields frequently surpassing 90% (Nayak et al., 2005; Peixoto et al., 2008; Vicente et al., 2009a).

1.2.2 Concentration/purification

As mentioned in the preceding section, concentration is a critical step, ubiquitous in DSP of virus particles (Grzenia et al., 2008). The stream volume should be reduced as earlier in the process as possible in order to reduce the upfront investment in downstream equipment and materials. Moreover, it enhances processing safety as some of the virus preparations may require BSL2 or BSL3 manufacturing laboratories and the handling of bulky volumes may prove challenging. The goal, at this stage, is to remove effectively low molecular weight

(MW) HCP, fragmented HC DNA, and possibly fragmented product-related impurities, eg., viral proteins (Fig. 1.1). The concentration factor should be as high as achievable, however, aggregation must be considered as for example in adenovirus (Konz et al., 2005) or baculovirus (Barsoum, 1999) concentration. It is advisable under such situations to evaluate whether or not aggregation can be prevented by addition of certain additives (Wright et al., 2005). This is also why ultracentrifugation-based purification processes present normally very low recovery yields as irreversible aggregation might be taking place during virus banding or pelleting. It is then critical to have prompt analyticals to assess particle aggregation; dynamic light scattering (DLS) can be used very straightforwardly to monitor this issue during the concentration step (Trilisky and Lenhoff, 2007; Vicente et al., 2010d) in alternative to capillary (zone) electrophoresis and/or analytical ultracentrifugation.

For some of the cell systems used, there is a large content of HC DNA constituting a major threat to the required target purity (10 ng/dose with up to 200 bp fragment length (FDA, 2010)). In order to reduce the amount of nuclease units necessary for efficient nucleic acid digestion (typically Benzonase^{TM}), it is advisable in most of the cases to perform this incubation immediately after concentration and prior to the diafiltration step for buffer exchange.

Positive chromatography, i.e., operated in bind-elute mode, constitutes an alternative for the concentration/purification step. When chromatography is operated as a capture step at this stage, good concentration factors can be achieved upon elution if the product is rather diluted in the bulk and if the capacity of the chosen matrix is significant; this has been an option in purification of retroviral vectors (Rodrigues et al., 2007b) or influenza virus vaccines (Kalbfuss et al., 2007). Membrane adsorbers and monolithic matrices constitute relevant options for capture at this early stage, as these materials present higher capacities and faster processing for large bioparticles making them suitable for non-concentrated clarified feedstocks.

Nonetheless, other chromatographic chemistries have been efficiently used including hydrophobic interaction (Chahal et al., 2007; Wolff et al., 2010), hydroxyapatite (O'Riordan et al., 2000; Kuiper et al., 2002) and sulfated (Wolff et al., 2010) ligands, the latter two considered as "pseudo"-affinity chromatography ligands.

High-performance TFF (HPTFF) has shown to be a very promising concentration/purification step for mAb refining (van Reis et al., 1997; Fontes and van Reis, 2009). HPTFF employs charged ultrafiltration membranes that promote selectivity for protein-protein separations. The rational framework implemented by van Reis and colleagues (van Reis

et al., 1997) can be used as a guideline for HPTFF of viruses or VLPs. For systems that have other challenges as, for example, a mixture of two virus particles differing slightly in their physico-chemical properties, this kind of approach might be worthwhile pursuing. Adeno-associated viruses (AAVs) produced in insect cells by baculovirus infection (Merten et al., 2005) or lentivirus from baculovirus transduction (Lesch et al., 2008) are such examples where this approach might outperform current concentration steps.

The scalability and cost-effectiveness of the described membrane processes (including membrane chromatography) should be highlighted (van Reis and Zydney, 2007; Peixoto et al., 2008). These unit operations are very amenable to any cGMP process scheme; they often fill the serious gap of the labour- and time-consuming density-gradient procedures, making them impracticable at larger scales for viral vector/VLP manufacturing.

1.2.3 Polishing

Polishing is a critical step for the purification of biopharmaceuticals; purity is mandatory and product quality/potency must be as high as achievable so that its final clinical application is effective and safe. Therefore, this step is typically quite challenging as it should resolve impurities—either process- or product-related—very closely related to the product of interest.

Chromatographic processes are the workhorses for this step as they allow high resolution separations (Lyddiatt, 2002; Przybycien et al., 2004; Morenweiser, 2005). Ion-exchange (IEX) chromatography constitutes a process of choice for resolving HCP-virus particle, HC DNA-virus particle, or damaged virus particle-virus particle feedstreams. A significant number of case studies can be found in the literature where this solution is implemented (Barsoum, 1999; Debelak et al., 2000; Vellekamp et al., 2001; Kaludov et al., 2002; Yamada et al., 2003; Davidoff et al., 2004; Specht et al., 2004; Rodrigues et al., 2006; Trilisky and Lenhoff, 2007; Wu et al., 2007; Kalbfuss et al., 2007; Vicente et al., 2008; Peixoto et al., 2008; Rodrigues et al., 2008; Kutner et al., 2009; Vicente et al., 2009a; Okada et al., 2009; Dormond et al., 2010). It is often the case that IEX chromatography is used vertically within the DSP strategy as it easily fits from early capture to final purification steps. IEX is typically operated in positive (bind-elute) mode: most of the impurities are collected in the flowthrough pool, while the virus particles and some of the impurities are retained in the matrix. Due to the differences in charge of the different components, it is possible to use this process with high resolution elution gradients, separating the adsorbed materials into fractionated cuts, even though they are closely related.

Negative (flowthrough) mode has also potential as it can be implemented for adsorption of resilient impurities as HCP or product-related impurities. Case studies from the mAb process scale purification (Zhou et al., 2006; Gottschalk, 2008) should serve as a basis for implementation of such process also for large biopharmaceuticals.

Gel filtration or size-exclusion chromatography (SEC) and ultrafiltration/diafiltration (usually by TFF) are two other widely used processes at the very latest stage for formulating the product (Rodrigues et al., 2007b; Peixoto et al., 2007; Dormond et al., 2010). Both rely on size making them suitable for buffer exchange, the former permitting milder conditions. TFF scales more easily (adding membrane area) than SEC which is limited to a process scale chromatography column (the load should not exceed 10% of column bed volume).

1.3 In pursuit of an ideal DSP platform

The fundamental *desideratum* in the large scale manufacturing process of any product is that the technologies and resources involved must be cost-effective. Such "tenet" is also applicable for complex biopharmaceuticals. However, as these products are designed to clinical applications, the safety concerns require complex, thus not inexpensive, DSPs.

The ideal DSP platform for virus particles must decrease the impurity levels to acceptable values while maintaining and concentrating the product in its functional state. Given the complexity of such particles and their physico-chemical properties, variable for different viruses, setting up a universal and high-yield DSP platform shall be extremely challenging or even impossible. For example, non-enveloped viruses as AAVs or adenoviruses are prone to aggregation with HC DNA (Konz et al., 2005) or other impurities whereas enveloped viruses as lenti- or influenza-viruses are much more shear-sensitive, thus labile, due to the extra lipid membrane harboring glycoproteins essential for viral infectivity. Similarly, the requirements for enveloped viruses will be different depending on their use: gene therapy applications will require smoother DSPs to preserve receptors than vaccines, where epitopes are often enough to elicit an immunological reaction.

Nonetheless, more restrict DSP platforms can still be designed for the purification of, at least, subset classes of virus particles. Indeed, if the physico-chemical properties do not differ much, the products should behave similarly upon processing. As in any platform, minor refinements can then be done in order to maximize throughput and recovery yield.

Furthermore, in what concerns the technologies used, new DSP matrices are being regarded as common denominators to the purification of large biopharmaceuticals. Dis-

posable membrane adsorbers and monoliths are being used as excellent alternatives to packed-bed chromatography. A number of reports have shown these to be suitable choices for purification of various virus particles (Branovic et al., 2003; Kramberger et al., 2004; Charcosset, 2006; Etzel and Riordan, 2009; Whitfield et al., 2009; Gutiérrez-Aguirre et al., 2009).

1.3.1 Classical *versus* rational process development

Process optimization still relies mainly on empirical-based strategies because there is much to be known about the biophysico-chemical properties of such particles. However, more rational strategies bringing together a variety of fundamentals, analytical and predictive modeling tools shall provide deeper insights into a more efficient, thus cost-effective and quicker process optimization. This section overviews efforts being taken by researchers and developers towards this trend where product- and process-knowledge is obtained aiming at a more rational design and improvement for the existing processes. These would contribute to a faster process development at very early stages (or even later for fine-tuning) in the product development lifecycle; furthermore, such rationale serves as solid ground for the implementation of Quality by Design (QbD) rules meeting the Process Analytical Technology (PAT) initiative (Mollerup et al., 2008).

Fig. 1.2 depicts the two main paths one can use for process optimization. Such schematic should be interpreted widely: it can be equally grasped as a step-by-step diagram either for one-step optimization (e.g., a chromatographic unit operation) or for integrated process optimization, learning, for example, from lessons on other complex biopharmaceutical systems (Cruz et al., 2002). On the left, the stacked boxes space representing a significant experimental work and resources (costs of goods and time included) to obtain the optimal operating conditions should be highlighted; in the rational process development strategy, by implementing scaled-down tools and concomitant suitable mathematical modeling for such unit operations, the amount of resources spent are substantially reduced to obtain an increased amount of data/process insight. One should also emphasize the fundamentals of the Quality by Design (QbD) approach being depicted here as key: a focused seeking of process understanding and control via product characterization permits the definition of improved design of experiments (DoE). The feedback of knowledge gathered brings clear benefits in terms of what is known about the product at the different stages of the manufacturing process but also for more easily defining the design space where fine-tunings can be done safely, predicting the expected gains in terms of productivity/yield or savings in

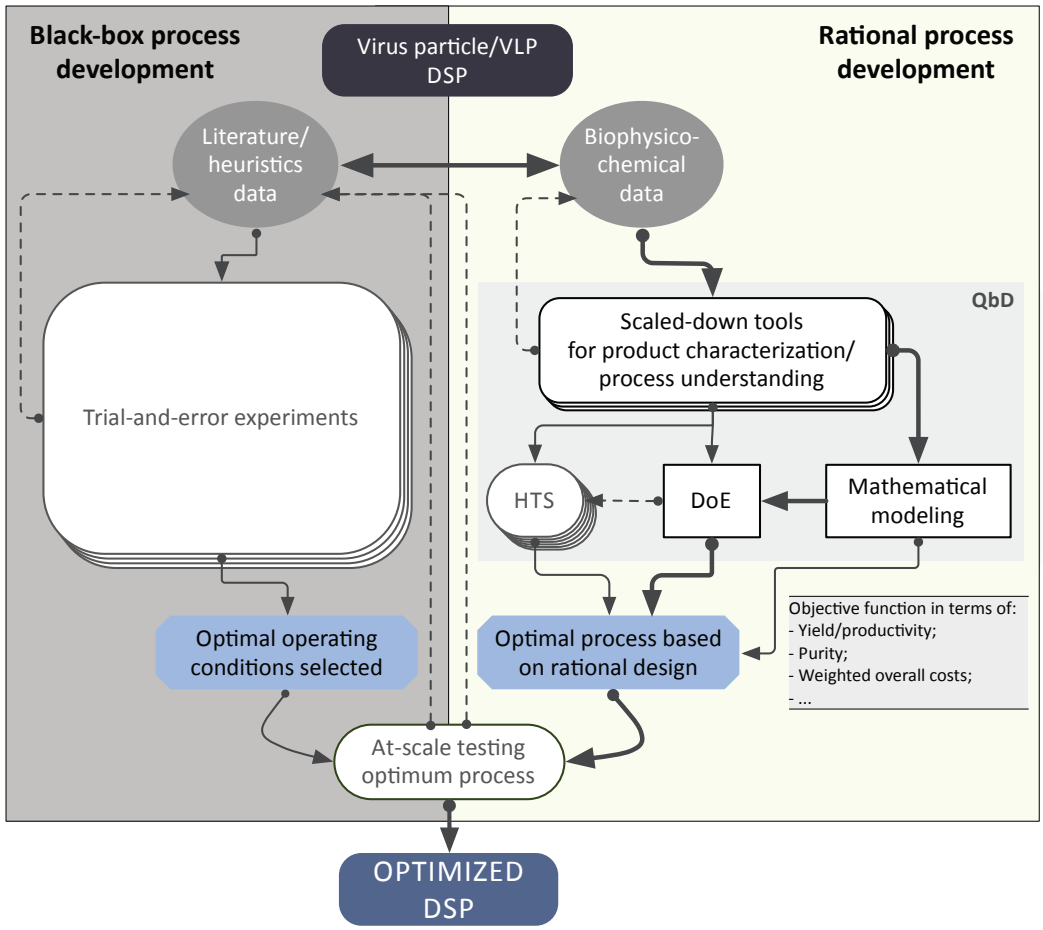

Figure 1.2: *Schematic representation of a process development task for viral vector/VLP biopharmaceuticals: a perspective on rational versus black-box optimization. Elliptical, curved and squared box shapes stand respectively for 'current knowledge/data analysis', 'experimental work' and 'implemented tool'. Notice that the 'scaled-down tools' boxes are purposely curved as these tools also encompass experimental work. Thicker arrows represent the authors' standpoint on the most sound strategy for process development; HTS, DoE, QbD stand for, respectively, high throughput screening, design of experiments and quality by design.*

resources.

We agree with Nfor and colleagues (Nfor et al., 2009) in that rational purification process development will become more entrenched in the biopharmaceutical industry. Overly complex and computationally demanding mathematical models may render process optimization untractable, which may lead to failure due to lack of basic experimental data, if the tools are chosen based on a sensible rationale, the chances to success make it worth trying. Basic understanding adds value by allowing to identify earlier the critical issues and devising ways to overcome them.

Analyticals and their critical role in process development

Analyticals play a pivotal role for whatever approach used (Kelner and Bhalgat, 2007). When dealing with complex biological particles, a number of assays must be in place to properly assess product identity, quality, titer, purity and consistency throughout the manufacturing process. It is clear that one should determine what is effect of any changes in an operating condition; this applies equally to trial-and-error experimentation or during *in silico* design of a certain unit operation. For the case of virus particles the list may include: infective virus titer determination (via cell based assays using immunocyto- or histo-chemistry assays or FACS), real-time quantitative PCR (for viral genome titration), transmission or scanning electron microscopy (for particle visualization), SDS-PAGE (one- or two-dimensional for protein profiling), Western Blotting (for protein identity matching), ELISA (for quantitative particle concentration measurement), total protein assessment, total endotoxin assessment, total DNA assessment, glycoprotein analysis and/or N- or C-terminal protein sequencing (for exposed, essential protein identity matching), mass spectrometry (for protein identity matching), capillary zone electrophoresis (for enhanced particle or protein size/molecular weight measurement), size exclusion chromatography HPLC, dynamic light scattering (DLS) (for size and ζ-potential measurements), and surface plasmon resonance (SPR) (for equilibrium or sorption kinetics of product or impurities). This rather extensive wishlist stresses the challenges and complexity underlying purification of these complex biopharmaceuticals.

1.3.2 The special case of adsorptive chromatography

Chromatography has been for a number of decades the most widely used unit operation in biotechnological downstream processing (Nfor et al., 2009; Gottschalk, 2008). It offers tremendous opportunities as far as resolution power/selectivity, throughput and scalability

are concerned. Due to the increasing costs of chromatography within a given DSP, a great deal of effort is still being devoted to this separation process, especially in the area of complex biopharmaceuticals as viral vectors or vaccines.

We limit our more technical discussion in this review to the rational advances put forward in the field of adsorptive chromatography, in particular, to IEX chromatography. Unlike the rather expensive affinity chromatography processes with good recovery yields based on immobilized metal affinity (Jiang et al., 2004; Ye et al., 2004), heparin or others (Chen et al., 2009; Wu et al., 2007; Opitz et al., 2007), IEX processes are generally much more affordable at large scales and offer a broad spectrum of stationary phases for the capture of virus particles. IEX chromatography is based on the charge of the biological particles instead of on the existence of very specific ligands on the stationary phase; the latter may leach from the matrix thus contaminating the product and often require very harsh elution conditions (that may degrade the product). Although there is now considerable literature reporting on the successful implementation of IEX chromatography for the purification of virus particles, there is still room for improvement and opportunities to take advantage of while using this IEX chromatography for biopharmaceutical purification.

As pointed out in the previous sections, IEX processes can be operated in positive or negative mode. In bind-and-elute mode, a large amount of process-related and/or product-related impurities are removed in the flowthrough, while most of the product from the bulk is retained adsorbed over the matrix surface functionalized with a given IEX ligand. The inverse procedure—retention of impurities in the matrix while the product freely flows through and is collected polished—is also feasible because either the buffer can be adjusted at a given pH or a ligand of opposite charge can be used.

Recently, the interest on the implementation of other types of chromatographic matrices based on porous membrane layers or monoliths has risen. These porous matrices are particularly suited for very large particles, as viral vectors or VLPs, due to some key reasons confirmed by a number of studies. First, the specific surface areas (*per* unit volume) of porous matrices with pore sizes of 0.8 μm (Mustang^{TM} membrane adsorbers from Pall), 3 μm (Sartobind^{TM} membrane adsorbers from Sartorius-Stedim Biotech) or > 1 μm (Jungbauer and Hahn, 2008) (CIM^{TM} monoliths from BIA Separations, Ljubljana, Slovenia) are significantly larger than those of resin beads used in packed-bed chromatography, whose pores go up to 10-20 nm for conventional resins or 400 nm for perfusive resins (Trilisky and Lenhoff, 2009). Virus particles, ranging from 20 nm to 300 nm, are hindered from binding onto the internal surface area of the resin, resulting in sub-optimal usage of such matrices.

Second, due to the porous nature of these matrices, diffusional mass transfer resistances are reduced to a minimum. Indeed, they allow the use of fairly high linear velocities promoting convective transport. For the case of binding of large particles that have rather small diffusion coefficients, as compared to smaller biologicals as proteins, these matrices clearly present an advantage over packed-bed chromatography. Third, and as a corollary of the latter, these matrices permit very high process throughputs. Due to the very low pressure drops, higher flow rates can be used for loading and eluting the material using a given stepwise or linear gradient.

A very pertinent study has analyzed the influence of the pore size distribution of monolith, perfusive and conventional resin matrices (Trilisky and Lenhoff, 2009). Although high adsorption capacities are obtained for porous matrices, entrapment of the virus particles should be considered and the linear flow rates used should be also optimized in order to reduce this phenomenon; indeed, loading the virus bulk at a high flow rate and eluting at a lower flow rate should improve product recovery (Trilisky and Lenhoff, 2009).

Moreover, most of these porous matrices can now be purchased as disposable units representing a leap in processing flexibility, eliminating cleaning and sterilization as well as their validation costs. Other matrices harboring extenders, as tentacle resins, have been used with good results most likely because they improve the accessibility of their binding sites to the large virus particles (Rodrigues et al., 2007a). Yet, it is anticipated that packed-bed chromatography can also be of great interest if flowthrough mode is implemented for polishing purposes, removing low molecular weight biological impurities; however, to our knowledge, the implementation of such strategy has not yet been reported in the literature.

Optimization of IEX processes

For the optimization of IEX processes, ionic strength and pH of the buffer/medium containing the complex mixture bulk are critical parameters that should be taken into special consideration early in the development design (Pujar and Zydney, 1998; Schaldach et al., 2006; Vicente et al., 2008). These conditions modulate the IEX mechanisms defining the adsorption and desorption of the product and some of the impurities. To address these issues, our team has initiated efforts towards a more knowledgeable approach to distinguish the underlying fundamentals for complex biopharmaceuticals. Rotavirus-like particles have been purified with better yields by anion-exchange membrane chromatography (Vicente et al., 2008). The process has been modeled with reasonable accuracy, for the prediction of the VLP peaks eluted at given conditions using the steric mass-action model proposed by

Brooks and Cramer (1992). This widely used theoretical framework for IEX of smaller and simpler model biologicals appears to be equally applicable to the more complex particles. If good estimations of the characteristic charge, equilibrium constants and steric factors are available, the process can be modeled with significant predictive power. However, in that preliminary study, the contribution of the impurities (with unknown properties for most of them) were not included in the multicomponent model. This is a major drawback when implementing a model that fully predicts the behavior of all the components of an animal cell-derived bioreaction bulk containing a given virus particle.

It is thus desirable to create a methodology that allows for a better understanding on the complexity of these virus bulks. This can be done by analyzing the major components of the bulk, including the impurities that in most cases represent the major mass fraction of the bulk. Such study has been performed using recombinant baculoviruses as a model system. The product—the integral virus particle—was compared to major process-related impurities (e.g., protein, DNA) and major product-derived impurities (damaged virus particles, eg., deprived of viral envelope or external glycoprotein harbored in the virus envelope) in terms of adsorption capacities to an IEX surface (Vicente et al., 2010b). For that purpose, surface plasmon resonance (SPR) was used as a pseudo-chromatography tool for biological adsorption and desorption on an IEX surface (Vicente et al., 2010c). SPR conveniently results in a scaled-down analytical tool for predicting adsorption isotherms at varied ionic strengths. The same type of data typically requires a set of adsorption experiments on a lab-scale chromatographic matrix resulting in quite expensive optimization routines as these biologicals are costly. SPR thus offers the possibility to add more rationale in the typical DoE type of approach at reduced costs given the small volumes required for testing (Fig. 1.2).

Table 1.1 summarizes relevant scientific reports using rational tools to optimize IEX processes for viral vectors or VLPs. Trilisky and Lenhoff (2007) produced a pioneering report on a more rational selection of suitable ionic strength and pH conditions for optimizing adsorption of adenoviruses. Dynamic light scattering and batch uptake were implemented as tools for determining the ζ-potential of the adenovirus, detecting its point of zero charge and for devising recommendations for pH and ionic strength of the buffer. Batch uptake tests have also been part of other studies for ligand screening (Rodrigues et al., 2006; Vicente et al., 2009a). However, SPR as an analytical chromatographic tool, can be used as a cost-effective alternative for batch uptake resin/ligand selection or HTS (Roper and Nakra, 2006; Kokpinar et al., 2006; Roper, 2007; Vicente et al., 2010b). Indeed, scaled-

Table 1.1: *Overview of ion-exchange (IEX) chromatographic advances where process development for viral vectors or VLPs included rational tools.*

System	Type	Matrix	Tool	Major contribution/result	Reference
Rotavirus-like particle[d]	Anion-exchange	Porous membrane	Process mathematical modeling	Predictive insights into the anion-exchange process	Vicente et al. (2008)
Densonucleosis virus[a]	IEX	Porous membrane	CLSM[b]	Observation of capacity differences between virus particles and smaller biological contaminants as proteins	Wickramasinghe et al. (2006)
Adenovirus[a]	IEX	Conventional resin (narrow pore) *vs* perfusive resin (wide pore)	DLS, batch uptake modeling	Porous matrix heuristics	Trilisky and Lenhoff (2007)
Adenovirus[a]	IEX	Monolithic *vs* perfusive matrices	EM and breakthrough curve modeling	Porous matrix recommendations for virus particle purification	Trilisky et al. (2009)
Adenovirus[a]	IEX	Conventional resin (narrow pore) *vs* perfusive resin (wide pore)	Virus entrapment modeling	Recommendations on operating conditions suitable for minimized virus loss due to entrapment into large porous	Trilisky and Lenhoff (2009)
Retrovirus[c]	Anion-exchange	Tentacle resin	DLS	Selection of conditions for improved product quality	Rodrigues et al. (2008)
Baculovirus[c]	Anion-exchange	Valid for any type	SPR and modeling	Adsorption isotherm prediction of the product and relevant product-related and process-related impurities	Vicente et al. (2010b)
Baculovirus[c]	Anion-exchange	Valid for any type	DLS and modeling	Deterministic model for prediction of optimal selectivity conditions	Vicente et al. (2010b)
Baculovirus[c]	Anion-exchange	Porous membrane	SPR and process modeling	Elucidation of ligand density effect on process performance	Vicente et al. (2010a)

[a]non-enveloped virus; [b]confocal laser scanning microscopy; [c]enveloped virus; [d]triple-layered VLP

down models are being considered relevant options for early stage process development for other more advanced processes, as mAbs (Coffman et al., 2008; Rege et al., 2006; Wensel et al., 2008).

Following this lead, DLS has also been used as a main analytical support for the design of a deterministic model capable of discriminating the contribution of the different virus components of baculoviruses to the overall electrostatic particle potential (Vicente et al., 2010d). Such tool provides fundamental knowledge on the crucial role of the external glycoprotein of these virus particles, while predicting the optimal pH and ionic strength ranges for improved adsorption of integral virus particles with enhanced selectivity to other product-derived impurities. Studies on retroviruses and other viruses have been performed with DLS (Schaldach et al., 2006; Rodrigues et al., 2008).

These studies, yet scarce in the literature, provide strategies for selecting/improving the conditions and materials/technologies available for optimizing the IEX process. The final goal would be to separate with high yield a product in a sharp and clean peak, decreasing to acceptable values the impurity contents. The future, utopian perhaps, is reaching a purely *in silico* process optimization as defended by Nfor et al. (2009); however, for these more complex biologicals, the challenges are still too large. Bringing together relevant and much more advanced work with simpler biologicals should constitute a good starting point. It has been shown that it is possible to predict the IEX chromatographic behavior of proteins directly from their crystal structure (Ladiwala et al., 2005). Furthermore, the examination of the binding orientation of the protein adsorbates (Dismer et al., 2008; Dismer and Hubbuch, 2007) provides a molecular-based approach for designing the ideal matrix support with the ideal ligand spacing and density (Dismer and Hubbuch, 2010).

1.4 Outlook

Rational optimization of downstream processes for complex biopharmaceuticals, as viral vectors or VLPs, is still in its infancy. It is clear that a more knowledgeable approach shall highly reduce the "meandering" of the optimization path. With the strict demands in product purity, safety, potency and quality, QbD shall be key in the manufacturing of these biologicals. Rational tools, overviewed here into more detail for IEX process, will be crucial for a more sustained process design and development. These case studies add obvious gains in terms of product characterization and process understanding, which is transforming the way state-of-the-art and scalable DSP processes are being designed. The

trend is clear, needed and thus will keep evolving.

1.5 Scope of the thesis

Viral vectors and virus-like particles are examples of biological products holding a remarkable potential in various clinical applications for gene therapy or vaccination. Enveloped viruses are amongst the most complex biopharmaceuticals where basic knowledge to more rationally address their production issues is still lacking. Moreover, the implementation of robust and scalable downstream processes for these biopharmaceuticals is still in its infancy. In fact, very little is known about the fundamental issues underlying the purification processes of such viruses. This thesis aimed at improving the state-of-the-art purification processes for these viral particles by means of developing and using fundamental-based approaches for a more rational and efficient process development. We took the path highlighted in Fig. 1.2 as our rationale.

A virus-like particle from Rotavirus (RLP) system (presented In Chapter 2) provided a model system where the introduced anion-exchange membrane chromatography step could be modeled using mathematical tools. For the first time, a steric mass action (SMA) model for the prediction of the elution profile of purified RLP pulses using membrane chromatography was implemented with reasonable accuracy.

A leap forward was taken towards an enveloped virus system—our target object of study of this thesis—in Part II. Increasing the particle complexity by adding an envelope on top of a much larger viral vector (required to be infective), the VLP-derived knowledge proved extremely useful to tackle more efficiently the issues in the purification of this virus model—virus quality (because of the presence of damaged virus particles due, e.g., to the added lability of the envelope), potency (concentration is often not enough for many applications) and purity (contaminating HCP and/or HC DNA may still be too high depending on the dose required).

For that purpose, our SPR (Chapters 4 and 5) and DLS (Chapter 6) tools, used as scale-down methodologies to address the anion exchange membrane chromatographic step of the established cGMP-compliant DSP (Chapter 3) were able to generate a better understanding of the relevant undergoing phenomena. As a final outcome membrane adsorber prototypes could be evaluated quicker yielding enhanced process performance and providing a proof of concept where rational design and development can overcome some of the biological and technological issues in the downstream processing of complex biopharmaceuticals.

References

Aboud M, Wolfson M, Hassan Y, Huleihel M. Rapid purification of extracellular and intracellular moloney murine leukemia virus. Arch Virol 1982;71:185–95.

Barsoum J. Concentration of recombinant baculovirus by cation-exchange chromatography. Biotechniques 1999;26:834–6.

Branovic K, Forcic D, Ivancic J, Strancar A, Barut M, Kosutic-Gulija T, et al. Application of short monolithic columns for improved detection of viruses. J Virol Methods 2003;110:163–71.

Brooks CA, Cramer SM. Steric mass-action ion exchange: Displacement profiles and induced salt gradients. AIChE J 1992;38:1969–1978.

Buckland BC. The process development challenge for a new vaccine. Nat Med 2005;11:S16–9.

Carmo M, Dias JD, Panet A, Coroadinha AS, Carrondo MJT, Alves PM, et al. Thermosensitivity of the reverse transcription process as an inactivation mechanism of lentiviral vectors. Hum Gene Ther 2009; 20:1168–1176.

Chahal PS, Aucoin MG, Kamen A. Primary recovery and chromatographic purification of adeno-associated virus type 2 produced by baculovirus/insect cell system. J Virol Methods 2007;139:61–70.

Charcosset C. Membrane processes in biotechnology: an overview. Biotechnol Adv 2006;24:482–492.

Chen GY, Chen CY, Chang MDT, Matsuura Y, Hu YC. Concanavalin a affinity chromatography for efficient baculovirus purification. Biotechnol Prog 2009;25:1669–77.

Coffman JL, Kramarczyk JF, Kelley BD. High-throughput screening of chromatographic separations: I. method development and column modeling. Biotechnol Bioeng 2008;100:605–618.

Crommelin DJA, Storm G, Verrijk R, de Leede L, Jiskoot W, Hennink WE. Shifting paradigms: biopharmaceuticals versus low molecular weight drugs. Int J Pharm 2003;266:3 – 16. A Special Issue for Professor Hans E. Junginger on the occasion of his 60th birthday.

Cruz PE, Maranga L, Carrondo MJT. Integrated process optimization: lessons from retrovirus and virus-like particle production. J Biotechnol 2002;99:199–214.

Davidoff AM, Ng CY, Sleep S, Gray J, Azam S, Zhao Y, et al. Purification of recombinant adeno-associated virus type 8 vectors by ion exchange chromatography generates clinical grade vector stock. J Virol Methods 2004;121:209–15.

Debelak D, Fisher J, Iuliano S, Sesholtz D, Sloane DL, Atkinson EM. Cation-exchange high-performance liquid chromatography of recombinant adeno-associated virus type 2. J Chromatogr B Biomed Sci Appl 2000;740:195–202.

Dismer F, Hubbuch J. A novel approach to characterize the binding orientation of lysozyme on ion-exchange resins. J Chromatogr A 2007;1149:312–320.

Dismer F, Hubbuch J. 3d structure-based protein retention prediction for ion-exchange chromatography. J Chromatogr A 2010;1217:1343–1353.

Dismer F, Petzold M, Hubbuch J. Effects of ionic strength and mobile phase ph on the binding orientation of lysozyme on different ion-exchange adsorbents. J Chromatogr A 2008;1194:11–21.

Dormond E, Chahal P, Bernier A, Tran R, Perrier M, Kamen A. An efficient process for the purification of helper-dependent adenoviral vector and removal of helper virus by iodixanol ultracentrifugation. J Virol Methods 2010;165:83–9.

Etzel MR, Riordan WT. Viral clearance using monoliths. J Chromatogr A 2009;1216:2621–4.

FDA. Center for biologics evaluation and research guidelines. 2010.

Ferguson SD, Ahmed AU, Thaci B, Mercer RW, Lesniak MS. Crossing the boundaries: stem cells and gene therapy. Discov Med 2010;9:192–196.

Fontes N, van Reis R. Advances in technology and process development for industrial-scale monoclonal antibody purification. In U Gottschalk, ed., Process Scale Purification of Antibodies, pp. 203–221. John Wiley & Sons, 2009.

Gotoh T, Miyazaki Y, Sato W, Kikuchi K, Bentley WE. Proteolytic activity and recombinant protein production in virus-infected sf-9 insect cell cultures supplemented with carboxyl and cysteine protease inhibitors. J Biosci Bioeng 2001;92:248–55.

Gottschalk U. Bioseparation in antibody manufacturing: The good, the bad and the ugly. Biotechnol Prog 2008;24:496–503.

Grzenia DL, Carlson JO, Czermak P, Han B, Specht RK, Wickramasinghe SR. Purification of densonucleosis virus by tangential flow ultrafiltration. Biotechnol Prog 2006;22:1346–53.

Grzenia DL, Carlson JO, Wickramasinghe SR. Tangential flow filtration for virus purification. J Membr Sci 2008;321:373–380.

Gutiérrez-Aguirre I, Banjac M, Steyer A, Poljsak-Prijatelj M, Peterka M, Strancar A, et al. Concentrating rotaviruses from water samples using monolithic chromatographic supports. J Chromatogr A 2009; 1216:2700–4.

Hanslip S, Zaccai N, Middelberg A, Falconer R. Assembly of human papillomavirus type-16 virus-like particles: Multifactorial study of assembly and competing aggregation. Biotechnol Prog 2006;22:554–560.

Hjorth R. Expanded-bed adsorption in industrial bioprocessing: recent developments. Trends Biotechnol 1997;15:230–5.

Jiang C, Wechuck JB, Goins WF, Krisky DM, Wolfe D, Ataai MM, et al. Immobilized cobalt affinity chromatography provides a novel, efficient method for herpes simplex virus type 1 gene vector purification. J Virol 2004;78:8994–9006.

Jungbauer A, Hahn R. Polymethacrylate monoliths for preparative and industrial separation of biomolecular assemblies. J Chromatogr A 2008;1184:62–79.

Kalbfuss B, Wolff M, Geisler L, Tappe A, Wickramasinghe R, Thom V, et al. Direct capture of influenza a virus from cell culture supernatant with sartobind anion-exchange membrane adsorbers. J Membr Sci 2007;299:251–260.

Kaludov N, Handelman B, Chiorini JA. Scalable purification of adeno-associated virus type 2, 4, or 5 using ion-exchange chromatography. Hum Gene Ther 2002;13:1235–43.

Kelley B, Blank G, Lee A. Downstream processing of monoclonal antibodies: Current practices and future opportunities. In U Gottschalk, ed., Process Scale Purification of Antibodies, pp. 1–23. John Wiley & Sons, 2009.

Kelner D, Bhalgat M. Analytical strategy for biopharmaceutical development. In A Shukla, MR Etzel, S Gadam, eds., Process scale bioseparations for the biopharmaceutical industry. Taylor and Francis, 2007.

Kokpinar O, Harkensee D, Kasper C, Scheper T, Zeidler R, Reif OW, et al. Innovative modular membrane adsorber system for high-throughput downstream screening for protein purification. Biotechnol Prog 2006;22:1215–1219.

Konz JO, Lee AL, Lewis JA, Sagar SL. Development of a purification process for adenovirus: controlling virus aggregation to improve the clearance of host cell dna. Biotechnol Prog 2005;21:466–72.

Konz JO, Pitts LR, Sagar SL. Scaleable purification of adenovirus vectors. Methods Mol Biol 2008; 434:13–23.

Kramberger P, Petrovic N, Strancar A, Ravnikar M. Concentration of plant viruses using monolithic chromatographic supports. J Virol Methods 2004;120:51–7.

Kuiper M, Sanches RM, Walford JA, Slater NK. Purification of a functional gene therapy vector derived from moloney murine leukaemia virus using membrane filtration and ceramic hydroxyapatite chromatography. Biotechnol Bioeng 2002;80:445–53.

Kutner RH, Zhang XY, Reiser J. Production, concentration and titration of pseudotyped hiv-1-based lentiviral vectors. Nat Protoc 2009;4:495–505.

Ladiwala A, Rege K, Breneman CM, Cramer SM. A priori prediction of adsorption isotherm parameters and chromatographic behavior in ion-exchange systems. Proc Natl Acad Sci U S A 2005;102:11710–5.

Lesch HP, Turpeinen S, Niskanen EA, Mähönen AJ, Airenne KJ, Ylä-Herttuala S. Generation of lentivirus vectors using recombinant baculoviruses. Gene Ther 2008;15:1280–6.

Lewis GD, Metcalf TG. Polyethylene glycol precipitation for recovery of pathogenic viruses, including hepatitis a virus and human rotavirus, from oyster, water, and sediment samples. Appl Environ Microbiol 1988;54:1983–8.

Li Y, Kahn DW, Galperina O, Blatter E, Luo R, Wu Y, et al. Development of a platform process for the purification of therapeutic monoclonal antibodies. In U Gottschalk, ed., Process Scale Purification of Antibodies, pp. 187–201. John Wiley & Sons, 2009.

Lightfoot EN, Moscariello JS. Bioseparations. Biotechnol Bioeng 2004;87:259–73.

Lusky M. Good manufacturing practice production of adenoviral vectors for clinical trials. Hum Gene Ther 2005;16:281–91.

Lyddiatt A. Process chromatography: current constraints and future options for the adsorptive recovery of bioproducts. Curr Opin Biotechnol 2002;13:95–103.

Maranga L, Rueda P, Antonis AF, Vela C, Langeveld JP, Casal JI, et al. Large scale production and downstream processing of a recombinant porcine parvovirus vaccine. Appl Microbiol Biotechnol 2002; 59:45–50.

Mellado MC, Peixoto C, Cruz PE, Carrondo MJ, Alves PM. Purification of recombinant rotavirus vp7 glycoprotein for the study of in vitro rotavirus-like particles assembly. J Chromatogr B Analyt Technol Biomed Life Sci 2008;874:89–94.

Merten OW, Geny-Fiamma C, Douar AM. Current issues in adeno-associated viral vector production. Gene Ther 2005;12:S51–61.

Mollerup JM, Hansen TB, Kidal S, Staby A. Quality by design–thermodynamic modelling of chromatographic separation of proteins. J Chromatogr A 2008;1177:200–6.

Morenweiser R. Downstream processing of viral vectors and vaccines. Gene Ther 2005;12 Suppl 1:S103–10.

Morling F, Russell S. Enhanced transduction efficiency of retroviral vectors coprecipitated with calcium phosphate. Gene Ther 1995;2:504–508.

Nayak DP, Lehmann S, Reichl U. Downstream processing of mdck cell-derived equine influenza virus. J Chromatogr B Analyt Technol Biomed Life Sci 2005;823:75–81.

Nfor BK, Verhaert PDEM, van der Wielen LAM, Hubbuch J, Ottens M. Rational and systematic protein purification process development: the next generation. Trends Biotechnol 2009;27:673–9.

Okada T, Nonaka-Sarukawa M, Uchibori R, Kinoshita K, Hayashita-Kinoh H, Nitahara-Kasahara Y, et al. Scalable purification of adeno-associated virus serotype 1 (aav1) and aav8 vectors, using dual ion-exchange adsorptive membranes. Hum Gene Ther 2009;20:1013–21.

Opitz L, Salaklang J, Buttner H, Reichl U, Wolff MW. Lectin-affinity chromatography for downstream processing of mdck cell culture derived human influenza a viruses. Vaccine 2007;25:939–947.

O'Riordan CR, Lachapelle AL, Vincent KA, Wadsworth SC. Scaleable chromatographic purification process for recombinant adeno-associated virus (raav). J Gene Med 2000;2:444–54.

Peixoto C, Ferreira T, Carrondo M, Cruz P, Alves P. Purification of adenoviral vectors using expanded bed chromatography. J Virol Methods 2006;132:121–126.

Peixoto C, Ferreira TB, Sousa MFQ, Carrondo MJT, Alves PM. Towards purification of adenoviral vectors based on membrane technology. Biotechnol Prog 2008;24:1290–1296.

Peixoto C, Sousa MFQ, Silva AC, Carrondo MJT, Alves PM. Downstream processing of triple layered rotavirus like particles. J Biotechnol 2007;127:452–461.

Prashad M, Tarrach K. Depth filtration: Cell clarification of bioreactor offloads. Filtr Sep 2006;43:28 – 30.

Przybycien TM, Pujar NS, Steele LM. Alternative bioseparation operations: life beyond packed-bed chromatography. Curr Opin Biotechnol 2004;15:469–78.

Pujar NS, Zydney AL. Electrostatic effects on protein partitioning in size-exclusion chromatography and membrane ultrafiltration. J Chromatogr A 1998;796:229–38.

Rege K, Pepsin M, Falcon B, Steele L, Heng M. High-throughput process development for recombinant protein purification. Biotechnol Bioeng 2006;93:618–30.

Rodrigues T, Alves A, Lopes A, Carrondo MJ, Alves PM, Cruz PE. Removal of envelope protein-free retroviral vectors by anion-exchange chromatography to improve product quality. J Sep Sci 2008;31:3509–18.

Rodrigues T, Carrondo MJT, Alves PM, Cruz PE. Purification of retroviral vectors for clinical application: Biological implications and technological challenges. J Biotechnol 2007a;127:520–541.

Rodrigues T, Carvalho A, Carmo M, Carrondo M, Alves P, Cruz P. Scaleable purification process for gene therapy retroviral vectors. J Gene Med 2007b;9:233–243.

Rodrigues T, Carvalho A, Roldao A, Carrondo MJT, Alves PM, Cruz PE. Screening anion-exchange chromatographic matrices for isolation of onco-retroviral vectors. J Chromatogr B 2006;837:59–68.

Roper DK. Determining surface plasmon resonance response factors for deposition onto three-dimensional surfaces. Chem Eng Sci 2007;62:1988–1996.

Roper DK, Nakra S. Adenovirus type 5 intrinsic adsorption rates measured by surface plasmon resonance. Anal Biochem 2006;348:75–83.

Saha K, Lin YC, Wong PK. A simple method for obtaining highly viable virus from culture supernatant. J Virol Methods 1994;46:349–52.

Schaldach CM, Bourcier WL, Shaw HF, Viani BE, Wilson WD. The influence of ionic strength on the interaction of viruses with charged surfaces under environmental conditions. J Colloid Interface Sci 2006;294:1–10.

Shukla A, Kandula J. Harvest and recovery of monoclonal antibodies: Cell removal and clarification. In U Gottschalk, ed., Process Scale Purification of Antibodies, pp. 53–78. John Wiley & Sons, 2009.

Shukla AA, Hubbard B, Tressel T, Guhan S, Low D. Downstream processing of monoclonal antibodies–application of platform approaches. J Chromatogr B Analyt Technol Biomed Life Sci 2007;848:28–39.

Smith RH, Yang L, Kotin RM. Chromatography-based purification of adeno-associated virus. Methods Mol Biol 2008;434:37–54.

Specht R, Han B, Wickramasinghe SR, Carlson JO, Czermak P, Wolf A, et al. Densonucleosis virus purification by ion exchange membranes. Biotechnol Bioeng 2004;88:465–73.

Trilisky EI, Koku H, Czymmek KJ, Lenhoff AM. Relation of structure to performance characteristics of monolithic and perfusive stationary phases. J Chromatogr A 2009;1216:6365–76.

Trilisky EI, Lenhoff AM. Sorption processes in ion-exchange chromatography of viruses. J Chromatogr A 2007;1142:2–12.

Trilisky EI, Lenhoff AM. Flow-dependent entrapment of large bioparticles in porous process media. Biotechnol Bioeng 2009;104:127–33.

Tsoka S, Ciniawskyj OC, Thomas ORT, Titchener-Hooker NJ, Hoare M. Selective flocculation and precipitation for the improvement of virus-like particle recovery from yeast homogenate. Biotechnol Prog 2000;16:661–667.

van Reis R, Gadam S, Frautschy LN, Orlando S, Goodrich EM, Saksena S, et al. High performance tangential flow filtration. Biotechnol Bioeng 1997;56:71–82.

van Reis R, Zydney A. Bioprocess membrane technology. J Membr Sci 2007;297:16–50.

Vellekamp G, Porter FW, Sutjipto S, Cutler C, Bondoc L, Liu YH, et al. Empty capsids in column-purified recombinant adenovirus preparations. Hum Gene Ther 2001;12:1923–36.

Vicente T, Faber R, Alves PM, Carrondo MJT, Mota JPB. Impact of ligand density on the optimization of ion-exchange membrane chromatography for viral vector purification 2010a;in final preparation.

Vicente T, Mota JPB, Peixoto C, Alves PM, Carrondo MJT. Analysis of adsorption of a baculovirus bioreaction bulk on an ion-exchange surface by surface plasmon resonance. J Biotechnol 2010b;148:171–181.

Vicente T, Mota JPB, Peixoto C, Alves PM, Carrondo MJT. Modeling protein binding and elution over a chromatographic surface probed by surface plasmon resonance. J Chromatogr A 2010c;1217:2032–2041.

Vicente T, Peixoto C, Alves PM, Carrondo MJT. Modeling electrostatic interactions of baculovirus vectors for ion-exchange process development. J Chromatogr A 2010d;1217:3754–3764.

Vicente T, Peixoto C, Carrondo MJT, Alves PM. Purification of recombinant baculoviruses for gene therapy using membrane processes. Gene Ther 2009a;16:766–775.

Vicente T, Peixoto C, Carrondo MJT, Alves PM. Virus production for clinical gene therapy. Methods Mol Biol 2009b;542:447–470.

Vicente T, Sousa MFQ, Peixoto C, Mota JPB, Alves PM, Carrondo MJT. Anion-exchange membrane chromatography for purification of rotavirus-like particles. J Membr Sci 2008;311:270–283.

Vieira HLA, Estevao C, Roldao A, Peixoto CC, Sousa MFQ, Cruz PE, et al. Triple layered rotavirus vlp production: Kinetics of vector replication, mrna stability and recombinant protein production. J Biotechnol 2005;120:72–82.

Wensel DL, Kelley BD, Coffman JL. High-throughput screening of chromatographic separations: Iii. monoclonal antibodies on ceramic hydroxyapatite. Biotechnol Bioeng 2008;100:839–854.

Whitfield RJ, Battom SE, Barut M, Gilham DE, Ball PD. Rapid high-performance liquid chromatographic analysis of adenovirus type 5 particles with a prototype anion-exchange analytical monolith column. J Chromatogr A 2009;1216:2725–9.

Wickramasinghe SR, Carlson JO, Teske C, Hubbuch J, Ulbricht M. Characterizing solute binding to macroporous ion exchange membrane adsorbers using confocal laser scanning microscopy. J Membr Sci 2006;281:609–618.

Wolff MW, Siewert C, Hansen SP, Faber R, Reichl U. Purification of cell culture-derived modified vaccinia ankara virus by pseudo-affinity membrane adsorbers and hydrophobic interaction chromatography. Biotechnol Bioeng 2010;107:312–320.

Wright JF, Le T, Prado J, Bahr-Davidson J, Smith PH, Zhen Z, et al. Identification of factors that contribute to recombinant aav2 particle aggregation and methods to prevent its occurrence during vector purification and formulation. Mol Ther 2005;12:171–8.

Wu C, Soh KY, Wang S. Ion-exchange membrane chromatography method for rapid and efficient purification of recombinant baculovirus and baculovirus gp64 protein. Hum Gene Ther 2007;18:665–72.

Yamada K, McCarty DM, Madden VJ, Walsh CE. Lentivirus vector purification using anion exchange hplc leads to improved gene transfer. Biotechniques 2003;34:1074–8, 1080.

Ye K, Jin S, Ataai MM, Schultz JS, Ibeh J. Tagging retrovirus vectors with a metal binding peptide and one-step purification by immobilized metal affinity chromatography. J Virol 2004;78:9820–7.

Zhou JX, Tressel T, Gottschalk U, Solamo F, Pastor A, Dermawan S, et al. New q membrane scale-down model for process-scale antibody purification. J Chromatogr A 2006;1134:66–73.

Part I

Stepping into complexity: downstream processing of a VLP

Chapter 2

ANION-EXCHANGE MEMBRANE CHROMATOGRAPHY FOR PURIFICATION OF ROTAVIRUS-LIKE PARTICLES

Adapted from:

Vicente T, Sousa MQ, Peixoto C, Mota JPB, Alves PM, Carrondo MJT. Anion exchange membrane chromatography for purification of rotavirus-like particles. J Membr Sci 2008; 311:270–283.

Abstract

Anion-exchange chromatography is one of the separation processes of choice for the recovery/purification of proteins and complex bio-structures as viruses or virus-like particles (VLPs), e.g., rotavirus-like particles (RLPs) representing a potential biopharmaceutical, where a safer vaccine technology is endeavored. Purification strategies of complex bioparticles are as yet rather empirical. The breakthrough pursued hereby was to gain theoretical and predictive knowledge on the anion-exchange membrane chromatography processing of this type of products. Currently, the use of membrane chromatography is expanding due to its scalability, robustness and disposable nature, allowing high fluxes, rapid processing, little buffer consumption and a validation-free environment. A novel matrix, Sartobind^{TM} D membrane adsorber from Sartorius, was used and thoroughly studied for the adsorption of VLPs. Screening studies showed the sensitive effect of the ionic strength and the pH of the equilibration buffer on product final recovery. Steric mass action (SMA) model formulation was implemented for the prediction of the elution profile of purified RLP pulses. Experimental data fitting gave good model validation therefore yielding insights on the fundamental understanding of the ion-exchange separation mechanism of virus-like particles and, potentially, for other similar structures. Anion-exchange membrane chromatography was finally used in a larger scale downstream process, confirming that rotavirus VLPs can be reproductively purified to clinical grade at 46% global recovery yield, concomitant with nearly 100% removal of host bulk DNA and approximately 98% of host cell proteins.

Contents

2.1 Introduction

Given existing and potential applications in vaccines and gene therapy, complex biological structures as VLPs justify the efforts that bioengineers invest in bioprocess development so as to boost productivities while enabling cost-effective solutions.

Viruses or virus-like particles aimed as biopharmaceuticals are examples of complex high-added value biologicals where in-depth studies clarifying the downstream purification steps are scarce. The variability and complex composition of the bulks produced in animal cell bioreactors include, besides the desired product, mixtures containing host cell proteins, DNA, adventitious agents and/or other contaminant particles. These components greatly contribute for the complexity of the systems, complicating the understanding and integration of the purification steps.

The purification section of a biological process assumes up to 80% of the total costs of the process (Lightfoot and Moscariello, 2004); downstream processing (DSP) is still recurrently a bottleneck greatly limiting final productivities (Aldridge, 2006). Process optimization strategies are thus critical; beyond empirical/systematic know-how, predictive knowledge of the process mechanisms establishing appropriate objective functions can become a major driver in directly targeting both final product yield and purity improvements.

RLPs constitute an interesting example of a vaccine candidate for the worldwide burden of early infant Rotavirus diarrhea (Glass et al., 2005). This specific virus-like particle is an assembly of the Rotavirus protein building blocks, VP2 and VP6, and an outer glycoprotein layer, VP7, essential for the immunization response (Bertolotti-Ciarlet et al., 2003). Avoiding the viral components responsible for infection (e.g., DNA or other proteins) these particles represent a potential advantage over attenuated-live or deactivated viral vaccines (Nguyen et al., 2003). Self-assembled RLPs are classically produced by the Baculovirus Expression Vector System / Insect Cell (BEVS/IC) bioreaction and purified using ultracentrifugation methods (Crawford et al., 1994), impracticable for large scale biomanufacturing. Strategies involving ultrafiltration and chromatography DSP schemes are currently the best choices for RLPs. The use of hollow fiber cross-flow filtration followed by packed-bed size exclusion chromatography has been demonstrated by our team with improved overall yields (37% overall product recovery) compared to the traditional ultracentrifugation processes (Peixoto et al., 2007). The present study extends this effort to adsorptive chromatography using a weak anion exchange membrane matrix commercially available from Sartorius Stedim Biotech, Sartobind^{TM} D, a diethylamine anion exchanger (DEAE) matrix. For instance, weak anion exchanger matrices have been used with good results for purification of retroviruses (Rodrigues et al., 2006). Additionally, adsorption onto DEAE matrices seems to be in agreement with the theoretical net negative charge of the RLPs at neutral pHs (see characteristics in Table 2.1).

Disposable membrane adsorbers have already been used in purification schemes of viruses (Karger et al., 1998; Specht et al., 2004) as well as employed efficaciously in clearance steps of viral particles (Zhou et al., 2006). Adsorptive membranes have the advantage over traditional resin-bed chromatography of decreasing diffusional effects to a minimum. Convection is the prevailing mass transfer phenomenon throughout the membrane matrix allowing a much easier and faster solute approach onto the ligand sites available. Adsorption is consequently favored under these conditions (Teeters et al., 2002; Lightfoot and Moscariello, 2004). High adsorptive uptake efficiencies, particularly for very large

Table 2.1: *Properties of Rotavirus-like particles (RLP) building block proteins and the full particle.*

Material	Molecular mass (kDa)	Theoretical isoelectric point[a] (-)	Theoretical number in assembled particle	Layer	Typical form in solution	Observations
VP2	102.7	5.63	60 dimers[b]		Assembled 60 dimer VP2 particles[b]	Insoluble in aqueous solutions[b]
VP6	44.9	5.48	260 trimers[c]		Soluble glycoprotein[c]	Outer glycoprotein prone to "peel off" in the absence of calcium cation[e]
VP7	37.2	4.74	780 monomers[c]		Trimers, tubes, or spheres of VP6[d]	Ionic strength / pH dependent forms[d]
Assembled RLP	76362	∼5–6			∼75–85 nm[d]	

[a]computed via ExPASy URL (http://www.expasy.org); [b]Labbe et al. (1991); [c]Prasad et al. (1988); [d]Lepault et al. (2001); [e]Ruiz et al. (1996)

biomolecules (e.g., virus particles) with small diffusivities, are the main features of these units (Teeters et al., 2002). Additionally, the possibility of having rather small bed height-to-diameter ratios facilitates high fluid velocities and consequently high fluxes, therefore reducing process time, a major advantage when dealing with a product prone to disassembly, including the "peel-off" of the glycoprotein layer (Peixoto et al., 2007). Up-scaling of membrane processes tends to be straightforward, since increasing both cross sectional areas and bed heights without compromising binding efficiency or performance is feasible using a membrane-like matrix (Teeters et al., 2002).

Ion-exchange process theories can be used to describe and model the mechanisms involved in the anion-exchange membrane chromatography process. Plate models as developed by Yamamoto and colleagues (Yamamoto et al., 1983; Yamamoto, 1995) or Rate models can be taken as a basis (Shene et al., 2006). Given its conceptual simplicity and robust formalism, the Steric Mass Action (SMA) description tool was chosen to be implemented and adapted to the RLP system (Brooks and Cramer, 1992; Shi et al., 2005; Jakobsson et al., 2005). By establishing proper material differential balance equations and boundary conditions, the characterization of the elution behavior of the multicomponents

of a certain mixture becomes feasible (Brooks and Cramer, 1992). This formalism has been successfully applied for describing the dynamics of the ion-exchange mechanism while yielding process development and optimization strategies for antibody purification (Iyer et al., 1999) and should be applicable to complex biopharmaceuticals.

Briefly, in this model it is assumed that the sorption phenomena taking place in an ion-exchange chromatographic process are explained by the exchange reactions between the free proteins or particles in solution in equilibrium with a certain number of ions adsorbed onto the ligands covering the matrix surface (Brooks and Cramer, 1992; Gallant et al., 1996). Herein, the focus is at the simulation of the elution curves of the different species present in the RLP system describing the sorption processes using a membrane adsorber matrix.

This work aimed at the evaluation of the Sartobind D matrix provided by Sartorius Stedim Biotech. A screening of operational conditions provided experimental input for the modeling of the anion-exchange membrane chromatography using the SMA model. Finally, an integration of the membrane adsorber process in the whole DSP route was achieved, effectively increasing overall recovery yields over the state of the art strategy recently reported (Peixoto et al., 2007). Modeling of RLPs was thus possible within a membrane adsorber technology, representing a rational tool for further process optimization on this and, probably, other viral(-like) systems. Moreover, a successful application of anion-exchange membrane chromatography for RLPs was demonstrated hereby enlarging the significance of this technology for the purification of these complex biopharmaceuticals.

2.2 Materials and methods

2.2.1 RLP production

RLPs were produced with a *Spodoptera frugiperda* Sf-9 cell line obtained from the European Collection of Cell Cultures (ECACC #89070101, United Kingdom) using the baculovirus expression vector system (BEVS). The three baculoviruses, containing rotaviral vp2, vp6 and vp7 genes were kindly provided by Dr. Didier Poncet from Centre National de la Recherche Scientifique (Institut National Recherche Agronomique (INRA), Gif-sur-Yvette, France). The cells were routinely cultured in shake flasks and propagated in spinner flasks (125 mL working volume). These cultures were used as inoculum for a 10 L working volume Wavebag bioreactor (Wave Europe, Cork, Ireland) using Gibco^{TM} Sf-900 II SFM medium (Invitrogen, Paisley, United Kingdom); cells were co-infected with a multiplicity of

infection of 2–5 pfu/cell for each type of the three baculoviruses at a cell concentration at infection of 3.0×10^6 cells/mL. At the time of infection and every 48 h afterwards, the culture was supplemented with protease inhibitors (1 μg/mL leupeptin and 1.6 μg/mL aprotinin (Sigma-Aldrich, München, Germany)); the bioreaction broth was harvested at 120 h post-infection. Cell concentration and viability were assessed using a Schärfe System CASY^{TM} 1 TTC system (Innovatis, Reutlingen, Germany) and confirmed, whenever necessary, by haemocytometer (Brand, Wertheim, Germany) with cell viability evaluated by 0.4 % trypan blue exclusion dye (Merck, Darmstadt, Germany) in phosphate-buffered saline (PBS).

2.2.2 RLP standard purification protocol

Bioreactor bulk fractions were harvested and kept at -20°C and the standard purification strategy adopted the methodology established in-house (Peixoto et al., 2007). Briefly, cell lysis and lipid removal from the bulk were done by incubation with 1% (v/v) Triton^{TM} X-100 (Sigma-Aldrich) for 30 min at 37°C. Samples were withdrawn before and after each step for assessment of RLPs recoveries by Western Blot and SDS-PAGE. The clarification was carried out using a Sartopure^{TM} PP2 depth filter cartridge with nominal 3 μm pores (Sartorius Stedim Biotech, Göttingen, Germany) through a peristaltic pump (Watson-Marlow, Wilmington, USA) at a rotation rate of up to 450 mL/min (6.4 mm tubing bore diameter, 1.6 mm tubing wall thickness) controlling possible overpressure (initial and maximum/final backpressures were approximately 1 and 2 bar). The clarified bulk was concentrated afterwards in a cross-flow ultrafiltration/diafiltration QuixStand^{TM} Benchtop System using a hollow fiber cartridge with a lumen diameter of 1 mm, a nominal molecular weight cut-off (MWCO) of 750 kDa, a membrane area of 0.042 m^2 and a flow-path length of 30 cm (UFP-750-E-4MA, all GE Healthcare, Uppsala, Sweden). Prior to use, the membrane was flushed with deionized water and equilibrated with Gibco^{TM} D-PBS (Invitrogen). The apparatus' reservoir was loaded with up to 1.7 L of pre-clarified cell lysate; transmembranar pressure (TMP) was set within the range of 5-10 psi which resulted in a permeate flow rate range of 5-20 mL/min. When the volumetric concentration factor reached 2-5, the retentate was diluted five times with D-PBS and further concentrated to 50 mL. The degree of washout of permeable components should be up to 10-20 % (see mass balance results in Table 5). Samples of the final retentate and permeate were taken to assess process yield.

The clarified and concentrated RLPs were then purified using size exclusion chromatography with a XK26/60 column (2.6 cm diameter, 60 cm bed height) packed in house with

Sephacryl^{TM} S-500 coupled to an ÄKTAexplorer^{TM} 100 liquid chromatography system (all GE Healthcare) equipped with UV (three simultaneous wavelength measurements) and conductivity/pH monitors. System operation and data gathering/analysis was done using the UNICORN^{TM} 5.0 software (GE Healthcare). The column was loaded with 5 % of the column volume and the elution was carried out with a flow rate of 2 mL/min (22.6 cm/h) at room temperature with D-PBS as running buffer. A final concentration step was performed by ultracentrifugation at 100000 g for 60 min at 4°C. The RLPs pellets were typically re-suspended in 1 mL of D-PBS. Hereafter, this processing route will be referred to as the "standard purification protocol".

2.2.3 Analyticals

To assess the RLP content and the relative concentration of the different proteins (VP2, VP6 and VP7), samples collected during the purification process were loaded onto NuPAGE^{TM} Novex 4-12 % Bis-Tris pre-cast polyacrilamide gels (Invitrogen) using standard running conditions (Laemmli, 1970). Protein visual detection was performed using SilverXpress^{TM} Silver Staining kit (Invitrogen).

Protein transfer onto nitrocellulose membrane was done with a semi-dry transfer unit (GE Healthcare); immunochemical detection for the three recombinant Rotavirus proteins, VP2, VP6 and VP7 was carried out using a polyclonal anti Rotavirus serum produced in rabbit, provided by Dr. Annie Charpilienne (CNRS INRA, France) followed by incubation with an alkaline phosphatase conjugated anti-rabbit IgG antibody (Sigma-Aldrich) and developed using 1-step^{TM} NBT/BCIP (Pierce, Rockford, United States of America).

SDS-PAGE (for protein purity assessment) and Western Blot (for RLP yield estimation) band profiles were analyzed by ImageJ software using an available add-in designed for gel band densitometry quantification and normalization.

Total protein content of samples was determined using the BCA protein assay kit (96-well plate protocol) from Pierce (Rockford, USA).

The quantification of DNA content throughout processing was undertaken using the PicoGreen^{TM} dsDNA Assay kit (Invitrogen) using 96-well plates according to the manufacturer's instructions.

Total baculovirus particles used for the BEVS/IC were quantified by real time quantitative PCR (q-PCR) following the methodology described before (Vieira et al., 2005).

RLP's integrity and morphology (shape, size) was assessed by electron microscopy. Briefly, 3 μL of sample was adsorbed onto a formvar coated 400-mesh copper grid (Electron

Microscopy Sciences, Hatfield, USA) for 60 s. The grid was then soaked in 1 % uranyl acetate for 30 s and dried in air at room temperature. The purified samples were examined in a JEM 200 Ex electron microscope (JEOL, Sollentuna, Sweden).

2.2.4 Anion-exchange membrane adsorber studies

Sartobind D MA 75 membrane adsorber provided from Sartorius Stedim Biotech (see Table 2.2 for details), was connected to the ÄKTA system as if dealing with a packed-bed column by means of proper luer connections allowing to monitor online the adsorption and elution processes.

Table 2.2: *Manufacturer parameters and operational standards for Sartobind D MA 75 anion exchange membrane adsorber.*

Characteristic	Value
Membrane material	Reinforced stabilized cellulose
Functional group	R-CH_2-N-$(C_2H_5)_2$
Adsorption area (cm^2)	75
Diameter (cm)	2.5
Sectional area (cm^2)	4.91
Number of layers	15
Bed height (mm)	4
Equivalent bed volume (mL)	2.06
Adsorption area / equivalent volume ratio (cm^2/mL)	36.4
Manufacturer's typical flux[a] (mL/(min.cm^2))	80
Minimum static binding capacity[b] (mg/unit)	45
Specific minimum static binding capacity[b] (mg/cm^2)	0.6

[a]nominal measurement at 1 bar operating pressure; [b]considering bovine serum albumin as reference protein

Preliminary membrane testing

A preliminary experiment with a clarified sample of RLPs (presenting a high load of impurities at this point) was performed in order to check for the potential applicability of this specific ion-exchange adsorption matrix as a capture/concentration step. The membrane was equilibrated with D PBS and elution was achieved using a linear salt gradient up to 1 M NaCl in 4 "colum" volumes (CVs). The pool of the flowthrough and fractions of detected elution peaks were obtained by the fraction collector and further analyzed via SDS-PAGE and immunoblot testing.

Systematic evaluation of the anion exchange process

Samples of RLPs obtained by the standard purification method were used to perform a scouting study for the ionic strength and pH of the equilibration/binding buffer.

For each chromatographic evaluation run, 50 μL of a concentrated and purified RLP feedstock (∼800 μg/mL) was diluted 10-fold in the desired buffer. For a pH range of 6.7-7.9 a 0.1 M Tris buffer supplemented with 3-mM $CaCl_2$ and 1.5 mM $MgCl_2$ (all Merck, Darmstadt, Germany) was used. Buffers at desired pHs and ionic strengths were prepared using the automated buffer preparation feature of the ÄKTA system operated with the UNICORN software. Essentially, it takes advantage of the two pumps connected to two stream selectors (one per pump) allowing four inlet streams. The four feeding solutions mixed by the system in appropriate proportions were: 0.1 M Tris buffer mentioned above, 0.1 M HCl, Ultra-pure water and 2 M NaCl. An automated method for the operation of the standard membrane chromatographic process was implemented. In brief, the flow rate was set to 2 mL/min (24 L/(h.cm^2)); equilibration of the membrane was set to 5 CVs; linear gradient elution (up to 1.5 M NaCl) was performed assuming a specified slope; membrane cleaning at 1.5 M NaCl and final re-equilibration with binding buffer were set to a total volume of 5 CVs for both steps. Automated scouting runs were then performed for the variation of a specific parameter. Conductivities of different equilibration buffers ranging from 2.5 to 7.1 mS/cm were tested as well as the pH within the range from 6.7 to 7.9 (fixing a selected ionic strength at 5.4 mS/cm). Additionally, varied linear gradient slopes were employed: 1.5, 3, 6, 9 and 12 CVs. All chromatographic runs were performed at room temperature.

2.2.5 Modeling and theoretical considerations

In the present study the SMA approach was used for the prediction of the exchange behavior of RLPs in anion-exchange chromatography. The SMA formalism implies the definition of three major parameters, the characteristic charge, ν_i, the steric factor, σ_i, and the equilibrium constant, K_i, that characterize the adsorption process as a stoichiometric exchange reaction of each solute with a certain number of adsorbed counterions (Brooks and Cramer, 1992):

$$c_i + \nu_i q_0 \rightleftarrows q_i + \nu_i c_0 \qquad i = 1, ..., N_c, \tag{2.1}$$

where c_i and q_i denote the solute concentration in the mobile phase and in the stationary phase, respectively, c_0 represents the salt concentration in the mobile phase, and q_0 is the concentration of bound salt available for exchange. The corresponding equilibrium

constant, K_i, is written as:

$$K_i = \frac{q_i}{c_i}\left(\frac{c_0}{q_0}\right)^{\nu_i} \qquad i = 1, ..., N_c. \tag{2.2}$$

Each solute may sterically obstruct to some extent some salt counterions on the adsorptive surface; the concentration of the "blocked" salt counterions is given by:

$$q_0^* = \sum_{i=1}^{N_c} \sigma_i q_i \qquad i = 1, ..., N_c. \tag{2.3}$$

The condition of electroneutrality requires that

$$\Lambda = q_0 + \sum_{i=1}^{N_c} (\nu_i + \sigma_i) q_i, \tag{2.4}$$

where Λ is the maximum ionic capacity of the membrane. Equations 7.4 and 7.6 constitute a system of nonlinear equations describing the multicomponent equilibrium. The dynamics of the membrane adsorber, which is assumed to behave as a chromatographic column (with geometric parameters listed in Table 2.2), is described by an equilibrium dispersed plug-flow model (Guiochon et al., 1994). The differential material balance for the component i can be written as

$$\frac{\partial c_i}{\partial \theta} + \frac{1-\epsilon}{\epsilon}\frac{\partial q_i}{\partial \theta} = \frac{1}{Pe}\frac{\partial^2 c_i}{\partial x^2} - \frac{\partial c_i}{\partial x} \qquad (0 < x < 1), \tag{2.5}$$

with he usual boundary conditions

$$\begin{aligned} c_i - \frac{1}{Pe}\frac{\partial c_i}{\partial x} &= c_i^{in} \qquad \text{for } x = 0, \\ \frac{\partial c_i}{\partial x} &= 0 \qquad \text{for } x = 1, \end{aligned} \tag{2.6}$$

where ϵ is the void fraction, $x = z/L$ is the dimensionless axial position (z is the axial position within the L height of the membrane), $\theta = t/\tau$ is the dimensionless temporal coordinate ($\tau = L/u$ is the reference time with u the interstitial linear velocity), Pe is the Péclet number for axial dispersion, and c_i^{in} is the inlet concentration. The membrane adsorber is initially solute-free and equilibrated with salt concentration, c_0^0, the initial

conditions for the membrane adsorber can be written as

$$\begin{aligned} c_0(0,x) &= c_0^0, \quad q_0(0,x) = \Lambda \\ c_i(0,x) &= 0, \quad q_i(0,x) = 0, \qquad i = 1, ..., N_c. \end{aligned} \tag{2.7}$$

For a linear-gradient elution the following conditions apply:

$$\begin{aligned} c_0(\theta,0) &= \begin{cases} c_0^0, & \theta < \theta_F \\ c_0^0 + G(\theta - \theta_F), & \theta \geqslant \theta_F \end{cases} \\ c_i(\theta,0) &= \begin{cases} c_i^F, & \theta < \theta_F \\ 0, & \theta \geqslant \theta_F \end{cases} \end{aligned} \tag{2.8}$$

where θ_F is the dimensionless length of the feed pulse, c_i^F is the feed concentration, and G is the gradient slope.

The equations are implemented and numerically solved using gPROMS (Process Systems Enterprise, London, United Kingdom), a software package for the modeling and simulation of lumped and distributed-parameter process models with combined discrete and continuous characteristics. The spatial derivatives are discretized using third-order orthogonal collocation on finite elements with a sufficiently fine resolution to provide a grid-independent solution.

Some model parameters are fixed by the experimental setup, while others can be determined via simulation and curve-fitting using the built-in estimation capabilities of gPROMS. The characteristic charge, ν_i, the equilibrium constant, K_i, and the steric factor, σ_i are unknown parameters. These parameters should be invariant from experiment to experiment, as they define the characteristic behavior of a certain solute in the SMA model framework. In a system with good mass-transfer characteristics operated at reasonable flow rates (as with membrane adsorbers), the Péclet numbers become fairly high (unless an extremely low throughput is employed). In this case, dispersion should not be significantly altered within the velocity window used (there is a physical limitation for the flow). One should keep in mind, however, that for large values of this parameter, its estimation in the present work is subjected to a large statistical uncertainty due to the mentioned low sensitivity of dispersion (and consequent chromatogram shape) as a function of the Péclet number variation.

Under diluted conditions with respect to particle concentration ($\Sigma_{i=1}^{N_c} c_i \to 0$), as is the

case in this study, the adsorption isotherms reduce to the linear or Henry's law form:

$$q_0 \rightarrow \Lambda, \qquad q_i \rightarrow K_i \left(\frac{\Lambda}{c_0}\right)^{\nu_i} c_i \qquad i = 1, ..., N_c. \tag{2.9}$$

Thus, the steric factor becomes redundant, but the partition coefficient retains the strongly nonlinear dependence upon salt concentration. For the case of linear gradient chromatography, the retention time, θ^*, of an infinitely diluted peak can be predicted using the linear solvent theory (Gallant et al., 1996):

$$\theta^* = 1 + \frac{\left[\gamma_i G + (c_0^0)^{\nu_i+1}\right]^{1/(\nu_i+1)} - c_0^0}{G}, \qquad \gamma_i = (\nu_i + 1)\frac{1-\epsilon}{\epsilon} K_i \Lambda^{\nu_i} \tag{2.10}$$

By fitting Eq. 7.12 to the retention times of several chromatographic runs with different gradient slopes, G, and different initial salt concentrations, c_0^0 estimations of K_i and ν_i can be obtained.

Additional effects might also become important for the refinement of the estimated fittings. Initial concentrations for each solute can be prominent; although these values are imposed by the chosen pulse, they refer to very small amounts, so that the inherent errors on the pipetting, dilution and injection onto the membrane could reflect variations on the amount of RLPs that were in fact loaded and further detected in the eluted peaks. Moreover, if we close the material balances, ie, the integral of the modeled outlet concentration (summing both RLP species) have to meet the sum of the experimental peak areas calculated; then, c_1^F and c_2^F become mutually dependent by means of:

$$\int_0^\infty (c_{\text{tot}}^{\text{out}})_{\text{simulation}} dt = (c_1^F + c_2^F)_{\text{simulation}} \times \Delta t_{\text{injection}} = \int_0^\infty (c_{\text{tot}}^{\text{out}})_{\text{experimental}} dt \tag{2.11}$$

An additional effect that is recurrently observed is the tailing of the peaks. This effect arises normally when the column is overloaded and operated in the nonlinear region of the adsorption equilibrium, which is not the case here as the RLPs are very diluted, or when there is a back-mixing effect generated by dead volumes in the system. The latter effect was taken into consideration by lumping all mixing effects onto a single mixing cell placed downstream of the membrane adsorber. Assuming a perfectly mixed cell, the solute balance material can be written as:

$$\frac{d(c_i^{\text{mix}})}{d\theta} = \frac{\tau F}{V_{\text{mix}}}(c_i(\theta, 1) - c_{\text{tot}}^{\text{mix}}) \tag{2.12}$$

where V_{mix} is the volume of the mixing cell, F is the flow rate, $c_i(\theta, 1)$ is the individual RLP concentration at the outlet of the membrane, and $c_{\text{tot}}^{\text{mix}} = c_1^{\text{mix}} + c_2^{\text{mix}}$ denotes the concentration measured by the UV monitor placed downstream of the membrane. This equation lumps the overall tailing effects interfering in the system. Indeed, by using the buffer preparation feature of the UNICORN software coupled to the ÄKTA system, automated mixing occurs with the four different inlet solutions and the injected samples which, in turn, impacts the overall elution behavior and consequently the peaks' shape. In addition, the dead volume present in the membrane adsorber may also have an active contribution to the tailing effect.

2.2.6 Revisiting downstream purification of RLPs

The anion-exchange membrane chromatography process was integrated into the downstream scheme by imposing some alterations on the standard purification protocol.

The buffer selected for assaying the Sartobind unit in a larger scale was Tris buffer used in the characterization studies with a conductivity of about 6 mS/cm and a pH fixed to 7.3 (these were the conditions that maximized product uptake).

The hollow fiber ultrafiltration process duration was reduced by restricting the concentration step to approximately 2-fold. The retentate hereby collected was divided in equal parts for further processing in the membrane adsorber in quadruplicate (to provide reproducibility assessment). Ultrafiltered bulk was then submitted to the anion-exchange process defining the following operational conditions: flow rate was set to 10 mL/min (122 mL/(h.cm^2)) except for elution, at 8 mL/min (98 mL/(h.cm^2)) due to operational pressure limitations; amounts of 250 mL were injected into the membrane followed by a washing step with equilibration buffer with 8 CVs; the linear gradient slope was programmed to 20 CVs followed by membrane cleaning with maximum salt concentration and re-equilibration with the starting buffer, both during 5 CVs. This capture and concentration step resulted in apparent low purity of the withdrawn fractions. Hence, the purification scheme had to proceed to a desalting step with a standard HiPrep$^{\text{TM}}$ 26/10 Desalting column (GE Healthcare), exchanging to the Tris buffer used before, allowing further processing. The pool of captured/concentrated particles was then polished by gel filtration as mentioned in the standard purification protocol. The pool of particles obtained at this stage is nearly 1.5-fold diluted (comparing to the previous step) and a final concentration step was carried out with a second anion-exchange membrane chromatography using the same operational method already described.

Samples were collected throughout the experiments for SDS-PAGE, Western Blot, total protein, DNA assay and host baculovirus q-PCR assessments.

2.2.7 Viral spiking study

To validate the process concerning the regulations imposed for a clinical grade product, a spiking study was designed to assess the possible binding of baculoviruses to this matrix.

Consecutively diluted samples of 2.8×10^9 total particles (TP)/mL of a monocistronic baculovirus stock with the vp2 gene were injected in the membrane adsorber in a series of runs and eluted under the same conditions. The decimal logarithmic reduction in total viral particles was assessed.

2.3 Results and discussion

The ultimate goal of a biotechnological process delivering a highly valuable end product is to maximize the overall process productivity while meeting the necessary purity requirements. Taking into consideration the process strategy presented in the literature mainly consisting of an ultradiafiltration followed by size exclusion chromatography (Peixoto et al., 2007), an attempt was made here to further improve recoveries while increasing the understanding of the underlying principles of the unit operations.

The results presented in this article can be sorted out as follows: i) the Sartobind D MA 75 membrane chromatography matrix from Sartorius was utilized and its performance studied in detail to detect its flaws and optimize the throughput; ii) the elution behavior was simulated based in SMA modeling approach used for proteins for improved process understanding and design; finally, iii) this step was integrated into the whole processing scheme to evaluate whether incorporation of the anion-exchange membrane chromatography improved the process.

2.3.1 Identification of a potential capture/concentration step

Samples of a pre-clarified bulk were injected in order to test the membrane for possible adsorption of RLPs; as depicted in Fig. 3.1, the chromatograms suggest adsorption of RLPs: the eluate peaks, which were collected as a single fraction, demonstrated the presence of RLPs as measured by Western blotting (see Fig. 3.1B). The molecular weights of the VP proteins resulting from this analysis differ from the values shown in Table 2.1. This is, however, rather common for pre-stained markers which do not always provide realistic marker

weights (see Invitrogen marker application notes). RLPs were furthermore not detected in the flowthrough pool, even with a reasonable contaminant load mainly composed of host cell proteins, DNA or baculoviruses (bulk). These encouraging results mandated a further evaluation of this chromatographic matrix.

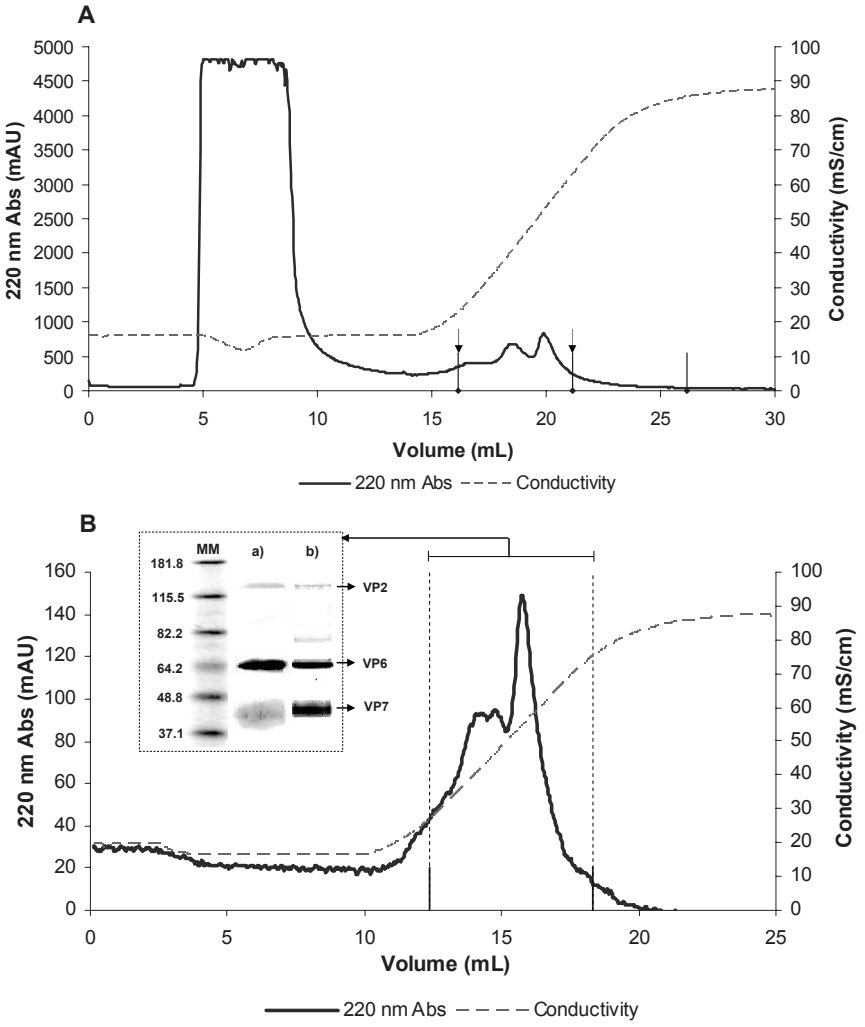

Figure 2.1: *Chromatograms demonstrating the binding uptake of RLPs present in a clarified sample: the matrix was equilibrated with D-PBS, then a 5 mL sample was loaded and eluted in 4 column volumes (CVs) with a linear gradient of up to 1 M NaCl; The pool of the two fractions delimited in A with arrows was injected in the membrane (post washing in high salt concentrations and re-equilibration with D-PBS) and chromatogram B was generated; the pool of peaks in B was analyzed by Western blot, a), and by SDS-PAGE stained with silver, b); Lane MM: BenchMark^{TM} Pre-Stained Protein Ladder, Invitrogen and correspondent weights in kDa.*

2.3.2 Evaluation of Sartobind D with purified RLPs

Adsorption isotherms or breakthrough curves determinations are typical procedures when a more in-depth study in chromatography is proposed. However, these procedures were avoided due to strong limitations on product availability, since manufacturing of perfectly assembled RLPs is complex and costly. Moreover, claimed dynamic binding capacities for this membrane adsorber are reasonably high (Table 2.2). Thus, an experimental setting was planned where a low amount of RLP would be necessary. As such, looking for the best conditions for operation of the selected membrane adsorber, a series of experiments were performed, injecting strict pulses of a purified RLP stock. The following operational variables, ionic strength and pH, were evaluated. It was observed in this set of chromatographic runs that the flowthrough pools did not present quantifiable amounts of RLPs as analyzed by Western blot (data not shown). Nonetheless, residual amounts of RLPs in these fractions shall demonstrate different peak areas reflecting different product uptake efficiencies in the following studies.

Effect of salt concentration

Buffering of injected RLP samples in a set of solutions differing on salt concentration was shown to affect the binding efficiency of the product onto the matrix. To address this issue, narrow variations on salt concentration in the chosen buffer were screened; the aim was to observe whether or not the equilibration step of the membrane and subsequent dilution of the sample in the same buffer upon injection/loading would be influenced by such subtle changes. The same linear salt gradients were applied starting from the imposed salt concentration present in the system. Even for a low amount of product expected to adsorb, a maximum for the binding capacity was attained, directly related to the detected peak areas (Fig. 3.2). This maximum for the RLPs peak areas was obtained when using a salt concentration of approximately 50 mM corresponding to $\sim$5.3 mS/cm. In agreement with the previous experiment (Fig. 3.1), two peaks were also observed. This may be due to the presence of either an excess of unassembled RLP proteins or even RLPs with slight different net density charges. The external protein VP7, presenting a theoretical isoelectric point lower than the remaining viral particle proteins, can have a stronger adsorption to the matrix as, in principle, more intense negative charge densities occur. This hypothesis was not confirmed as no differences could be measured in VP7 amounts for both peaks by any of the tests used: immunoblot, SDS-PAGE, electron microscopy or analytical size exclusion analyses (data not shown). No clear differences were detected in the analytical

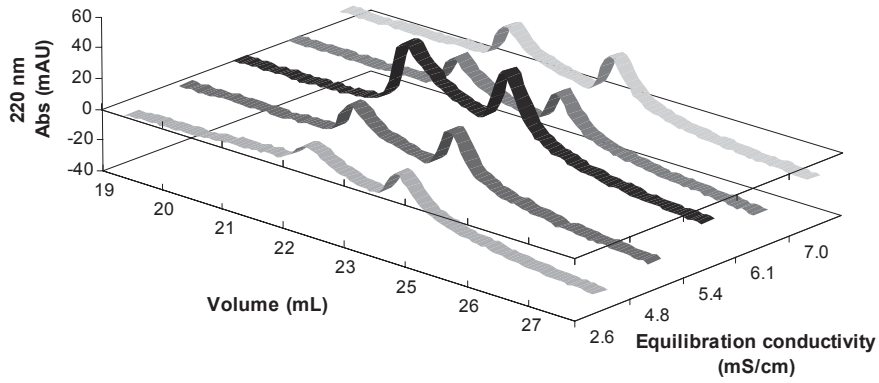

Figure 2.2: *Effect of the binding/equilibration buffer conductivity on the elution profile of RLPs. All five chromatograms were obtained by following a scouting method implemented in UNICORN coupled to the ÄKTA system where equilibration buffer conductivity was allowed to change to the indicated values; same RLP feedstock was used and the remaining operating variables and gradient elution parameters were kept fixed (detailed in Materials and methods section).*

Superdex 200 chromatograms as well as on Sephacryl S-500 runs; these were very similar to the ones normally obtained when using the classical DSP strategy (Peixoto et al., 2007). On the other hand, besides the presence of two distinct populations, the same RLP may have two modes of binding onto the studied matrix therefore yielding two distinct adsorption binding strengths. If, for instance, two preferential (but physicochemically slightly different) points of contact on the RLP surface become available for establishing electrostatic interactions with the DEAE ligands on the surface of the matrix, then, two different adsorption/desorption equilibria may occur. Due to the non-elucidation of the nature of the two peaks shown here (and throughout this work (see Figs. 3.2, 3.3, 3.4, 3.5, 3.6 and 2.9), the end product was defined in this manuscript as the pool of the two peaks.

pH scouting

Another critical variable in ion-exchange processes is the pH of the buffer solution used in the binding mode. The net charge density of proteins is a function of the proton concentration in solution (Voet and Voet, 1990). Thus, as was acknowledged above the impact on the peak areas by tight variations on ionic strength, a pH scouting was done in order to observe whether or not such variable could have a similar influence. As expected (Fig. 3.3), increasing pH until a certain level resulted in higher peak areas. This is in agreement with the theory for a single protein: the farther the pH is from the pI of the RLP the higher the global ionic surface charge is. Therefore, higher electrostatic forces should favor an improved approach/adsorption of the RLPs to the membrane adsorber. However, a de-

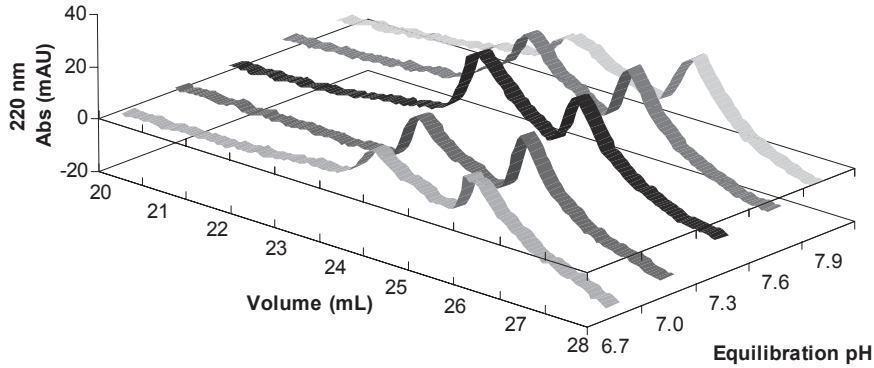

Figure 2.3: *Effect of binding/equilibration buffer pH on the elution profile of RLPs. All five chromatograms were obtained by following a scouting method implemented in UNICORN coupled to the ÄKTA system where the pH of equilibration buffer was set to vary from run to run; same RLP feedstock was used and the remaining operating variables and gradient elution parameters were kept fixed (detailed in Materials and methods section).*

crease in the peak areas was observed when increasing the pH to values higher than 7.6. As unexpectedly seen above, when lowering conductivity resulted in decreased capacity, by increasing the charge density (pH>7.6) the binding capacity decreased. A possible explanation could be that in a more alkaline environment (stronger particle negative charge) or in lower conductivities (weaker solvated particle), the first RLPs being injected may assume stronger electrostatic binding which in turn sterically hinder other incoming RLPs resulting in a non-ideal arrangement in the matrix surface, consequently diminishing capacity. This phenomenon has been observed both with monoclonal antibodies (Harinarayan et al., 2006) and antibody fragments (Ljunglof et al., 2007).

2.3.3 Spiking studies

By spiking the RLP samples with a known contaminant in reasonable amounts one could assess the outcome and distinguish the peaks detected in our chromatography system. In a set of chromatographic runs, a series of samples were spiked with monocistronic baculoviruses used in the bioreaction in different total viral particle titers; assessment for possible viral uptake onto the matrix was carried out by quantitative-PCR. Fig. 3.4 shows an example of such an experiment where the slower linear gradient was used. Additionally, a negative control where only RLPs were present was run to allow chromatogram comparison. These results suggest that adsorptive materials other than RLPs had bound to the matrix. It is worthwhile referring that the baculovirus stock used here was a clarified supernatant stock containing likely host cell proteins and/or other contaminants that may

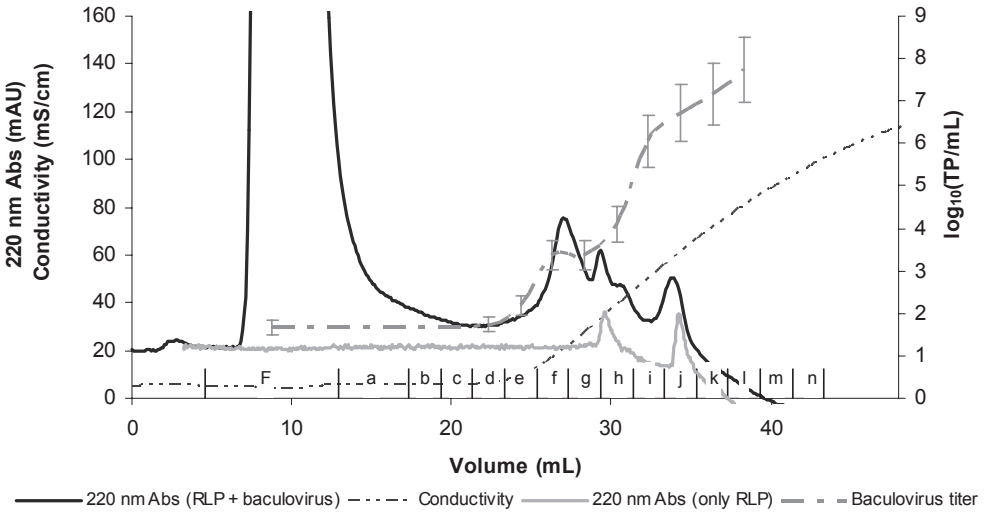

Figure 2.4: *Anion-exchange membrane chromatography curve obtained in a baculovirus spiking run: a co-injection of ∼40 µg of purified RLP and 10^9 TP/mL of a stock of baculovirus ("220 nm Abs (RLP + baculovirus)") was injected and further eluted in a gradient with a slope of 12 CVs using 1 M NaCl. A control run maintaining only the RLP content of the co-injection run was used to serve as control ("220 nm Abs (RLP only)").*

absorb at 220 nm. Possible adsorption of baculoviruses could somehow present an issue as it contaminates the desired clinical grade preparation of the RLPs. On the other hand, this observation opens a landscape for processing of such baculoviruses for use in, for example, gene therapy (Kukkonen et al., 2003). As assessed by q-PCR, baculoviruses corresponded to the highest retention times, as can be observed in Fig. 3.4. Thus one could foresee the need for a gel filtration polishing step to assure baculovirus clearance from RLPs.

2.3.4 Modeling of anion-exchange process

The dynamic concentrations of the different species for the anion-exchange membrane chromatography process are the numerical solutions of the set of Eqs. 7.7, therefore conversion of the collected absorbance data during the experiments (220 or 280 nm UV absorbances) into concentration units are required allowing the comparison between experimental and modeled data. Assuming perfectly assembled RLP particles (Lepault et al., 2001) (molecular weight of 76362 kDa), extinction coefficients of approximately 5.6×10^{-9} mmol/mAU (220 nm) and 4.0×10^{-8} mmol/mAU mmol/mAU (280 nm) are roughly estimated based on tests done with a known concentration of RLP pure stock.

In order to use the established SMA model, chromatographic runs at different gradient slopes were performed to provide experimental data input for model testing and further

fitting. The gradient velocity is, in fact, one of the most important variables in linear gradient elution of IEX processes as it can impose a great variation of retention times of the species present in the mixture impacting, amongst others, resolution.

Model training

In order to assess the suitability of the proposed model in the RLP case study, simulations were performed in gPROMS using initial guesses for unknown SMA parameters presented in the literature for other protein solutes (Gallant et al., 1996; Iyer et al., 1999; Pedersen et al., 2003; Arnau et al., 2006). It is worthwhile noting that this modeling tool could cope with the set of the multicomponent equations mentioned before within reasonably short computational times (e.g.: the simulation of an anion-exchange membrane chromatography linear-gradient experiment took approximately 50 seconds of CPU time on an 3.00 GHz Intel^{TM} Pentium^{TM} IV machine with 2 Gb of RAM, for a spatial grid of 50 finite elements).

Different chromatograms using a pure RLP stock in diluted conditions were rendered by the ÄKTA system for runs performed at different gradient slopes allowing estimation of the two important SMA parameters ν_i and K_i (see Table 2.3 and Fig. 3.5). Numerical solutions for the Eq. 7.12 could be obtained using a regular MS Excel^{TM} solver for the experiments carried out under the two slowest gradients (see Table 2.3). These values were thus used for the subsequent model testing. Provided that K_i, ν_i and remaining operational conditions listed in Table 2.3 and Table 2.4 were available, simulations could be conducted. The remaining parameters were proposed initially and further estimated by curve-fitting: namely, the Péclet number, accounting for the system's dispersion and the initial concentration of the RLP species as well as the feed concentrations c_1^F and c_2^F.

Curve-fitting and parameter estimation

By setting up the above conditions and assumptions, the estimation tool on gPROMS was run in order to fit the simulated output to the experimental data. Apart from the values obtained for the SMA parameters (Table 2.4), estimations for the feeding concentrations, c_1^F and c_2^F, as well as Péclet number were accomplished (Table 2.3).

As can be seen in Fig. 3.5, very good adjustments were obtained with this approach. Fine-tuned fits could however be obtained had one performed individual experimental curve-fitting. Nevertheless, here it was intended to present the broadest result possible that granted meaningful and predictive knowledge on the description of the elution profiles.

Not only could the estimated SMA parameters deal with the exchange between the

Table 2.3: *Chromatographic runs performed under different linear elution gradients and corresponding experiment-dependent parameters estimated by curve-fitting.*

	Established		**Estimated**		
Run	G(mM/min)	c_0^0 (mM)	$c_1^F + c_2^F$ (mM)	c_1^F/c_2^F (-)	$\frac{(c_1^F+c_2^F)_{\text{Run } i}}{(c_1^F+c_2^F)_{\text{Run 1}}}$ (-)
1	113.6	58.6	2.6	0.62	1.0
2	196.7	57.5	3.5	0.67	1.3
3	322.6	57.3	4.2	0.89	1.6
4	394.4	47.4	3.4	0.91	1.3

Table 2.4: *Non experiment-dependent parameters assessed within the SMA formalism.*

Λ (mM)[a]	208
ϵ[a]	0.95*
F (mL/min)[a]	2.0
Pe (-)[b]	7882
ν_0 (-)[b]	1.0
ν_1 (-)[b]	7.34
ν_2 (-)[b]	7.29
K_0 (-)[b]	1.0
K_1 (-)[b]	4.26×10^3
K_2 (-)[b]	2.05×10^5
V_{mix} (mL)[b]	0.33

*value obtained according to V_0 determined in a run with a pulse of salt; [a]estimated using frontal analysis (Gadam et al., 1993); [b]curve-fitting estimated parameters

double component RLPs appearing in the two peaks, but also when estimating proper feeding concentrations and Péclet numbers even better fits were achieved thus confirming that the formalism implemented gives strong robustness, even with slight alterations in the initial ionic strength.

If the information regarding the impact of ionic strength on product uptake during binding to the matrix (Fig. 3.2 and Fig. 3.3) is integrated, then the slight variations on the sum of feed RLP concentrations presented in Table 2.3 become reasonable. Nevertheless, it should be observed that the model has not assumed residual losses of product in the flowthrough; in fact, the experimental chromatograms are inconclusive on this issue. Therefore, the imposed material balance explains the increment on the feeding concentrations (Eq. 2.12). Overall, these results serve as a proof of principle that, indeed, modeling is possible for this system.

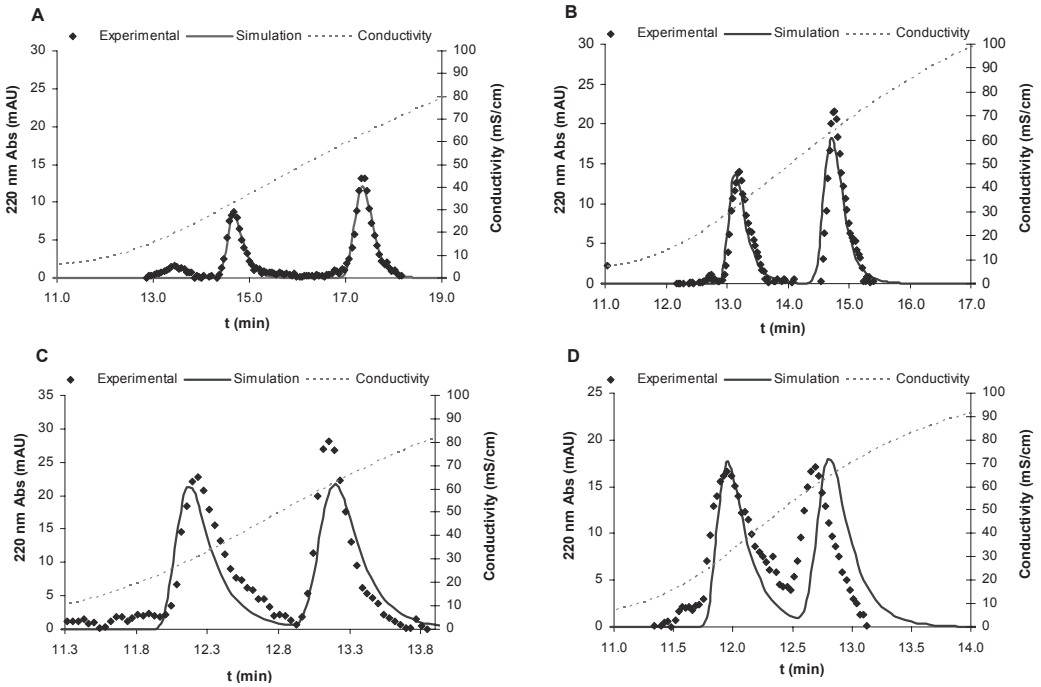

Figure 2.5: *Simulations performed against experimental data of anion-exchange membrane chromatography runs of purified RLPs varying the linear gradient slope: A, 12 CV; B, 6 CV; C, 3 CV; D, 1.5 CV. Details of the experimental chromatographic experiments are shown in the text; simulations and curve-fitting to experimental data-set were done using the gPROMS simulation software; time zero refers to the injection start.*

2.3.5 Scaled-up integration of the anion-exchange membrane chromatography

Integrated process

Finding an optimized utilization for a process that simultaneously integrates concentration and purification steps can be a time- and labor-consuming task since the room for possible experiments, i.e., selecting operational conditions, is large. Taking into account the results obtained in the matrix evaluation studies, a sensible integration of the anion-exchange membrane chromatography step in the standard purification protocol was attempted (see Fig. 3.8): an ultradiafiltered bulk (obtained by the standard procedure) only nearly 2-fold concentrated was used after exchanging with the chosen buffer – 0.010 mM Tris buffer plus 0.050 M NaCl (calcium supplemented) – that was equally divided and used in order to repeat the process and provide some support to our results. This quite diluted bulk permitted to significantly accelerate the hollow fiber ultrafiltration process where the permeate flux tends to decrease with time due to membrane clogging. In addition, there is

a gain in both product conservation and processing time as RLPs exposure to high shear stresses is reduced for a shorter period (the standard procedure step using hollow fiber could last up to 4 hours, to reach feasible concentration factors considering the subsequent gel filtration polishing step).

Afterwards, equal retentate quantities where pumped through the membrane adsorber via the ÄKTA system and subsequently eluted using a linear gradient. Here, the operational conditions were modified so that they would allow the fastest processing possible. By increasing the scale, the load flow rate had also to be up-scaled, therefore 10 mL/min was considered as reasonable. Using this flow rate the membrane capacities were assessed close to the limit in terms of adsorption kinetics (very low residence times are imposed). In fact, as can be checked in Table 5, the yield in this step was around 55%; indeed, the presence of RLPs was detected by immunoblotting in the flowthrough fraction (data not shown). This problem can be overcome by using different strategies: slowing the flow rates thus allowing a longer residence time or using a recirculation mode, letting the feed pass a sufficient number of times over the matrix. It can be of interest to opt for a series of injection steps if the adsorption to the surface matrix is a limiting step; using highly porous membrane adsorbers, residence times tend to be quite short (especially if it is intended to keep the flux or flow rate as high as possible). Worth mentioning in this regard is also that possible contaminants might adsorb as well and occupy ligand sites therefore counteracting product uptake and further recovery. Membrane fouling can furthermore become relevant when very high loads of protein and other contaminants are processed. Future investigation is needed to further clarify these possible issues.

The elution flow rate was programmed to 8 mL/min using 20 CVs as a linear gradient slope to allow fair resolutions as well as providing an additional result to confront with the developed theoretical model.

A stepwise elution mode could be applied here but since it was decided to obtain as much data as possible as well as comparable with the approach used in the evaluation studies and modeling a linear salt gradient was used. As can be seen in the chromatogram depicted in Fig. 3.6, in this step a huge load of contaminants being washed out from the membrane in the loading mode was observed as expected; furthermore the two eluted peaks now appear at a higher order of magnitude and with a smaller resolution due in part to some contaminant binding. Although contaminant binding was not expected, a less complete ultrafiltration may permit that proteins kept on this bulk, showing similar charge properties, would also compete for the matrix binding sites.

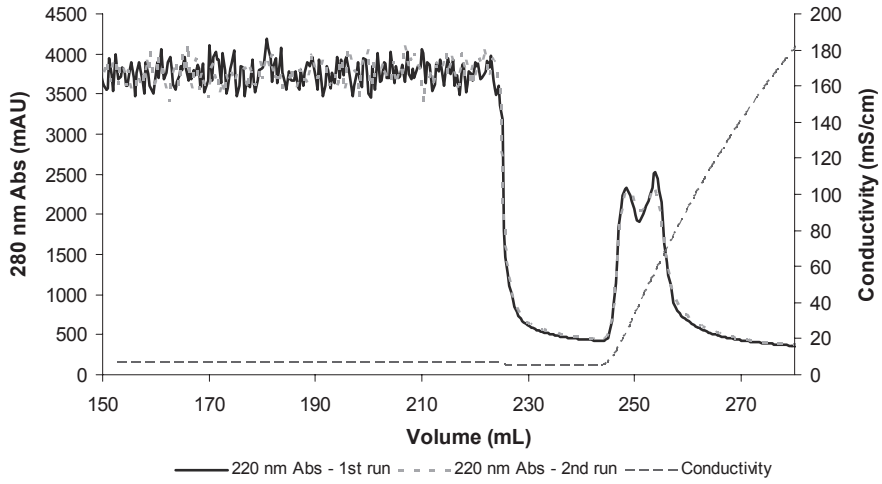

Figure 2.6: *Chromatograms obtained in two of the four anion-exchange membrane chromatography runs carried out for the larger processing scale; only two curves are present, so as to facilitate reader observation (chromatograms were very highly reproducible); loads of 220 mL with a flow rate of 10 mL/min were used after which a 2 CVs washing with equilibration buffer and elution performed for 20 CVs, now using 8 mL/min flow rates.*

At this point in the DSP route, the peak fractions containing RLPs obtained during elution were several times purer but, still in agreement with the discussion above, a reasonable quantity of host cell proteins could be macroscopically observed by giving a characteristic color to the solution (present in early step bulks and usually never present, in our experience, even in concentrated RLP suspensions). This was supported by SDS-PAGE profile analysis (Fig. 3.7).

At this point, taking into account that this type of products can be very sensitive when dealt under aggressive conditions, a size exclusion chromatography, serving as a polishing step was introduced (Peixoto et al., 2007). This step dilutes our product approximately 1.5-fold; therefore, the option was to use anion-exchange membrane chromatography once again, similarly operated, but this time, mainly acting as a final concentration step. The outline of the integrated process is depicted in Fig. 3.8; the space between the two dashed lines in this diagram corresponds to the real volume proportions of the material throughout each DSP step providing a visual perception of the concentration factors. Yields of around 47% were obtained (Table 2.5) while removing most of the DNA and host-cell protein load (the final product has about 1.4 μg DNA/mg RLP). The concern underlined before on the presence of contaminant baculoviruses was avoided by gel filtration as has also been shown before (Peixoto et al., 2007). The DSP strategy presented here shows an improved overall yield being faster and more economic than the process described in Peixoto et al. (2007)

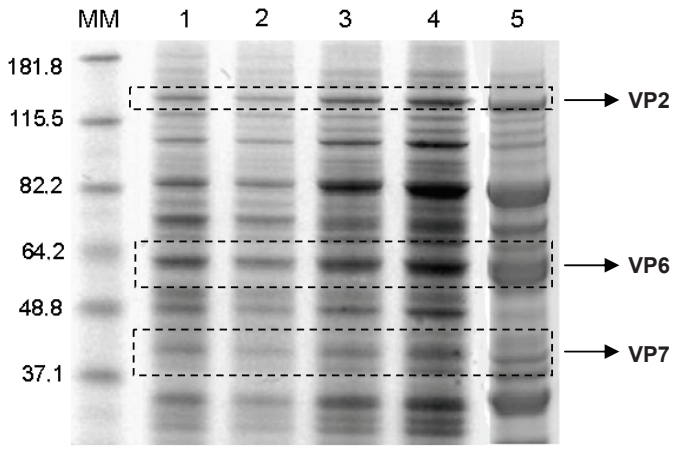

Figure 2.7: *Coomassie blue stained SDS-PAGE protein profiles of intermediate DSP steps samples. Lane MM: BenchMarkł Pre-Stained Protein Ladder, Invitrogen and correspondent weights in kDa; lane 1: 2 µL of bioreaction bulk sample; lane 2: 2 µL of sample after treatment with 1%Triton X-100; lane 3: 6 µL of sample after 3 µm depth filter clarification; lane 4: 6 µL of retentate sample after ultra/diafiltration; lane 5: 20 µL of the elution peak fraction of the first Sartobind D step.*

using an expensive and difficult to scale-up ultracentrifugation as the final step. The use of a membrane adsorber requires lower buffer consumptions for the different steps and uses a disposable and scalable technology thus avoiding cleaning costs and validation for cGMP operations.

Table 2.5: *Essential values for the assessment of each step and overall outcome.*

Process step	Purity[a] (%)	Step Yield[b] (%)	Concentration factor[c] (-)	%DNA removal	LRV[c] (-)
Bioreaction bulk	3.0	-	-	-	0.0
Cell disruption	2.9	97.6	0.9	37	-
Clarification	5.5	97.0	0.9	856	-
UF/DF	12.5	90.3	1.9	68	-
IEx (capture)	55.0	55.2	29.2	90	1.3
Gel filtration	74.0	99.7	17.5	98	3.5
IEx (concentration)	98.0	97.6	134.6	∼100	4.5
Overall	98	46	135	∼100	4.5

[a]ratio SDS-PAGE RLP bands signal/total protein signal; [b]step mass yield calculated via BCA total protein determination adjusted by the corresponding purity degree; [c]volume concentration factor assuming the bulk volume as reference; [d]$\log_{10}$ of total bVP2 baculovirus titer (obtained by qPCR) reduction assuming the bulk viral titer as reference

Predicted simulation

To validate the attempt to model this complex system, the implementation of the shown formalism was then tested in a more realistic situation, when this process is used to capture the product from a complex bulk containing a large load of contaminants. When changing the operational conditions, i.e., flow rate (binding and elution phases), time schedule of

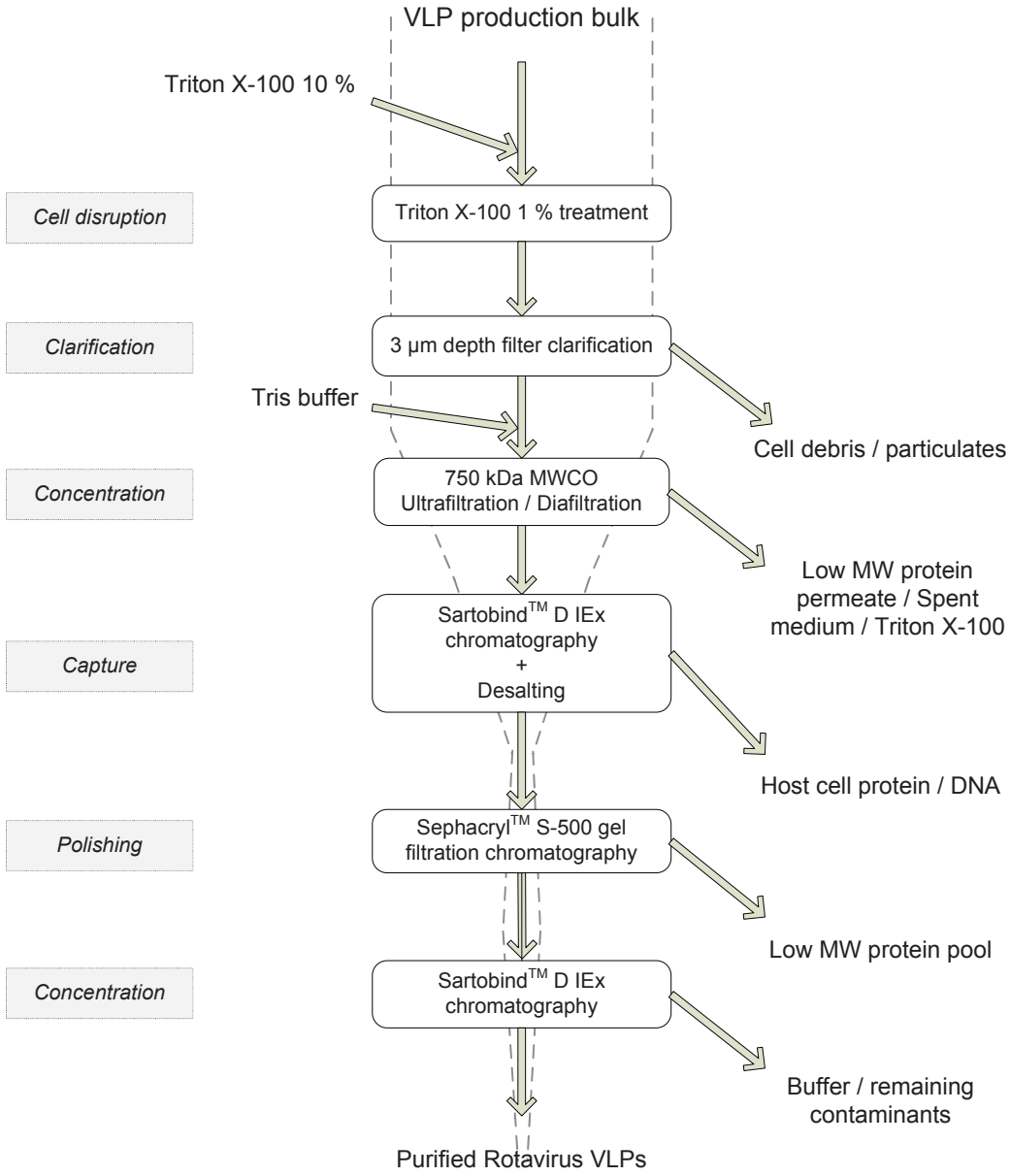

Figure 2.8: *Flow diagram for the integrated use of anion-exchange membrane chromatography in the DSP of RLPs.*

the process, elution gradient used, and remaining up-scaled operational parameters, good simulations are obtained (Fig. 2.9) taking into account the following operations. Again, some operationally related considerations had to be imposed, such as the feeding concentrations which are not known beforehand as well as the ionic maximum capacity, Λ, that is fixed. Assuming that the RLPs at this capture stage were more concentrated than the RLP diluted stock used in the evaluation studies, the computed c_1^F and c_2^F were adjusted (weighing the concentrations of the RLPs in the evaluation studies and in this capture step) and the ionic maximum capacity was arbitrarily decreased one quarter, so as to take into account the contaminant binding that was observed. Within the performed scalability testing, where the membrane was led to its limits in terms of material loading, the capacity was most likely achieved. As seen in Table 2.5, a loss of RLPs is detected in the flowthrough pool which is probably due to contaminant binding onto the membrane matrix (see purity in Table 2.5). Indeed, if an unaltered maximum ionic capacity had been used, the simulation would mispredict the product peaks (Fig. 2.9). The intrinsic ionic maximum capacity was obviously not physically altered here (at least with an unspoiled membrane). Effectively, this adjustment was only an artifact to assess whether or not the model could be applied to a larger scale situation under real contaminant conditions by assuming that the membrane capacity was in fact fully utilized. Alternatively to this explanation, one can speculate that in this situation the steric factor may play an important role and that would generate non-linear SMA isotherms. The applicability of the SMA theory is still meaningful for the larger scale, as in this case, while it opens new possibilities of investigation in order to elucidate the possible steric effects and contaminant binding studies in the preparative scale.

Overall, under the mentioned assumptions and approximations, these results provide evidence on model applicability and validation for larger scale, stressing the relevance of these calculated SMA parameters.

2.4 Conclusions

An anion-exchange chromatographic process was extensively studied in a membrane adsorber pattern for the purification of RLPs. A process evaluation study using this robust, scalable and cost-effective DSP step resulted in the determination of a narrow window of ionic strength and pH conditions where RLP recoveries were maximized. Additionally, an effort to understand the anion-exchange process mechanism ended up in a model formula-

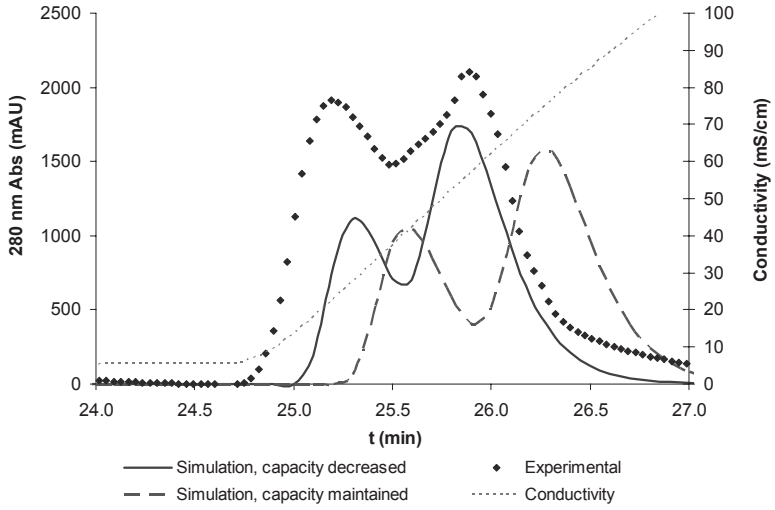

Figure 2.9: *Simulation versus experimental anion-exchange membrane chromatography elution curves obtained for one of the performed process runs; time zero refers to the injection start.*

tion that accurately described the behavior of the linear gradient step of these particles. This SMA model utilization was expanded from proteins as earlier presented in the literature and shown to be able to cope with much larger biological structures as virus-like particles with an incomparably higher degree of complexity. Moreover and as a proof of principle, SMA theory not only could be applied to the RLPs purification but also is suitable for improved understanding of membrane adsorber mechanisms. These results therefore deliver a starting point for dynamic modeling of separation mechanisms using non-model protein systems.

In future work, refinements of the model implementation can be carried out by considering contaminant binding; objective functions may then be more accurately assigned for both purity and recovery optimization depending on operational set-points.

Having ascertained that the anion-exchange membrane chromatography could be efficiently integrated into the DSP of RLPs, improved recoveries and yields could be effectively achieved (46% of overall product yield over the 37% previously reported by Peixoto et al. (2007)) yet meeting clinical-grade product requirements for potential medical applications.

Acknowledgements

Dr. Didier Poncet and Dr. Annie Charpilienne from Centre National de la Recherche Scientifique (Institut National Recherche Agronomique, Gif-sur-Yvette, France) are acknowl-

edged for providing the monocistronic baculoviruses and antibodies. We are grateful to Dr. Uwe Gottschalk from Sartorius Stedim Biotech (Göttingen, Germany) for providing the Sartobind membrane adsorber units. Dr. John Konz (Merck & Co, West Point PA, USA) is gratefully thanked for critically reviewing this manuscript. The authors thank Dr. António Roldão for support on the bioreaction as well as on discussions concerning simulation and modeling. We acknowledge funding from the European Commission (Baculogenes, LSHB-2006-037541 and Clinigene – Network of Excellence, LSHB-2006-018933) and the Portuguese *Fundação para a Ciência e a Tecnologia* (PTDC/EQU-EQU/71645/2006 and SFRH/BD/31257/2006).

Nomenclature

Symbols

c_i	concentration of the component i in the liquid phase (mobile phase) (mM)
c_0^0	initial salt concentration (mM)
c_i^F	feed concentration of the component i (mM)
c_i^{in}	initial concentration of the component i in the liquid phase (mM)
$c_{\text{tot}}^{\text{mix}}$	sum of solutes' concentrations on the outlet (mM)
c_i^{mix}	measured outlet concentration of the component i (mM)
F	flow rate (mL/min)
G	linear gradient slope (mM/min)
K_i	SMA equilibrium constant (-)
L	membrane adsorber bed height (cm)
N_c	number of total components (-)
q_i	concentration of the component i in the adsorbed phase (stationary phase) (mM)
q_0^*	concentration of salt counterions shielded by the solutes in the adsorbed phase (mM)
t	time since the beginning of anion-exchange membrane chromatography injection (min)
v	interstitial velocity (cm/min)
V	membrane adsorber volume (mL)
V_{mix}	volume of the mixing cell (mL)
x	Axial coordinate, $x = z/L$ (-))

Greek letters

ϵ	void fraction (-)
Λ	maximum ionic capacity of the membrane (mM)

ν_i characteristic charge coefficient of the component i (-)

σ_i steric factor of the component i (-)

τ reference time, $\tau = v/L$ (min)

θ temporal coordinate, $\theta = t/\tau$ (-)

θ_F dimensionless length of the feed pulse (-)

References

Aldridge S. Overcoming the critical issues in scale-up - improvements in titer shift the bottlenecks downstream to purification. Genetic Engineering News 2006;26:46–52.

Arnau J, Lauritzen C, Petersen GE, Pedersen J. Current strategies for the use of affinity tags and tag removal for the purification of recombinant proteins. Protein Expr Purif 2006;48:1–13.

Bertolotti-Ciarlet A, Ciarlet M, Crawford SE, Conner ME, Estes MK. Immunogenicity and protective efficacy of rotavirus 2/6-virus-like particles produced by a dual baculovirus expression vector and administered intramuscularly, intranasally, or orally to mice. Vaccine 2003;21:3885–900.

Brooks CA, Cramer SM. Steric mass-action ion exchange: Displacement profiles and induced salt gradients. AIChE J 1992;38:1969–1978.

Crawford SE, Labbe M, Cohen J, Burroughs MH, Zhou YJ, Estes MK. Characterization of virus-like particles produced by the expression of rotavirus capsid proteins in insect cells. J Virol 1994;68:5945–52.

Gadam SD, Jayaraman G, Cramer SM. Characterization of non-linear adsorption properties of dextran-based polyelectrolyte displacers in ion-exchange systems. J Chromatogr 1993;630:37–52.

Gallant SR, Vunnum S, Cramer SM. Optimization of preparative ion-exchange chromatography of proteins: linear gradient separations. J Chromatogr A 1996;725:295–314.

Glass RI, Bresee JS, Parashar U, Turcios R, Fischer T, Jiang B, et al. Rotavirus vaccines: past, present, and future. Arch Pediatr 2005;12:844–7.

Guiochon G, Golshan-Shirazi S, Katti A. Fundamentals of Preparative and Nonlinear Chromatography. Academic Press, Boston, MA, 1994.

Harinarayan C, Mueller J, Ljunglöf A, Fahrner R, Van Alstine J, van Reis R. An exclusion mechanism in ion exchange chromatography. Biotechnol Bioeng 2006;95:775–787.

Iyer H, Tapper S, Lester P, Wolk B, van Reis R. Use of the steric mass action model in ion-exchange chromatographic process development. J Chromatogr A 1999;832:1–9.

Jakobsson N, Karlsson D, Axelsson JP, Zacchi G, Nilsson B. Using computer simulation to assist in the robustness analysis of an ion-exchange chromatography step. J Chromatogr A 2005;1063:99–109.

Karger A, Bettin B, Granzow H, Mettenleiter TC. Simple and rapid purification of alphaherpesviruses by chromatography on a cation exchange membrane. J Virol Methods 1998;70:219–224.

Kukkonen SP, Airenne KJ, Marjomaki V, Laitinen OH, Lehtolainen P, Kankaanpaa P, et al. Baculovirus capsid display: a novel tool for transduction imaging. Mol Ther 2003;8:853–62.

Labbe M, Charpilienne A, Crawford SE, Estes MK, Cohen J. Expression of rotavirus vp2 produces empty corelike particles. J Virol 1991;65:2946–52.

Laemmli UK. Cleavage of structural proteins during the assembly of the head of bacteriophage t4. Nature 1970;227:680–5.

Lepault J, Petitpas I, Erk I, Navaza J, Bigot D, Dona M, et al. Structural polymorphism of the major capsid protein of rotavirus. Embo J 2001;20:1498–507.

Lightfoot EN, Moscariello JS. Bioseparations. Biotechnol Bioeng 2004;87:259–73.

Ljunglof A, Lacki KM, Mueller J, Harinarayan C, van Reis R, Fahrner R, et al. Ion exchange chromatography of antibody fragments. Biotechnol Bioeng 2007;96:515–24.

Nguyen TV, Iosef C, Jeong K, Kim Y, Chang KO, Lovgren-Bengtsson K, et al. Protection and antibody responses to oral priming by attenuated human rotavirus followed by oral boosting with 2/6-rotavirus-like particles with immunostimulating complexes in gnotobiotic pigs. Vaccine 2003;21:4059–70.

Pedersen L, Mollerup J, Hansen E, Jungbauer A. Whey proteins as a model system for chromatographic separation of proteins. J Chromatogr B 2003;790:161–173.

Peixoto C, Sousa MFQ, Silva AC, Carrondo MJT, Alves PM. Downstream processing of triple layered rotavirus like particles. J Biotechnol 2007;127:452–461.

Prasad BV, Wang GJ, Clerx JP, Chiu W. Three-dimensional structure of rotavirus. J Mol Biol 1988; 199:269–75.

Rodrigues T, Carvalho A, Roldao A, Carrondo MJT, Alves PM, Cruz PE. Screening anion-exchange chromatographic matrices for isolation of onco-retroviral vectors. J Chromatogr B 2006;837:59–68.

Ruiz MC, Charpilienne A, Liprandi F, Gajardo R, Michelangeli F, Cohen J. The concentration of ca2+ that solubilizes outer capsid proteins from rotavirus particles is dependent on the strain. J Virol 1996; 70:4877–83.

Shene C, Lucero A, Andrews BA, Asenjo JA. Mathematical modeling of elution curves for a protein mixture in ion exchange chromatography and for the optimal selection of operational conditions. Biotechnol Bioeng 2006;95:704–713.

Shi Q, Zhou Y, Sun Y. Influence of ph and ionic strength on the steric mass-action model parameters around the isoelectric point of protein. Biotechnol Prog 2005;21:516–23.

Specht R, Han B, Wickramasinghe SR, Carlson JO, Czermak P, Wolf A, et al. Densonucleosis virus purification by ion exchange membranes. Biotechnol Bioeng 2004;88:465–73.

Teeters MA, Root TW, Lightfoot EN. Performance and scale-up of adsorptive membrane chromatography. J Chromatogr A 2002;944:129–139.

Vieira HLA, Estevao C, Roldao A, Peixoto CC, Sousa MFQ, Cruz PE, et al. Triple layered rotavirus vlp production: Kinetics of vector replication, mrna stability and recombinant protein production. J Biotechnol 2005;120:72–82.

Voet D, Voet JG. Biochemistry. John Wiley & Sons, New York, 1990.

Yamamoto S. Plate height determination for gradient elution chromatography of proteins. Biotechnol Bioeng 1995;48:444–451.

Yamamoto S, Nakanishi K, Matsuno R, Kamijubo T. Ion exchange chromatography of proteins - predictions of elution curves and operating conditions. ii. experimental verification. Biotechnol Bioeng 1983;25:1373–1391.

Zhou JX, Tressel T, Gottschalk U, Solamo F, Pastor A, Dermawan S, et al. New q membrane scale-down model for process-scale antibody purification. J Chromatogr A 2006;1134:66–73.

Part II

Rational design and development of downstream processing for baculoviruses: a challenging enveloped virus model

Chapter 3

PURIFICATION OF AN ENVELOPED VIRAL VECTOR FOR CLINICAL APPLICATIONS USING MEMBRANE PROCESSES

Adapted from:

Vicente T, Peixoto C, Carrondo MJT, Alves PM. Purification of recombinant baculoviruses for gene therapy using membrane processes. Gene Ther 2009; 16:766–775.

and

Vicente T, Peixoto C, Carrondo MJT, Alves PM. Virus production for clinical gene therapy. Methods Mol Biol 2009; 542:447–470.

Abstract

Recombinant baculoviruses are widely used as vectors for the production of recombinant proteins in insect cells. More recently, these viral vectors have been gaining increasing attention due to their emerging potential as gene therapy vehicles to mammalian cells. Their production in stirred bioreactors using insect cells is an established technology; however, the downstream processing (DSP) of baculoviruses envisaged for clinical applications is still poorly developed. In the present work, the recovery and purification of recombinant baculoviruses aiming at injectable-grade virus batches for gene therapy trials was studied. A complete downstream process comprising three steps – depth filtration, ultra/diafiltration and membrane sorption – was successfully developed. Optimal operational conditions for each individual step were achieved yielding a scalable downstream processing for recombinant baculoviruses (rBV) as vectors for gene therapy. The processing route designed hereby presents global recovery yields reaching 40 % (at purities over 98 %) and, most importantly, relies on technologies easy to transfer to process scales under cGMP guidelines.

Contents

3.1 Introduction

Recombinant baculovirus (rBV) has emerged as a novel vector for in vivo and in vitro gene delivery (Hu, 2006). Indeed, applications of baculovirus-mediated gene transfer have widely expanded to drug screening, eukaryotic gene display, cancer therapy and tissue engineering (Chuang et al., 2007). In addition, rBV envelope can be used for protein/peptide display rendering rBVs the potential as a vaccine delivery platform (Hu, 2006; Tani et al., 2008).

Current efforts to improve rBVs as gene delivery vehicles for mammalian cells are motivated by their advantages over existing gene transfer vectors, e.g.: non-pathogenicity to mammalian hosts; ability to accommodate very large foreign DNA inserts; reliable production at high titers using insect cell lines (Palomares et al., 2006; Hu, 2008). However, the baculovirus distinct properties, in particular surface heterogeneity and non-spherical, rod-shaped structure, represent major challenges in the development of robust downstream strategies to produce clinical grade preparations. Moreover, *in vivo* clinical applications require high doses of viral vectors to achieve the targeted therapeutic effect and effective removal of contaminants since these can inhibit transduction efficiency or can initiate host immune responses leading to unwanted adverse effects. Thus, these challenges on potency and quality urge for the development of efficient and scalable purification and concentration methods to optimize the production of rBVs (Hu, 2006).

The literature is scarce on what concerns the concentration/purification of rBVs as compared to other viral vectors. Routinely, rBVs are purified and concentrated by a series of centrifugation and ultracentrifugation steps after harvesting from cell culture (O'Reilly et al., 1994). However, ultracentrifugation protocols are time- and labor-consuming often leading to significant loss of infectivity (potency) probably due to irreversible aggregation of the viral particles; hence, low recovery yields with low reproducibility are typically obtained (Jorio et al., 2006). A purification strategy combining ultracentrifugation and size exclusion chromatography has been proposed but the overall recovery yield obtained barely reaches 25% (Transfiguracion et al., 2007). A concentration step based on the electrostatic surface charge of rBV using cation exchange ligands was also described (Barsoum, 1999; Wu et al., 2007). Recently, the concentration of biotinylated rBV vectors using magnetic beads was reported with success (Kaikkonen et al., 2008). Nevertheless, for applications requiring non-conjugated rBV vectors, there is still no fully scalable downstream processing (DSP) strategy available.

Animal cell culture derived impurities such as host cell DNA, host cell protein and endotoxins are major concerns when a clinical application is envisaged (FDA, 2010). The available purification protocols for rBVs barely address these issues. Viral vectors involved in a large number of clinical trials, for instance, adenoviruses or retroviruses require a combination of DSP steps (concentration, capture and polishing steps) capable of decreasing these contaminants to acceptable values (Altaras et al., 2005; Rodrigues et al., 2007; FDA, 2010).

The aim of this study was the development of a simple, robust and cost-effective DSP strategy for rBV purification. An efficient purification process mostly based on membrane technology was devised where processing times and validation costs were significantly reduced comparing to existing methodologies, thus streamlining the technology transfer to cGMP operations. The DSP strategy presented herein is divided into three major parts: (i) clarification by depth filtration, followed by (ii) concentration by cross-flow ultradiafiltration, and (iii) purification using anion exchange membrane adsorbers emerging as an alternative for purification of rBV, with great potential for large scale manufacturing.

3.2 Materials and methods

3.2.1 Recombinant baculovirus stock propagation

Sf9 insect cells (ECACC #89070101, UK) were routinely grown in Gibco^{TM} Sf-900 II SFM (serum-free) culture medium (Invitrogen, Paisley, UK) using spinner (stirred at 150 rpm in a magnetic stirrer) or Erlenmeyer vessels (shaken at 110 rpm in an orbital shaker). Cell concentration and viability were routinely assessed by haemocytometer (Brand, Wertheim, Germany) with cell viability evaluated by 0.4 % trypan blue exclusion dye (Merck, Darmstadt, Germany) in phosphate-buffered saline.

Infection procedures were done using rBV seed stocks kindly provided by Dr. Kari Airenne (AIV Institute/UKU, Kuopio, Finland) at multiplicities of infection (MOI) of approximately 0.1 plaque-forming units (pfu)/cell. Two vectors were used: rBV GF-Pvp39Nterm (encoding for the baculovirus major structural capsid protein, vp39, containing on its N-terminal a GFP protein reporter (Kukkonen et al., 2003)) referred to as rBV-GFP, and rBV DsRed2-mCherryvp39Nterm (encoding for vp39 fused with mCherry, a cherry-red fluorescent protein, plus an additional mammalian expression cassette composed of a strong mammalian cell promoter, CMV, and DsRed2, a red fluorescent protein) referred to as rBV-cherry-dsred2.

3.2.2 Production of rBV stocks

Stock aliquots of rBV-GFP were produced in Sf9 cells grown in a 25 L working volume wavebag bioreactor (Wave Europe, Cork, Ireland) using Sf-900 II medium. Sf9 cells were infected at a viable cell concentration at infection of 1-2$\times 10^6$ cells/mL using an MOI of 0.1 pfu/cell. Cell viability and cell infection were monitored for five days post infection (Cruz et al., 2000). Quantification of the infected cells during the process was done by flow cytometry assessing GFP-expressing cell populations using a CyFlow^{TM} Space flow cytometer system (Partec, Münster, Germany). Data analysis was done using the manufacturer acquisition software FloMax^{TM} (Partec). The rBV production bulk was harvested when the cell viability reached values of 50 %. Infection bulks were clarified either by centrifugation at 1500 g for 20 minutes or by depth-filtration using 3 and 0.65 μm retention Sartopure PP2 filter capsules (Sartorius Stedim Biotech, Göttingen, Germany) detailed in the Downstream Processing methods section. Clarified aliquots were stored at 4 °C in the dark until further use.

rBV-cherry-dsred2 stock aliquots were produced in 2 L Erlenmeyer flasks incubated

at 27°C orbital shaker at 110 rpm. Sf9 infections were done for five days post infection (when the cell viability reached 50 %). Cell infection was monitored using a fluorescence microscope for the detection of the mCherry signal produced.

3.2.3 Downstream processing

Ultracentrifugation-based purification

rBV standards used as reference for purity and recovery yields were obtained following a classical ultracentrifugation-based purification protocol using sucrose gradients as described in the literature (Airenne et al., 2000).

Clarification assays

A clarification scheme was devised based on disposable depth-filter capsules that are easily integrated downstream of the bioreactor apparatus. Sterile tubing (1/4" inside diameter) connections were prepared coupling the outlet of the bioreactor to 3 μm retention Sartopure PP2 filter capsules followed by 0.65 μm retention Sartopure PP2 filter capsules in series. Virtually, all large cell particulates/aggregates were removed from the rBV containing supernatant. Filtration flow rates ranging within 3-5 L/h (or a flux of 15-25 L/(m^2h)) were achieved by using a peristaltic pump (Watson-Marlow, Wilmington, MA, USA) run at room temperature. The depth-filters were pre-equilibrated with D-PBS (supplemented with Ca^{2+} and Mg^{2+}) (Invitrogen). Samples were collected for analytical purposes before and after the clarification step.

Concentration/Buffer exchange assays

As an intermediate purification/concentration process, ultrafiltration combined with diafiltration using tangential cross-flow filtration was developed. The cross-flow filtration runs were performed in an automated ÄKTAcrossflow system controlled by the UNICORN^{TM} software (all GE Healthcare, Uppsala, Sweden). The feed, retentate and permeate side pressures as well as the retentate and permeate flow rates were digitally controlled by the equipment software. 200 cm^2 Hydrosart^{TM} membranes with 100 kDa nominal molecular weight cut-off (MWCO) (Sartorius Stedim Biotech) were mounted on the holder and connected to the ÄKTA system. Three retentate flow rates were evaluated: 25, 35 and 50 mL/min; at each of these retentate flow rates, a range of transmembrane pressures (TMP) within 0.25 to 2 bar was screened. Additionally, the impact of DVs (number of buffer vol-

umes used for medium exchange) in the permeate protein content was assessed collecting samples throughout the process.

After setting the optimal operational conditions (35 mL/min retentate flow rate and TMP of 1.2 bar (see Results and Discussion section)), a two-step program was used: (i) concentration until a desired concentration factor; and, (ii) continuous diafiltration until a desired diafiltration volume exchanging the spent medium for D-PBS buffer. All ultrafiltration/diafiltration runs were interspersed with 1 M NaOH cleaning in place sessions, water washes, water flux tests (where Flux vs. TMP plots are produced to prove membrane stability and performance for further process runs) and D-PBS system equilibration. All these protocols were performed using the program templates available in the UNICORN software package for ÄKTAcrossflow system and modified accordingly. All experiments were performed at room temperature.

Capture assays

A capture step relying on a bind-elute chromatographic step was chosen as the core of the rBV purification process. A preliminary screening of potential sorption chromatographic ligands was performed by simple batch adsorption using equal amounts of resin (5 mL settled material) and rBV supernatant (5-fold diluted in Tris-base buffer (Merck, Darmstadt, Germany) at pH 8.0) to a total of 10 mL. Beakers containing each resin type test were shaken in an orbital shaker at 200 rpm for a period of 75 minutes. Samples were collected throughout the experiment for rBV quantitation. In parallel, a control experiment was done using the same amount of 5-fold diluted rBV lacking any resin in suspension. Resins screened included a weak anion-exchange resin, Capto^{TM} DEAE (GE Healthcare), two strong anion exchange resins, Capto^{TM} ViralQ (GE Healthcare) and UnoSphere^{TM} Q (Bio-Rad, California, USA), and an affinity-based resin composed of sulfate groups designed for large particles that can also behave as cation-exchanger, Cellufine^{TM} Sulfate (Chisso Corporation, Tokyo, Japan).

The best results were obtained with DEAE (see Results and discussion section); taking into account the selection of this ligand, a comparison study between two types of chromatography matrices was performed: an anion-exchange membrane chromatography matrix using Sartobind D MA 75 (Sartorius Stedim Biotech) units with 75 cm^2 effective membrane area (equivalent to approximately 2 mL of membrane volume) containing DEAE, and, a packed column-based anion exchange chromatography matrix using Capto DEAE resin. Both matrices were coupled to an ÄKTAexplorer 100 chromatography sys-

tem controlled with UNICORN software (all GE Healthcare), equipped with online UV absorbance cell detector, conductivity meter, pH sensor, and a fraction collector. Both matrices were equilibrated with D-PBS prior to sample loading with amounts of 100 mL of previously ultra/diafiltered rBV supernatants. Flow rates varied from 5 mL/min (resin) to 10 mL/min (membrane). After sample loading, D-PBS buffer was allowed to pass through the matrices to remove unbound/contaminant material. Elution of the viral peaks was carried out using serial isocratic steps at buffer conductivities of around 48, 73 and 120 mS/cm (using D-PBS containing 1.5 M NaCl as the second mixing buffer).

The dynamic binding capacity of Sartobind D was estimated at 5 mL/min using a smaller unit, Sartobind D MA 15 (15 cm^2 effective membrane area or approximately 0.4 mL equivalent volume), injecting the same rBV material as above and collecting samples for rBV titration in each fraction. In addition, the impact of residence time was addressed by testing sample load recirculation at 10 MV/min; samples were collected for detection of rBV throughout the recirculation loading process.

After purification with the membrane adsorber units, the rBV fraction pools were submitted to a final desalting step using a standard HiPrep^{TM} 26/10 desalting column (GE Healthcare). Sterile microfiltration of final material was performed using Acrodisc^{TM} Syringe Filters with Supor^{TM} PES Membrane (Pall, New York, USA) or Sartorius Minisart^{TM} NML (Sartorius Stedim Biotech) before storage at 4°C in the dark. These experiments were performed at room temperature.

3.2.4 Analyticals

Total rBV particles titration

The number of genome containing particles referred to as total rBV titer (total particles (TP)) was monitored by real-time PCR (qPCR). Viral DNA was extracted and purified with the High Pure Viral Nucleic Acid Kit (Roche Diagnostics, Mannheim, Germany). Purified rBV viral DNA stocks previously quantitated by another validated qPCR method were used as external standard (Vieira et al., 2005).

The wild-type baculovirus *ie*-1 gene sequence was used as a template for the amplification of a chosen amplicon of 150 bp (protocol adapted (Lo and Chao, 2004)). DNA amplifications were done using the Light Cycler system with Fast Start Master SYBR Green I kit (Roche Diagnostics). For a 20 μL PCR reaction, 10 μL DNA template and 10 μL of master mix were added to each capillary. The master mix was prepared to obtain a final concentration of 4 mM $MgCl_2$ and 0.5 μM of each primer in each capillary.

Selected primers used for the *ie*-1 gene amplification were: forward, 5'-CCCGTAACGGACCTCGTACTT-3' and reverse, 5'-TTATCGAGATTTATTTGCATACAACAAG-3'. The PCR program was set to: DNA denaturation for 10 min at 95 °C; standard amplification using 45 three-step cycles: (i) denaturation-heating at 95 °C for 30 second; (ii) annealing-cooling at 63 °C during 5 seconds and; (iii) elongation-heating at 72 °C for 6 seconds. Fluorescence data was acquired at the end of the elongation step of each cycle. Data was analyzed using the LightCycler software (Roche Diagnostics) by means of the 'fit points method' described elsewhere (Rasmussen et al., 1998).

rBV transduction assays

Infective virus titers (IP) were determined either with the traditional end-point dilution assay method (O'Reilly et al., 1994) (for rBVs-cherry-dsred2) or with a flow cytometer-based assay (for rBVs-GFP) as developed by Karkkainen et al. (2009). Briefly, the end-point method was done with 96-well plates containing 100 μL of cellular suspension at a density of 0.5×10^6 cells/mL incubated for 1 hour at 27 °C. Dilutions of the virus samples were performed serially in culture medium, from $1{:}10^4$ to $1{:}10^{11}$, and 100 μL were used to infect the seeded Sf9 cells monolayers after removing the medium from the plate wells. Ten replicates for each dilution were performed in the same plate, and two independent plates were infected for each viral sample. A dilution of $1{:}10^2$ was used as positive control; culture medium was used as negative control. Plates were screened after seven days for mCherry fluorescence detection under an inverted fluorescence microscope. The 50 % tissue-culture infectious dose (TCID50) and consequent pfu (or number of infective particles) were calculated using the equations described elsewhere (King and Possee, 1992).

In the flow cytometric method, 500 μL of Sf9 cell suspension at 1.5×10^6 cells/mL, seeded into 2.2 mL 96-well plates (ABgene Limited, Epsom, UK), were infected with 500 μL of serial rBV sample dilutions. After incubating the plates at 27 °C for approximately 18 h in a shake flask orbital shaker at 420 rpm, cell suspensions were directly submitted to flow cytometer analysis using a 96-well plate autosampler (Partec) serially feeding each sample to the flow cytometer for GFP-expressing cell population assessment (Karkkainen et al., 2009). The maximum GFP-expressing cell population percentage (corresponding to a non-diluted viral sample) was used as a normalization factor for reliable titer calculation (Karkkainen et al., 2009).

HepG2 cell line was used as a target cell line for testing of rBV-cherry-dsred2 transduction potency. HepG2 cells were routinely cultured in Modified Eagle's Medium (MEM)

supplemented with 10 % fetal bovine serum (FCS) and grown at 37 °C in a humidified atmosphere equilibrated with 5 % CO_2. For rBV transduction with samples, HepG2 cells were seeded in 12-well plates at approximately 50 % confluence; 24 h later the culture medium was depleted from the wells, and the cells were washed with cold PBS; rBV samples were either directly added or diluted 1:2 (likewise for all samples) in MEM medium containing 1% FBS prior to incubation at 37 °C (with 5 % CO_2) for 3 h. Negative control wells containing MEM medium deprived of any viral sample were used. The virus dilution suspensions from each well were then exchanged with MEM (supplemented with 10 % FBS) after a brief PBS wash. Transduction was monitored for up to 15 days by cell visualization under an inverted fluorescence microscope coupled with a digital camera.

SDS-PAGE and Western Blot

Protein profiling of samples collected after each of the purification steps were performed using NuPAGE™ Novex 4-12% Bis-Tris pre-cast polyacrilamide gels (Invitrogen, Paisley, UK) using standard running conditions. Visual detection was carried out using SimplyBlue™ Safe Stain (Invitrogen).

Protein transfer onto nitrocellulose membrane was done with a semi-dry transfer unit (GE Healthcare); immunochemical detection of baculovirus main envelope glycoprotein, gp64, was carried out using a commercially available mouse monoclonal antibody (mAb) against gp64, AcV5 clone, affinity purified (1:2000 dilution) (eBioscience, San Diego, CA, USA) followed by incubation with an alkaline phosphatase conjugated anti-mouse IgG antibody (1:5000 dilution) (Sigma-Aldrich, München, Germany) and developed using 1-step™ NBT/BCIP (Pierce, Rockford, USA).

SDS-PAGE and Western Blot band profiles were analyzed by ImageJ software (NIH, Maryland, USA) using an available add-in designed for gel band densitometry quantification and normalization.

Total protein quantification

Total protein content of samples was determined using the BCA protein assay kit (96-well plate protocol) from Pierce following the manufacturer's protocol.

dsDNA quantification

The quantification of total dsDNA content in solution throughout processing was performed using the PicoGreen dsDNA Assay kit (Invitrogen) in 96-well plates according to

the manufacturer's instructions.

Endotoxin quantification

The endotoxin level in the end products was determined by LAL test using the Limulus Amebocyte Lysate QCL-1000 kit (Cambrex, Walkerville, MD, USA) following the manufacturer's instructions.

Electron microscopy analysis

rBV integrity and morphology were monitored by transmission electron microscopy. Briefly, 3 μL of sample was adsorbed onto a formvar coated 400-mesh copper grid (Electron Microscopy Sciences, Hatfield, USA) for 60 s. The grid was then soaked in 1% uranyl acetate for 30 s and dried in air at room temperature. The purified samples were examined in a JEM 200 Ex electron microscope (JEOL, Sollentuna, Sweden).

Dynamic light scattering analysis

Hydrodynamic size estimations of sample particles were obtained by dynamic light scattering (DLS) using a Zetasizer Nano-ZS Series ZEN3600 equipped with a 633 nm He-Ne laser (Malvern, Worcestershire, UK). Viral samples were diluted 25- to 60-fold in D-PBS; size measurements were performed in semi-micro polystyrene, 10×4 mm, cuvettes. Bovine serum albumin (BSA) (Merck, Darmstadt, Germany) diluted in D-PBS was used as a control experiment. The rendered experimental correlation functions from DLS were analyzed by the CONTIN method to obtain distributions of decay rate profiles which provided distributions of apparent diffusion coefficient and, consequently, of the apparent hydrodynamic diameter (through the Stokes-Einstein equation). Replicates with over 20 % deviation were neglected. Before data acquisition, the instrument software automatically optimizes operational conditions such as signal attenuation, focal distance and number of scans.

3.3 Results and discussion

3.3.1 Clarification and concentration

The clarification of the rBV bulk was performed using two depth filters in series: a 3 μm pore size followed by 0.65 μm pore size. A recovery of infective particles of 95±5 % was obtained. This two-stage mode technology allows for the removal of the centrifugation step, while maintaining the product stream sterile as the filters are autoclavable. Furthermore,

the filters are easy to use and represent a low up-front capital investment. The typical sequence used for most of the initial clarification steps in cell line based processes is 0.45 followed by 0.2 μm retention in order to prevent contamination; however, as rBVs are very large (Blissard and Rohrmann, 1990), larger pore sizes were chosen to reduce eventual viral coagulation and retention in the filters. Moreover, the selected pore size allowed for a more effective utilization of the entire depth of the porous filter for rBVs (Roush and Lu, 2008).

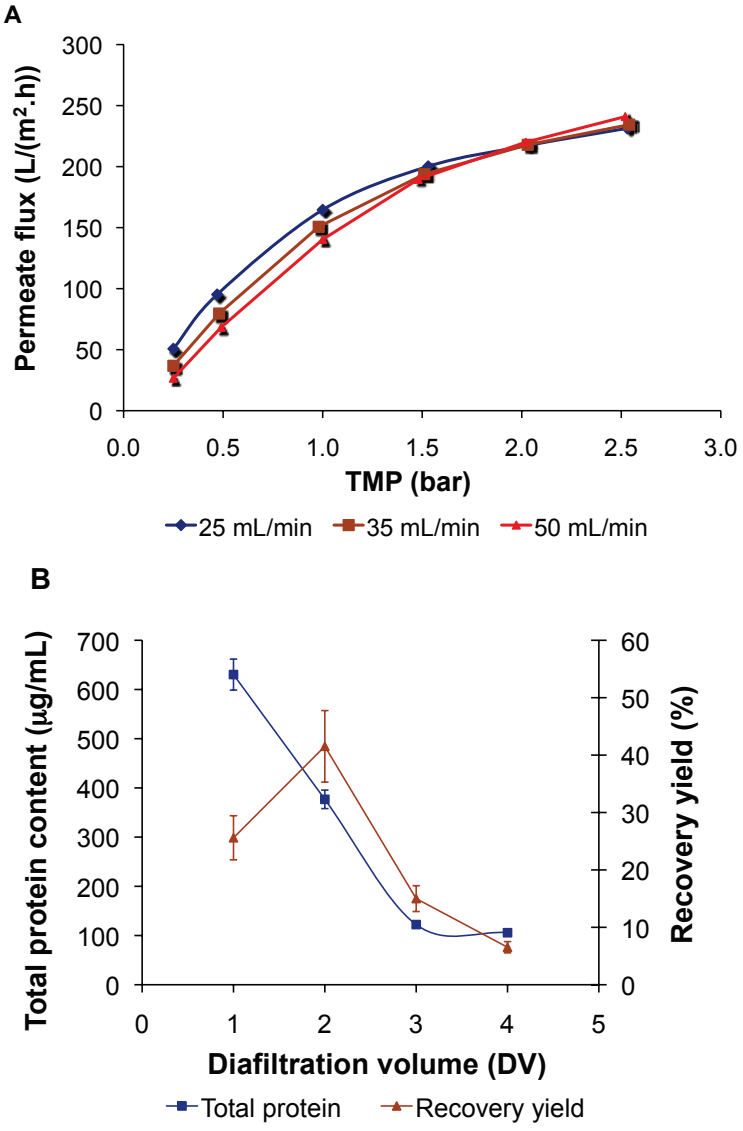

Figure 3.1: *Depth filter clarification of rBV: (A) Effect of transmembrane pressure (TMP) on permeate flux at different retentate flow rates: 25, 35 and 50 mL/min. (B) Relationship between increasing diafiltration volumes (DVs) and the amount of total protein in the process sample obtained when using continuous diafiltration along with ultrafiltration step.*

Concentration of rBVs and removal of low molecular weight contaminants was performed using tangential flow filtration (TFF); this is a technique routinely used at large scale to concentrate and purify viral products Altaras et al. (2005). The best retentate flow rates and TMP operating conditions were determined aiming at an optimized utilization of the membrane while reducing membrane fouling and consequent product loss (Fig. 3.1A). A TMP of 1.2 bar was selected, since for higher values a tendency for stabilization of the permeate flux occurred for the three different retentate flow rates tested. This stabilization of the permeate flux occurs most probably due to gel layer formation, which may explain the decrease in rBV recoveries. Nevertheless, when operated at the TFF optimized conditions, recovery yields of 70±5 % (based on infective rBV titers) were obtained; moreover, concentration factors of, at least, up to 6 were feasibly achieved. Higher concentration factors are likely to be accomplished if one could further control the resilient gel layer formation; in fact, this seems to be the most critical issue, as it has been recently reported that rBVs resist well to other factors such as shear stress (Michalsky et al., 2008).

Table 3.1: *Assessment of ultrafiltration/diafiltration step reproducibility using different rBV vectors and different methods for quantification of infective rBV titers.*

rBV stock, #Experiment	Method used for determination of infectious titer	Recovery yield of UF/DF step (%)
rBV-GFP, #1	Flow cytometer	70±5
rBV-GFP, #2	$TCID_{50}$	68±6
rBV-cherry-dsred2, #1	$TCID_{50}$	65±10
rBV-cherry-dsred2, #2	$TCID_{50}$	70±4

Since at this point the purity did not meet the quality requirements for use in *in vitro* (or *in vivo*) clinical testing, the product was conditioned for a next downstream process step, an ion exchange process. The relationship between increasing diafiltration volumes (DVs) and the amount of total protein removed and recovery yield obtained when using continuous diafiltration was thus also evaluated (Fig. 3.1B). From these results, it is possible to conclude that 2 DVs is a good compromise between purity and recovery yield; after reaching a maximum around 2 DVs, a steep decrease is observed for the recovery yield for higher DVs accompanying the total protein content decrease (Fig. 3.1B). The reproducibility of this technique was also investigated with rBVs from different batches for different applications (Table 3.1). These results indicate that, independently of the batch or the method used for infective titer determination, the recovery yield obtained was within the same order of magnitude confirming process robustness. The recovery yields obtained do not differ much from the recoveries reported in the literature when cation exchange chromatography or ultracentrifugation steps were used to concentrate the virus (Barsoum,

1999; Transfiguracion et al., 2007). Moreover, the TFF has several advantages over the methods previously described in the literature, as it can process larger volumes in shorter times and can be used as disposable material thus facilitating cGMP operations.

3.3.2 Capture

To remove remaining contaminating proteins and DNA from the concentrated rBV stocks another purification step was investigated. Four different chromatographic media were tested (see Material and methods). The ligands selected for this study have been extensively used in protein purification; however, there are no reports in the literature addressing their applicability to rBV purification. The buffer used in the batch adsorption assay was Tris-base at pH 8.0 to avoid any pH limitation for virus binding onto the anion-exchange matrices. Anion-exchange functional ligands are good candidates for virus binding considering the low pI of the external rBV gp64 glycoprotein (Duisit et al., 1999). Samples were prepared by diluting 1/5 the baculovirus feedstock (approximately 10^8 viral particles/mL (TP/mL)); for each parallel experiment, approximately 2×10^7 TP/mL was used. The same viral load was subjected to equal conditions serving as an internal control. The results indicate that Capto DEAE and Capto ViralQ are the best matrices in terms of adsorption kinetics; from 30 to 50 min Capto DEAE shows slightly faster dynamics than Capto ViralQ although reaching both the same final plateau (Fig. 3.2). UnoSphere Q shows a lower capacity comparing to the Capto resins; Cellufine Sulfate does not significantly adsorb rBVs. Additionally, as it can be seen, rBV stability was not an issue as no significant rBV titer decrease was observed in the control beaker. As the main objective here was to select a ligand to proceed with the process development, DEAE seemed to be a reasonable choice.

Membrane chromatography has been applied with success for virus purification (Duffy et al., 2005; Lajmi et al., 2007); therefore, we investigated the performance of membrane adsorbers using the same diethylaminoethyl functional group (DEAE). rBV samples previously clarified by depth filtration and concentrated by TFF were loaded onto Sartobind D MA 75 for comparison against Capto DEAE resin packed in a column bed (10 mL column volume). Three elution steps were defined: (i) 48 mS/cm; (ii) 73 mS/cm; (iii) 120 mS/cm. The chromatogram profiles obtained are shown in Fig. 3.3.

The step elution mode provides a higher concentration factor and allows for the use of higher flow rates and column loads. Although two well resolved peaks were observed in both experiments, the Western Blot analysis using a monoclonal antibody anti-gp64 envelope protein (the major rBV enveloped protein) indicated that both fraction pools contain rBVs

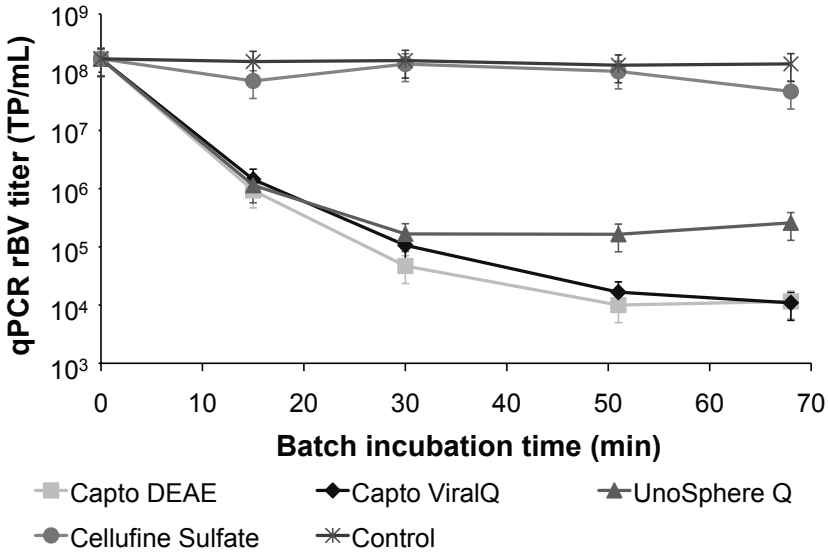

Figure 3.2: *Capture step selection: batch adsorption screening of baculoviral vectors to different ligands. The control corresponds to supernatant with no chromatographic matrix in suspension.*

(data not shown). This can be due to the different interactions taking place between the heterogeneous viral surface and the matrix. However, in terms of recovery yields and processing time, the Sartobind D membrane adsorber showed improved performance when compared to Capto DEAE resin in packed bed; indeed, the recovery yield of total rBV particles was around 20 % higher using the membrane process.

The loss of rBVs in the flowthrough and wash pools suggested that the residence time of the rBV feedstock load on the membrane unit could have been too short to allow full adsorption (data not shown); thus, a recirculation strategy was also evaluated for the membrane adsorber. An rBV sample was recirculated for 30 min at 10 membrane volumes *per* minute (MV/min) and flowthrough samples were withdrawn over time for analysis by Western Blot (Fig. 3.4). After 6 min of recirculation (roughly corresponding to 2 membrane passages), gp64 was no longer detectable in the flowthrough indicating that the recirculation mode did not significantly improve the adsorption kinetics of rBV and consequent recovery yield of baculovirus. One should highlight that a low amount of material was used as feedstock to remain well below the maximum binding capacity of the matrix (see below for dynamic binding capacity estimation) in order to assess only the adsorption dynamics. Alternatively, we decided to reduce the loading flow rate (down to half of the initial flow rate used) in order to allow the same residence times.

To fully characterize the membrane anion-exchange chromatography matrix, its dy-

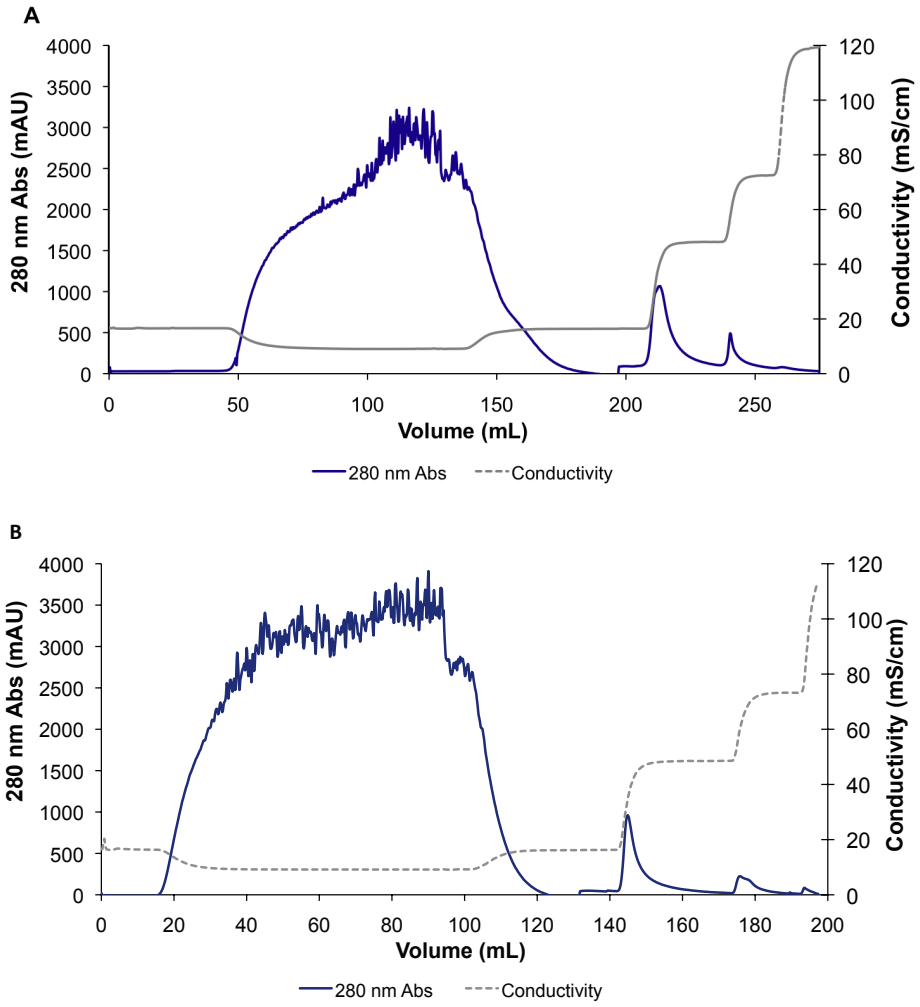

Figure 3.3: *Comparison between different matrices support: baculoviral vectors elution profile on Capto DEAE resin bed (A) and Sartobind D (B) matrices. The sample was previously concentrated by ultrafiltration and the elution steps were performed setting the elution buffer conductivities serially at 48, 73 and 120 mS/cm for the two different matrices.*

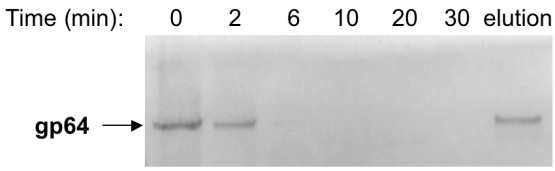

Figure 3.4: *Effect of feed recirculation on recovery of baculoviruses in membrane matrices: Western Blot for detection of gp64 (the major envelope baculovirus glycoprotein) in the flowthrough samples of Sartobind D loaded at 10 MV/min.*

namic binding capacity for rBVs was measured using a sample previously clarified and concentrated using the methodologies described above; the rBV sample was loaded onto a Sartobind D MA 15 unit (Fig. 3.5). A flow rate of 5 mL/min was used and viral particles were analyzed by qPCR. The breakthrough curve demonstrates that the dynamic binding capacity for rBVs, at these dynamic conditions and at 10 % breakthrough, is approximately 7.7×10^{10} TP/mL, or *per* membrane effective area, 8.5×10^{8} TP/cm^2; further, up to 70±5 % of the bound virus can be eluted with addition of D-PBS supplemented with 600 mM NaCl.

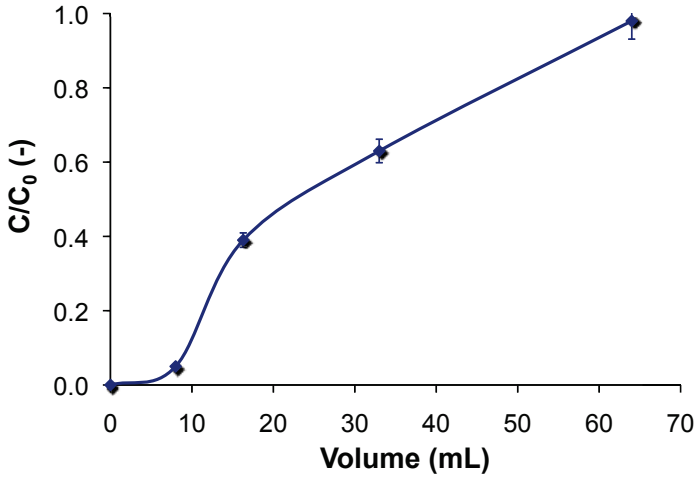

Figure 3.5: *Dynamic binding capacity study from breakthrough curve for the capture of baculovirus from concentrated and diafiltrated supernatant. The sample was loaded onto Sartobind D MA 15 at 5 mL/min. C_0 is the initial qPCR titer of rBV and C is the qPCR titer of rBV at sampling instant.*

The purified rBVs samples were also analyzed using SDS-PAGE (Fig. 3.6). The profile obtained with the membrane strategy (lane 4) is comparable to rBVs purified by sucrose gradient ultracentrifugation (lane 5) showing even higher purity; several bands disappeared in the SDS-PAGE pattern when the Sartobind D process was used.

To assess the eligibility for clinical purposes, DNA levels and endotoxin contents of purified samples were assessed. Endotoxin levels of end-product samples were below 10 EU/mL, *ie*, of sufficient purity, whereas the amount of host cell derived dsDNA was approximately 2 μg/(10^9 TP). However, this value can be significantly decreased if an additional operation specifically aimed at reducing DNA is incorporated, *eg*, by adding a nuclease incubation step or DNA precipitation (Goerke et al., 2005).

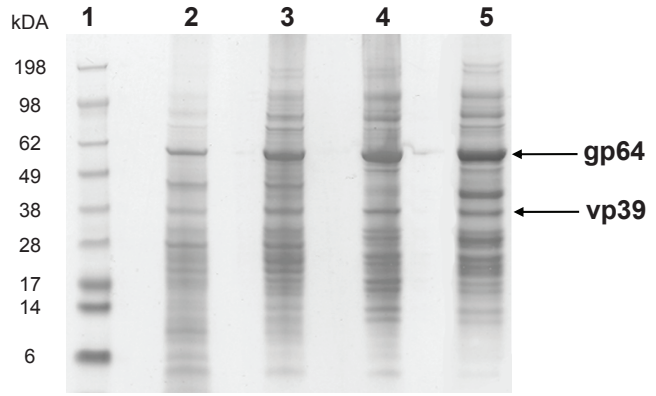

Figure 3.6: *SDS-PAGE analysis of samples obtained from rBV purification using membrane technology and by classical ultracentrifugation-based purification: (1) molecular weight markers; (2) baculoviruses clarified with depth-filters; (3) concentrated and diafiltrated sample (4) peak eluted from Sartobind D (5) rBVs purified with sucrose gradient.*

To further characterize the rBV samples obtained after purification with the membrane adsorber, DLS was used to estimate the hydrodynamic size of the particles; bovine serum albumin (BSA) and trimers of gp64 (obtained as described elsewhere (Mellado et al., 2008)) were used to serve as comparison entities (internal controls) against rBV particles coming from sucrose gradient purification and from the proposed purification strategy (Fig. 3.7A). These results show that rBVs purified using the strategy described are comparable with the size obtained from the classical sucrose gradient purified rBV sample. A two modal distribution of sizes can be observed which is most likely due to the rod-shape geometry of the rBV particles. The extended peak observed to almost 800 nm may also be an indication of some aggregation as compared to the expected size of the isolated baculovirus particle of around 300-400 nm in length. Morphological characterization was performed by transmission electron microscopy. As shown in Fig. 3.7B, the purified rBVs consist of intact, rod-shaped particles with a size roughly 70 nm $\times$ 320 nm, values slightly lower than the ones obtained with DLS (90-100 nm $\times$ 300-400 nm). However, one must recall

that the size determined by DLS is, in fact, an estimation of a hydrodynamic size, *ie*, with rBVs suspended in buffer conditions; as such, this might lead to some particle swelling as compared to the dried particle observed by transmission electron microscopy.

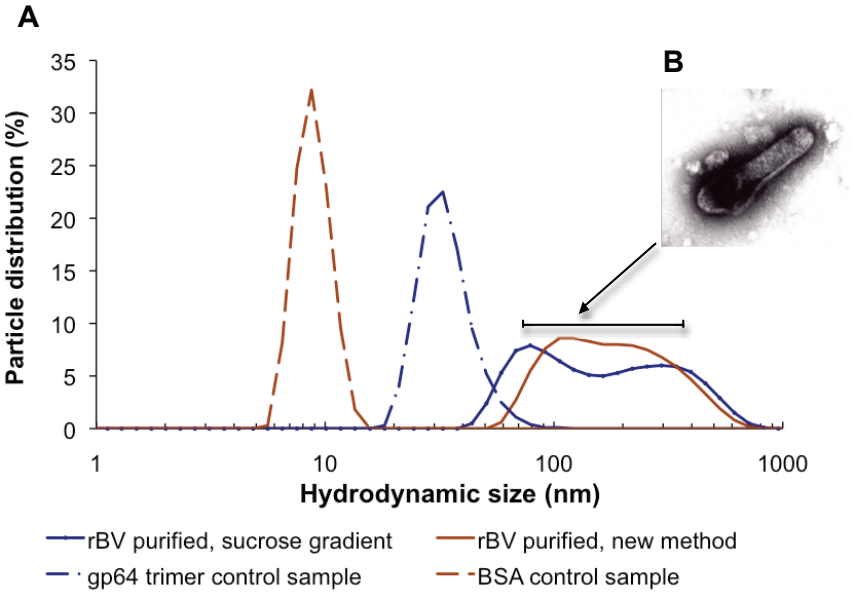

Figure 3.7: *Characterization of purified rBVs: (A) hydrodynamic size estimations by dynamic light scattering using D-PBS as dilution buffer, at 25 °C; gp64 trimer sample were obtained as a by-product of the strategy published in-house (Mellado et al., 2008). Plots are obtained from triplicate runs and subsequent application of Stokes-Einstein equation for size determination. (B) Transmission electron microscopy photograph from purified rBV sample with the proposed purification process (120 k-fold magnification).*

Upon achieving high purity with the three membrane purification steps, a desalting step was introduced after the anion-exchange membrane process, to obtain the rBVs in the desired salt concentration and pH for storage and/or clinical administration. Finally, a 0.2 μm microfiltration was performed to assure sterility of the final product; the infective rBV recovery yields were dramatically dependent on the filters used, which might have been caused by the entrapment of the rod-shaped rBVs particles in the porous membrane. Two different filters were investigated and the best recoveries, 90±10 %, were obtained for the filter manufactured with two layers (pre-filter of 0.8 μm + 0.2 μm membrane) (from Pall, East Hills, NY, USA) as opposed to filters with no pre-filter (data not shown). One can circumvent this final sterile filtration drawback by designing a fully closed aseptic process, possible in cGMP operations. However, completely closed processing has its own issues and all of the tools involved may turn the investment capital higher than regular processing.

Summing up, the indicators of the proposed integrated downstream process are pre-

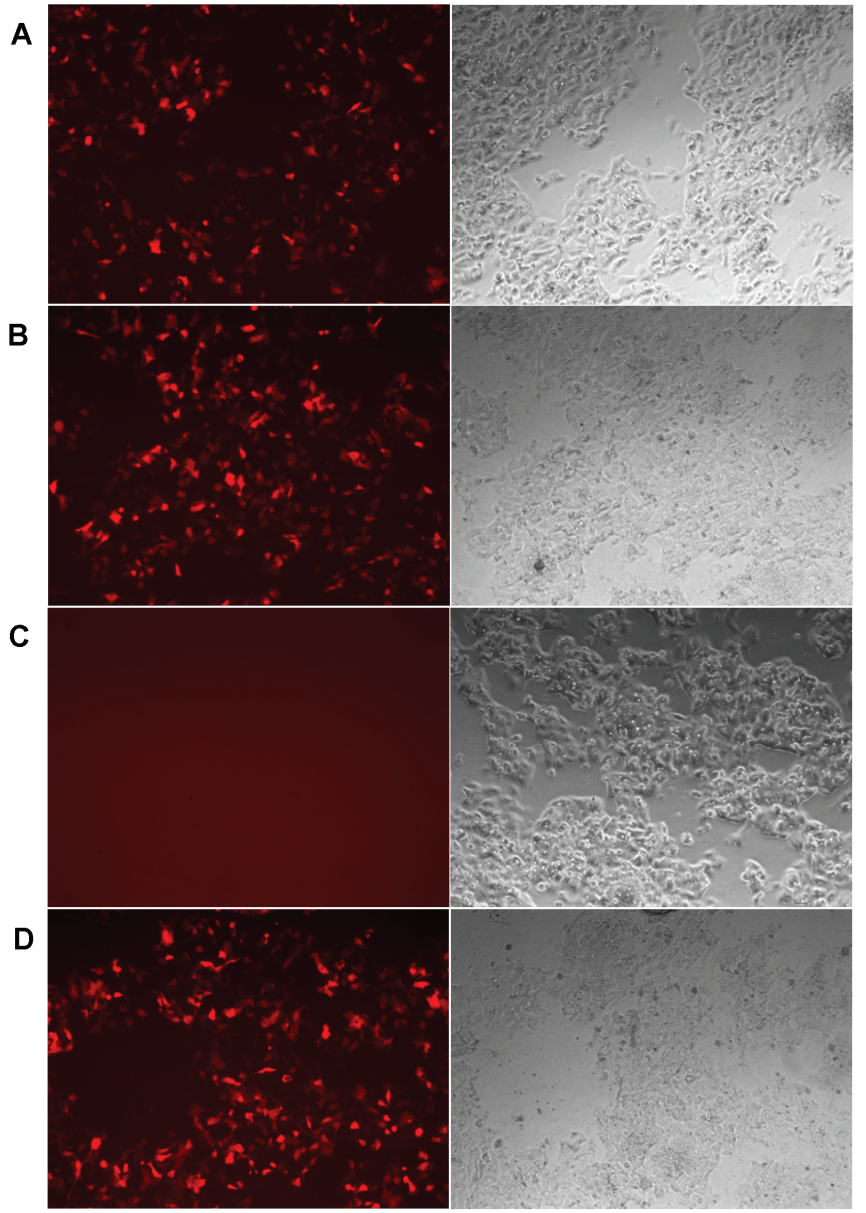

Figure 3.8: *Transduction assays carried out with rBV-cherry-dsred2 samples: HepG2-expressed DsRed2 protein signal was detected under a fluorescent microscope 24h post-transduction (left panels); phase contrast micrographs are shown on the right hand side panels; equal volumetric amount of sample was used in each assay; (A) clarified supernatant sample; (B) concentrated/diafiltrated baculovirus sample; (C) flowthrough sample from Sartobind D step; and, (D) eluted sample from Sartobind D step.*

sented in Table 3.2. A final recovery yield of 38±5 % was obtained with a final ratio between total particles and infective particles (IP) below 20. In order to confirm the gene delivery functionality of the rBVs throughout the complete downstream process, transduction assays were carried out using HepG2 as mammalian testing cells. Fig. 8 shows *in vitro* fluorescence images of targeted cells 24 hours post-transduction using a low dilution factor (see Materials and methods) to guarantee unambiguous positive (or negative) DsRed2 expression signal, *ie*, with at least 100 plaque-forming units (pfu) *per* target cell in the positive signal samples. Whereas the flowthrough fractions did not induce any positive signal, the supernatant and, especially, the concentrated samples after TFF and eluted peak from Sartobind D showed evidence of bright red fluorescence under green light excitation demonstrating that the rBVs particles are functional throughout the purification process.

Table 3.2: *Evaluation of downstream process steps for baculovirus purification using membrane technology (depth-filtration, ultra/diafiltration, and membrane chromatography).*

Process Step	TP/IP[a,c]	μg DNA / 10^9 TP	Protein (μg/10^9 TP)	Endotoxin (EU/mL)	Recovery yield of IP[b,c] (%)
Clarification	NA	1980	3983	NA	98±2
Ultrafiltration	53	823	194	NA	70±5
AEX membrane	NA	5	66	NA	65±5
Desalting	NA	NA	NA	NA	95±3
Sterile filtration / Final product	18	2	70	<10	90±10

[a]TP/IP: Ratio between total (TP) and infective (IP) rBVs is an indicator of product quality of the outlet of the specified step; [b]Based on the fraction between the total amount of infective rBVs in the outlet (used for the subsequent process step) and the total amount of infective rBVs in the feed of the specified step; [c]Total amount of rBVs (TP and/or IP) were used for these calculations, *ie*, by multiplying the specified titer by the total volumetric amount of material; NA: Not assessed.

3.4 Concluding remarks

This work describes a complete and integrated purification scheme for rBVs mostly based on disposable membrane technology. An intermediate recovery yield of 70 % was obtained using TFF and Sartobind D membrane chromatography after optimization of the critical operating parameters. An overall recovery yield of 40 % while meeting purity requirements was achieved. In conclusion, the approach devised here represents a substantial improvement for the production process of clinical grade rBVs.

Acknowledgements

Dr. Kari Airenne (University of Kuopio, Kuopio, Finland) is gratefully acknowledged for providing the recombinant baculoviruses used in this work. The authors want to thank Dr. Uwe Gottschalk (Sartorius Stedim Biotech, Göttingen, Germany) for providing the Sartobind units. The authors also wish to acknowledge Ana Alves for excellent support on analytical procedures, Marcos Sousa for expertise on the wavebag bioreaction and Dr. Catarina Brito for support on fluorescent microscopy. We acknowledge funding from the European Commission (Baculogenes, LSHB-2006-037541 and Clinigene – Network of Excellence, LSHB-2006-018933) and the Portuguese *Fundação para a Ciência e a Tecnologia* (PTDC/EQU-EQU/71645/2006 and SFRH/BD/31257/2006).

References

Airenne KJ, Hiltunen MO, Turunen MP, Turunen AM, Laitinen OH, Kulomaa MS, et al. Baculovirus-mediated periadventitial gene transfer to rabbit carotid artery. Gene Ther 2000;7:1499–504.

Altaras NE, Aunins JG, Evans RK, Kamen A, Konz JO, Wolf JJ. Production and formulation of adenovirus vectors. Adv Biochem Eng Biotechnol 2005;99:193–260.

Barsoum J. Concentration of recombinant baculovirus by cation-exchange chromatography. Biotechniques 1999;26:834–6, 838, 840.

Blissard GW, Rohrmann G. Baculovirus diversity and molecular biology. Annu Rev Entomol 1990;35:127–55.

Chuang CK, Sung LY, Hwang SM, Lo WH, Chen HC, Hu YC. Baculovirus as a new gene delivery vector for stem cell engineering and bone tissue engineering. Gene Ther 2007;14:1417–24.

Cruz PE, Peixoto CC, Devos K, Moreira JL, Saman E, Carrondo MJT. Characterization and downstream processing of hiv-1 core and virus-like-particles produced in serum free medium. Enzyme Microb Technol 2000;26:61–70.

Duffy AM, O'Doherty A M, O'Brien T, Strappe PM. Purification of adenovirus and adeno-associated virus: comparison of novel membrane-based technology to conventional techniques. Gene Ther 2005; 12:S62–72.

Duisit G, Saleun S, Douthe S, Barsoum J, Chadeuf G, Moullier P. Baculovirus vector requires electrostatic interactions including heparan sulfate for efficient gene transfer in mammalian cells. J Gene Med 1999; 1:93–102.

FDA. Center for biologics evaluation and research guidelines. 2010.

Goerke AR, To BC, Lee AL, Sagar SL, Konz JO. Development of a novel adenovirus purification process utilizing selective precipitation of cellular dna. Biotechnol Bioeng 2005;91:12–21.

Hu YC. Baculovirus vectors for gene therapy. Adv Virus Res 2006;68:287–320.

Hu YC. Baculoviral vectors for gene delivery: a review. Curr Gene Ther 2008;8:54–65.

Jorio H, Tran R, Kamen A. Stability of serum-free and purified baculovirus stocks under various storage conditions. Biotechnol Prog 2006;22:319–25.

Kaikkonen MU, Viholainen JI, Narvanen A, Yla-Herttuala S, Airenne KJ. Targeting and purification of metabolically biotinylated baculovirus. Hum Gene Ther 2008;19:589–600.

Karkkainen HR, Lesch HP, Maatta AI, Toivanen PI, Mahonen AJ, Roschier MM, et al. A 96-well format for a high-throughput baculovirus generation, fast titering and recombinant protein production in insect and mammalian cells. BMC Res Notes 2009;2:63.

King L, Possee R. The baculovirus expression vector system: a laboratory guide. Chapman and Hall, London, 1992.

Kukkonen SP, Airenne KJ, Marjomaki V, Laitinen OH, Lehtolainen P, Kankaanpaa P, et al. Baculovirus capsid display: a novel tool for transduction imaging. Mol Ther 2003;8:853–62.

Lajmi AR, Kutner R, Reiser J. A membrane chromatography application: a rapid, high capacity gene therapy vector purification tool, vol. 31. Taylor and Francis, NW, 2007.

Lo HR, Chao YC. Rapid titer determination of baculovirus by quantitative real-time polymerase chain reaction. Biotechnol Prog 2004;20:354–60.

Mellado MC, Peixoto C, Cruz PE, Carrondo MJ, Alves PM. Purification of recombinant rotavirus vp7 glycoprotein for the study of in vitro rotavirus-like particles assembly. J Chromatogr B Analyt Technol Biomed Life Sci 2008;874:89–94.

Michalsky R, Pfromm PH, Czermak P, Sorensen CM, Passarelli AL. Effects of temperature and shear force on infectivity of the baculovirus autographa californica m nucleopolyhedrovirus. J Virol Methods 2008; 153:90–96.

O'Reilly D, Miller L, Verne A. Baculovirus Expression Vectors: A Laboratory Manual. Freeman, New York, 1994.

Palomares LA, Estrada-Mondaca S, Ramírez O. Principles and Applications of the Insect Cell-Baculovirus Expression Vector System. Taylor and Francis, New York, 2006.

Rasmussen R, Morrison T, Herrmann M, Wittwer C. Quantitative pcr by continuos fluorescence monitoring of a double strand dna specific binding dye. Biochemica 1998;No.2:8–11.

Rodrigues T, Carrondo MJT, Alves PM, Cruz PE. Purification of retroviral vectors for clinical application: Biological implications and technological challenges. J Biotechnol 2007;127:520–541.

Roush DJ, Lu Y. Advances in primary recovery: centrifugation and membrane technology. Biotechnol Prog 2008;24:488–95.

Tani H, Abe T, Matsunaga TM, Moriishi K, Matsuura Y. Baculovirus vector for gene delivery and vaccine development. Future Virol 2008;3:35–43.

Transfiguracion J, Jorio H, Meghrous J, Jacob D, Kamen A. High yield purification of functional baculovirus vectors by size exclusion chromatography. J Virol Methods 2007;142:21–8.

Vieira HLA, Estevao C, Roldao A, Peixoto CC, Sousa MFQ, Cruz PE, et al. Triple layered rotavirus vlp production: Kinetics of vector replication, mrna stability and recombinant protein production. J Biotechnol 2005;120:72–82.

Wu C, Soh KY, Wang S. Ion-exchange membrane chromatography method for rapid and efficient purification of recombinant baculovirus and baculovirus gp64 protein. Hum Gene Ther 2007;18:665–72.

Chapter 4

ESTABLISHING A NOVEL SCALED-DOWN CHROMATOGRAPHIC TOOL BASED ON SURFACE PLASMON RESONANCE FOR BINDING AND ELUTION ANALYSIS

Adapted from:

Vicente T, Mota JPB, Peixoto C, Alves PM, Carrondo MJT. Modeling protein binding and elution over a chromatographic surface probed by surface plasmon resonance. J Chromatogr A 2010; 1217:2032–2041.

Abstract

Surface plasmon resonance (SPR) spectroscopy is used as a scaled-down, analytical, pseudo-chromatography tool for analyzing protein binding and elution over an ion-exchange surface under cyclic sorption conditions. A micrometric-scale adsorption surface was produced by immobilizing a typical ion exchange ligand—diethylaminoethyl (DEAE)—onto commercially-available planar gold sensor chip surfaces pre-derivatized with a self-assembled monolayer of 11-mercaptoundecanoic acid with known density. An explicit mathematical formulation is provided for the deconvolution and interpretation of the SPR sensorgrams. An adsorption rate model is proposed to describe the SPR sensorgrams for bovine serum albumin, used here as model protein, when the DEAE surface is subjected to a cyclic series of binding and elution steps. Overall, we demonstrate that the adsorption rate model is capable of quantitatively describing BSA binding and elution for protein titers from dilute conditions up to overloaded conditions and a broad range of salt concentrations.

Contents

4.1 Introduction

Process design and optimization are critical tasks in any pharmaceutical industrial process; the time and resources allotted for R&D tasks are relevant issues (Davies et al., 2005; Pampel et al., 2008). This becomes particularly crucial within the scope of biopharmaceuticals for gene therapy or vaccination, comprising complex structures, such as monoclonal antibodies, virus-like particles, or viruses. Indeed, these products commonly derive from highly costly animal cell-based upstream productions. Hence, the optimization of such processes becomes mandatory in the interest of cost and time savings. Scaled-down models, often used in high-throughput technologies, are being considered as viable options for early stage process development (Coffman et al., 2008; Rege et al., 2006; Wensel et al., 2008), including downstream processing steps such as ion-exchange chromatography, which is one of the core purification steps for biopharmaceuticals (Vicente et al., 2008; Rodrigues et al., 2006; Specht et al., 2004; Yamada et al., 2003; Zydney et al., 2008; Trilisky and Lenhoff, 2007; Kaludov et al., 2002; Vicente et al., 2009). High-throughput robotics operating with multi-micro-sized matrices are able to generate a considerable amount of data covering the n-dimensional design space for the selected n-critical process variables (Kelley et al., 2008).

By using these high-throughput methodologies, the bottleneck seems now to be moving towards data processing and subsequent integration. This drawback opens up the need for a more focused scaled-down rationale, capable of ultimately yielding better and more selective data for facilitating further optimization choices. In the context of multicomponent adsorption processes, including ion-exchange chromatography, the understanding of how the different contaminants interact with the stationary phase provides clues and guidelines for finding the best strategy for process design and optimization.

Surface plasmon resonance (SPR) is a spectroscopic technique with a wide variety of applications (established over the last couple of decades) whenever an interaction between two entities is involved — a ligand, immobilized on a surface, and an analyte, flowing over that surface (Hoa et al., 2007; Pattnaik, 2005; Rich and Myszka, 2008). Moreover, SPR permits simpler and faster label-free, real-time interaction analyzes between those two entities than other analytical technologies (Myszka et al., 1998). By producing interaction data using highly reduced amounts of material in each run, SPR can play a significant role in the design of adsorption processes, including ion-exchange chromatography. Such analytical technology may be used as a cost-effective aid for the early stage systematic screenings of stationary phases, buffer conditions, and chromatographic steps.

An SPR sensor mainly consists of a surface support with a metal (typically gold) and a film of fluid flowing over the surface, thus allowing for possible interactions between the gold surface and the liquid. Commercially available SPR-based sensors can be extremely sensitive; in fact, they can detect, within a fraction of a second, very small refractive index (RI) changes within the film delimited in the depth of the sensing evanescent electromagnetic field (Jung et al., 1998). When such a sensor is functionalized with selective ligands for any given molecule (either chemical or biochemical), then selective (bio)chemical sensors can be custom-made. A straightforward and self-controlled means to prepare a functionalized sensor surface from an untreated gold one is to use self-assembled monolayers (SAMs) using thiolate compounds (Mrksich and Whitesides, 1996). SAMs — particularly those formed by adsorption of long chain alkanethiols over gold surfaces — are especially suited for studying interactions between post-functionalized surfaces and proteins or other particles (Mrksich and Whitesides, 1996). These compounds self-generate well defined, synthetic surfaces with known molecular and macroscopic properties, thus allowing for consistent fundamental studies. This is particularly relevant if a SAM is used as a linker to a layer of covalently coupled functional groups (at known stoichiometry) (Whitesides et al., 2005). 11-mercaptoundecanoic acid (MUA) has been utilized in different applications for the cova-

lent immobilization of ligands with complex structures, such as viruses (Roper and Nakra, 2006; Kim et al., 2006).

The quantitative interpretation and modeling of SPR rendered data, including cases where different SAM layers are used, has been addressed in the literature (Myszka et al., 1998; Jung et al., 1998). However, a detailed analysis for a sensor chip surface functionalized with a layer of ion-exchange ligands, mimicking the undergoing mechanisms of adsorption equilibrium and kinetics on a typical adsorbent surface, is still unavailable.

In the present work SPR spectroscopy is used as a scaled-down, analytical tool for analyzing protein binding and elution over an ion-exchange surface under cyclic adsorption conditions. We review the principles of SPR spectroscopy and establish the required calibration procedures and analytical formulae for converting the SPR signal shift into surface concentration of adsorbed protein. We propose two different adsorption rate models that qualitatively describe the general trends observed in the SPR sensorgrams for bovine serum albumin (BSA) — used here as model protein — when the DEAE surface is subjected to a cyclic series of binding and elution steps. By carefully analyzing the adsorption/desorption plateaus we show that it is possible to exclude one of the kinetic models. Furthermore, by performing SPR experiments at different salt concentrations, the dependency of binding capacity and rate constants on salt concentration can be established. Overall, we demonstrate that the resulting adsorption rate model quantitatively describes the SPR sensorgrams for protein titers from dilute conditions up to overloaded conditions and a broad range of salt concentrations.

4.2 Materials and methods

4.2.1 Sensor surface preparation

Biacore gold sensor chip surfaces (Biacore/GE Healthcare, Uppsala, Sweden) were modified according to protocols described in the literature (Mrksich and Whitesides, 1996; Roper and Nakra, 2006), but with some adjustments. 11-mercaptoundecanoid acid (MUA) (NanoThinks^{TM} ACID11 solution from Sigma-Aldrich, München, Germany) and 2-diethylaminoethylamine (DEAEA) (99% purity grade from Sigma-Aldrich) were used as thiolate for SAM preparation and ligand coupling compound, respectively. A Leica AR200 digital handheld refractometer (Leica Microsystems, Wetzlar, Germany) was used to monitor the RI changes throughout the MUA-SAM immobilization procedure.

The gold sensor chip surface was first equilibrated with ultra-pure, deionized water, at

18.2 MΩ·cm. The surface was sanitized with 0.1 M NaOH and 1% Triton^{TM} X-100 (Sigma-Aldrich) and then re-equilibrated in 10 mM 4-Morpholineethanesulfonic acid (MES) buffer (Sigma-Aldrich) at pH 5.0. Ethanol was then used to washout the buffer and the surface was exposed directly to the ACID11 solution (5 mM MUA in ethanol) and left overnight in a closed compartment inside a laminar flow bench. The freshly formed SAM of MUA was rinsed with ethanol and re-equilibrated with the 10 mM MES buffer previously used until the RI stabilized. The sensor chip was then docked into the SPR system — a Biacore^{TM} 2000 (Biacore/GE Healthcare) — for DEAEA immobilization by amide coupling chemistry. The same MES solution was used as running buffer for the duration of the immobilization procedure.

Freshly prepared solutions of 0.4 M 1-ethyl-3-(3-dimethylamino-propyl)carbodiimide hydrochloride (EDC) and 1.0 M N-hydroxysuccinimide (NHS) (amine coupling kit from Biacore/GE Healthcare) in water were mixed 1:1 and injected in a pulse of 200 μL at 20 μL/min to activate the terminal carboxyl group for amide bond formation. 1.0 M DEAEA in MES running buffer was added in serial 100 μL pulses at 20 μL/min until the SPR signal stabilized. Although there are four flow sensing cells available in the Biacore sensor chip, only one flow cell was derivatized with DEAEA to allow the comparison of SPR adsorption data from MUA against MUA-DEAE. All buffers and solutions were prepared sterile and degassed prior to use.

4.2.2 SPR experiments

The SPR experiments were performed on a Biacore 2000 system at 25°C. Analytical grade (> 98% electrophoresis purity) BSA was purchased from Merck KGaA (Darmstadt, Germany). It is well known that commercial BSA samples contain a substantial fraction (5–20%) of covalent dimmer; the actual amount in our freshly prepared BSA solutions is estimated to be ca. 6%, from analytical size-exclusion chromatography on a Superdex 200 column. This residual fraction is believed to have only a minor influence on the experimental results. This assumption is supported by the closeness between our estimate of the thickness of the adsorbed monolayer, obtained from calibration experiments at a high salt concentration (see discussion below), and the BSA diameter calculated from its molecular weight and mass density; these two lengths are much smaller than the diameter of the covalent dimmer. All buffers were prepared sterile and degassed prior to use in the equipment.

The experiments were performed at constant flow rate of running buffer and sample

injection of 100 μL/min. Each run consisted of the following sequence of steps repeated over three or four cycles: (i) equilibration of the flow cell with running buffer at a prescribed NaCl concentration (c_0); (ii) injection of 100 μL of BSA solution at given concentration (c_0, c_B); and (iii) desorption and equilibration with running buffer (again, at c_0). Before starting a new run, the flow cell was subjected to an aggressive desorption step using 100 μL of 1.5 M NaCl in 20 mM phosphate buffer at pH 6.8 ($c_{0,\mathrm{ref}}$), and then cleaned/sanitized with 100 μL of 0.1 M NaOH for complete regeneration of the surface.

DEAE ligands and SAM's have been shown to be fully resistant to pulses of NaOH (or HCl) up to 1 M (Knoll et al., 1998). The baseline stability was controlled throughout the course of each experiment. All sensorgrams were duplicated by repeating each run once for confirmation of their reproducibility and surface regeneration.

4.3 Supporting theory for SPR data analysis

In order to quantitatively analyze SPR data under adsorption conditions one must first understand the underlying probing mechanism of the Biacore machine — the medium's RI within the sensing evanescent field depth. The RI of an aqueous salt solution (0) with concentration c_0 is

$$\eta_0 = \tilde{\eta}_\mathrm{w} + (\tilde{\eta}_0 - \tilde{\eta}_\mathrm{w})\nu_0 c_0, \tag{4.1}$$

where c_0 (M) is the salt concentration, ν_0 is the molar volume of the salt ions (M^{-1}), $\tilde{\eta}_\mathrm{w}$ is the RI of water, and $\tilde{\eta}_0$ is the RI of the salt ions. Similarly, the RI of the aqueous salt solution with a given dissolved solute (B) (this can take the form of any analyte, e.g., a protein), can be expressed as

$$\eta_\mathrm{B} = \eta_0 + (\tilde{\eta}_\mathrm{B} - \eta_0)v_\mathrm{B} c_\mathrm{B}, \tag{4.2}$$

where c_B (M), v_B (M^{-1}) and $\tilde{\eta}_\mathrm{B}$ are the concentration, specific volume, and RI of the dissolved solute, respectively.

The Biacore's signal, $R(\eta)$, expressed in resonance units (RU), is a function of the measured RI in the flow cell, η; if η does not vary greatly (i.e., if the shift $\Delta\eta$ is not very large), then the corresponding change in the Biacore signal, ΔR, will be proportional to the change in η, that is, $\Delta R = m\Delta\eta$ (Jung et al., 1998). It is also known that η is not probed uniformly over the depth of the flow cell height, but proportionally to the intensity of light at each point. Thus, the effective RI measured by the Biacore system, η_eff, is the

average of η over the depth of the evanescent electromagnetic field (Jung et al., 1998):

$$\eta_{\text{eff}} = \frac{1}{d_{\text{p}}} \int_0^\infty \eta(z) e^{-z/d_{\text{p}}} \, \mathrm{d}z, \tag{4.3}$$

where d_{p} is the effective penetration depth; for the case of the Biacore 2000 machine, $d_{\text{p}} \approx 150$ nm.

Let us first consider the case of a uniform adsorbent film of thickness d_{s}, attached to the metal sensor surface, under conditions where there is no adsorption from the fluid solution flowing over its surface (this is the case, e.g., when the salt concentration is large enough to suppress solute binding). The RI of this adsorbent film, η_{s}, is constant unless there are external perturbations, such as a temperature change in the flow cell, which is not the case in the present work. Assuming that η_{s} is constant, Eq. 4.3 can be rewritten as follows:

$$\begin{aligned} \eta_{\text{eff}} &= \frac{\eta_{\text{s}}}{d_{\text{p}}} \int_0^{d_{\text{s}}} e^{-z/d_{\text{p}}} \, \mathrm{d}z + \frac{1}{d_{\text{p}}} \int_{d_{\text{s}}}^\infty \eta(z) e^{-z/d_{\text{p}}} \, \mathrm{d}z \\ &= \eta_{\text{s}}(1 - e^{-d_{\text{s}}/d_{\text{p}}}) + \frac{1}{d_{\text{p}}} \int_{d_{\text{s}}}^\infty \eta(z) e^{-z/d_{\text{p}}} \, \mathrm{d}z \\ &= \eta_{\text{s}}(1 - \phi_{\text{s}}) + \eta'_{\text{eff}}, \end{aligned} \tag{4.4}$$

where $\phi_{\text{s}} = \exp(-d_{\text{s}}/d_{\text{p}})$. In the absence of adsorption, $\eta(z) = \eta$ for $z > d_{\text{s}}$, where η is the bulk solution's RI, and $\eta'_{\text{eff}} = \eta\phi_{\text{s}}$. Therefore, under non-adsorbing conditions, η_{eff} is given by

$$\eta_{\text{eff}} = \eta_{\text{s}} + \phi_{\text{s}}(\eta - \eta_{\text{s}}). \tag{4.5}$$

When the salt solution has no dissolved solute ($c_0 > 0$, $c_{\text{B}} = 0$), the effective RI, $\eta_{0,\text{eff}}$, is given by Eq. 4.5 with η replaced by η_0 defined by Eq. 4.1; the result is

$$\eta_{0,\text{eff}} = \eta_{\text{s}} + \phi_{\text{s}}[(\tilde{\eta}_0 - \tilde{\eta}_{\text{w}})\nu_0 c_0 + \tilde{\eta}_{\text{w}} - \eta_{\text{s}}]. \tag{4.6}$$

If the baseline (or reference) signal is established for a salt solution with concentration $c_{0,\text{ref}}$, then the change in the effective RI when the salt concentration is altered to c_0 is

$$(\eta_0 - \eta_{0,\text{ref}})_{\text{eff}} = \phi_{\text{s}}(\tilde{\eta}_0 - \tilde{\eta}_{\text{w}})\nu_0(c_0 - c_{0,\text{ref}}). \tag{4.7}$$

The corresponding signal shift in the Biacore system is

$$\Delta R = m(\eta_0 - \eta_{0,\text{ref}})_{\text{eff}} = m_0(c_0 - c_{0,\text{ref}}), \tag{4.8}$$

where $m_0 = m\phi_s(\tilde{\eta}_0 - \tilde{\eta}_w)\nu_0$ is the slope of the linear fitting (with intercept set to zero) of ΔR against $(c_0 - c_{0,\mathrm{ref}})$.

When solute is added to the reference salt solution ($c_0 = c_{0,\mathrm{ref}}$, $c_B > 0$) and flown over the sensing surface under non-adsorbing conditions, the effective RI is given by

$$(\eta_{B,\mathrm{ref}})_{\mathrm{eff}} = \eta_s + \phi_s(\eta_{B,\mathrm{ref}} - \eta_s), \tag{4.9}$$

where $\eta_{B,\mathrm{ref}}$ is defined by Eq. 4.2 with $\eta_0 = \eta_{0,\mathrm{ref}}$. The corresponding change in the RI is obtained as follows:

$$\begin{aligned}(\eta_{B,\mathrm{ref}} - \eta_{0,\mathrm{ref}})_{\mathrm{eff}} &= \phi_s(\tilde{\eta}_B - \eta_{0,\mathrm{ref}})v_B c_B \\ &= \phi_s[(\tilde{\eta}_B - \tilde{\eta}_w) - (\tilde{\eta}_0 - \tilde{\eta}_w)\nu_0 c_{0,\mathrm{ref}}]v_B c_B \end{aligned} \tag{4.10}$$

and the shift of the Biacore signal is given by

$$\Delta R = m(\eta_{B,\mathrm{ref}} - \eta_{0,\mathrm{ref}})_{\mathrm{eff}} = (m_B - m_0 v_B c_{0,\mathrm{ref}})c_B \tag{4.11}$$

where $m_B = m\phi_s(\tilde{\eta}_B - \tilde{\eta}_w)v_B$. Note that $m_B - m_0 v_B c_{0,\mathrm{ref}}$ is the slope of a linear fitting (with intercept set to zero) of ΔR vs. c_B. Once m_0 and m_B are known, we can predict the shift in the Biacore signal due to the change in the effective RI, $(\eta_B - \eta_{0,\mathrm{ref}})_{\mathrm{eff}}$, of an aqueous buffer with salt concentration c_0 and solute concentration c_B (assuming that the baseline was defined for the buffer salt solution with concentration $c_{0,\mathrm{ref}}$) using the expression

$$\Delta R = (m_B - m_0 c_0 v_B)c_B + m_0(c_0 - c_{0,\mathrm{ref}}). \tag{4.12}$$

The more complex case where there is solute adsorption onto the adsorbent sensor surface film is depicted in Fig. 4.1. The aqueous buffer solution in the bulk has salt concentration c_0 and protein concentration c_B; the thickness of the adsorbed layer is d_m and its inter-solute volume is filled with buffer solution assumed to contain the same salt concentration as that of the bulk. In Fig. 4.1, d_m is assumed to be equal to the diameter of the adsorbed solute molecules, in accordance with the formulation of a single adsorbed monolayer, though this is not a restriction imposed in our formulation. The effective RI probed by the Biacore machine, $\eta_{m,\mathrm{eff}}$, is

$$\eta_{m,\mathrm{eff}} = \frac{\eta_s}{d_p}\int_0^{d_s} e^{-z/d_p}\,\mathrm{d}z + \frac{\eta_m}{d_p}\int_{d_s}^{d_s+d_m} e^{-z/d_p}\,\mathrm{d}z + \frac{\eta_B}{d_p}\int_{d_s+d_m}^{\infty} e^{-z/d_p}\,\mathrm{d}z, \tag{4.13}$$

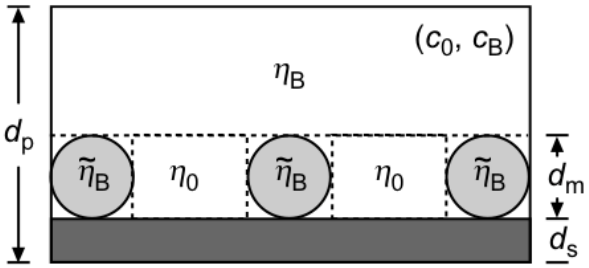

Figure 4.1: *Schematic of solute monolayer adsorbed onto the film of thickness d_s in the Biacore sensor chip flow cell. The bulk aqueous concentration has salt concentration c_0 and solute concentration c_B; the isolated (dry) solute's RI is $\tilde{\eta}_B$; aqueous solution is assumed to fill the gaps between adsorbed solute molecules, with salt concentration c_0 and RI η_0; the thickness of the adsorbed monolayer, d_m, is roughly equal to the diameter of the adsorbed solute.*

yielding

$$\eta_{m,eff} = \eta_s + \phi_s(\eta_m - \eta_s) + \phi_s\phi_m(\eta_B - \eta_m), \tag{4.14}$$

where $\phi_m = \exp(-d_m/d_p)$. Here, η_m and η_B are the RI's of the adsorbed monolayer and of the bulk aqueous solution (c_0, c_B), respectively.

Considering the adsorption model shown in Fig. 4.1, and assuming that the solute, when adsorbed, does not change neither its RI nor its specific (or molar) volume, then the adsorbed monolayer's RI is

$$\eta_m = \eta_0 + (\tilde{\eta}_B - \eta_0)v_B c_m, \tag{4.15}$$

where c_m (M) is the solute concentration in the volume occupied by the adsorbed monolayer; c_m can be converted into a surface concentration, q (g/dm^2), through the simple formula $q = d_m c_m$. If the baseline's RI is $(\eta_{0,ref})_{eff}$ (obtained with a salt solution of concentration $c_{0,ref}$), then the change in the effective RI probed by the Biacore machine will be

$$(\eta_m - \eta_{0,ref})_{eff} = \phi_s(\eta_m - \eta_{0,ref}) + \phi_s\phi_m(\eta_B - \eta_m). \tag{4.16}$$

Expanding the two right-hand side differences yields

$$(\eta_m - \eta_{0,ref})_{eff} = \phi_s(\tilde{\eta}_B - \eta_0)v_B[c_m + \phi_m(c_B - c_m)] + \phi_s(\eta_0 - \eta_{0,ref}). \tag{4.17}$$

The corresponding shift in the Biacore signal is

$$\Delta R = (m_B - m_0 c_0 v_B)[c_m + \phi_m(c_B - c_m)] + m_0(c_0 - c_{0,ref}). \tag{4.18}$$

Solving for c_{m} gives

$$c_{\mathrm{m}} = \frac{\Delta R - m_0(c_0 - c_{0,\mathrm{ref}})}{(1-\phi_{\mathrm{m}})(m_{\mathrm{B}} - m_0 c_0 v_{\mathrm{B}})} - \frac{\phi_{\mathrm{m}}}{1-\phi_{\mathrm{m}}} c_{\mathrm{B}}. \tag{4.19}$$

Equations 4.18 and 4.19 are the most general ones since they encompass all the cases discussed above. For example, setting $\phi_{\mathrm{m}} = 1$ (i.e., $d_{\mathrm{m}} = 0$) eliminates the adsorbed monolayer; setting $c_{\mathrm{m}} = c_{\mathrm{B}}$ sets the solute concentration in the adsorbed monolayer equal to that in the bulk solution and the two phases become optically indistinguishable. In both cases, Eq. 4.18 correctly reduces to Eq. 4.12.

Equation 4.11 shows that m_{B} can be determined from the slope b of the linear fitting (with intercept equal to zero) of ΔR against c_{B}, as $m_{\mathrm{B}} = b + m_0 v_{\mathrm{B}} c_{0,\mathrm{ref}}$. These calibration experiments, however, must be carried out under conditions where the solute does not adsorb; this may be difficult to achieve in practice. When the buffer conditions are such that a large fraction of the surface is shielded against adsorption, the adsorbed phase will quickly reach saturation conditions, that is, c_{m} will attain a constant value for moderate values of c_{B}. Equation 4.18 shows that, in this case, a plot of ΔR against c_{B} still exhibits a linear relationship for sufficiently large values of c_{B} (i.e., those values of c_{B} for which $c_{\mathrm{m}} \approx$ const.), but with slope equal to $\phi_{\mathrm{m}}(m_{\mathrm{B}} - m_0 v_{\mathrm{B}} c_{0,\mathrm{ref}})$ and intercept equal to $(1-\phi_{\mathrm{m}})(m_{\mathrm{B}} - m_0 v_{\mathrm{B}} c_{0,\mathrm{ref}}) c_{\mathrm{m}}$. Under these conditions, an estimate of ϕ_{m}, and of the resulting d_{m}, can be obtained by noticing that the slope of $(\eta_0 - \eta_{0,\mathrm{ref}})_{\mathrm{eff}}$ against $(c_0 - c_{0,\mathrm{ref}})$ yields $\phi_{\mathrm{s}}(\tilde{\eta}_0 - \tilde{\eta}_{\mathrm{w}})\nu_0 = m_0/m$ (cf. Eqs. 4.7 and 4.8) and that the slope of $(\eta_{\mathrm{B}} - \eta_{0,\mathrm{ref}})_{\mathrm{eff}}$ against c_{B} gives $\phi_{\mathrm{s}}(\tilde{\eta}_{\mathrm{B}} - \eta_{0,\mathrm{ref}})v_{\mathrm{B}} = [\phi_{\mathrm{m}}(m_{\mathrm{B}} - m_0 v_{\mathrm{B}} c_{0,\mathrm{ref}})]/m$ (cf. Eqs. 4.10 and 4.11); such measurements can be performed with a refractometer.

4.4 Adsorption/desorption rate model

In this section we formulate a general adsorption/desorption rate model capable of quantitatively explaining the SPR sensorgrams for the interaction of BSA with the DEAE-SAM surface under continuous cycling of the solute concentration. As described in §4.2.2, each SPR experiment consisted of a series of adsorption/desorption cycles, where during the adsorption step the sensor chip was contacted with buffer solution with given salt and protein concentrations; after binding, buffer alone was introduced to monitor the desorption kinetics. This sequence was repeated over three or four cycles. We observed partial irreversible binding of the protein onto the DEAE-SAM surface (or subject to a very slow dissociation kinetics which was imperceptible for the duration of the desorption step) and

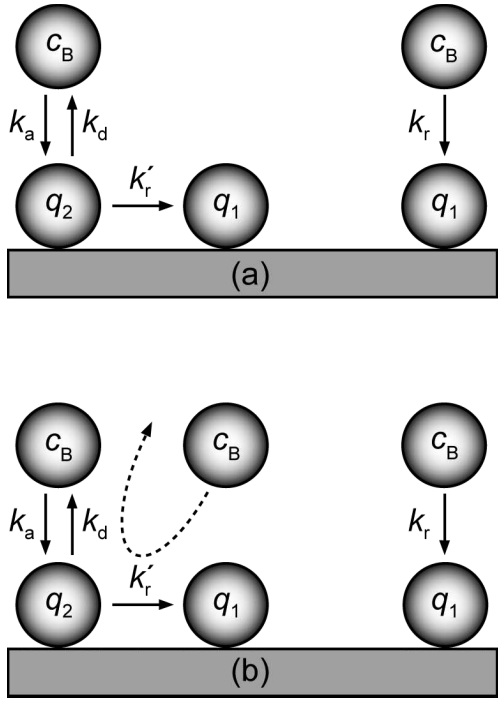

Figure 4.2: *Kinetic model for reversible/irreversible protein adsorption.*

a slight increase of the binding plateau from cycle to cycle, but tending to a constant, asymptotical value.

Based on these observations, it is assumed that only part of the protein is reversibly adsorbed, whereas the other part binds irreversibly to the stationary phase. Moreover, we consider that the irreversible adsorption process is the result of two binding mechanisms operating in parallel: one in which irreversible adsorption takes place from the reversibly adsorbed phase, and another in which irreversible adsorption takes place directly from the liquid phase. Two possible types of irreversible binding mechanisms are considered: in mechanism A, irreversible adsorption from the reversibly adsorbed phase is an autonomous process that is independent of the protein concentration in the liquid phase; in mechanism B, irreversible adsorption from the reversibly adsorbed phase depends on the frequency of collisions or interactions between the proteins in the reversibly adsorbed phase and those contacting liquid solution. The two mechanisms are illustrated in Fig. 4.2.

Let q_1 be the concentration of irreversibly bound protein and q_2 the protein concentration in the reversibly adsorbed phase. For mechanism A, the irreversible binding kinetics can be written as

$$\frac{dq_1}{dt} = k_{\mathrm{r}} c_{\mathrm{B}} (\tilde{q}_1^{\infty} - q_1) + k_{\mathrm{r}}' q_2, \tag{4.20}$$

where k_r is the rate constant for irreversible adsorption from the bulk, k'_r is the rate constant for irreversible binding from the reversibly adsorbed phase and $\tilde{q}_1^\infty$ is the apparent capacity of the stationary phase for irreversible binding; this capacity is apparent because some of the sites for irreversible binding may be shielded by the presence of reversibly adsorbed proteins. Hence,

$$\tilde{q}_1^\infty = q_1^\infty - \sigma_{12} q_2, \tag{4.21}$$

where σ_{12} is a steric factor: it gives the number of irreversible binding sites shielded by the reversibly adsorbed proteins. For mechanism B, the corresponding equation is

$$\frac{dq_1}{dt} = k_\mathrm{r} c_\mathrm{B} (\tilde{q}_1^\infty - q_1) + k'_\mathrm{r} c_\mathrm{B} q_2. \tag{4.22}$$

The difference between mechanisms A and B is that for the former the rate of irreversible adsorption from the reversibly adsorbed phase is proportional to q_2 whereas for the latter it is proportional to $c_\mathrm{B} q_2$ (cf. Fig. 4.2).

Assuming a Langmuirian kinetic model for reversible adsorption, we can write for mechanism A

$$\frac{dq_2}{dt} = k_\mathrm{a} c_\mathrm{B} (\tilde{q}_2^\infty - q_2) - (k_\mathrm{d} + k'_\mathrm{r}) q_2, \tag{4.23}$$

where k_a and k_d are the forward and reverse rate constants for reversible adsorption, respectively, and $\tilde{q}_2^\infty$ is the apparent capacity of the stationary phase for reversible binding. Again, the adsorption capacity is apparent because some of the sites for reversible binding may be shielded by the presence of irreversibly adsorbed proteins:

$$\tilde{q}_2^\infty = q_2^\infty - \sigma_{21} q_1. \tag{4.24}$$

For mechanism B the kinetic model is

$$\begin{aligned} \frac{dq_2}{dt} &= k_\mathrm{a} c_\mathrm{B} (\tilde{q}_2^\infty - q_2) - k_\mathrm{d} q_2 - k'_\mathrm{r} c_\mathrm{B} q_2 \\ &= k_\mathrm{a} c_\mathrm{B} (\tilde{q}_2^\infty - q_2) - (k_\mathrm{d} + k'_\mathrm{r} c_\mathrm{B}) q_2. \end{aligned} \tag{4.25}$$

At equilibrium (which we denote by an overbar):

$$\left(\overline{\frac{dq_1}{dt}} \right) = \left(\overline{\frac{dq_2}{dt}} \right) = 0, \tag{4.26}$$

which allows us to determine closed-form expressions for the adsorption isotherms, $\overline{q}_1(c_\mathrm{B})$

and $\overline{q}_2(c_\mathrm{B})$.

One way to discriminate between the two types of irreversible binding mechanisms is to compare the dependencies between $\overline{q}_1$ and $\overline{q}_2$ given by Eqs. 4.20 and 4.22. For mechanism A, we get

$$\overline{q}_1 = q_1^\infty + \left(\frac{k_\mathrm{r}'}{k_\mathrm{r}} - \sigma_{12} c_\mathrm{B}\right) \frac{\overline{q}_2}{c_\mathrm{B}}, \tag{4.27}$$

whereas for mechanism B the expression is

$$\overline{q}_1 = q_1^\infty + \left(\frac{k_\mathrm{r}'}{k_\mathrm{r}} - \sigma_{12}\right) \overline{q}_2. \tag{4.28}$$

Clearly, for mechanism B, $\overline{q}_1$ varies linearly with $\overline{q}_2$ with an ordinate and a slope that are independent of c_B.

Let us assume temporarily that the shielding effect can be neglected. In this case, Eqs. 4.27 and 4.28 simplify to

$$\overline{q}_1 = q_1^\infty + \left(\frac{k_\mathrm{r}'}{k_\mathrm{r}}\right) \frac{\overline{q}_2}{c_\mathrm{B}} \quad \text{(mechanism A)} \tag{4.29}$$

$$\overline{q}_1 = q_1^\infty + \left(\frac{k_\mathrm{r}'}{k_\mathrm{r}}\right) \overline{q}_2 \quad \text{(mechanism B)}. \tag{4.30}$$

Thus for mechanism A, $\overline{q}_1$ varies linearly with $\overline{q}_2/c_\mathrm{B}$, whereas for mechanism B, $\overline{q}_1$ varies linearly with $\overline{q}_2$; in both cases the ordinate and slope are positive.

The saturation capacities, q_1^∞ and q_2^∞, and hence the total saturation capacity $q^\infty = q_1^\infty + q_2^\infty$, are expected to be modulated by the salt concentration, as is the case for a typical ion-exchange matrix. The higher the counterion concentration, the lower the binding of a given solute assuming that no other effects are impacting the overall adsorption process onto the SPR sensor chip. Thus, an empirical correlation of the form

$$q^\infty = q_0^\infty e^{k c_0} \quad \text{or} \quad q^\infty = q_0^\infty c_0^k \tag{4.31}$$

is adopted here; in Eq. 4.31, q_0^∞ is the maximum attainable adsorption capacity at residual ionic strength and $k < -1$ is an empirical constant. The second expression for q^∞ in Eq. 4.31 is similar to the mathematical formulation used in the steric mass action formalism for the interpretation of adsorption by ion exchange (Brooks and Cramer, 1992).

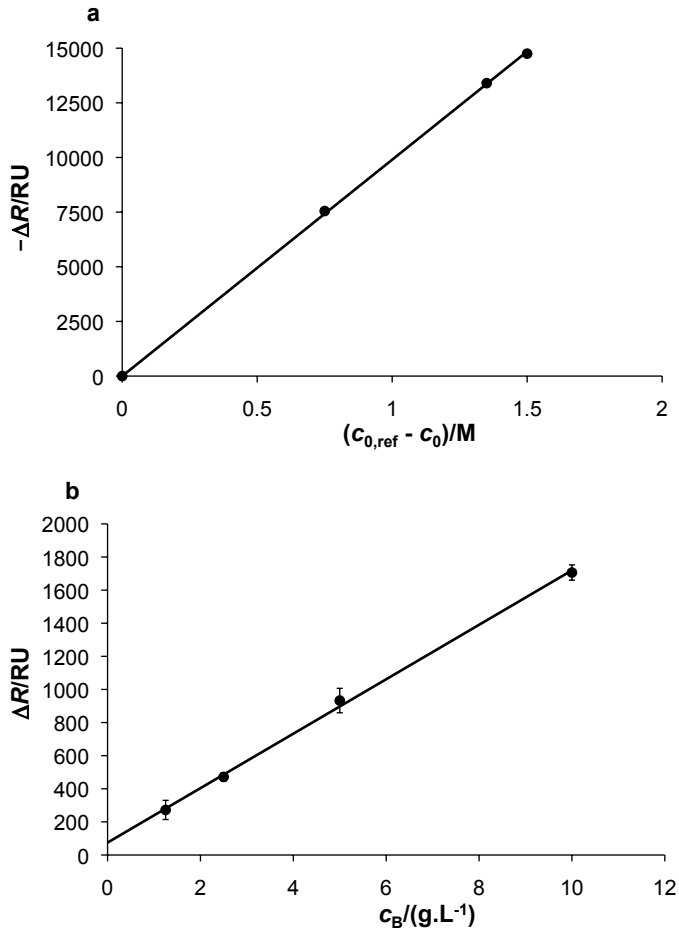

Figure 4.3: *(a) Experimental SPR signal shift, ΔR, as a function of salt concentration, $c_0 - c_{0,\mathrm{ref}}$ ($c_{0,\mathrm{ref}}$ = 1.5 M NaCl); (b) experimental SPR signal shift, ΔR, as a function of bulk protein concentration, c_B, under low binding conditions ($c_0 = c_{0,\mathrm{ref}} = 1.5$ M NaCl).*

4.5 Results and discussion

4.5.1 Calibration of Biacore signal

The Biacore signal was calibrated using various solutions with different salt (c_0) and BSA (c_B) concentrations and a baseline defined for a buffer solution with salt concentration $c_{0,\mathrm{ref}}$ = 1.5 M NaCl. First, salt solutions with different c_0 values were injected into the Biacore cell and the corresponding signal shifts measured (Fig. 4.3a). The linear fitting (with intercept set to zero) of ΔR against $(c_0 - c_{0,\mathrm{ref}})$ yielded $m_0 = m\phi_\mathrm{s}(\tilde{\eta}_0 - \tilde{\eta}_\mathrm{w})\nu_0 =$ 9898.1 RU/M with an excellent regression coefficient (r^2 = 0.9998); this linearity is in complete agreement with Eq. 4.8. This calibration accounts for the salt concentration

Table 4.1: *BSA physical properties (Bosma and Wesselingh, 1998).*

Molecular Weight	66.7 kDa
Dimensions	4 nm × 4 nm × 14 nm
Radius based on sphere	2.69 nm
Density	1360 g/L
Isoelectric point	4.9

effect without the presence of solute in suspension.

To account for the effect of BSA in solution ($c_0, c_B > 0$) a set of BSA concentrations in buffer with salt concentration $c_0 = c_{0,ref} = 1.5$ M NaCl was used (Fig. 4.3b). This salt concentration was high enough to reduce BSA adsorption to a residual level, so that the Biacore signal shifts yielded a straight line when plotted against c_B in accordance with Eq. 4.18 when c_m has a constant value. The linear fitting of ΔR vs c_B yielded a slope $\phi_m(m_B - m_0 v_B c_{0,ref}) = 164.43$ RU/(g/L), again with a very good regression coefficient: $r^2 = 0.9986$ (Fig. 4.3b).

The main physical properties of BSA are listed in Table 4.1 (Bosma and Wesselingh, 1998); from the data, $v_B = 7.553 \times 10^{-4}$ L/g, hence $m_0 v_B c_{0,ref} = 10.92$ RU/(g/L) and $m_B = 164.43/\phi_m + 10.92 = 179.79$ RU/(g/L). Equation 4.19 can now be applied for converting the SPR signal (ΔR) into concentration values of adsorbed protein, c_m (g/L) and q (g/dm^2) $= 10^{-8} d_m c_m$, with d_m in nm.

In solution, BSA is a prolate ellipse (cigar-shaped) with an axial ratio of about four; if the assumed BSA radius is calculated from its molecular weight and mass density, then the thickness of the planar monolayer will be $d_m = 2 \times 26.9$ Å $= 53.8$ Å (Bosma and Wesselingh, 1998). According to our model, d_m can be determined from the obtained values of m_0 and m_B and RI measurements as follows: plotting $(\eta_0 - \eta_{0,ref})_{eff}$ against $(c_0 - c_{0,ref})$ yields the slope

$$\phi_s(\tilde{\eta}_0 - \tilde{\eta}_w)\nu_0 = m_0/m \tag{4.32}$$

and plotting $(\eta_B - \eta_{0,ref})_{eff}$ against c_B yields the slope

$$\phi_s(\tilde{\eta}_B - \eta_{0,ref})v_B = \left[\phi_m(m_B - m_0 v_B c_{0,ref})\right]/m. \tag{4.33}$$

From these linear plots the calculated value d_m is $d_{m,\eta-based} \approx 5.6$ nm, which is closely comparable to the reference value of 5.38 nm. This supports the applicability of Eqs. 4.18 and 4.19 derived from our theory for SPR data analysis.

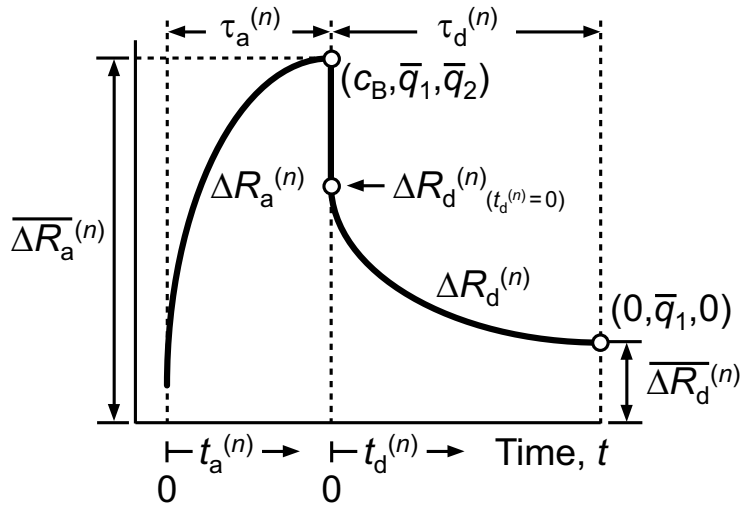

Figure 4.4: *Schematic of the nth adsorption/desorption cycle for a Biacore experiment.*

4.5.2 Analysis of BSA sensorgrams

The SPR experiments were performed at Biacore's maximum flow rate (100 μL/min) to avoid mass transfer limitations. These were, in fact, negligible when compared to the sorption rates at the tested conditions; a two-compartment, mass transport model coupled to our kinetic model showed no detectable impact on the apparent adsorption/desorption rates (see section 4.7).

Figure 4.4 shows the schematic of an adsorption/desorption cycle (say the nth one) for a Biacore experiment. The durations of the adsorption and desorption steps are $\tau_{\mathrm{a}}^{(n)}$ and $\tau_{\mathrm{d}}^{(n)}$, respectively. At the end of the adsorption step the SPR signal is $\overline{\Delta R}_{\mathrm{a}}^{(n)}$ and corresponds to $\left\{c_{\mathrm{B}}, \overline{q}_1^{(n)}, \overline{q}_2^{(n)}\right\}$, i.e., {bulk protein} + {irreversibly adsorbed protein} + {reversibly adsorbed protein}. When the desorption step begins, the bulk protein is immediately removed due to the high flow rate used (100 μL/min) compared to the flow chamber volume (approximately 60 nL) and the conditions in the flow cell change to $\left\{0, \overline{q}_1^{(n)}, \overline{q}_2^{(n)}\right\}$; the SPR signal then decays until it stabilizes at a value $\overline{\Delta R}_{\mathrm{d}}^{(n)}$ corresponding to $\left\{0, \overline{q}_1^{(n)}, 0\right\}$, i.e., when only irreversibly adsorbed protein remains in the sensor chamber.

If the step durations, $\tau_{\mathrm{a}}^{(n)}$ and $\tau_{\mathrm{d}}^{(n)}$, are long enough, then the SPR signals, $\overline{\Delta R}_{\mathrm{a}}^{(n)}$ and $\overline{\Delta R}_{\mathrm{d}}^{(n)}$, at the end of the respective steps correspond to steady state conditions in the sensor chamber (which are denoted by an overbar in our rate model); these are characterized by an horizontal plateau in the sensorgrams (i.e., the SPR signal becomes constant). This was found to be the case for most of the runs, particularly for the desorption steps. For those

cases where the SPR signal had not yet attained a constant value at the end of the step, the signal was extrapolated to infinite time by fitting the asymptotic part of the signal to a first-order dynamics,

$$\Delta R(t) = \alpha - \beta \exp(-t/\tau), \tag{4.34}$$

where α, β and $\tau > 0$ are fitting parameters; the asymptotic value of $\Delta R(t)$ for large values of time was estimated as the value of the fitted parameter α. Using Eq. 4.18, the value of $\overline{\Delta R}_{\mathrm{a}}^{(n)}$ was converted into the value of $\overline{q}_1^{(n)} + \overline{q}_2^{(n)}$ and that of $\overline{\Delta R}_{\mathrm{d}}^{(n)}$ into the value of $\overline{q}_1^{(n)}$.

From the analysis of the adsorption/desorption plateaus it is possible to make a first assessment of the adequacy of the two rate models — mechanisms A and B developed in §4.4 — incorporating different mechanisms for irreversible binding. According to mechanism A, $\overline{q}_1^{(n)}$ should vary linearly with $\overline{q}_2^{(n)}/c_{\mathrm{B}}$ with positive ordinate and slope, whereas for mechanism B, $\overline{q}_1^{(n)}$ should change linearly with $\overline{q}_2^{(n)}$ with positive ordinate and slope. As shown in Fig. 4.5, the experimental results reject mechanism A and support mechanism B.

Therefore, the most suitable kinetic model (mechanism B) can be stated as

$$\frac{dq_1}{dt} = k_{\mathrm{r}} c_{\mathrm{B}} (q_1^{\infty} - \sigma_{12} q_2 - q_1) + k'_{\mathrm{r}} c_{\mathrm{B}} q_2, \tag{4.35}$$

$$\frac{dq_2}{dt} = k_{\mathrm{a}} c_{\mathrm{B}} (q_2^{\infty} - \sigma_{21} q_1 - q_2) - (k_{\mathrm{d}} + k'_{\mathrm{r}} c_{\mathrm{B}}) q_2. \tag{4.36}$$

For this type of kinetic model, the reversible adsorption isotherm (i.e., the equilibrium dependency of $\overline{q}_2$ with c_{B}) is

$$\overline{q}_2 = \frac{(q_2^{\infty} - \sigma_{21} q_1^{\infty}) k_{\mathrm{a}} c_{\mathrm{B}}}{k_{\mathrm{d}} + [k'_{\mathrm{r}} + k_{\mathrm{a}} + \sigma_{21}(k'_{\mathrm{r}}/k_{\mathrm{r}} - \sigma_{12}) k_{\mathrm{a}}] c_{\mathrm{B}}}, \tag{4.37}$$

which is a Langmuir-type isotherm, i.e.,

$$\overline{q}_2 = \frac{\gamma b_2 c_{\mathrm{B}}}{1 + b_2 c_{\mathrm{B}}}, \tag{4.38}$$

where

$$b_2 = \frac{k'_{\mathrm{r}} + k_{\mathrm{a}}[1 + \sigma_{21}(k'_{\mathrm{r}}/k_{\mathrm{r}} - \sigma_{12})]}{k_{\mathrm{d}}}, \quad \gamma b_2 = \frac{k_{\mathrm{a}}(q_2^{\infty} - \sigma_{21} q_1^{\infty})}{k_{\mathrm{d}}}. \tag{4.39}$$

Figure 4.6 shows plots of $1/\overline{q}_1$ and $1/\overline{q}_2$ against $1/c_{\mathrm{B}}$. From the plot of the inverse of $\overline{q}_2$ against the inverse of c_{B} it is evident that Eq. 4.37 does apply for the reversible adsorption isotherm, $\overline{q}_2(c_{\mathrm{B}})$, and that the irreversible component, $\overline{q}_1(c_{\mathrm{B}})$, is the sum of a Langmuir isotherm model and a constant — derived in our model as q_1^{∞} — in accordance with Eqs. 4.30 and 4.37 (cf. Fig. 4.6). Note that the linear regression coefficients in

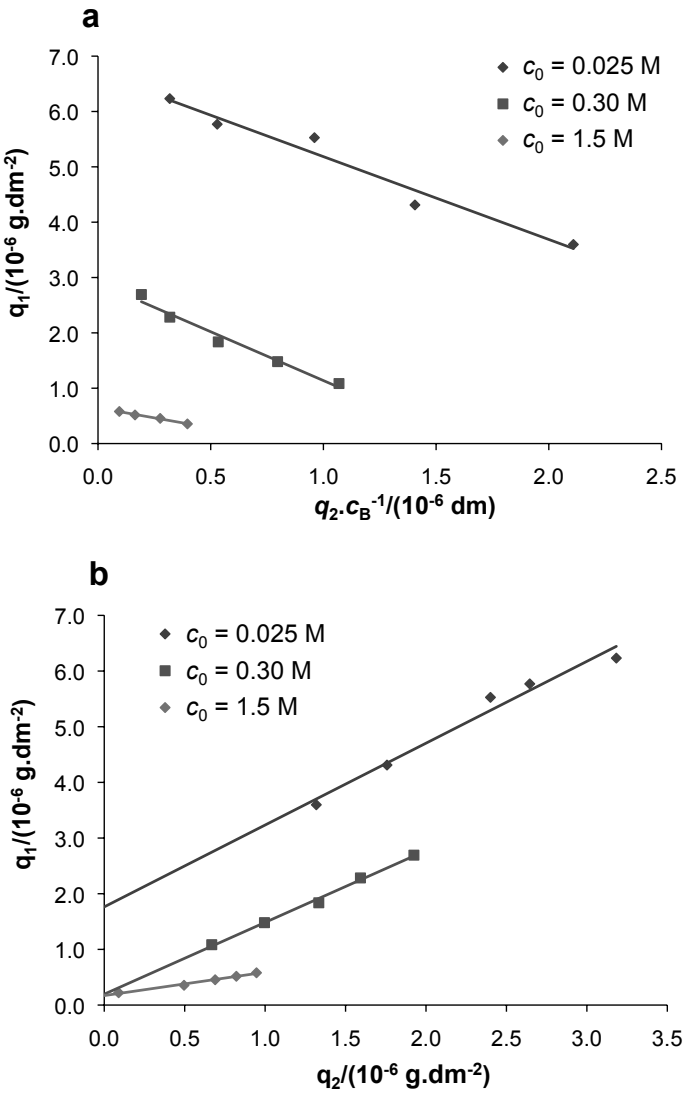

Figure 4.5: *Evaluation of the suitability of mechanisms A and B for the description of the dynamics of the SPR adsorption/desorption cycles: (a)* $\overline{q}_1$ *vs* $\overline{q}_2/c_B$ *plot (mechanism A); linear regression coefficient,* r^2*, is 0.964, 0.975, and 0.983 for* $c_0 = 0.025$ *M,* $c_0 = 0.30$ *M, and* $c_0 = 1.5$ *M, respectively; note that all slopes are negative in disagreement with Eq. 4.29; (b)* $\overline{q}_1$ *vs* $\overline{q}_2$ *plot (mechanism B);* r^2 *is 0.951, 0.995, and 0.999 for* $c_0 = 0.025$ *M,* $c_0 = 0.30$ *M, and* $c_0 = 1.5$ *M, respectively; note that all slopes are positive in agreement with Eq. 4.30.*

Fig. 4.6b are very acceptable, confirming the Langmuir-type adsorption behavior implied by Eq. 4.38. The inverse plot for $\overline{q}_1$ shows also a very reasonable correlation; this can be explained by Eq. 4.28, which expresses the irreversible adsorption component as an irreversible adsorption capacity (q_1^{∞}) plus a Langmuir-type isotherm ($\overline{q}_2$) scaled by a constant ($k'_r/k_r - \sigma_{12}$).

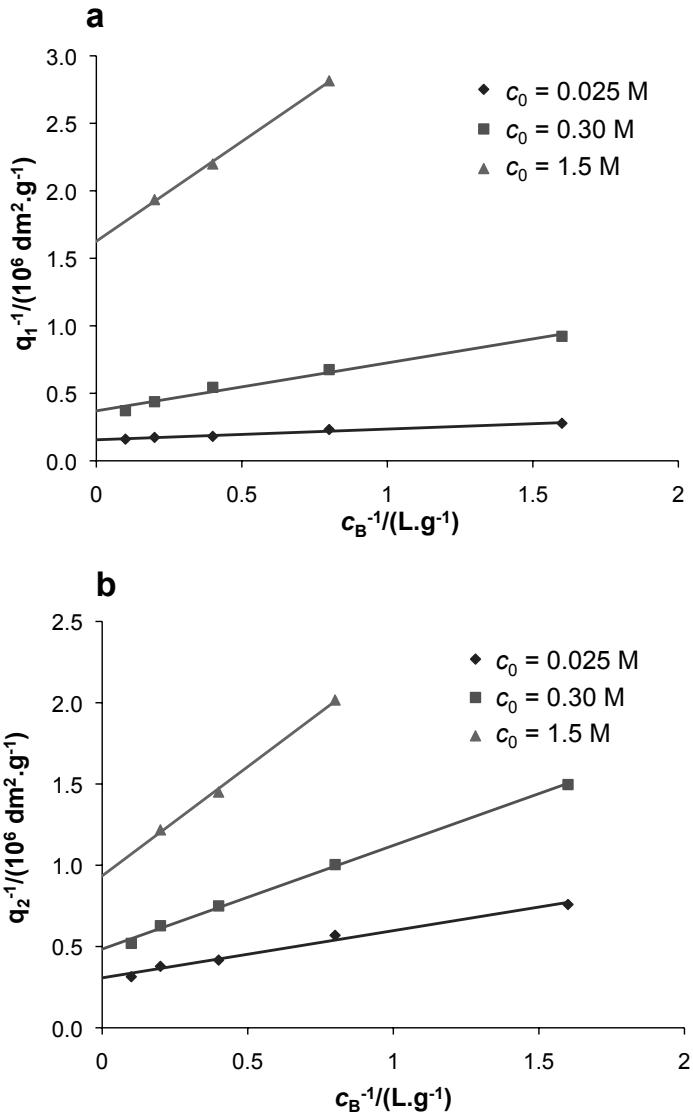

Figure 4.6: *Inverse plots of adsorption against bulk concentration: (a)* $1/\overline{q}_1$ *vs* $1/c_B$*; linear regression coefficient,* r^2*, is 0.999, 0.984, and 0.975 for* $c_0 = 0.025$ *M,* $c_0 = 0.30$ *M, and* $c_0 = 1.5$ *M, respectively; (b)* $1/\overline{q}_2$ *vs* $1/c_B$*;* r^2 *is 0.998, 0.998, and 0.986 for* $c_0 = 0.025$ *M,* $c_0 = 0.30$ *M, and* $c_0 = 1.5$ *M, respectively.*

As shown in both inverse plots of Fig. 4.6, the slope and intercept are functions of the salt concentration showing evidence of an ion exchange-type mechanism modulated by the concentration of the salt counterion, Cl^-. Although it is not apparent from the inverse plots, the adsorption equilibrium data extracted from the various SPR sensorgrams span protein concentrations from dilute conditions, where Henry's law prevails, up to overloaded conditions, where the adsorbed monolayer is near completed.

Let us now analyze the adsorption and desorption rates. During the desorption step, $c_{\mathrm{B}} = 0$; the equations governing the dynamics for this step (under the assumption of negligible mass transfer resistance between the bulk and the sensor surface) are:

$$\frac{dq_1^{(n)}}{dt} = 0, \tag{4.40}$$

$$\frac{dq_2^{(n)}}{dt} = -k_{\mathrm{d}} q_2^{(n)}. \tag{4.41}$$

The solution is simply

$$q_1^{(n)} = \overline{q}_1^{(n)}, \quad q_2^{(n)} = \overline{q}_2^{(n)} \exp\left(-k_{\mathrm{d}} t_{\mathrm{d}}^{(n)}\right). \tag{4.42}$$

Therefore,

$$\ln q_2^{(n)} = \ln \overline{q}_2^{(n)} - k_{\mathrm{d}} t_{\mathrm{d}}^{(n)}, \tag{4.43}$$

which shows that the rate constant k_{d} can be estimated from a $\ln q_2^{(n)}$-vs-$t_{\mathrm{d}}^{(n)}$ regression plot.

From Eq. 4.18 it easy to deduce that

$$\Delta R_{\mathrm{d}}^{(n)} = \frac{(m_{\mathrm{B}} - m_0 c_0 v_{\mathrm{B}})(1-\phi_{\mathrm{m}})\left[\overline{q}_1^{(n)} + q_2^{(n)}\right]}{d_{\mathrm{m}}} + m_0(c_0 - c_{0,\mathrm{ref}}). \tag{4.44}$$

The irreversible component, $q_1^{(n)} = \overline{q}_1^{(n)}$, is constant during the desorption step, but the reversible component, $q_2^{(n)}$, decreases from $\overline{q}_2^{(n)}$ to 0 as $t_{\mathrm{d}}^{(n)}$ advances from 0 towards large time (∞). Let $\overline{\Delta R}_{\mathrm{d}}^{(n)} = \lim_{t_{\mathrm{d}}^{(n)} \to \infty} \Delta R_{\mathrm{d}}^{(n)}$; then

$$\Delta R_{\mathrm{d}}^{(n)} - \overline{\Delta R}_{\mathrm{d}}^{(n)} = (m_{\mathrm{B}} - m_0 c_0 v_{\mathrm{B}})(1-\phi_{\mathrm{m}}) q_2^{(n)} / d_{\mathrm{m}} \tag{4.45}$$

and

$$\ln\left[\Delta R_{\mathrm{d}}^{(n)} - \overline{\Delta R}_{\mathrm{d}}^{(n)}\right] = \ln[(m_{\mathrm{B}} - m_0 c_0 v_{\mathrm{B}})(1-\phi_{\mathrm{m}})/d_{\mathrm{m}}] + \ln q_2^{(n)}. \tag{4.46}$$

Therefore, $\ln\left[\Delta R_{\mathrm{d}}^{(n)} - \overline{\Delta R}_{\mathrm{d}}^{(n)}\right]$ and $\ln q_2^{(n)}$ both change with time at the same rate; in both cases the slope of the linear change with t is k_{d}.

Let us assume the case when shielding is negligible, i.e. when σ_{12} and σ_{21} both tend

Table 4.2: *Model parameters estimated from three Biacore training experiments with BSA injections at $c_B = 2.5$ g/L and different salt concentrations, c_0.*

c_0 (M)	k_d (s^{-1})	k_r ($dm^3 g^{-1} s^{-1}$)	k'_r ($dm^3 g^{-1} s^{-1}$)	k_a ($dm^3 g^{-1} s^{-1}$)	$10^6 q_1^\infty$ ($g\,dm^{-2}$)	$10^6 q_2^\infty$ ($g\,dm^{-2}$)	σ_{12}	σ_{21}
0.025	0.051	0.017	0.0192	0.034	2.79	5.29	≈ 0	0.023
0.300	0.056	0.017	0.0221	0.020	0.20	4.45	≈ 0	0.025
1.500	0.128	0.016	0.0031	0.085	0.17	1.13	≈ 0	0.025

to 0. In this case, Eqs. 4.35 and 4.36 simplify to

$$\frac{dq_1}{dt} = k_r c_B (q_1^\infty - q_1) + k'_r c_B q_2, \tag{4.47}$$

$$\frac{dq_2}{dt} = q_2^\infty k_a c_B - [k_d + (k_a + k'_r) c_B] q_2. \tag{4.48}$$

From Eq. 4.30 it is possible to determine q_1^∞ and k'_r/k_r. Rearranging Eq. 4.37 gives

$$\frac{1}{\overline{q}_2} = \frac{k_a + k'_r}{q_2^\infty k_a} + \frac{k_d}{q_2^\infty k_a}\frac{1}{c_B} = \alpha + \beta\frac{1}{c_B}. \tag{4.49}$$

From the linear fitting of $\overline{q}_2$ vs c_B we get $q_2^\infty k_a = k_d/\beta$ and $k_a + k'_r = k_d\alpha/\beta$. With this analysis, values of k_d, $q_2^\infty k_a$ and $k_a + k'_r$ can be estimated; these are the required lumped parameters to solve Eq. 4.48. As to Eq. 4.47, the values of q_1^∞ and the ratio k'_r/k_r are already known; by curve fitting, k_r and k'_r parameters can be estimated and all remaining unknown parameters can easily be calculated.

Once all parameters were estimated using the procedure described above, their values were refined by taking protein shielding into account. In this case the shielding factors, σ_{12} and σ_{21}, were determined by nonlinear curve-fitting using the complete kinetic model. These fittings were performed using gPROMS, a software package for the modeling and simulation of lumped and distributed-parameter process models with combined discrete and continuous characteristics (PSE, 2009). The fittings were applied to sets of sensorgrams obtained at different salt concentrations. Table 4.2 summarizes the model parameters obtained using the procedure explained above: starting from an estimate of k_d using Eq. 4.46, the simplified model (Eqs. 4.48 and 4.47) was used to determine k_r; all parameters were then introduced in the complete model formulation (Eqs. 4.35 and 4.36) to refine the parameters and to estimate values for σ_{12} and σ_{21}.

Figure 4.7 shows the comparison between simulations and experimental data at different salt concentrations. The results indicate a fairly good agreement between the experimental curves and our adsorption/desorption rate model with the the estimated parameters (Table 4.2). The proposed assumption that two distinct adsorption mechanisms occur si-

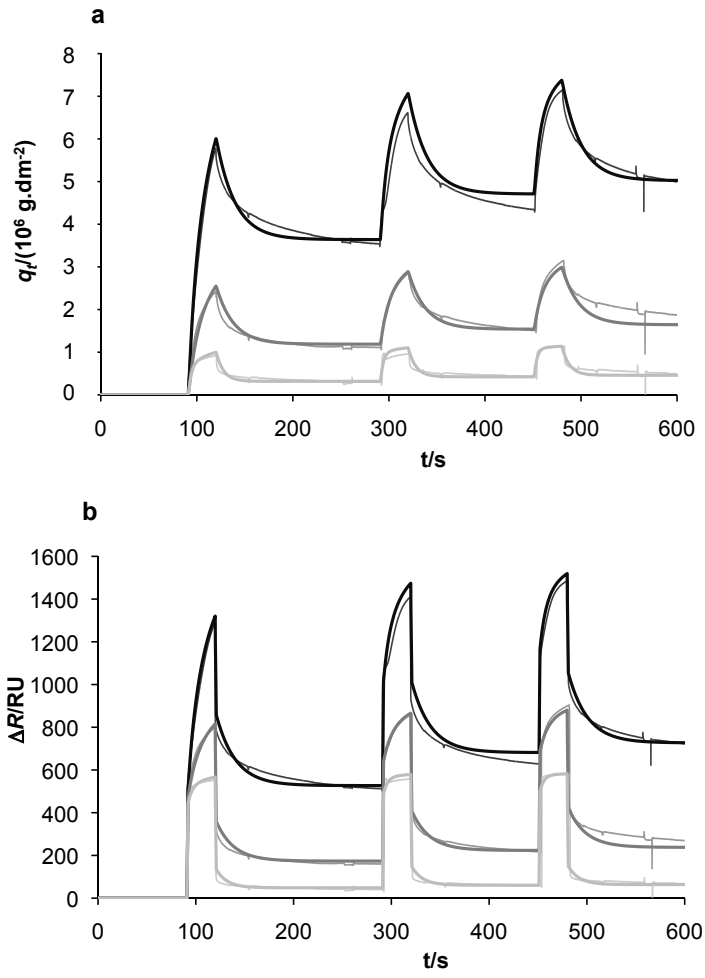

Figure 4.7: *Model training using three SPR experiments with BSA at* $c_B = 2.5$ *g/L and different salt concentrations,* $c_0 = 0.025$*, 0.30, and 1.5 M: (a)* $q = q_1 + q_2$ *vs t; (b)* ΔR *vs t. The thick and thin lines correspond, respectively, to the model predictions and experimental data; increasing dark tone in gray lines corresponds to decreasing salt concentrations; q is estimated from the experimental data using Eq. 4.19 and* $d_m = 5.6$ *nm.*

multaneously, one being reversible and similar to an exchange reaction between the free protein and a certain number of bound ions, and another, with an extremely low desorption rate, formally defined as an irreversible mechanism, seems to suit well the experimental data.

Table 4.2 shows that the total BSA binding capacity of the derivatized surface, $q_1^\infty + q_2^\infty$, is ca. 0.81 mg/m^2 at 25 mM salt concentration; this value is less than the 5 mg/m^2 typically found for a protein monolayer. It is important to note, however, that the binding capacity is strongly dependent on the ligand density of the derivatized surface, and our guess is that the ligand density was low in our MUA-DEAE surfaces. This guess is supported, in part, by the low values of the binding constants, e.g., $b_2 = 1.04$ L/g at 25 mM NaCl, derived from the Langmuir adsorption isotherm model (cf. Eqs. 4.38 and 4.39). Another indication of low ligand density are the small values of the shielding factors, σ_{12} and σ_{21}, obtained from the fitting of the kinetic model; small values of σ indicate that the bound BSA molecules are spread over the derivatized surface with a mean distance between neighboring molecules large enough for the shielding to have only a mild effect.

Figures 4.5b, 4.6, and 4.7, as well as Table 4.2, show that both the reversible and irreversible adsorption mechanisms are sensitive functions of the salt concentration. A speculation for this effect on the irreversible adsorption component is that the degree of solvation of both the protein and the DEAE ligand sites, which is directly a function of salt concentration, inhibits the irreversible adsorption mechanism as it does for the reversible part. Indeed, when the ionic strength or, more precisely, the salt concentration, are increased, both the reversible and irreversible equilibrium adsorption amounts decrease exponentially with the salt concentration, c_0. Thus, similar trends are observed for the dependencies of q_1^∞ and q_2^∞ with c_0: the larger the salt counterion concentration, the smaller the amount of adsorbed protein, in line with a typical ion-exchange surface using commercial matrices.

These observations emphasize that the micrometric-scale DEAE surface mimics well an ion-exchange surface in terms of intrinsic adsorption capacities to different materials, even though other effects, such as the three-dimensionality of a chromatography matrix or mass transfer resistances, are not considered. Nevertheless, it is clear that by changing the ligand type and/or its density, which can be accomplished using different SAM compositions, our SPR-based method is well suited to small-scale studies of protein adsorption. In fact, a scale-down factor of over 1200-fold is accomplished using this strategy when compared to a commercially available Sartobind D MA 15 unit from Sartorius-Stedim Biotech (with

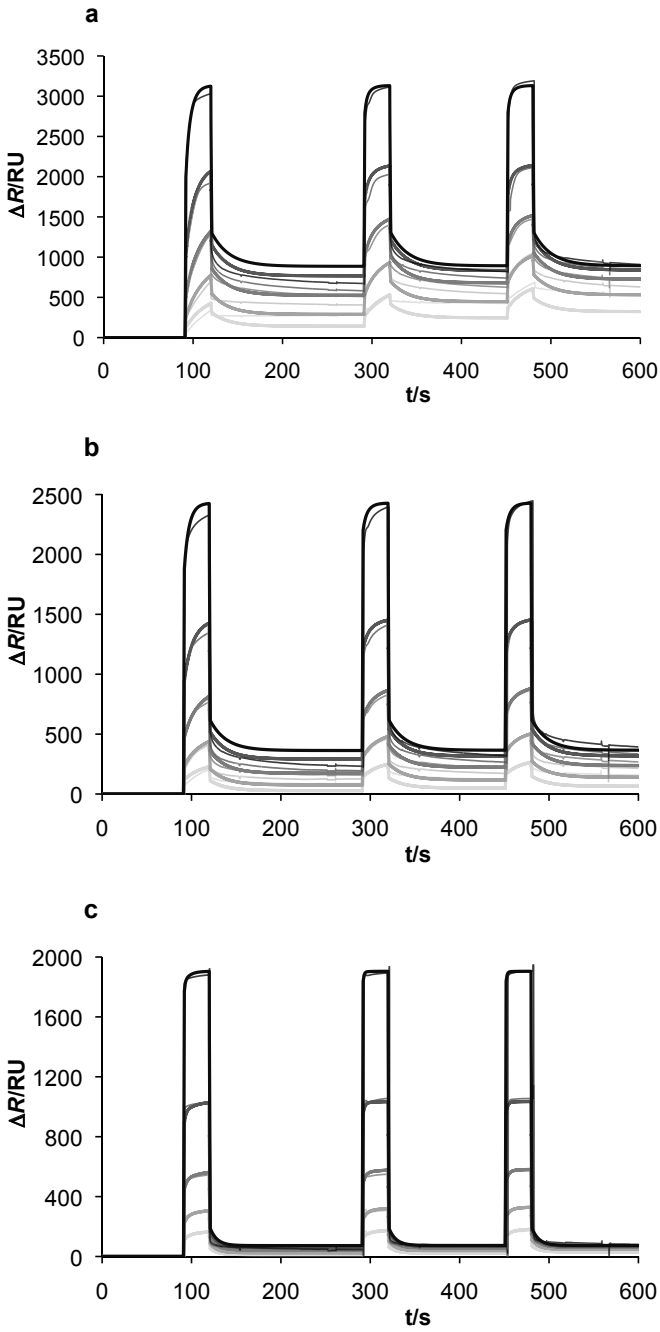

Figure 4.8: *Model validation with cyclic SPR experiments of BSA binding and elution over micrometric DEAE surface at different injected BSA concentrations,* $c_B = 0.625$*, 1.25, 2.5, 5, and 10 g/L; (a)* $c_0 = 0.025$ *M, (b)* $c_0 = 0.30$ *M, (c)* $c_0 = 1.5$ *M. The thick and thin lines correspond, respectively, to the model predictions and experimental data; increasing dark tone in gray lines corresponds to increasing protein concentration,* c_B*.*

15 cm^2 total effective area).

In order to further validate the proposed model, SPR runs with different injected BSA concentrations were compared against predicted simulation curves; the results are shown in Fig. 4.8. This data set was used to test the extrapolation capability of the kinetic model with the parameter values estimated above. Note that the model parameters were estimated from SPR experiments at fixed c_B and varying c_0. The results depicted in Fig. 4.8 show that the changes in injected protein concentration are rather well predicted by the model simulations; additionally, changes in c_0 result in lower adsorption and faster kinetics confirming the expected low or residual adsorption.

4.6 Conclusions

Adsorption equilibrium and kinetics on a derivatized surface, containing an ion-exchange functional DEAE group, have been measured and analyzed by SPR spectroscopy. BSA was used as a model protein for system development, implementation and testing. A complete mathematical description of the SPR sensor mechanism was derived giving rise to simple algebraic expressions relating the protein concentration in the adsorbed monolayer with SPR signal shift and protein and salt concentration in the bulk solution. Using the calibrations performed for salt and free protein in solution, the concentration of the adsorbed protein monolayer could be directly obtained from the SPR sensorgram data at different conditions of load and salt concentration.

An adsorption/desorption rate model, incorporating two different adsorption mechanisms, was proposed as a means to explain the SPR sensorgrams. The model is based on the assumption that only part of the protein adsorbs reversibly, according to a Langmuirian kinetic model, whereas the other part binds irreversibly to the DEAE surface; the kinetics of the latter is proportional to the protein concentrations in the bulk and in the reversibly adsorbed phase. The dependency between the estimated reversible and irreversible adsorbed concentrations in the stationary phase (herein mimicked by the customized chip surface) allowed us to discriminate between two possible adsorption mechanisms; this analysis suggests the presence of an adsorption scheme compatible with a first-order kinetics controlled by the reversibly adsorbed solute and its concentration in the mobile phase. From the SPR experiments it was possible to determine the adsorption isotherms for different salt conditions and to estimate the parameters of the developed rate model. The results provided evidence that the DEAE-SAM derivatized surface is a good mimic of an

ion-exchange surface, as far as intrinsic ion exchange-related interactions are concerned, without considering transport or exclusion phenomena only present in a chromatographic matrix.

Acknowledgements

We acknowledge funding from the European Commission (Baculogenes, LSHB-2006-037541 and Clinigene – Network of Excellence, LSHB-2006-018933) and the Portuguese *Fundação para a Ciência e a Tecnologia* (PTDC/EQU-EQU/71645/2006 and SFRH/BD/31257/2006).

4.7 Appendix: Influence of mass transport on measured binding rate constants

Figure 4.9 shows a schematic of the Biacore's flow chamber. We assume that laminar flow is fully developed over the entire length l of the flow cell and neglect any variations along the z coordinate. Under these assumptions, the velocity field (u, v), which is the solution for fully developed laminar flow between two parallel flat plates, is

$$u = 6\,\overline{u}\left(\frac{y}{h}\right)\left(1-\frac{y}{h}\right), \quad v = 0, \tag{4.50}$$

where u and v are the velocity components along the x and y coordinates, respectively, and $\overline{u}$ is the average velocity; $\overline{u}$ is related to the volumetric flow rate Q through $\overline{u} = Q/(hw)$ (see Fig. 4.9 for the meaning of w and h). Given that $h \gg d_\mathrm{p}$, we can linearize the velocity field near $y = 0$; this gives

$$u(y) \approx \frac{6\overline{u}}{h} y \quad \text{for} \quad y \approx 0. \tag{4.51}$$

At a flow rate of 100 μL/min = 100 mm^3/min, the average axial velocity of an analyte molecule in the flow cell is $\overline{u} = 66.7$ mm/s; However, the average axial velocity of the analyte molecules within the fluid film delimited in the depth $y \leq d_\mathrm{p}$ of the evanescent electomagnetic field is reduced to $\overline{u}' = 0.6$ mm/s. Nevertheless, the characteristic residence time of these molecules in the volume of fluid probed the Biacore sensor is only $l_\mathrm{c}/\overline{u}' = 1.6/0.6 = 2.8$ seconds (cf. Fig. 4.9).

The effect of mass transfer on the analysis of the SPR signal is usually described by a

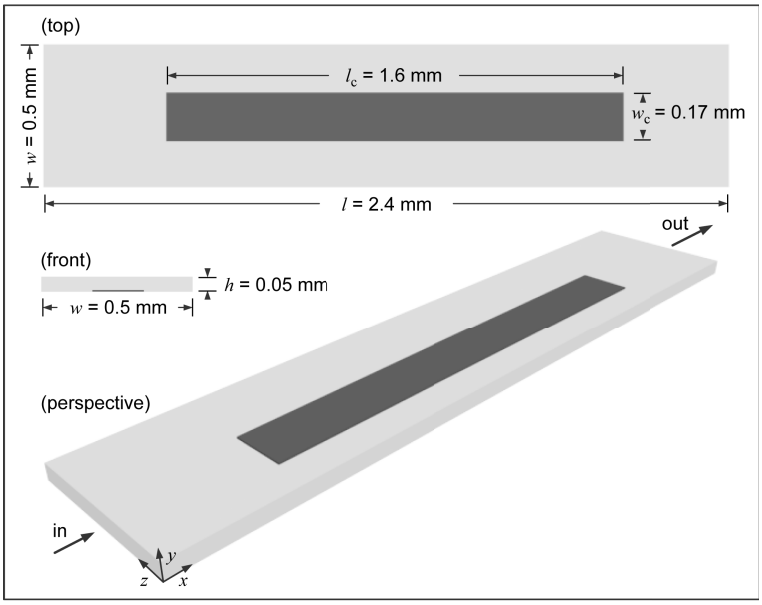

Figure 4.9: *Schematic of Biacore's flow cell.*

two-compartment model (Myszka et al., 1998):

$$d_{\mathrm{p}}\frac{dc_{\mathrm{B}}}{dt}+\left(\frac{dq_1}{dt}+\frac{dq_2}{dt}\right)=k_{\mathrm{m}}(c_{\mathrm{B}}^{\mathrm{o}}-c_{\mathrm{B}}), \tag{4.52}$$

where k_{m} is the transport coefficient describing the diffusional flux of solute from the bulk of the flow chamber, where its concentration is $c_{\mathrm{B}}^{\mathrm{o}}$, into the inner compartment, where its concentration is c_{B}. As a matter of convenience, the inner compartment can be taken as the layer of fluid delimited in the depth of the evanescent electromagnetic field, whose volume is $l_{\mathrm{c}}w_{\mathrm{c}}d_{\mathrm{p}}$ (cf. Fig. 4.9).

As discussed by Lok et al. (Lok et al., 1983) and Sjölander and Urbaniczky (Sjölander and Urbaniczky, 1991), it can be shown that, to a good approximation,

$$k_{\mathrm{m}}\approx 1.282\left(\frac{\overline{u}'D^2}{d_{\mathrm{p}}l_{\mathrm{c}}}\right)^{1/3}, \tag{4.53}$$

where D is the molecular diffusion coefficient.

Transport effects will not influence the adsorption kinetics if $k_{\mathrm{m}}\gg k_{\mathrm{r}}q_1^{\infty}$ and $k_{\mathrm{m}}\gg k_{\mathrm{a}}q_2^{\infty}$; similarly, the desorption kinetics will not be influenced by mass transfer if $k_{\mathrm{m}}c_{\mathrm{B}}^{\mathrm{o}}\gg k_{\mathrm{d}}q_2^{\infty}$. For our SPR experiments with BSA, $D=9\times10^{-7}\mathrm{cm}^2/\mathrm{s}$ and $k_{\mathrm{m}}=0.0035$ cm/s. From the data listed in Table 4.2, it is clear that mass transport effects can be safely neglected in the analysis of the SPR experiments carried out during this work.

References

Bosma JC, Wesselingh JA. ph dependence of ion-exchange equilibrium of proteins. AIChE J 1998;44:2399–2409.

Brooks CA, Cramer SM. Steric mass-action ion exchange: Displacement profiles and induced salt gradients. AIChE J 1992;38:1969–1978.

Coffman JL, Kramarczyk JF, Kelley BD. High-throughput screening of chromatographic separations: I. method development and column modeling. Biotechnol Bioeng 2008;100:605–618.

Davies A, Greene A, Lullau E, Abbott WM. Optimisation and evaluation of a high-throughput mammalian protein expression system. Protein Expr Purif 2005;42:111–21.

Hoa XD, Kirk AG, Tabrizian M. Towards integrated and sensitive surface plasmon resonance biosensors: a review of recent progress. Biosens Bioelectron 2007;23:151–60.

Jung LS, Campbell CT, Chinowsky TM, Mar MN, Yee SS. Quantitative interpretation of the response of surface plasmon resonance sensors to adsorbed films. Langmuir 1998;14:5636–5648.

Kaludov N, Handelman B, Chiorini JA. Scalable purification of adeno-associated virus type 2, 4, or 5 using ion-exchange chromatography. Hum Gene Ther 2002;13:1235–43.

Kelley BD, Switzer M, Bastek P, Kramarczyk JF, Molnar K, Yu T, et al. High-throughput screening of chromatographic separations: Iv. ion-exchange. Biotechnol Bioeng 2008;100:950–963.

Kim HS, Jung SH, Kim SH, Suh IB, Kim WJ, Jung JW, et al. High-throughput analysis of mumps virus and the virus-specific monoclonal antibody on the arrays of a cationic polyelectrolyte with a spectral spr biosensor. Proteomics 2006;6:6426–32.

Knoll W, Schmitt FJ, Klein C, Guder HJ, Liley M, Spinke J. Universal binding film. US Patent 5763191 1998.

Lok BK, Cheng YL, Robertson CR. Protein adsorption on crosslinked polydimethylsiloxane using total internal reflection fluorescence. J Colloid Interface Sci 1983;91:104–116.

Mrksich M, Whitesides GM. Using self-assembled monolayers to understand the interactions of man-made surfaces with proteins and cells. Annu Rev Biophys Biomol Struct 1996;25:55–78.

Myszka DG, He X, Dembo M, Morton TA, Goldstein B. Extending the range of rate constants available from biacore: interpreting mass transport-influenced binding data. Biophys J 1998;75:583–94.

Pampel LW, Boushaba R, Titchener-Hooker NJ. A methodical approach to ultra-scale-down of process sequences: application to casein removal from the milk of transgenic animals. Biotechnol Prog 2008; 24:192–201.

Pattnaik P. Surface plasmon resonance: applications in understanding receptor-ligand interaction. Appl Biochem Biotechnol 2005;126:79–92.

PSE. Process systems enterprise, gproms, www.psenterprise.com/gproms, 1997-2009. 2009.

Rege K, Pepsin M, Falcon B, Steele L, Heng M. High-throughput process development for recombinant protein purification. Biotechnol Bioeng 2006;93:618–30.

Rich RL, Myszka DG. Survey of the year 2007 commercial optical biosensor literature. J Mol Recognit 2008;21:355–400.

Rodrigues T, Carvalho A, Roldao A, Carrondo MJT, Alves PM, Cruz PE. Screening anion-exchange chromatographic matrices for isolation of onco-retroviral vectors. J Chromatogr B 2006;837:59–68.

Roper DK, Nakra S. Adenovirus type 5 intrinsic adsorption rates measured by surface plasmon resonance. Anal Biochem 2006;348:75–83.

Sjölander S, Urbaniczky C. Integrated fluid handling system for biomolecular interaction analysis. Anal Chem 1991;63:2338–2345.

Specht R, Han B, Wickramasinghe SR, Carlson JO, Czermak P, Wolf A, et al. Densonucleosis virus purification by ion exchange membranes. Biotechnol Bioeng 2004;88:465–73.

Trilisky EI, Lenhoff AM. Sorption processes in ion-exchange chromatography of viruses. J Chromatogr A 2007;1142:2–12.

Vicente T, Peixoto C, Carrondo MJT, Alves PM. Purification of recombinant baculoviruses for gene therapy using membrane processes. Gene Ther 2009;16:766–775.

Vicente T, Sousa MFQ, Peixoto C, Mota JPB, Alves PM, Carrondo MJT. Anion-exchange membrane chromatography for purification of rotavirus-like particles. J Membr Sci 2008;311:270–283.

Wensel DL, Kelley BD, Coffman JL. High-throughput screening of chromatographic separations: Iii. monoclonal antibodies on ceramic hydroxyapatite. Biotechnol Bioeng 2008;100:839–854.

Whitesides GM, Kriebel JK, Love JC. Molecular engineering of surfaces using self-assembled monolayers. Sci Prog 2005;2005:17–48.

Yamada K, McCarty DM, Madden VJ, Walsh CE. Lentivirus vector purification using anion exchange hplc leads to improved gene transfer. Biotechniques 2003;34:1074–8, 1080.

Zydney AL, Harinarayn C, Reis Rv. Modeling electrostatic exclusion effects during ion exchange chromatography of monoclonal antibodies. Biotechnol Bioeng 2008;102:1131–40.

Chapter 5

ANALYSIS OF ADSORPTION OF A BACULOVIRUS BIOREACTION BULK ON AN ION-EXCHANGE SURFACE BY SURFACE PLASMON RESONANCE

Adapted from:

Vicente T, Mota JPB, Peixoto C, Alves PM, Carrondo MJT. Analysis of adsorption of a baculovirus bioreaction bulk on an ion-exchange surface by surface plasmon resonance. J Biotechnol 2010; 148:171–181.

Abstract

The binding and elution of the key components of a bioreaction bulk for production of recombinant baculoviruses—a promising viral vector for gene therapy and vaccination—on a model ion-exchange surface have been successfully measured and interpreted by surface plasmon resonance (SPR) spectroscopy. The micro-scaled, ion-exchange surface was produced by immobilizing a typical ion-exchange ligand, diethylaminoethyl, onto commercially available planar gold sensor chip surfaces, which were pre-derivatized with a self-assembled monolayer of 11-mercaptoundecanoic acid. Each isolated analyte was injected into the SPR cell at defined operating conditions of salt and solute concentrations to determine the adsorption equilibrium plateau, and then eluted at the same salt concentration, upon which a well-defined, residual desorption equilibrium plateau was observed. From the analysis of the binding and elution curves and equilibrium plateaus for seven key biomolecules, it is possible to determine the adsorption isotherms over a broad range of equilibrium conditions for the three main cuts of the baculovirus bioreaction bulk: the product (the infective baculovirus), the main product-related impurities, and the main process-related impurities. A model that quantitatively explains the SPR-derived adsorption/desorption data was successfully developed for this complex biological system.

Contents

5.1 Introduction

Ion-exchange processes are ubiquitously used in downstream processing of complex biologics for clinical use. The optimization of charge-dependent unit operations relies on the evaluation of pivotal operating conditions, such as ionic strength and pH of the suspension buffer. These procedures tend to become exceptionally costly when a high added-value product is recovered from a complex preparation, such as an animal cell derived bioreaction bulk. Hence, the optimization of such unit processes becomes mandatory in the interest of cost and time savings. Scaled-down models, often used in high-throughput technologies, are being considered as options of choice for early stage process development (Coffman et al., 2008; Rege et al., 2006; Wensel et al., 2008).

Recombinant baculoviruses (rBVs) constitute a challenging model system within the collection of promising complex biopharmaceuticals for clinical therapies. Besides being used as a robust expression system with insect cell lines (BEVS), the potential of these viral vectors has evolved to human gene therapy or vaccination due to important (and alternative) advantages over other more studied vectors such as adeno- or retroviruses (Kost et al., 2005; Airenne et al., 2009). Since the mid-nineties (Hofmann et al., 1995), it has been shown that these insect-specific viruses can be genetically modified to transduce vertebrate cells, by means of a proper mammalian promoter, without replicating themselves or causing cytotoxic effects. Due to this non-pathogenicity to mammalian cells, the ability to accommodate very large foreign DNA inserts and the easiness of production at high viral titers in insect cell cultures, this system presents significant potential and important advantages over other vectors used in clinical trials (Hu, 2008; Airenne et al., 2009).

The typical insect cell clarified bioreaction bulk comprises a complex mixture of components: the desired product—the recombinant baculoviruses, infective/bioactive particles—, the product-related impurities, which decrease the quality of the product, and the process-related impurities—DNA, host-cell protein, and/or eventual endotoxin. The understanding of how these impurities behave in an ion-exchange process provides useful information for designing and optimizing the chromatographic purification process.

Surface plasmon resonance (SPR) spectroscopy is an extremely sensitive analytical technique with many applications in fundamental surface science (Hoa et al., 2007; Pattnaik, 2005; Rich and Myszka, 2008). SPR biosensors allow label-free, real-time, quantitative and qualitative characterization of the specific binding of a mobile analyte to a ligand immobilized on a metal surface (Schuck, 1997). When working with highly expensive biological materials, such as viral vectors produced in cell culture, SPR can play a supporting role for the optimization of adsorption-based, downstream purification processes, including ion-exchange chromatography, by providing quantitative information on the binding kinetics and equilibria of the various biomolecules of the bioreaction bulk to an immobilized functionalization layer mimicking the adsorbent. Because of the highly reduced sample volume used in a typical SPR experiment, a critical amount of data on the adsorbed film for a broad range of analyte loading and salt concentration can be obtained with a small amount of material.

We have recently applied SPR sensing to the monitoring and quantitative analysis of protein binding and elution over a micro-scaled, ion-exchange surface under cyclic adsorption conditions (Vicente et al., 2010). It is the purpose of the present study to employ SPR

and its mathematical formalism for quantitative interpretation of ion-exchange equilibria for a much more complex biological system: a recombinant baculovirus bioreaction bulk.

For convenience, we shall split the biological bulk into three cuts or fractions—the product, the main product-related impurities, and the main process-related impurities—and identify the key biomolecules governing the chromatographic behavior of each fraction. We will then use SPR sensing to measure the adsorption equilibrium of each isolated biomolecule over a broad range of solute and salt concentrations. Overall, we shall report on seven different adsorbates. A kinetic model is proposed to explain the measured SPR responses for the adsorbed films of the various biomolecules. Our results show that SPR can be a handy predictive tool by providing fundamental data for the design of downstream chromatographic purification processes, and thus very useful in early-stage process development of complex biopharmaceuticals.

5.2 Materials and methods

5.2.1 Cell culture and baculovirus production

Sf9 insect cells (ECACC #89070101, UK) were routinely grown in Gibco^{TM} Sf-900 II SFM (serum-free) culture medium (Invitrogen, Paisley, UK) using spinner (stirred at 150 rpm in a magnetic stirrer) or Erlenmeyer vessels (shaken at 110 rpm in an orbital shaker). Cell concentration and viability were routinely assessed by haemocytometer (Brand, Wertheim, Germany) with cell viability evaluated by 0.4% trypan blue exclusion dye (Merck, Darmstadt, Germany) in phosphate-buffered saline.

The vector used, rBV-green fluorescent protein (GFP), encodes for the baculovirus major structural capsid protein, vp39, containing on its N-terminal a GFP protein reporter (Kukkonen et al., 2003). Stock aliquots of rBV-GFP were produced in Sf9 cells grown in a 25 liter working volume wavebag bioreactor (Wave Europe, Cork, Ireland) using Sf-900 II medium. Sf9 cells were infected at a viable cell concentration of 1–2$\times 10^6$ cells/mL, using a multiplicity of infection (MOI) of 0.1 plaque forming units (PFU)/cell. Cell viability and cell infection were monitored for five days post infection. Quantification of the infected cells during the process was done by flow cytometry assessing GFP-expressing cell populations using a CyFlow^{TM} space-flow cytometer system (Partec, Münster, Germany). Data analysis was done using the manufacturer's data acquisition software, FloMax^{TM} (Partec). The rBV production bulk was harvested when the cell viability reached values of 50%. Infection bulks were clarified as described elsewhere (Vicente et al., 2009).

5.2.2 Purification of baculoviruses and isolation of product-derived impurities

Infective baculovirus particles, rBV_i, which are the target product, were isolated by ultracentrifugation based on sucrose density gradients (Airenne et al., 2000), yielding standard rBV_i stocks. Briefly, primary clarification and concentration were accomplished by depth-filtration and tangential flow filtration using conditions recently described (Vicente et al., 2009). 3 μm retention Sartopure PP2 filter capsules, followed by 0.65 μm retention Sartopure PP2 filter capsules, were operated in series. Tangential flow filtration was run on an ÄKTAcrossflow system controlled by the UNICORN^{TM} software (all GE Healthcare, Uppsala, Sweden) with a 200 cm^2 Hydrosart^{TM} membrane with 100 kDa nominal molecular weight cut-off (MWCO) (Sartorius Stedim Biotech) at 35 mL/min retentate flow rate and a transmembrane pressure of 1.2 bar; buffer exchange to D-PBS was accomplished by continuous diafiltration as described elsewhere (Vicente et al., 2009).

rBV_i concentrated stocks were transferred into ultracentrifuge tubes on top of two discrete sucrose density layers: 8 mL of 50% (w/v) and 6 mL of 20% (w/v) sucrose in D-PBS (bottom); the tubes were centrifuged at 100,000 *g* and 4°C for 1 h. The virus bands were pooled, resuspended into 35 mL of ice-cold D-PBS, transferred into ultracentrifuge tubes containing 3 mL of 25% (w/v) sucrose in D-PBS, and centrifuged as above. The concentrated virus buffer was exchanged to D-PBS using a prepacked HiPrep^{TM} 26/10 desalting column coupled to an ÄKTAexplorer system (all GE Healthcare, Uppsala, Sweden).

Sterile microfiltration of final material was performed using Acrodisc^{TM} Syringe Filters with Supor^{TM} PES membrane (Pall, New York, USA) before storage at 4°C in the dark (Vicente et al., 2009). Purified rBV_i preparations were subjected to enzymatic digestion using subtilisin (Sigma-Aldrich, Steinheim, Germany) to produce glycoprotein deficient vectors, rBV_{gp64^-}, or lipid removal using Triton^{TM} X-100 (Sigma) to produce envelope deficient vectors, rBV_{env^-}. Briefly, 0.5 mL of a concentrated subtilisin stock, prepared in digestion buffer, was added to the purified particles resulting in a final subtilisin concentration of 1 mg/mL. The incubation was done for 2 h at 37°C, after which 5 μg/mL of phenylmethanesulphonylfluoride (Sigma) was added to suppress the protease; the material was stored at 4°C in the dark until use. Lipid removal of the rBV particles was performed by addition of a concentrated stock of 20% Triton X-100 to achieve a final concentration of 0.5% (v/v), followed by incubation of the samples at 37°C for 30 min. After both incubations, buffer is exchanged to D-PBS using a prepacked HiTrap^{TM} desalting column (GE Healthcare) coupled to an ÄKTAexplorer system to remove subtilisin or Triton X-100 from

the resulting baculovirus materials.

The number of genome containing particles was quantified by real-time PCR (qPCR) following the protocol described elsewhere (Vicente et al., 2009). Infective virus titers (IP) were determined with a flow cytometer-based assay (for rBVs-GFP) (Vicente et al., 2009; Karkkainen et al., 2009). To assess the presence of cholesterol in viral samples, Amplex^{TM} Red cholesterol assay kit (Molecular Probes, Eugene OR, USA) was used and DNA was measured using the Quant-iT^{TM} PicoGreen DNA assay kit (Molecular Probes).

5.2.3 Process derived-impurities

In this work reference biologicals have been used to study their isolated behaviors in the ion-exchange-based process. Host-cell dsDNA was obtained from an Sf9 insect cell culture after DNA extraction using the High Pure PCR template Acid Kit (Roche Diagnostics, Mannheim, Germany). Lipopolysaccharide (LPS) is of analytical grade from Sigma-Aldrich. Bovine serum albumin (BSA) is of analytical grade (> 98% electrophoresis purity) purchased from Merck KGaA (Darmstadt, Germany); the amount of covalent dimer in the freshly prepared BSA solutions is estimated to be ca. 6%, from analytical size-exclusion chromatography on a Superdex 200 column. All solutes were conditioned in 20 mM phosphate buffer at pH 6.8 with the specified NaCl supplementation.

5.2.4 Sensor surface preparation

Biacore gold sensor chip surfaces (Biacore/GE Healthcare, Uppsala, Sweden) were modified according to protocols described in the literature (Roper and Nakra, 2006; Vicente et al., 2010). 11-mercaptoundecanoid acid (MUA) (NanoThinks^{TM} ACID11 solution from Sigma-Aldrich, München, Germany) and 2-diethylaminoethylamine (DEAEA) (99% purity grade from Sigma-Aldrich) were used as thiolate for self-assembled monolayer (SAM) preparation and ligand coupling compound, respectively. The refractive index (RI) was monitored throughout the MUA-SAM immobilization procedure with a Leica AR200 digital hand-held refractometer (Leica Microsystems, Wetzlar, Germany). Briefly, the gold sensor chip surface was first equilibrated with ultra-pure, deionized water at 18.2 M$\Omega \cdot$cm. The surface was sanitized with 0.1 M NaOH and 1% Triton^{TM} X-100 (Sigma-Aldrich) and then re-equilibrated in 10 mM 4-Morpholineethanesulfonic acid (MES) (Sigma) buffer at pH 5.0. Ethanol was then used to washout the buffer and the surface was exposed directly to the NanoThinks ACID11 solution (5 mM MUA in ethanol) and left overnight in a closed compartment inside a laminar flow bench. The freshly formed SAM of MUA

was rinsed with ethanol and re-equilibrated with the 10 mM MES buffer previously used until the refractive index stabilized. The sensor chip was then docked in the SPR system, a Biacore^{TM} 2000 (Biacore/GE Healthcare), at this stage for DEAEA immobilization by amide coupling chemistry. The same MES buffer was used as running buffer for the duration of the immobilization procedure.

Freshly prepared solutions of 0.4 M 1-ethyl-3-(3-dimethylamino-propyl)carbodiimide hydrochloride (EDC) and 1.0 M N-hydroxysuccinimide (NHS) (amine coupling kit from Biacore/GE Healthcare) in water were mixed 1:1 and injected in a pulse of 200 μL at 20 μL/min to activate the terminal carboxyl group for amide bond formation. 1.0 M DEAEA in MES running buffer was added in serial 100 μL pulses at 20 μL/min until the SPR signal stabilized. Although there are four flow sensing cells available over the Biacore sensor chip, only one flow cell was derivatized with DEAE so that SPR sorption data from MUA could be compared against MUA-DEAE; the background was low as compared to the MUA-DEAE.

5.2.5 SPR experiments

The SPR experiments were performed on a Biacore 2000 system at 25°C. Product (rBV_i), product-related impurities (rBV_{gp64^-}, rBV_{env^-}, and gp64 glycoprotein) and process-related impurities (DNA, BSA, and LPS) were diluted to a given concentration (c_B) in 20 mM phosphate buffer at pH 6.8 with the specified NaCl supplementation (c_0). All buffers were prepared sterile and degassed prior to use in the equipment.

The experiments were performed at constant flow rate of running buffer and sample injection of 100 μL/min. Each run consisted of the following sequence of steps: (i) equilibration of the flow cell with running buffer at a given NaCl concentration (c_0); (ii) injection of 100 μL of analyte solution at given concentration (c_0, c_B); and (iii) desorption and equilibration with running buffer (again, at c_0). Before starting a new run, the flow cell was subjected to an aggressive desorption step using 100 μL of 1.5 M NaCl in 20 mM phosphate buffer at pH 6.8 ($c_{0,ref}$), and then cleaned/sanitized with 100 μL of 0.1 M NaOH for complete regeneration of the surface.

DEAE ligands and SAM's have been shown to be fully resistant to pulses of NaOH (or HCl) up to 1 M (Knoll et al., 1998). The baseline stability was controlled throughout the course of each experiment. All sensorgrams were duplicated by repeating each run once for confirmation of their reproducibility and surface regeneration.

5.3 SPR data analysis

SPR sensors measure small changes in the refractive index (RI) profile of the sample within the evanescent field above the sensor surface (Schuck, 1997). The fundamental equation for interpretation of an SPR sensor's response to an adsorbed film is (Jung et al., 1998)

$$R = \frac{m}{d_\mathrm{p}} \int_0^\infty \eta(z)\, e^{-z/d_\mathrm{p}}\, dz, \tag{5.1}$$

where R is the sensor's signal; $\eta(z)$, the RI at a distance z from the sensor surface; m, a proportionality constant; and d_p, the effective penetration depth of the evanescent electromagnetic field; for the case of our Biacore 2000 machine, $d_\mathrm{p} \approx 150$ nm. The maximum distance from the sensor surface that is effectively probed by the evanescent electromagnetic field is $z_\mathrm{max} \approx 5.3 d_\mathrm{p}$, because the truncation of the integral in Eq. (5.1) at that depth,

$$\frac{1}{d_\mathrm{p}} \int_0^{z_\mathrm{max}} \eta(z)\, e^{-z/d_\mathrm{p}}\, dz \approx 0.995, \tag{5.2}$$

shows that the cumulative effect of larger distances contributes less than 0.5% to the SPR signal.

Within the usual range of SPR applications, the sample's refractive index is, to a good approximation, the weighted arithmetic mean of the RI's of its isolated constituents with weights equal to their volume fractions in the sample (Jung et al., 1998). This is the basis for converting the SPR signal into a surface concentration.

In a typical ion-exchange experiment, the solute (B) is dissolved into a buffer solution whose ionic strength is controlled by a dissolved salt (0). By picturing the adsorbed film as shown in the schematic of Fig. 5.1, it is possible to work out explicit formulae for deconvoluting the SPR signal into adsorbate concentration, c_m, bulk adsorptive concentration, c_B, and salt concentration, c_0 (Vicente et al., 2010).

Under general conditions (i.e., measurable solute adsorption), and assuming a constant pH, the SPR signal shift, ΔR, obtained as response to a typical ion-exchange adsorption process on the sensor surface is given by (Vicente et al., 2010)

$$\Delta R = (m_\mathrm{B} - m_0 c_0 v_\mathrm{B})\,[c_\mathrm{m} + \phi_\mathrm{m}(c_\mathrm{B} - c_\mathrm{m})] + m_0(c_0 - c_{0,\mathrm{ref}}), \tag{5.3}$$

where m_0 and m_B are the calibration constants associated with the SPR response to changes in c_0 and c_B, respectively; v_B, the molar volume of the adsorbed solute; c_m, the solute concentration in the volume of the adsorbed monolayer; $\phi_\mathrm{m} = \exp(-d_\mathrm{m}/d_\mathrm{p})$ where

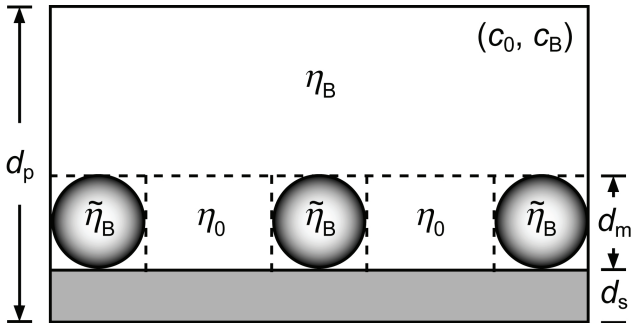

Figure 5.1: *Schematic diagram of an adsorbate monolayer over a ligand-functionalized surface of thickness d_s in the Biacore sensor chip flow cell. The thickness of the adsorbed monolayer, d_m, is roughly equal to the diameter of the adsorbed molecules molecules. d_p is the effective penetration depth of the evanescent electromagnetic field; for the case of the Biacore 2000 machine, $d_p \approx 150$ nm. The bulk aqueous solution has salt concentration c_0 and solute concentration c_B; the isolated (dry) solute's refractive index is $\tilde{\eta}_B$. Aqueous solution is assumed to fill the gaps between adsorbed solute molecules, with salt concentration c_0 and refractive index η_0.*

d_m is the thickness of the adsorbed monolayer and d_p the characteristic penetration depth of the evanescent electromagnetic field (Fig. 5.1); and $c_{0,ref}$, the salt concentration in the buffer solution used to equilibrate the flow cell and to define the baseline of the SPR's signal. The adsorbed concentration, c_m, can be converted into a surface concentration through the simple formula $q = d_m c_m$.

The constant m_0 can be determined from the slope of the linear fitting of ΔR against c_0 for a set of experiments on buffer solutions with different salt concentrations, but no solute ($c_B = c_m = 0$). The constant m_B, on the other hand, can be obtained from the slope of the linear part of the plot of ΔR vs c_B for a constant, large value of c_0. At high salt concentrations, most of the ion-exchange sites on the surface are shielded and the available binding sites are completely saturated for moderately small values of c_B. For larger values of c_B, for which c_m is constant, Eq. (5.3) shows that ΔR is a linear function of c_B with slope $(m_B - m_0 c_0 v_B)\phi_m$ if the buffer solution is not changed.

Solving Eq. (5.3) for c_m gives

$$c_m = \frac{\Delta R - m_0(c_0 - c_{0,ref})}{(1-\phi_m)(m_B - m_0 c_0 v_B)} - \frac{\phi_m}{1-\phi_m} c_B. \tag{5.4}$$

Equations (5.3) and (5.4) can be applied to the complex baculovirus system under study if the d_m values for the different species comprising the bioreaction bulk are measured or estimated (see Tables 5.1 and 5.2).

5.4 Adsorption/desorption rate model

In this section an adsorption/desorption rate model that quantitatively explains the SPR sensorgrams probing the interactions of the studied biomolecules with the DEAE-SAM surface is proposed. A binding/elution rate model, using BSA as a reference protein, was validated elsewhere (Vicente et al., 2010); here, we demonstrate that a similar formulation is equally applicable to the complex biological system of baculoviruses.

Let us first consider a reaction model for the intrinsic adsorption kinetics and assume, for the moment, that the mass transport by convection and diffusion does not influence neither the adsorption nor the desorption kinetics. The validity of this assumption will be discussed in detail later on when the experimental results are presented.

As indicated in a previous section, each SPR experiment consisted of an adsorption/desorption sequence, where the adsorption step consisted of injecting buffer solution with given salt and solute concentrations through the sensor chip; after binding, buffer alone with the same salt concentration was injected to monitor the desorption kinetics. Partial irreversible binding of the biomolecules onto the DEAE-SAM surface was observed (or subject to an extremely slow desorption rate) because the elution step consistently gave rise to a well-defined, residual equilibrium plateau whose height decreased with increasing salt concentration in the buffer.

Given this observation, it is assumed that only part of the solute adsorbs reversibly, whereas the other part binds irreversibly to the stationary phase. In our previous study with BSA (Vicente et al., 2010) it was observed that irreversible binding took place from the bulk solution as well as from the reversibly adsorbed phase; moreover, irreversible protein adsorption from the reversibly adsorbed phase was seen to be likely dependent on the frequency of collisions, or interactions, between the proteins in the bulk and those in the reversibly adsorbed phase. A similar adsorption/desorption mechanism is assumed to apply here. The mechanism is illustrated in Fig. 5.2.

Let q_1 be the concentration of irreversibly bound solute and q_2 the solute concentration in the reversibly adsorbed phase. The rate model for irreversible binding to the DEAE-SAM surface is

$$\frac{dq_1}{dt} = k_\mathrm{r} c_\mathrm{B} (\tilde{q}_1^\infty - q_1) + k'_\mathrm{r} c_\mathrm{B} q_2, \tag{5.5}$$

where k_r is the rate constant for irreversible adsorption from the bulk, k'_r is the rate constant for irreversible binding from the reversibly adsorbed phase, and $\tilde{q}_1^\infty$ is the capacity of the stationary phase for irreversible binding. To make the analysis as general as possible, the

Table 5.1: *Characteristic features of baculovirus and baculovirus-derived impurities.*

Species	Size	Structure	Infectivity
rBV_i	$d_m = 120$ nm $L_m = 350$ nm		Yes; contains gp64 + envelope + genome with capsid
rBV_{gp64^-}	$d_m = 100$ nm $L_m = 340$ nm		No; gp64 peplomers lacking
rBV_{env^-}	$d_m = 60$ nm $L_m = 300$ nm		No; envelope lacking
gp64 trimers	$d_m = 15$ nm		N.A.

Table 5.2: *Characteristic features of process-related impurities.*

Impurity	Structure
BSA	protein with diameter $d_m = 5.4$ nm
DNA	Linear structure with equivalent diameter $d_m = 50$ nm
LPS	Linear structure with equivalent diameter $d_m = 15$ nm

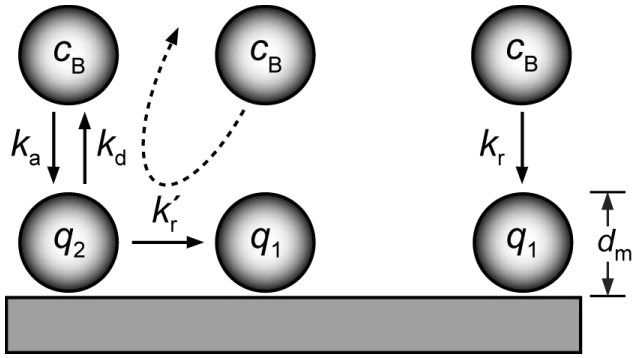

Figure 5.2: *Kinetic model for reversible/irreversible adsorption; d_m, is roughly equal to the diameter of the adsorbed solute. k_a and k_d are the forward and reverse rate constants for reversible adsorption from the bulk solution, respectively; k_r, the rate constant for irreversible adsorption from the bulk solution; and k_r', the rate constant for irreversible adsorption from the reversibly adsorbed phase.*

capacity $\tilde{q}_1^\infty$ is assumed to be apparent, because some of the sites for irreversible binding may be shielded by the presence of reversibly adsorbed solutes. Hence, we write

$$\tilde{q}_1^\infty = q_1^\infty - \sigma_{12} q_2, \tag{5.6}$$

where σ_{12} is a steric factor: it gives the number of irreversible binding sites shielded by the reversibly adsorbed solutes.

Assuming a Langmuirian kinetic model for reversible adsorption, one obtains

$$\begin{aligned} \frac{dq_2}{dt} &= k_\mathrm{a} c_\mathrm{B} (\tilde{q}_2^\infty - q_2) - k_\mathrm{d} q_2 - k'_\mathrm{r} c_\mathrm{B} q_2 \\ &= k_\mathrm{a} c_\mathrm{B} (\tilde{q}_2^\infty - q_2) - (k_\mathrm{d} + k'_\mathrm{r} c_\mathrm{B}) q_2, \end{aligned} \tag{5.7}$$

where k_a and k_d are the forward and reverse rate constants for reversible adsorption, respectively, and $\tilde{q}_2^\infty$ is the capacity of the stationary phase for reversible binding. Again, this adsorption capacity is assumed to be apparent, because some of the sites for reversible binding may be shielded by the presence of irreversibly adsorbed proteins:

$$\tilde{q}_2^\infty = q_2^\infty - \sigma_{21} q_1. \tag{5.8}$$

At equilibrium,

$$\left(\overline{\frac{dq_1}{dt}} \right) = \left(\overline{\frac{dq_2}{dt}} \right) = 0, \tag{5.9}$$

which allows closed-form expressions for the adsorption isotherms, $\overline{q}_1(c_\mathrm{B})$ and $\overline{q}_2(c_\mathrm{B})$, to be determined.

The functional dependency between $\overline{q}_1$ and $\overline{q}_2$ can be derived by applying the equilibrium conditions to Eqs. (5.5) and (5.7); the result is

$$\overline{q}_1 = q_1^\infty + \left(\frac{k'_\mathrm{r}}{k_\mathrm{r}} - \sigma_{12} \right) \overline{q}_2. \tag{5.10}$$

If the shielding can be neglected, Eq. (5.10) simplifies to

$$\overline{q}_1 = q_1^\infty + \left(\frac{k'_\mathrm{r}}{k_\mathrm{r}} \right) \overline{q}_2, \tag{5.11}$$

which shows that, under these simplified conditions, $\overline{q}_1$ varies linearly with $\overline{q}_2$ with positive ordinate and slope.

The adsorption isotherm (i.e., the equilibrium dependency of $\overline{q}_2$ with c_B), for the general

case where shielding cannot be neglected, is

$$\overline{q}_2 = \frac{(q_2^\infty - \sigma_{21} q_1^\infty) k_\mathrm{a} c_\mathrm{B}}{k_\mathrm{d} + [k'_\mathrm{r} + k_\mathrm{a} + \sigma_{21}(k'_\mathrm{r}/k_\mathrm{r} - \sigma_{12}) k_\mathrm{a}] c_\mathrm{B}}, \tag{5.12}$$

which is a Langmuir-type isotherm, i.e.,

$$\overline{q}_2 = \frac{\gamma b_2 c_\mathrm{B}}{1 + b_2 c_\mathrm{B}}, \tag{5.13}$$

where

$$b_2 = \frac{k'_\mathrm{r} + k_\mathrm{a}[1 + \sigma_{21}(k'_\mathrm{r}/k_\mathrm{r} - \sigma_{12})]}{k_\mathrm{d}}, \quad \gamma b_2 = \frac{k_\mathrm{a}(q_2^\infty - \sigma_{21} q_1^\infty)}{k_\mathrm{d}}. \tag{5.14}$$

For a typical ion-exchange process, the saturation capacities, q_1^∞ and q_2^∞, and hence the total saturation capacity, $q^\infty = q_1^\infty + q_2^\infty$, are modulated by the salt concentration. The higher the counterion concentration, the lower the binding of a given solute assuming that no other factors influence the overall adsorption process in the SPR sensor chip. An empirical correlation of the form

$$q^\infty = q_0^\infty e^{k c_0}, \tag{5.15}$$

is adopted here, where q_0^∞ is the maximum attainable adsorption capacity at residual ionic strength and $k < 0$ is an empirical constant.

5.5 Results and discussion

5.5.1 Calibration of Biacore signal

The Biacore signal was calibrated with various solutions with different salt (c_0) and BSA (c_B) concentrations and a baseline defined for a buffer solution with salt concentration $c_{0,\mathrm{ref}} = 1.5$ M NaCl. Salt solutions with different c_0 values were injected into the Biacore cell and the corresponding signal shifts measured. The linear fitting (with intercept set to zero) of ΔR against $(c_0 - c_{0,\mathrm{ref}})$ yielded $m_0 = 9898.1$ RU/(g/L) with an excellent regression coefficient ($r^2 = 0.9998$). This calibration accounts for the salt concentration effect without the presence of solute in suspension.

To account for the effect of protein in solution ($c_0, c_\mathrm{B} > 0$) a set of BSA concentrations in buffer with salt concentration $c_0 = c_{0,\mathrm{ref}} = 1.5$ M NaCl was used. This salt concentration was high enough to reduce BSA adsorption to a small level, so that the plot of the Biacore signal shifts against c_B yielded a straight line in accordance with Eq. (5.3) when c_m has a constant value (when $c_0 = c_{0,\mathrm{ref}}$ the adsorbed mono-

layer is completed for small values of c_B because the saturation capacity of the DEAE-SAM surface is very low at that salt concentration). The linear fitting of ΔR vs c_B yielded a slope $\phi_m(m_B - m_0 v_B c_{0,ref}) = 164.43$ RU/(g/L) with a good regression coefficient, $r^2 = 0.9986$; with $m_0 v_B c_{0,ref} = 10.92$ RU/(g/L), it is possible to determine $m_B = 164.43/\phi_m + 10.92 = 179.79$ RU/(g/L).

Equation 5.4 can now be applied for converting the SPR signal (ΔR) into concentration values of adsorbed biomolecule, c_m (g/L) and q (g/dm^2) $= 10^{-8} d_m c_m$, with the d_m (nm) estimated for each of the different biomolecules under study (Tables 5.1 and 5.2).

5.5.2 Applicability of sorption model to a complex biological system

As a matter of convenience for a future design of the ion-exchange chromatographic process, a key step of current downstream purification strategy (Vicente et al., 2009), it is best to split the biological bulk into three cuts, or fractions—(i) the product, (ii) the main product-related impurities, and (iii) the main process-related impurities—and to define for each fraction the key components governing its chromatographic behavior.

In the present case, the infective baculovirus (rBV_i), which is the integral/functional particle, is assumed to be the desired product. The baculovirus defective in gp64 glycoprotein trimers (rBV_{gp64-}) on its envelope (if any) and the envelope defective baculovirus (rBV_{env-}), i.e., rBV_i without envelope (a "naked" capsid) or with any disrupted version of it, are considered to be the main product-related impurities; gp64 viral glycoprotein is a byproduct of the production/degradation of rBVs and can be also included as a product-related impurity; this protein has been added to the present study in order to compare it with the rBV particles, either infective (rBV_i) or deficient in gp64 (rBV_{gp64-}). BSA is considered as a host cell protein analogue; LPS and host insect DNA are references for endotoxin and DNA contaminants, respectively; these are established as the three major process-related impurities (Vicente et al., 2009).

Each target biomolecule was injected into the Biacore sensor cell, under various conditions of solute and salt concentrations, and the corresponding SPR sensorgrams analyzed using the analytical and modeling tools described above. The conversion of the experimental SPR sensorgram, $\Delta R(t)$, expressed in RU units, into and equivalent sensorgram of adsorbed concentration, $q(t)$, expressed in g/dm^2, was done directly using the aforementioned calibrations, assuming the following density constants or inverse specific volumes, $1/v_{iB}$: 1.36 g/mL for BSA and gp64 (Bosma and Wesselingh, 1998), 1.2 g/mL for the

recombinant baculovirus particles (Mazzone, 1998), 1.55 g/mL for dsDNA (Sambrook and Russel, 2001), and 1.4 g/mL for LPS (Ulevitch and Johnston, 1978); the assumed adsorption layer thicknesses, d_{m}, are those listed in Tables 5.1 and 5.2.

The proposed kinetic model was tested on the baculoviruses, baculovirus-related impurities, and major process-related impurities. Values of $\overline{q}_1$ and $\overline{q}_2$ were obtained from the horizontal plateaus of the adsorption/desorption steps for each of the previously isolated biological solutes.

Figure 5.3 shows the experimental SPR sensorgrams for one of the studied biomolecules —the product, $\mathrm{rBV_i}$— using the binding/elution procedure; an explanatory nomenclature is superposed on the topmost sensorgram. The sensorgrams shown in Fig. 5.3 are representative of the sensorgrams obtained for the other biomolecules: in all cases, an initial steep rise is observed, followed by a curved response typical of a pseudo-first-order kinetics, then a steep fall in the signal upon elution of the sensor cell, and finally a shallow decaying curve that stabilizes as an horizontal plateau. BSA was seen to desorb slower than the larger biomolecules. Using Eq. (5.4), the SPR sensorgrams of Fig. 5.3 can be converted into equivalent surface chromatograms of adsorbed concentration; the latter are shown in Fig. 5.4.

Before proceeding with the discussion of the results it is important to assess whether or not our SPR experiments were limited by convective-diffusive mass transport. Previous studies showed that diffusion through the unstirred fluid film over the sensor surface can limit the binding kinetics under certain conditions (Glaser, 1993; Hall et al., 1996; Schuck, 1997; Myszka et al., 1997, 1998; Goldstein et al., 1999; Mason et al., 1999). Especially at low flow rates, large biological particles, like the ones evaluated here, do present diffusion restrictions (Roper and Nakra, 2006); we have observed this effect in exploratory experiments run at low flow rates.

However, as shown next, for the flow rate used in our SPR runs, 100 μL/min, the experiments were not limited by mass transport. A two-compartment mass transport model (Myszka et al., 1998) is usually employed to distinguish intrinsic adsorption rates from slower diffusive mass transport of the solute across the fluid layer adjacent to the sensor surface. The model can be written as

$$h_{\mathrm{i}}\frac{dc_{\mathrm{B}}}{dt}+\left(\frac{dq_1}{dt}+\frac{dq_2}{dt}\right)=k_{\mathrm{m}}(c_{\mathrm{B}}^{\mathrm{o}}-c_{\mathrm{B}}), \tag{5.16}$$

where k_{m} is the transport coefficient describing the effective diffusional flux of solute from an outer compartment, where its concentration is $c_{\mathrm{B}}^{\mathrm{o}}$, into an inner compartment adjacent

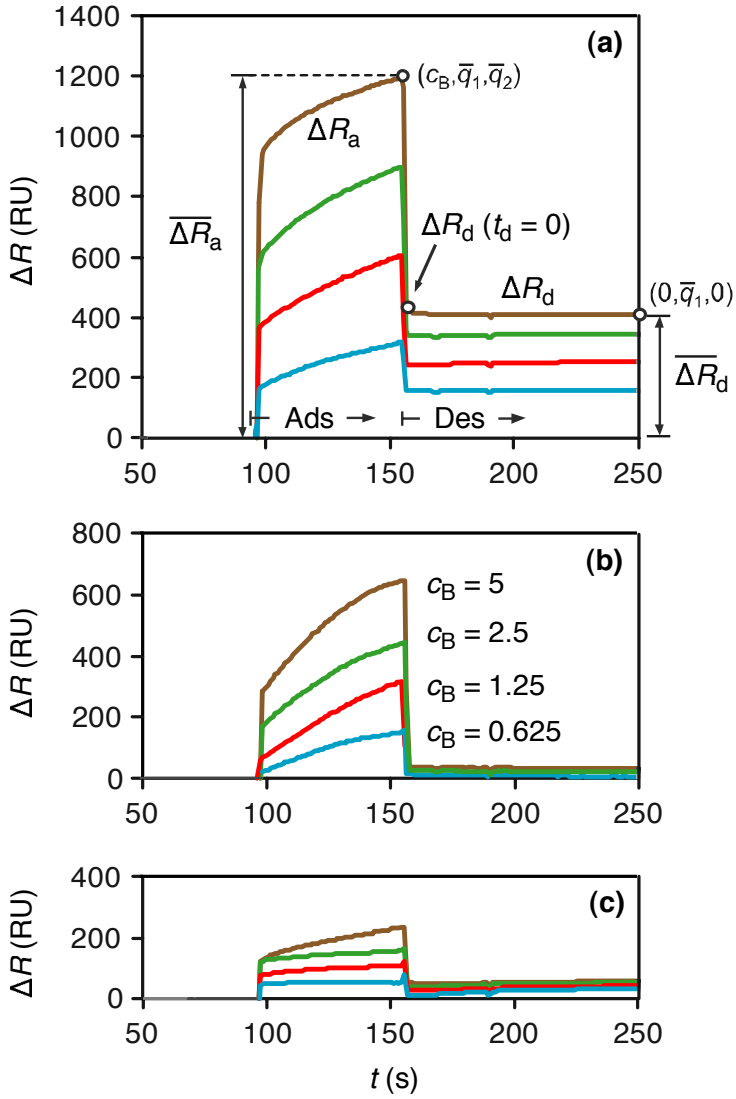

Figure 5.3: *Experimental sensorgrams of adsorption/desorption runs for different rBV_i and salt concentrations: (a) $c_0 = 0.023$ M, (b) $c_0 = 0.50$ M, and (c) $c_0 = 1.26$ M; the rBV_i concentrations in $(10^8$ pfu$)/$mL are indicated in the middle graphic and are same for all three graphics. The notation attached to the topmost sensorgram has the following meaning: subscript 'a', binding/adsorption step ('Ads'); subscript 'd', elution/desorption step ('Des'); ΔR, SPR signal; overbar, equilibrium value; $(c_B, q_1, q_2) =$ (bulk solute concentration, irreversibly adsorbed concentration, reversibly adsorbed concentration).*

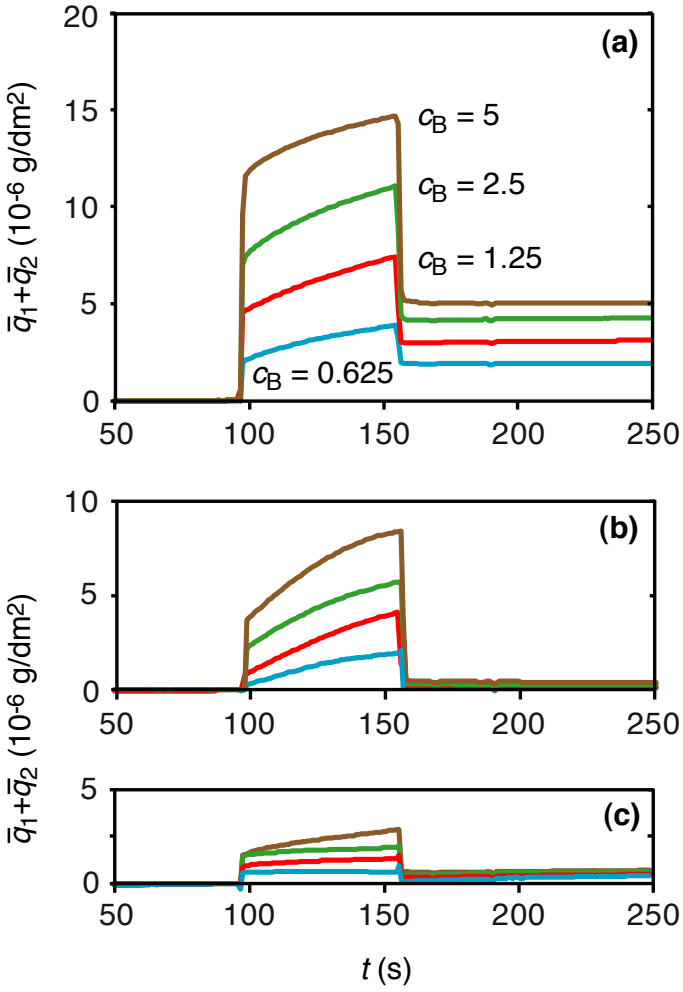

Figure 5.4: *Conversion of the experimental SPR sensorgrams shown in Fig. 5.3, for the rBV_i binding/elution runs, into equivalent surface chromatograms of adsorbed concentration by means of Eq. (5.4). Salt concentrations: (a) $c_0 = 0.023$ M, (b) $c_0 = 0.50$ M, and (c) $c_0 = 1.26$ M; the rBV_i concentrations in $(10^8$ pfu$)/mL$ are indicated in the top graphic and are same for all three graphics.*

to the sensor surface, where its concentration is c_B; h_i is the height of the inner compartment and its value is somewhat arbitrary, because it has been shown that, after a brief initial transient, the binding kinetics are independent of the size of the inner compartment (Goldstein et al., 1999).

To a good approximation (Lok et al., 1983; Sjölander and Urbaniczky, 1991),

$$k_\mathrm{m} = 1.282 \left(\frac{3}{2} \frac{\overline{u} D^2}{hl} \right)^{1/3}, \tag{5.17}$$

where $\overline{u} = Q/(hw)$ is the average velocity of the fluid in the flow cell; Q, the volumetric flow rate; h and w, the height and width of the flow cell; l, the length of the sensor surface; and D, the diffusion coefficient.

The diffusion coefficient for the fastest diffusing molecule of our set, BSA, is $D_\mathrm{BSA} = 9 \times 10^{-7}$ cm^2/s (Schmitz and Lu, 1983), whereas for the largest particles, say rBV$_\mathrm{i}$, the diffusion coefficient is $D_{\mathrm{rBV_i}} \approx 10^{-7}$ cm^2/s (Mazzone, 1998); from Eq. (5.17), the mass-transfer coefficient for the latter case is $k_\mathrm{m} \approx 3 \times 10^{-4}$ cm/s at 100 μL/min. Transport effects will not influence the adsorption kinetics if $k_\mathrm{m} \gg k_\mathrm{r} q_1^\infty$ and $k_\mathrm{m} \gg k_\mathrm{a} q_2^\infty$; these two inequalities are safely verified for our system: $k_\mathrm{m} \gg k_\mathrm{r} q_1^\infty \approx 3 \times 10^{-6}$ cm/s and $k_\mathrm{m} \gg k_\mathrm{a} q_2^\infty \approx 7 \times 10^{-6}$ cm/s, where we majored $q_1^\infty = 2 \times 10^{-7}$ g/cm^2, $q_2^\infty = 2 \times 10^{-7}$ g/cm^2, $k_\mathrm{a} = 10^{-2}$ dm$^3 \cdot$ g $\cdot$ s^{-1} and $k_\mathrm{r} = 10^{-2}$ dm$^3 \cdot$ g$^{-1} \cdot$ s^{-1}, the two latter values obtained from model fitting.

The sensorgrams for rBV$_\mathrm{i}$ shown in Fig. 5.3, as well as those for the other biomolecules, can now be interpreted without any worries about mass-transport issues. Although the primary objective of this work is to report on adsorption equilibrium data, in section 5.7 we provide an analytical solution for the kinetic model and SPR response in the absence of mass-transport limitations. Here we focus on the shape and equilibrium plateaus of the SPR sensorgrams.

The initial steep rise in the SPR signal upon start of the adsorption step is the result of replacing the buffer solution ($c_0, c_\mathrm{B} = 0$) with the injected sample ($c_0, c_\mathrm{B} = c_\mathrm{B}^\mathrm{o}$) over the sensor surface. The binding kinetics generates the convex curvature in the SPR response; this part of the sensorgram is described by Eq. (5.3) with c_B fixed at c_B^o, $c_\mathrm{m} = (q_1 + q_2)/d_\mathrm{m}$, and q_1 and q_2 given by the kinetic model defined by Eqs. (5.5)–(5.8). Under equilibrium conditions, the SPR signal stabilizes at an upper horizontal plateau, corresponding to $(c_\mathrm{B}, q_1, q_2) = (c_\mathrm{B}^\mathrm{o}, \overline{q}_1, \overline{q}_2)$, from where $\overline{q}_1 + \overline{q}_2$ can be determined.

Our SPR experiments with BSA showed that the total BSA binding capacity of the

derivatized surface is roughly 0.81 mg/m^2 at 25 mM salt concentration (Vicente et al., 2010); this value is less than the 5 mg/m^2 typically found for a protein monolayer. Since the binding capacity is strongly dependent on the ligand density, it appears that the ligand density was low in our MUA-DEAE surfaces. Under such conditions, bound biomolecules are expected to spread over the derivatized surface with a mean distance between neighboring molecules large enough for the shielding to have only a mild effect. This is also supported by the small values of the shielding factors obtained for BSA from the fitting of the full kinetic model. We have thus assumed in the analysis of our SPR experiments that the shielding effect can be neglected and that the binding kinetics is given by Eqs. (5.23) and (5.24) (see section 5.7).

In the elution step, buffer alone is injected into the SPR cell to monitor the desorption kinetics. The SPR response for this step is given by Eq. (5.3) with $c_{\mathrm{B}} = 0$, $c_{\mathrm{m}} = (q_1 + q_2)/d_{\mathrm{m}}$, $q_1 = \overline{q}_1$, and q_2 governed by Eq. (5.7). The steep fall in the SPR signal upon start of the elution step is the result of the cooperative effects of replacing the sample injected in the adsorption step (c_0,$c_{\mathrm{B}} = c_{\mathrm{B}}^{\mathrm{o}}$) by buffer alone ($c_0$,$c_{\mathrm{B}} = 0$) and of desorbing the reversibly bound solute, q_2. At the end of the elution step, the horizontal plateau in the SPR signal is due to the residual solute that is irreversibly bound to the derivatized surface. This residual horizontal plateau corresponds to $(c_{\mathrm{B}}, q_1, q_2) = (0, \overline{q}_1, 0)$. Thus the difference between the upper and lower plateaus, $(c_{\mathrm{B}}^{\mathrm{o}}, \overline{q}_1, \overline{q}_2) - (0, \overline{q}_1, 0)$, after the elution of solute from the bulk solution is taken into account, gives the equilibrium concentration of the reversibly adsorbed phase, $\overline{q}_2$.

As expected, for a fixed salt concentration in the buffer the height of the SPR sensorgrams, expressed in RU units, increases with increasing biomolecule concentration in the injected sample. On the other hand, the height of the SPR sensorgrams decreases strongly with increasing salt concentration in the buffer. The impact of salt concentration in the buffer is directly observed in the equilibrium value of ΔR_{a}, measured at the end of the adsorption step, and that of ΔR_{d}, measured after extended elution; these values are denoted in Fig. 5.3 by an overbar, as do all equilibrium variables in this work.

The dissolved salt in the buffer decreases the heights of the SPR sensorgrams for two reasons. The first one is the modulation of the ion-exchange interactions between the adsorbate molecules and the derivatized surface by the salt counter ion, Cl^-; this effect is visible when the sensorgrams are converted into surface chromatograms, such as those depicted in Fig. 5.4. The second reason is the decrease in the difference between the refractive index of the biomolecule and that of the buffer solution when the salt concentration is

increased. This effect can be understood from the schematic of Fig. 5.1 and from Eq. (5.3), the latter showing that ΔR is proportional to $(m_B - m_0 c_0 v_B)$: increasing c_0 will decrease ΔR for the same amount of adsorbed solute. The reason for this is a volume displacement effect: when a biomolecule adsorbs on the surface it displaces the volume of fluid that it is going to replace adjacent to the sensor surface; thus, the local refractive index will change proportionally to $\tilde{\eta}_B - \eta_0$ and not just to $\tilde{\eta}_B$ (see Fig. 5.1 for notation).

Upon conversion of RU into concentration units, Fig. 5.5 provides a direct overview of the effect of the salt concentration on the rBV_i's adsorption isotherm. It can be seen that both the irreversible and reversible parts of the overall adsorption isotherm are sensitive functions of the salt concentration; this is in agreement with the typical ion-exchange-type mechanism occurring in ion-exchange chromatography.

Figure 5.6 provides evidence that the proposed kinetic model is applicable to the biomolecules under study; indeed, the positive slopes and ordinates obtained from the good linear regressions of $\overline{q}_2$ vs $\overline{q}_1$ at all tested ionic strengths corroborate the applicability of Eq. (5.11). Moreover, the inverse plots of $1/\overline{q}_1$ and $1/\overline{q}_2$ against $1/c_B$ in Fig. 5.7 show that the good quality of the linear regressions is in agreement with Eq. (5.12), which expresses $q_2(c_B)$ as a Langmuir-type isotherm. Altogether, the results show that our kinetic sorption model is well suited to quantitatively explain the sensorgrams obtained in the Biacore machine. Similar trends have been observed for the remaining biological species considered in this study, including the impurities (data not shown). Thus, it appears that the sorption model proposed in the present work is sufficiently general for it to be applicable to the complex biologics of the baculovirus system.

5.5.3 Prediction of total adsorption capacities

The variations of the total adsorption capacities, including both reversible and irreversible components, with salt concentration show the typical trends observed in an ion-exchange process, in agreement with what was observed for the BSA protein model (Vicente et al., 2010). Indeed, the use of empirical fittings of the form given by Eq. (5.15), and shown in Figs. 5.8 and 5.9, is consistent with an ion-exchange-type mechanism governed by the salt concentration. One should note, though, that other effects, such as steric hindrance occurring in a typical chromatographic matrix, are not considered here. Exclusion effects, perturbing the typical dynamic binding capacity behavior as a function of salt concentration, have been reported in the literature, especially for large particles, such as virus-like particles (Vicente et al., 2008) or monoclonal antibodies (Harinarayan et al., 2006).

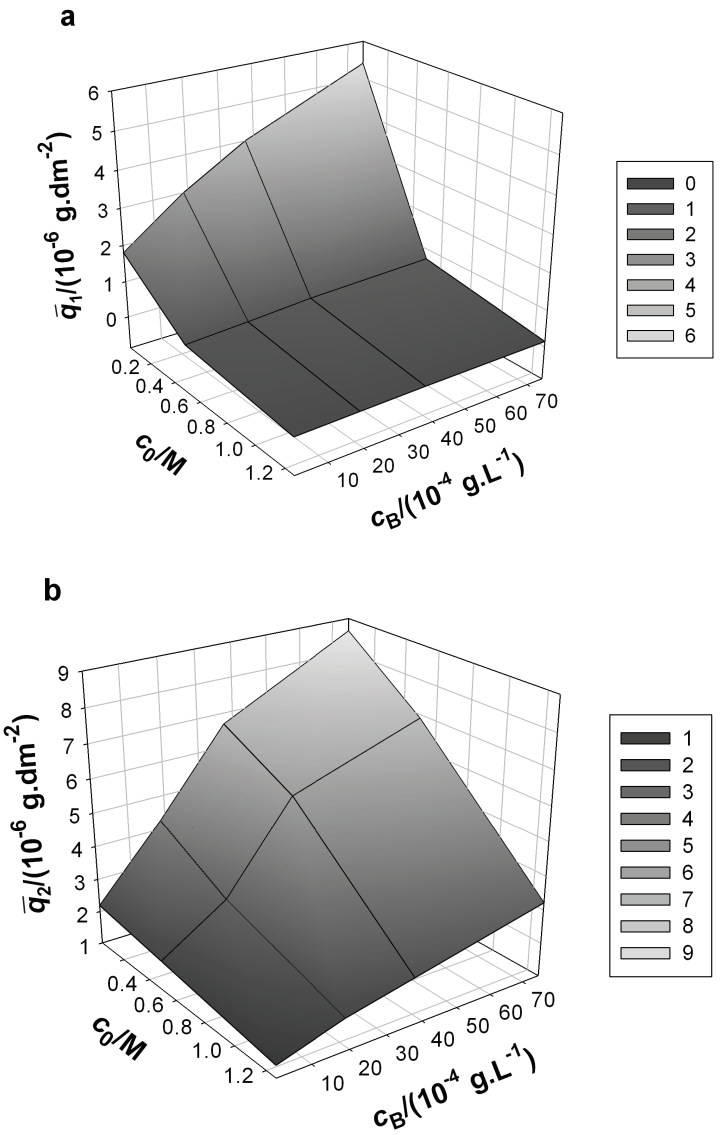

Figure 5.5: *Adsorption equilibrium of rBV*$_\mathrm{i}$ *particles: (a) irreversible component,* $\overline{q}_1$ *vs* (c_B, c_0)*; and (b) reversible component,* $\overline{q}_2$ *vs* (c_B, c_0)*;* c_B *for infective baculoviruses is calculated assuming a global particle weight of* 1.5×10^{-15} *g/pfu (Ilic et al., 2004).*

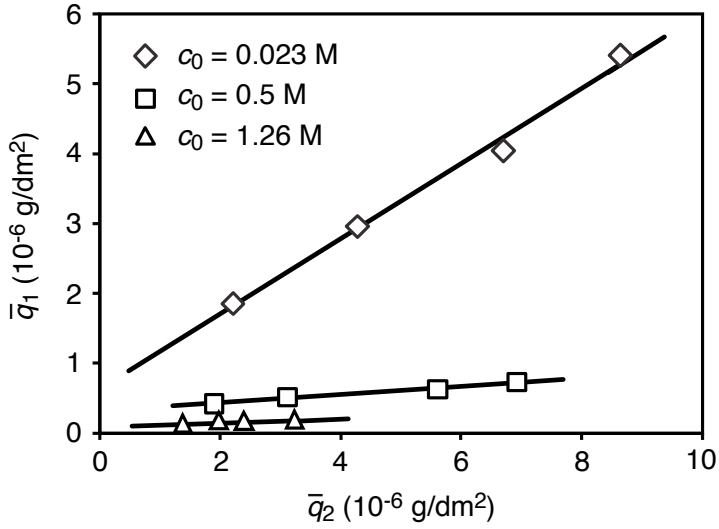

Figure 5.6: *Experimental plot of $\overline{q}_1$ against $\overline{q}_2$ (symbols) for rBV_i and corresponding fittings of Eq. 5.15 (lines).*

It can be observed that BSA, used here as an analogue of an adsorbing host-cell protein, endotoxin, and DNA show different binding capacities, which can be directly correlated with the different retention times obtained in chromatography runs. Retention times are the most fundamental data required to design a chromatographic process. However, the adsorption/desorption data obtained here required 1200-fold less material than that employed in a typical analytical chromatographic experiment. Moreover, Fig. 5.9 gives a clear indication that the DEAE-SAM surface has a much lower adsorption capacity for the product-related impurities, either non-enveloped baculoviruses or baculoviruses deficient in the external gp64 glycoprotein (essential for virus functionality (Monsma et al., 1996)), than for the desired/complete virus. Such information is valuable for shedding light on the characterization of the product pools after an ion-exchange chromatography step and contributing to select the best conditions to improve product quality and potency. For instance, it can be concluded from Figs. 5.8 and 5.9 that a salt concentration below 0.5 M would be optimal to obtain improved selectivity in the anion-exchange chromatographic process.

5.6 Conclusions

Sorption rates onto a micrometric derivatized surface, containing an ion-exchange functional DEAE group, have been measured and analyzed by SPR spectroscopy. A kinetic

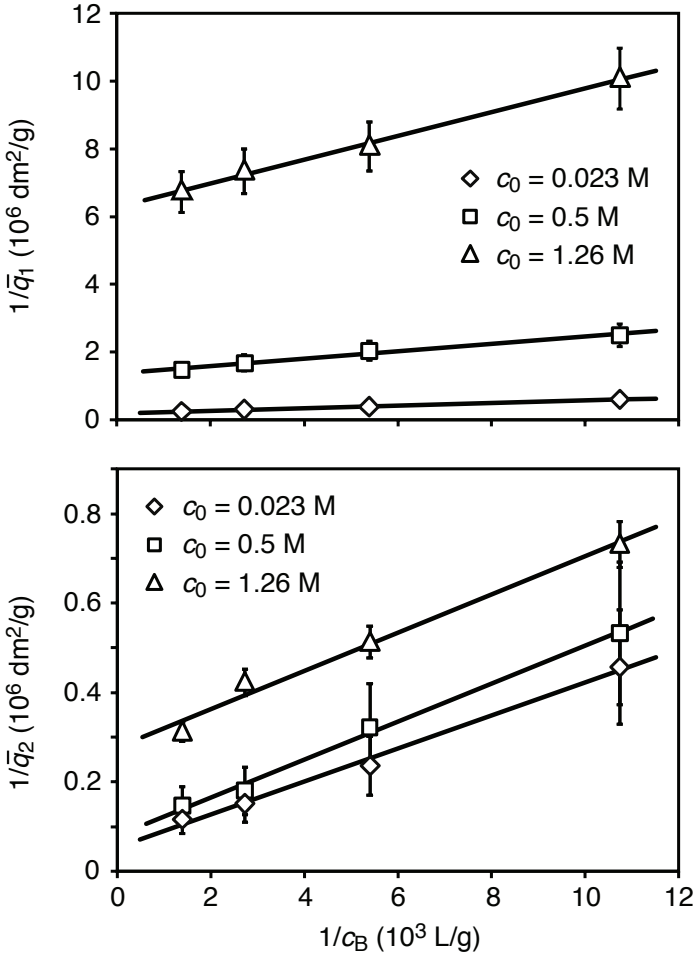

Figure 5.7: *Inverse plots for rBV_i particles: (a) $1/q_1$ vs $1/c_B$; (b) $1/q_2$ vs $1/c_B$; c_B for infective baculoviruses is calculated assuming a global particle weight of 1.5×10^{-15} g/pfu.*

model, incorporating two different adsorption mechanisms, was used to explain the SPR sensorgrams obtained for a complex biological system of enveloped viral vectors. The model assumes that a fraction of the biomolecules adsorbs reversibly according to a Langmuirian kinetic model, whereas the other fraction binds irreversibly to the stationary phase. Using the SPR experiments it was possible to determine the adsorption isotherms for different salt concentrations. The results provided evidence that the DEAE-SAM derivatized surface mimics well an ion-exchange surface, as far as intrinsic ion-exchange-related interactions are concerned, without considering transport or exclusion phenomena present in a real chromatographic matrix.

A model enveloped viral system has been studied as an example of a promising viral vector for clinical therapies – recombinant baculoviruses. The system was conveniently

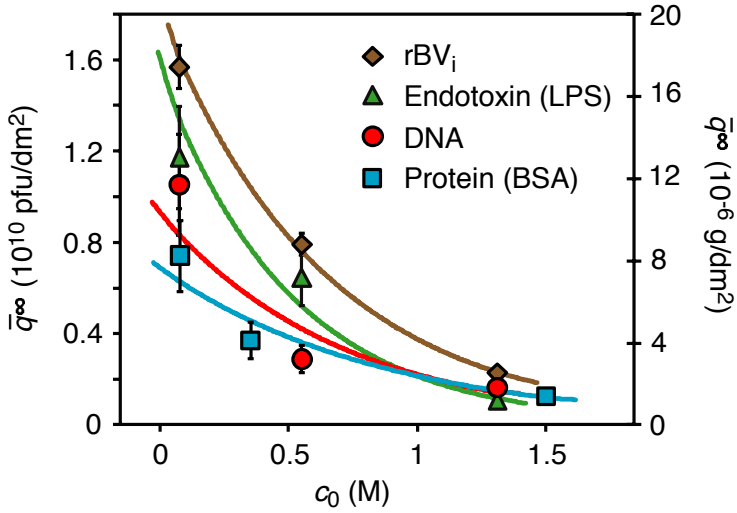

Figure 5.8: *Total adsorption capacity, $\overline{q}^{\infty} = \overline{q}_1^{\infty} + \overline{q}_2^{\infty}$, as a function of salt concentration, c_0, for rBV_i and major process-related impurities. rBV_i concentrations are read on the lefthand ordinate axis and all the others on the righthand ordinate axis.*

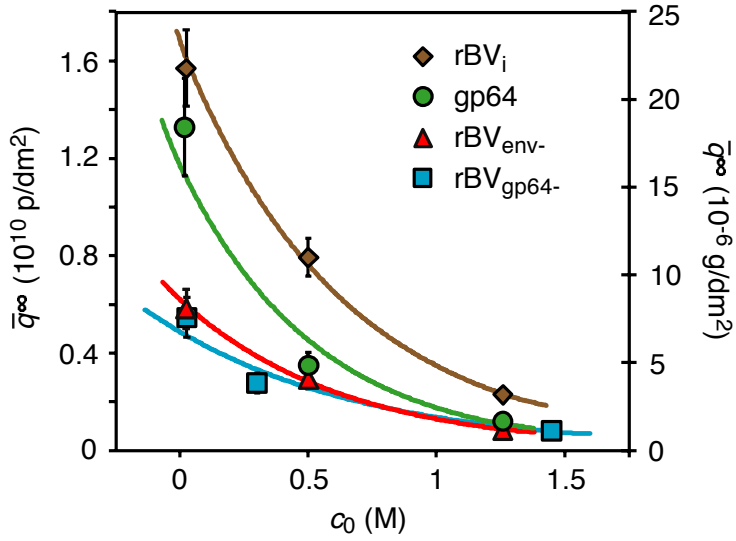

Figure 5.9: *Total adsorption capacity, $\overline{q}^{\infty} = \overline{q}_1^{\infty} + \overline{q}_2^{\infty}$, as function of salt concentration, c_0, for rBV_i, major-product related impurities (rBV_{gp64-} and rBV_{env-}), and and gp64. Units of p/dm^2 stand for particles (either rBV_i or other product-related impurity particles) per square decimeter. All concentrations, except those of gp64, are read on the lefthand ordinate axis; gp64 concentrations are read on the righthand ordinate axis.*

discriminated into (i) the desired product (a recombinant baculovirus), (ii) the major product-related impurities (damaged viral particles, hence non-infective), and (iii) the major process-related impurities (protein, DNA, endotoxin). This analysis resulted in the estimation of the adsorption isotherms of the isolated biomolecules as a function of salt

concentration. This tool, based on a simple stationary phase model, generates useful predictions of how the different components interact with a typical ion-exchange matrix used in a downstream process step. If the adsorption isotherms are known, suitable operating conditions can be determined through the application of design rules, such as those developed for simulated moving-bed processes or by computer-aided optimization. We shall resort to the latter approach for designing the biopurification process. It is worth noticing that the mechanistic knowledge obtained here for a complex biological system would not have been granted by other scaled-down approaches, e.g., high-throughput technologies, in the same time and with similar resources. Once this strategy is set up, it can be used to rationally enhance early-stage process screenings and increase basic knowledge on an industrial setting.

Acknowledgements

We thank Dr. Kari Airenne (University of Eastern Finland/Kuopio, Finland) for providing the recombinant baculoviruses used in this work; Ana F. Rodrigues is thanked for assistance in the cholesterol assay. We acknowledge funding from the European Commission (Baculogenes, LSHB-2006-037541 and Clinigene – Network of Excellence, LSHB-2006-018933) and the Portuguese *Fundação para a Ciência e a Tecnologia* (PTDC/EQU-EQU/71645/2006 and SFRH/BD/31257/2006).

5.7 Appendix: Analytical solution of the kinetic model and SPR response in the absence of mass-transport limitations

The initial steep rise in the SPR signal upon start of the adsorption step is the result of replacing the buffer solution ($c_0, c_\mathrm{B} = 0$) with the injected sample ($c_0, c_\mathrm{B} = c_\mathrm{B}^\mathrm{o}$) over the sensor surface for $z \leq z_\mathrm{max}$ [see Eq. (5.2)]. From Eqs. (5.3) and (5.16), this steep rise in the SPR signal can be approximated by

$$\Delta R = (m_\mathrm{B} - m_0 c_0 v_\mathrm{B}) c_\mathrm{B}, \quad h_\mathrm{i} \frac{dc_\mathrm{B}}{dt} = k_\mathrm{m}(c_\mathrm{B}^\mathrm{o} - c_\mathrm{B}), \tag{5.18}$$

whose solution for the initial condition $c_{\mathrm{B}}(0) = 0$ is

$$\Delta R = (m_{\mathrm{B}} - m_0 c_0 v_{\mathrm{B}}) c_{\mathrm{B}}^{\mathrm{o}} \left[1 - \exp\left(-\frac{k_{\mathrm{m}}}{h_{\mathrm{i}}} t \right) \right]. \tag{5.19}$$

This equation is valid for the early stages of the adsorption step; in particular, the derivative of Eq. (5.19) with respect to t for $t = 0$,

$$(m_{\mathrm{B}} - m_0 c_0 v_{\mathrm{B}}) c_{\mathrm{B}}^{\mathrm{o}} k_{\mathrm{m}} / h_{\mathrm{i}}, \tag{5.20}$$

approximates reasonably well the steep slope of the initial rise in the SPR signal.

The binding kinetics generates the convex curvature in the SPR response; this part of the sensorgram is described by Eq. (5.3) with c_{B} fixed at $c_{\mathrm{B}}^{\mathrm{o}}$, $c_{\mathrm{m}} = (q_1 + q_2)/d_{\mathrm{m}}$, and q_1 and q_2 given by the kinetic model defined by Eqs. (5.5)–(5.8). Under equilibrium conditions, the SPR signal stabilizes at an upper horizontal plateau corresponding to $(c_{\mathrm{B}}, q_1, q_2) = (c_{\mathrm{B}}^{\mathrm{o}}, \overline{q}_1, \overline{q}_2)$.

Given that $c_{\mathrm{B}} \approx c_{\mathrm{B}}^{\mathrm{o}}$ during binding because of unrestricted mass transfer, the kinetic model is governed by two ordinary differential equations amenable to a closed-form, analytical solution. The solution for the initial conditions $q_1(0) = q_2(0) = 0$, in the Laplace domain, is

$$Q_1(s) = \frac{\alpha_1(s + b_2) - \alpha_2 b_1}{[(s + a_1)(s + b_2) - a_2 b_1]s}, \quad Q_2(s) = \frac{\alpha_2(s + a_1) - \alpha_1 a_2}{[(s + a_1)(s + b_2) - a_2 b_1]s}, \tag{5.21}$$

where $Q_1(s)$ and $Q_2(s)$ are the Laplace transforms of $q_1(t)$ and $q_2(t)$, respectively; $\alpha_1 = k_{\mathrm{r}} q_1^{\infty} c_{\mathrm{B}}$, $a_1 = k_{\mathrm{r}} c_{\mathrm{B}}$, $b_1 = (\sigma_{12} k_{\mathrm{r}} - k_{\mathrm{r}}') c_{\mathrm{B}}$, $\alpha_2 = k_{\mathrm{a}} q_2^{\infty} c_{\mathrm{B}}$, $a_2 = \sigma_{21} k_{\mathrm{a}} c_{\mathrm{B}}$, and $b_2 = k_{\mathrm{d}} + (k_{\mathrm{a}} + k_{\mathrm{r}}') c_{\mathrm{B}}$. The solution can also be written in terms of time constants as

$$Q_1(s) = \frac{K_1(\tau_1' s + 1)}{[(\tau_1 s + 1)(\tau_2 s + 1) - \beta]s}, \quad Q_2(s) = \frac{K_2(\tau_2' s + 1)}{[(\tau_1 s + 1)(\tau_2 s + 1) - \beta]s}, \tag{5.22}$$

where $\tau_1 = 1/a_1$, $\tau_2 = 1/b_2$, $\beta = a_2 b_1 / a_1 b_2$, $K_1 = (\alpha_1 b_2 - \alpha_2 b_1)/a_1 b_2$, $\tau_1' = \alpha_1/(\alpha_1 b_2 - \alpha_2 b_1)$, $K_2 = (\alpha_2 a_1 - \alpha_1 a_2)/a_1 b_2$, and $\tau_2' = \alpha_2/(\alpha_2 a_1 - \alpha_1 a_2)$.

The effect of shielding on the binding kinetics is lumped into parameter β. The inversion of Eq. (5.22) for $\beta = 0$ gives

$$\frac{q_1(t)}{K_1} = 1 + \frac{\tau_1' - \tau_1}{\tau_1 - \tau_2} e^{-t/\tau_1} + \frac{\tau_1' - \tau_2}{\tau_2 - \tau_1} e^{-t/\tau_2}, \tag{5.23}$$

$$\frac{q_2(t)}{K_2} = 1 + \frac{\tau_2' - \tau_1}{\tau_1 - \tau_2} e^{-t/\tau_1} + \frac{\tau_2' - \tau_2}{\tau_2 - \tau_1} e^{-t/\tau_2}. \tag{5.24}$$

To assess the influence of β, first note that $a_2 b_1 < 0$ and so does β, and that $b_2 > a_1$. For nonzero, but small, values of $a_2 b_1$ the second-order polynomial $(s + a_1)(s + b_2) - a_2 b_1$ in the denominators of Eq. (5.21) is well approximated by $(s + a_1')(s + b_2')$, where $a_1' = a_1 - a_2 b_1/(b_2 - a_1)$ and $b_2' = b_2 + a_2 b_1/(b_2 - a_1)$. Thus, a_1 is increased by $\epsilon = |a_2 b_1|/(b_2 - a_1)$, whereas b_2 is decreased by the same value; since the time constants τ_1 and τ_2 are the reciprocals of a_1 and b_2, respectively, then is follows that τ_1 is decreased by shielding, whereas τ_2 is increased.

In the elution step, buffer alone is injected into the SPR cell to monitor the desorption kinetics. The SPR response for this step is given by Eq. (5.3) with $c_\mathrm{B} = 0$, $c_\mathrm{m} = (q_1 + q_2)/d_\mathrm{m}$, and q_1 and q_2 defined by

$$q_1 = \overline{q}_1, \quad \frac{dq_2}{dt} = -k_\mathrm{d} q_2. \tag{5.25}$$

If the time coordinate is reset to zero at the start of the elution step, the initial condition is $q_2(0) = \overline{q}_2$. The solution for the reversible component of the adsorbed phase concentration is thus

$$q_2(t) = \overline{q}_2 \exp(-k_\mathrm{d} t). \tag{5.26}$$

Nomenclature

Symbols

c_B	solute concentration in bulk solution
c_0	salt concentration in bulk solution
c_B^o	solute concentration in outer compartment
R	Biacore sensor's signal
z	distance from the sensor surface
$c_{0,\mathrm{ref}}$	reference salt concentration
d_p	penetration depth of the evanescent field
d_m	thickness of adsorbate monolayer
d_s	thickness of sensor surface film
c_m	adsorbate concentration
m	correlation coefficient between RI and Biacore's ΔR signal
m_0	slope of linear fitting of ΔR vs $(c_0 - c_{0,\mathrm{ref}})$
m_B	slope of linear fitting of ΔR vs c_B
D	diffusion coefficient

k_{m} mass transfer coefficient from bulk to sensor chip surface

h_{i} height of the inner compartment

$\overline{u}$ average velocity of the fluid in the flow cell, $Q/(hw)$

h height of the flow cell

w width of the flow cell

l length of the sensor surface

k_{a} reversible adsorption rate constant

k_{d} desorption rate constant

k_{r} rate constant for irreversible adsorption from the bulk solution

k'_{r} rate constant for irreversible adsorption from the reversibly adsorbed phase

q total adsorbed concentration

q_1 concentration of irreversibly bound solute

q_2 concentration of reversibly bound solute

q_1^{∞} capacity of the derivatized surface for irreversible binding

q_2^{∞} capacity of the derivatized surface for reversible binding

q^{∞} total capacity of the stationary phase

$\tilde{q}_1^{\infty}$ apparent capacity of the derivatized surface for irreversible binding

$\tilde{q}_2^{\infty}$ apparent capacity of the derivatized surface for reversible binding

$\overline{q}_1$ equilibrium concentration of irreversibly bound solute

$\overline{q}_2$ equilibrium concentration of reversibly bound solute

Greek letters

η_{B} refractive index of a salt solution with a dissolved biological solute

$\tilde{\eta}_{\mathrm{B}}$ refractive index of the (dry) solute

η_0 refractive index buffer solution with salt concentration c_0

ΔR Biacore signal

$\eta_{0,\mathrm{ref}}$ reference salt solution's RI (baseline buffer)

ϕ_{s} exponential ratio, $\exp(-d_{\mathrm{s}}/d_{\mathrm{p}})$

$\tilde{\eta}_0$ refractive index of the salt ions

v_{B} specific volume of the biological solute

ϕ_{m} exponential ratio, $\exp(-d_{\mathrm{m}}/d_{\mathrm{p}})$

σ_{12} steric factor for shielding of irreversible binding by reversibly bound adsorbates

σ_{21} steric factor for shielding of reversible binding by irreversibly bound adsorbates

ΔR_{a} sensorgram signal during adsorption

ΔR_{d} sensorgram signal during desorption

$\overline{\Delta R_a}$ equilibrium sensorgram signal upon adsorption

$\overline{\Delta R_d}$ equilibrium sensorgram signal upon desorption

References

Airenne KJ, Hiltunen MO, Turunen MP, Turunen AM, Laitinen OH, Kulomaa MS, et al. Baculovirus-mediated periadventitial gene transfer to rabbit carotid artery. Gene Ther 2000;7:1499–504.

Airenne KJ, Mähönen AJ, Laitinen OH, Ylä-Herttuala S. Baculovirus-mediated gene transfer: An emerging universal concept. In NS Templeton, ed., Gene and Cell Therapy: Therapeutic Mechanisms and Strategies. CRC Press, Boca Raton, 3rd ed., 2009.

Bosma JC, Wesselingh JA. ph dependence of ion-exchange equilibrium of proteins. AIChE J 1998;44:2399–2409.

Coffman JL, Kramarczyk JF, Kelley BD. High-throughput screening of chromatographic separations: I. method development and column modeling. Biotechnol Bioeng 2008;100:605–618.

Glaser R. Antigen-antibody binding and mass transport by convection and diffusion to a surface: a two-dimensional computer model of binding and dissociation kinetics. Anal Biochem 1993;213:152–161.

Goldstein B, Coombs D, He X, Pineda A, Wofsy C. The influence of transport on the kinetics of binding to surface receptors: application to cells and biacore. J Mol Recognit 1999;12:293–299.

Hall D, Cann J, Winzor D. Demonstration of an upper limit to the range of association rate constants amenable to study by biosensor technology based on surface plasmon resonance. Anal Biochem 1996; 235:175–184.

Harinarayan C, Mueller J, Ljunglöf A, Fahrner R, Van Alstine J, van Reis R. An exclusion mechanism in ion exchange chromatography. Biotechnol Bioeng 2006;95:775–787.

Hoa XD, Kirk AG, Tabrizian M. Towards integrated and sensitive surface plasmon resonance biosensors: a review of recent progress. Biosens Bioelectron 2007;23:151–60.

Hofmann C, Sandig V, Jennings G, Rudolph M, Schlag P, Strauss M. Efficient gene transfer into human hepatocytes by baculovirus vectors. Proc Natl Acad Sci U S A 1995;92:10099–10103.

Hu YC. Baculoviral vectors for gene delivery: a review. Curr Gene Ther 2008;8:54–65.

Ilic B, Yang Y, Craighead H. Virus detection using nanoelectromechanical devices. Appl Phys Lett 2004; 85:2604–2606.

Jung L, Campbell C, Chinowsky T, Mar M, Yee S. Quantitatite interpretation of the response of surface plasmon resonance sensors to adsorbed films. Langmuir 1998;14:5626–5648.

Karkkainen HR, Lesch HP, Maatta AI, Toivanen PI, Mahonen AJ, Roschier MM, et al. A 96-well format for a high-throughput baculovirus generation, fast titering and recombinant protein production in insect and mammalian cells. BMC Res Notes 2009;2:63.

Knoll W, Schmitt FJ, Klein C, Guder HJ, Liley M, Spinke J. Universal binding film. US Patent 5763191 1998.

Kost T, Condreay J, Jarvis D. Baculovirus as versatile vectors for protein expression in insect and mammalian cells. Nat Biotechnol 2005;23:567–75.

Kukkonen SP, Airenne KJ, Marjomaki V, Laitinen OH, Lehtolainen P, Kankaanpaa P, et al. Baculovirus capsid display: a novel tool for transduction imaging. Mol Ther 2003;8:853–62.

Lok BK, Cheng YL, Robertson CR. Protein adsorption on crosslinked polydimethylsiloxane using total internal reflection fluorescence. J Colloid Interface Sci 1983;91:104–116.

Mason T, Pineda A, C W, Goldstein B. Effective rate models for the analysis of transport-dependent biosensor data. Math Biosci 1999;159:123–144.

Mazzone H. CRC handbook of viruses: Mass-molecular weight values and related properties. CRC Press, Boca Raton, 1998.

Monsma SA, Oomens AG, Blissard GW. The gp64 envelope fusion protein is an essential baculovirus protein required for cell-to-cell transmission of infection. J Virol 1996;70:4607–16.

Myszka DG, He X, Dembo M, Morton TA, Goldstein B. Extending the range of rate constants available from biacore: interpreting mass transport-influenced binding data. Biophys J 1998;75:583–94.

Myszka DG, Morton TA, Doyle ML, Chaiken IM. Kinetic analysis of a protein antigen-antibody interaction limited by mass transport on an optical biosensor. Biophys Chem 1997;64:127–137.

Pattnaik P. Surface plasmon resonance: applications in understanding receptor-ligand interaction. Appl Biochem Biotechnol 2005;126:79–92.

Rege K, Pepsin M, Falcon B, Steele L, Heng M. High-throughput process development for recombinant protein purification. Biotechnol Bioeng 2006;93:618–30.

Rich RL, Myszka DG. Survey of the year 2007 commercial optical biosensor literature. J Mol Recognit 2008;21:355–400.

Roper DK, Nakra S. Adenovirus type 5 intrinsic adsorption rates measured by surface plasmon resonance. Anal Biochem 2006;348:75–83.

Sambrook J, Russel D. Molecular Cloning: A Laboratory Manual, vol. 2. Cold Spring Harbour Laboratory Press, New York, 2001.

Schmitz KS, Lu M. Effect of titration charge on the diffusion of bovine serum albumin. Proc Natl Acad Sci USA 1983;80:425–429.

Schuck P. Use of surface plasmon resonance to probe the equilibrium and dynamic aspects of interactions between biological macromolecules. Annu Rev Biophys Biomol Struct 1997;26:541–566.

Sjölander S, Urbaniczky C. Integrated fluid handling system for biomolecular interaction analysis. Anal Chem 1991;63:2338–2345.

Ulevitch R, Johnston A. The modification of biophysical and endotoxic properties of bacterial lipopolysaccharides by serum. J Clin Invest 1978;62:1313–1324.

Vicente T, Mota JPB, Peixoto C, Alves PM, Carrondo MJT. Modeling protein binding and elution over a chromatographic surface probed by surface plasmon resonance. J Chromatogr A 2010;1217:2032–2041.

Vicente T, Peixoto C, Carrondo MJT, Alves PM. Purification of recombinant baculoviruses for gene therapy using membrane processes. Gene Ther 2009;16:766–775.

Vicente T, Sousa MFQ, Peixoto C, Mota JPB, Alves PM, Carrondo MJT. Anion-exchange membrane chromatography for purification of rotavirus-like particles. J Membr Sci 2008;311:270–283.

Wensel DL, Kelley BD, Coffman JL. High-throughput screening of chromatographic separations: Iii. monoclonal antibodies on ceramic hydroxyapatite. Biotechnol Bioeng 2008;100:839–854.

Chapter 6

MODELING ELECTROSTATIC INTERACTIONS OF BACULOVIRUS VECTORS FOR ION-EXCHANGE PROCESS DEVELOPMENT

Adapted from:

Vicente T, Peixoto C, Alves PM, Carrondo MJT. Modeling electrostatic interactions of baculovirus vectors for ion-exchange process development. J Chromatogr A 2010; 1217:3754–3764.

Abstract

Product-related impurities constitute a major burden in the production of recombinant viral vectors for gene therapy and vaccination; it impairs not only the biological efficacy of the preparation but the process yield/productivity. Recombinant baculovirus was used as an enveloped virus model to address this issue. Given that ion-exchange chromatography is a process of choice for purification of viral vectors, the analysis of the electrostatic behavior can be instrumental for the improvement of impurity removal. The main species, product (infective virus particle) and product-derived impurities (dsDNA-, glycoprotein-, and envelope-deprived baculovirus particles), were isolated and correspondent ζ-potentials were analyzed through dynamic light scattering. A model of the virus based on the viral components critical for biological function is proposed. The contribution of these viral components to the overall particle electrostatic interaction energy profile (calculated between the particle and a putative ion-exchange surface) was assessed as a function of ionic strength and pH. This resulted in a deterministic tool capable of distinguishing the electrostatic properties of the infective virus particle from the major virus-related impurities. Within an ion-exchange bind-elute process, this knowledge helps narrow the optimization space in early stage process development for viral vectors by predicting the best selectivity conditions.

Contents

6.1 Introduction

The application of virus-like particles or recombinant viruses has been gaining momentum in the fields of vaccination or gene therapy for unmet medical needs (Merten et al., 2005; Rodrigues et al., 2007; Chuang et al., 2007; Cockrell and Kafri, 2007; Hu, 2008; Airenne et al., 2009). The growing number of preclinical studies and gene therapy trials require the purest grade materials in large-scale amounts (:20, 2008). Thus, it is becoming critical that tightly controlled, scalable and robust production processes become available for these complex biopharmaceuticals. Recombinant baculoviruses (rBVs) constitute a well established technology whose portfolio, in the last couple of decades, includes the production of many thousands of recombinant proteins using insect cells as host cell producers (Kost et al., 2005). The approved GSK Cervarix^{TM} vaccine against cervical cancer is an example of these biologics. Over the last decade, with the focus on human gene therapy paving the

way for innovative alternatives, the versatility of the rBV technology became clear by the increasing scientific evidence covering rBVs as successful vectors also in mammalian gene transfer (Kost et al., 2005; Airenne et al., 2009). In the mid-nineties, Hofmann *et al.* (Hofmann et al., 1995) have shown that these arthropod-specific viruses can be engineered to transiently transduce vertebrate cells by means of a proper mammalian promoter, although not replicating themselves or causing cytotoxic effects. Due to this non-pathogenicity to mammalian cells, the ability to accommodate very large foreign DNA sequences and the reliable production at high titers in insect cell cultures, rBV vectors hold significant advantages over other, more widely studied vectors (Hu, 2008; Airenne et al., 2009).

Nevertheless, as for other viral vectors or biologicals, bioengineers are currently seeing the process bottleneck shifting toward the downstream processing steps (Vicente et al., 2009; Gottschalk, 2008). In the specific case of viral vectors, given the increase in complexity, the workforce costs allocated to the compulsory analyticals and cell culture materials steeply augment thus resulting in costly process optimization. rBV vectors constitute a model system for this setting; clearly, a novel purification strategy developed by our laboratory for rBV vectors for clinical use has still room for improvement (Vicente et al., 2009). Crucial challenges need to be met: the large rod-shaped structure and envelope surface heterogeneity, the removal of resilient impurities and product derived impurities should be addressed in order to permit a more rational approach in the process fine-tuning and, ultimately, enhance yields/productivities of fully functional product.

Ion-exchange purification processes are state-of-the-art choices in purification processes for biopharmaceuticals (Urabe et al., 2006; Rodrigues et al., 2008; Vicente et al., 2008, 2009; Peixoto et al., 2008); they can be used efficiently to capture either the desired end product (bind-elute mode) or impurities (flow-through mode). Ionic strength and pH of the buffer/medium containing the complex mixture bulk are critical parameters one should observe with special attention (Pujar and Zydney, 1998; Schaldach et al., 2006; Vicente et al., 2008). Indeed, these conditions dramatically impact the ion-exchange process defining the binding strength at which the different bulk components undergo adsorption/desorption. To address these issues a more sound, knowledgeable based approach can be followed in an attempt to distinguish the underlying fundamental phenomena; hence, avoiding the need to cover all the possibilities using high-throughput methods used for blind design of experiments (DoE).

Dynamic light scattering (DLS) analysis can be easily conducted in benchtop machines with reduced consumable and biological material costs. In addition to the estimation

of hydrodynamic size and molecular weight of sub-micron particles, DLS can be used to study the electrokinetic properties of viral particles at chosen operational conditions of ionic strength and pH (Hiemenz, 1986); in particular, the estimation of the ζ potential provides a good measure of the electric double layer potential of the particle (Hiemenz, 1986). The integration of a conceptual model befitting these measurements can be instrumental in obtaining the conditions for best selectivity.

Following this rationale, DLS was used in this work to study in-depth the electrostatic features of baculovirus particles (as a model viral vector) and derived impurities. This resulted in relevant knowledge over the exploitable partitioning points that can be used for improved recovery of the functional viral vector from the remaining product-related impurities. This work is outlined into four major steps: (i) adapting a theoretical model to estimate the electrostatic potential of the relevant components of the viral particle; (ii) predicting the electrostatic interaction energies between the viral particle and a putative ion-exchange surface; (iii) validating the modeled predictions with experimental DLS data; and, (iv) establishing scenarios for best selectivity, hence, impurity removal.

6.1.1 Model of the virus particle and derived impurities

The virus used in this work – *Autographa californica* multicapsid nucleopolyhedrosis virus (AcMNPV) – in its budded virus phenotype is a rod-shaped enveloped virus (O'Reilly et al., 1994; King and Possee, 1992). This virus contains a rod-shaped (bacilliform) capsid composed of a protein sheath averaging 300 nm in body length and approximately 60 nm in diameter (Beaton and Filshie, 1976; Fraser, 1986). The capsid is an assembly of stacked ring subunits spaced 4.5 ± 0.2 nm apart (Beaton and Filshie, 1976), with distinct base and apex protein structures (Fraser, 1986). Although it is known that vp39 is the major capsid protein (Braunagel and Summers, 1994), there is still no further information on how the protein structurally assembles to form the ringlike capsomeres. The capsid encloses a molecule of dsDNA, typically within 128–140 kbp; electron dense capsids are observed under negative staining transmission electron microscopy indicating the presence of the baculovirus condensed genome (Fraser, 1986). These rod-shaped, DNA containing virions escape from the nucleus of the insect cell forming transient vacuoles that are further lost upon envelopment with lipid bilayers by budding from the cytoplasmic membrane (Fraser, 1986). Data from transmission electron microscopy and optical diffraction has shown that the minimum spacing between the envelope and the capsid is approximately 12 nm (Beaton and Filshie, 1976). The *de novo* enveloped virus contains an apical region covered with

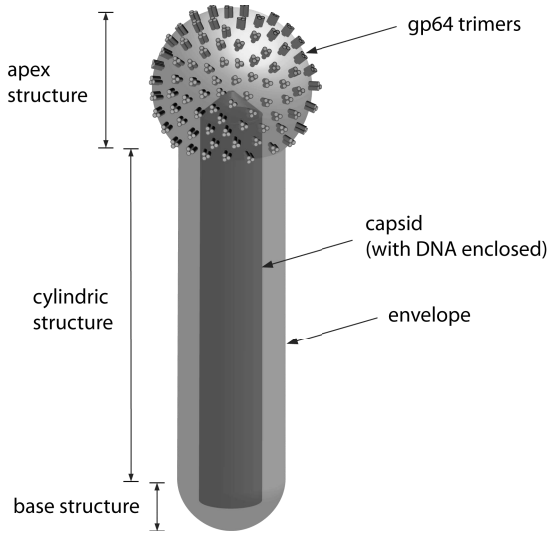

Figure 6.1: *Schematic representation of the baculovirus particle model used in this study. The particle can be physically decomposed into three parts: a* 135/180 *fraction of a sphere at the top, a cylindrical structure in the middle, and, a semi-sphere at the bottom.*

gp64 glycoprotein trimers which differentiates from the cylindrical body and bottom tip of the baculovirus (see Fig. 6.1) (Fraser, 1986). The postfusion crystal structure of gp64, mandatory for viral infection (Monsma et al., 1996), has been recently published; it consists of an elongated 15×5.5 nm structure composed of five protein domains *per* monomer (Kadlec et al., 2008). Gathering all the above structural data, the complete baculovirus particle averages approximately 390×90 nm in body length and diameter (with an apex, larger "head", with approximately 120 nm in diameter), respectively. Fig. 6.1 depicts the baculovirus model used in this work considering the described structural data; four major components are highlighted: the presence of the baculovirus genome here schematically represented as a dark (electron dense) rod-shaped capsid; the hollow tube capsid *per se*; the envelope surrounding the capsid; and gp64 trimers on the spherical-like apex surface of the particle.

We thus define in this study four recombinant baculovirus (rBV)-derived species: (i) infective baculovirus ($\mathrm{rBV_i}$), as the integral, functional particle; (ii) empty capsid baculovirus ($\mathrm{rBV_{e.c.}}$), lacking the viral genome (non-infective); (iii) gp64 defective baculovirus ($\mathrm{rBV_{gp64-}}$), with a defective amount of gp64 trimers (if any) on its envelope (non-infective); and (iv) envelope defective baculovirus ($\mathrm{rBV_{env-}}$), without envelope or with any disrupted version of it, i.e., a "naked" capsid (*a fortiori* non-infective). The relevant features and geometric data for the different model baculovirus-derived species considered in this work

are collected in Table 6.1.

Table 6.1: *Characteristic features of baculovirus and baculovirus-derived impurities considered in this work.*

Species	Apex structure	Cylindric and base structure	Schematic illustration	Infectivity	Critical interaction players
rBV_i	135°/180° of a sphere surface: $R_1 = 60$ nm	cylinder: $L = 240$ nm; $R_2 = 45$ nm + half-sphere: R_2		Yes; contains gp64 + envelope + genome containing capsid	gp64 trimers + envelope + capsid + viral dsDNA
$rBV_{e.c.}$	135°/180° of a sphere surface: $R_1 = 60$ nm	cylinder: $L = 240$ nm; $R_2 = 45$ nm + half-sphere: R_2		No; viral genome lacking	gp64 trimers + envelope + capsid
rBV_{gp64-}	135°/180° of a sphere surface: $R_{1'} = 50$ nm[a]	cylinder: $L = 240$ nm; $R_2 = 45$ nm + half-sphere: R_2	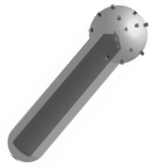	No; gp64 trimers lacking	envelope + capsid + viral dsDNA
rBV_{env-}	half-sphere: $R_3 = 30$ nm	cylinder: $L = 300$ nm; $R_3 = 30$ nm + half-sphere: R_3		No; envelope lacking	capsid + viral dsDNA

[a]considering that approximately 10 nm out of the 15 nm length of the gp64 trimer is exposed off the envelope (Kadlec et al., 2008)

6.1.2 Interaction energy between the model rBV particle and a flat plate

A means to understand the interactions governing an ion-exchange process is to obtain a quantitative estimation of the interaction energies between the different components of the mixture and the stationary phase. The interaction energy is defined as the Helmholtz free energy change associated when approaching the two charged surfaces (in this case, the viral particle and a flat surface) to a specific distance from infinite separation (Schmitz, 1996; Overbeek, 1990). The rBVs (and the remaining rBV-related species defined here (Table 6.1)) can be considered as colloidal particles, so that one can rely on the Derjaguin-Landau-Verwey-Overbeek (DLVO) theory to assess the van der Waals (vdW) and electro-

static double layer (EDL) interaction energies (Schaldach et al., 2006; Bhattacharjee and Elimelech, 1997). In fact, due to the non-specificity of the vDW potential energies the EDL contribution to the ion-exchange interaction energy is targeted here (Yoon and Lenhoff, 1992). The electric double layer interaction contribution is derived from the solution of the Poisson-Boltzmann equation (Hiemenz and Rajagopalan, 1997).

The surface element integration formalism available in the colloidal interface science literature (Bhattacharjee and Elimelech, 1997) represents an accurate method for the estimation of the interaction energy between a particle of arbitrary shape and an infinite flat plate from the corresponding interaction potential *per* unit area between two hypothetical infinite plates; in this approach, the differential interaction energy dU of a surface element dS at a distance h from an infinite flat plate can be expressed through the interaction energy *per* unit area between two infinite flat plates $\Psi(h)$ as $dU = \Psi(h)\mathbf{n} \cdot \mathbf{e_z} dS$, where $\mathbf{n}$ is the unit outward normal to the surface element and $\mathbf{e}_z$ is the unit normal to the xy plane (directed along the positive z axis (see Fig. 6.2)), h is the distance of the area element over the surface of the rBV particle and the infinite plate surface. The integral of the potential element over the surface of the rBV particle is then obtained by:

$$U = \int_x \int_y \Psi(h) \frac{\mathbf{n} \cdot \mathbf{e}_z}{\mid \mathbf{n} \cdot \mathbf{e}_z \mid} dxdy. \tag{6.1}$$

According to the definition of the different rBV particles species (Fig. 6.1, Table 6.1), this integral can be calculated by the summation of three contributions: (i) the surface of the apex of the particle; (ii) the cylindrical rod surface whose projected element in cylindrical coordinates is $LR_j d\theta$, L is the length of the cylindrical rod, and $\theta \in [0, \pi/2]$ (taking into account the symmetry of the cylinder) and j is 2 or 3 (according to Table 6.1); and, (iii) the semi-sphere surface of the bottom tip of the particle.

Assuming an α angle in the plane xy between the axis of the particle and the normal to the infinite plate surface as shown in Fig. 6.2, with $\alpha = \pi/2$, for the particle side facing the plate surface and using the expressions derived by Bhattacharjee and Elimelech

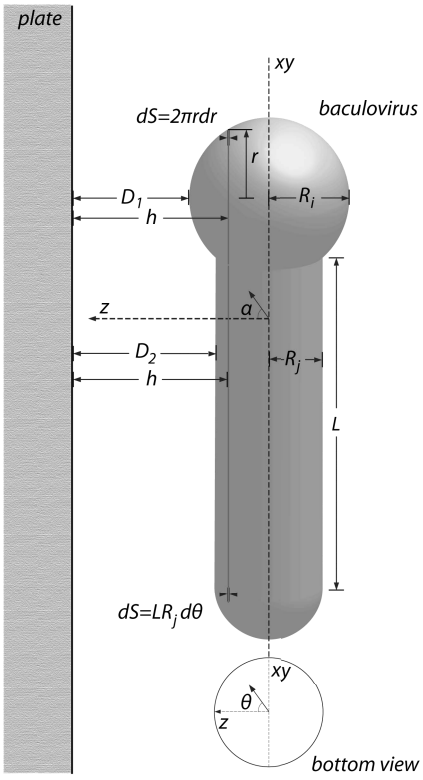

Figure 6.2: *Schematic representation of the recombinant baculovirus particle interacting with an hypothetical infinite flat plate: the ion-exchange surface is assumed as an infinite plate; for clarity, the baculovirus particle is simplified as compared to Fig. 6.1.*

(Bhattacharjee and Elimelech, 1997), one obtains

$$\begin{aligned} U_{+,v}(\alpha=\pi/2) &= f_1 \times 2\pi \int_0^{R_i} \Psi_{v,apex} \left[D_1 + R_i - R_i \left(1 - \frac{r^2}{R_i^2} \right)^{\frac{1}{2}} \right] rdr \\ &+ 2 \times LR_j \int_0^{\frac{\pi}{2}} \Psi_{v,rod}(D_2 + R_j - R_j \cos\theta) d\theta \\ &+ \frac{1}{2} \times 2\pi \int_0^{R_j} \Psi_{v,base} \left[D_2 + R_j - R_j \left(1 - \frac{r^2}{R_j^2} \right)^{\frac{1}{2}} \right] rdr. \end{aligned} \quad (6.2)$$

where $U_{+,v}$ is the interaction energy between the side of the rBV particle in study facing the flat plate and the plate itself, v refers to each of the four different species defined in the first column of Table 6.1; D_1 and D_2 are, respectively, the distances of closest approach between the plate surface and the top sphere surface and the plate surface and the cylindrical or

base surfaces. For $v = \mathrm{rBV_i}$ and $v = \mathrm{rBV_{e.c.}}$, $f_1 = 135/180$, $i = 1$ and $j = 2$ (i and j being an index of the parameter R in Table 6.1); for $v = \mathrm{rBV_{gp64^-}}$, $f_1 = 135/180$, $i = 1$' and $j = 2$; for $v = \mathrm{rBV_{env^-}}$, $f_1 = 1/2$, $i = 3$ and $j = 3$. The contribution for the total interaction energy between the side of the particle opposite to the flat plate and the flat plate has an analogous form, $U_{-,v}$, given by

$$\begin{aligned} U_{-,v}(\alpha = \pi/2) &= f_1 \times 2\pi \int_0^{R_i} \Psi_{v,apex} \left[D_1 + R_i + R_i \left(1 - \frac{r^2}{R_i^2} \right)^{\frac{1}{2}} \right] r dr \\ &+ 2 \times L R_j \int_0^{\frac{\pi}{2}} \Psi_{v,rod} (D_2 + R_j + R_j \cos\theta) d\theta \\ &+ \frac{1}{2} \times 2\pi \int_0^{R_j} \Psi_{v,base} \left[D_2 + R_j + R_j \left(1 - \frac{r^2}{R_j^2} \right)^{\frac{1}{2}} \right] r dr. \end{aligned} \quad (6.3)$$

The resulting interaction energy is $U_v(\alpha = \pi/2) = U_{+,v}(\alpha = \pi/2) - U_{-,v}(\alpha = \pi/2)$. As the particle contains only one symmetry axis (positioned on the longitudinal axis) one needs to take into consideration the possible orientations at the instant of interaction. The three pivotal orientations are: (i) $\alpha = 0$, when the particle has its apex facing the plate; (ii) $\alpha = \pi$, for the opposite orientation; and, (iii) $\alpha = \pi/2$, when the particle is parallelly aligned with the plate. The interaction energy is a function of α according to Eq. 6.1. Complying with the above motivation and for simplicity, herein we calculate the interaction energies for the three characteristic α angles, 0, $\pi/2$ and π, and interpolate for $\alpha \in [0, \pi/2]$ and $\alpha \in [\pi/2, \pi]$. For $\alpha = 0$, the analogous forms of Eqs. 6.2 and 6.3 become

$$U_{+,v}(\alpha = 0) = 2\pi \int_0^{R_i} \Psi_{v,apex} \left[D_1 + R_i - R_i \left(1 - \frac{r^2}{R_i^2} \right)^{\frac{1}{2}} \right] r dr \quad (6.4)$$

and

$$U_{-,v}(\alpha = 0) = f_2 \times 2\pi \int_0^{R_i} \Psi_{v,apex} \left[D_1 + R_i + R_i \left(1 - \frac{r^2}{R_i^2} \right)^{\frac{1}{2}} \right] r dr, \quad (6.5)$$

assuming that only the apex structure has a significant contribution to U, f_2 is 1/2 for $\mathrm{rBV_i}$, $\mathrm{rBV_{e.c.}}$ and $\mathrm{rBV_{gp64^-}}$, and 1 for $\mathrm{rBV_{env^-}}$. The resulting interaction energy is $U_v(\alpha = 0) = U_{+,v}(\alpha = 0) - U_{-,v}(\alpha = 0)$. For $\alpha = \pi$, one obtains

$$U_{+,v}(\alpha = \pi) = \frac{1}{2} \times 2\pi \int_0^{R_j} \Psi_{v,base} \left[D_2 + R_j - R_j \left(1 - \frac{r^2}{R_j^2} \right)^{\frac{1}{2}} \right] r dr, \quad (6.6)$$

where $U_v(\alpha = \pi) = U_{+,v}(\alpha = \pi)$, as only the half-sphere surface of the base structure is

considered for the interaction contribution in agreement with Eq. 6.1.

To calculate these contributions, expressions for the interaction energy *per* unit area, Ψ_v, between the two surfaces need to be established. An exact expression for the interaction energy derived from the solution of the linearized Poisson-Boltzmann equation, valid for small potentials ($\phi < 25$ mV), is given by (Hogg et al., 1966)

$$\Psi_v(h) = \frac{\epsilon_r \epsilon_0 \kappa}{2}(\phi_v^2 + \phi_p^2)\left[1 - \coth(\kappa h) + \frac{2\phi_v\phi_p}{\phi_v^2 + \phi_p^2}\mathrm{cosech}(\kappa h)\right], \tag{6.7}$$

where ϵ_0 is the permittivity of free space, ϵ_r is the dielectric constant of the external medium and κ is the inverse Debye length. Ψ_v is a function of the distance h between the two surfaces which is defined according to the schematic presented in Fig. 6.2 and spelt in terms of r and θ as shown in the arguments of the Ψ_v functions in Eqs. 6.2 and 6.3; Ψ_v is estimated using Eq. 6.7 provided that the surface potentials of the two surfaces experiencing interaction are assumed constant; ϕ_v and ϕ_p stand for the specific rBV particle species and flat plate surface potentials, respectively.

6.1.3 Relationship between interaction energy and chromatographic retention

In order to compare the chromatographic retention of $\mathrm{rBV_i}$ particles and their product-related impurities one can assume that the adsorption of these biological solutes is partly due to their accumulation in a diffuse layer close to the stationary-phase surface (defined above as the hypothetical flat plate) (Staahlberg, 1994). A detailed treatment of the thermodynamic interpretation of the capacity factor (or retention factor), k', for distance-dependent interactions has been presented previously in the literature (Staahlberg, 1994; Okada, 1999, 1998). k'_v is defined as

$$k'_v = \frac{t_v - t_0}{t_0}, \tag{6.8}$$

where v is the index corresponding to each of the biological particles studied, t_v and t_0 are the retention times of the species v and the void peaks, respectively. As derived by Ståhlberg (Staahlberg, 1994)

$$k'_v = \frac{A_S}{V_0}\int_h^{\kappa^{-1}}\left[\exp\left(-\frac{U_v}{RT}\right) - 1\right]dx, \tag{6.9}$$

where U_v is the free energy associated with transferring the solute v from a point in the bulk solution assumed here at a boundary distance κ^{-1}, which represents the medium Debye length, to a distance h separating the two surfaces, A_S and V_0 are the area and void volume of a given stationary phase, respectively. κ is calculated using

$$\kappa = \left(\frac{2 \times 1000 e^2 N_A I}{\epsilon_r \epsilon_0 k T} \right)^{\frac{1}{2}}, \tag{6.10}$$

where I is the ionic strength (in mol.L^{-1}) of the buffer, e is the elementary charge, N_A is the Avogadro's number, k is the Boltzmann constant and T is the absolute temperature. Eq. 6.9 allows to estimate a critical ion-exchange chromatography parameter as a function of the interaction energy calculated in Eq. 6.1, assuming that the EDL contribution is a determining factor for the sorption behavior —hence, retention— of the different particles. Under this hypothesis, the ratio of the capacity factor between any of the impurities (imp.) and rBV$_i$ becomes

$$\frac{k'_{\mathrm{rBV_{imp.}}}}{k'_{\mathrm{rBV_i}}} = \frac{\int_h^{\kappa^{-1}} \left[\exp\left(-\frac{U_{\mathrm{rBV_{imp.}}}}{RT} \right) - 1 \right] dx}{\int_h^{\kappa^{-1}} \left[\exp\left(-\frac{U_{\mathrm{rBV_i}}}{RT} \right) - 1 \right] dx}. \tag{6.11}$$

Eq. 6.11 is a measure of the selectivity that would be obtained in a bind-elute ion-exchange process.

6.1.4 EDL potential

Let us now consider the determination of ϕ of the different rBV species, ϕ_v, at defined buffer conditions (ionic strength and pH). These viruses can be considered colloid-sized particles, and, therefore, treated as charged particles with geometric characteristics listed in Table 6.1 immersed in an infinite medium with a characterized inverse Debye length, κ, surrounding its surface (Schaldach et al., 2004, 2006; Loveland et al., 1996). At small potentials, the linearized version of the Poisson-Boltzmann equation can be used to predict ϕ_v outside the rBV particle surface (Schaldach et al., 2006):

$$\phi_v(\delta) = \Phi_v \frac{R_k}{R_k + \delta} \exp(-\kappa\delta) \frac{1}{1 + \kappa R_k}, \tag{6.12}$$

where k is the radius' index listed in Table 6.1 and δ is the distance from the particle surface. The average surface potential Φ_v considering the charges within the particle is given by:

$$\Phi_v = \frac{1}{N} \sum_{m=1}^{N} \left[\sum_n \frac{q_n}{\epsilon r_{mn}} \exp\left(\frac{-r_{mn}}{\lambda} \right) \right], \tag{6.13}$$

where q_n is an elementary charge (amino acid, lipid or DNA), r_{mn} is the distance from that charge to the surface point, m, λ is the effective screening length due to compensating ions within the viral particle and N is the total number of m surface points considered for the calculation. This means that this model takes into account the presence (or absence) of the charges within the rBV particle. Eq. 6.12 allows for the estimation of the potential at specific conditions of ionic strength (impacting κ) and pH (impacting Φ_v). Two key points are: $\delta = 0$, producing ϕ_v included in the definition of Ψ_v due to the electrostatic double-layer effect; and, $\delta = \kappa^{-1}$ producing an estimation of the ζ potential as measured by DLS.

As stated before (summarized in Table 6.1), critical interaction players can be assigned: gp64 trimers, envelope, capsid and the viral dsDNA. We thus need to establish expressions to account for the different q_n charges considered for the summation in Eq. 6.13. Concomitantly, n comprises four sets of charges: n_1, n_2, n_3 and n_4 corresponding to the number of elementary charges due to the gp64 trimers, lipidic envelope, capsid protein, and viral dsDNA molecule, respectively.

gp64 trimers potential

The structure of the gp64 trimers has been recently published (Kadlec et al., 2008). From the Å-level resolution, Kadlec *et al.* (Kadlec et al., 2008) defined five main protomer domains (PDB ID code 3duz); herein we assume domain II and domain IV extended with 10 residues from the connected domain III portion (5 residues) and domain V (5 residues) (accounting for the 4 charged residues in this close vicinity) as the most exposed polypeptide sequences to the external medium where the ion-exchange interactions should be governed. From the polypeptide sequence of the gp64 protein (Combet et al., 2000; Kadlec et al., 2008), three separate polypeptide sequences can thus be highlighted: 44-60 and 218-271 (we indicate as region I), and 374-418 (we indicate as region II). Table 6.2 contains the content in charged residues for each of these regions and ionization constants in order to scrutinize the pH influence.

There is no available study assessing the average number of gp64 trimers *per* rBV particle. The mean infected Sf9 cell diameter (18-20 μm) (Palomares et al., 2001; Gotoh et al., 2008) and the number of trimers *per* cell has been estimated to be approximately 1.3×10^6 trimers.cell^{-1} (Monsma et al., 1996); additionally, from the baculovirus dimensions described, the fraction of envelope surface holding gp64 trimers is around 0.24. Thus, to account for this heterogeneity, the gp64 trimers should be localized on the cell membrane

Table 6.2: *Charged amino acid residues in exposed polypeptide sequences of gp64 (Kadlec et al., 2008) and acid dissociation constants.*

Amino acid	Number charges *per* region I *per* gp64 monomer (44-60 + 218-272)	Number charges *per* region II *per* gp64 monomer[a] (374-418)	pK_a[b]
Glutamate	3 + 2	3	4.5
Aspartate	2 + 5	5	4.5
Arginine	0 + 4	1	13.0
Lysine	2 + 7	2	10.1

[a]considering the residues 414-418 from the domain V we assume being critical due to the number of charged residues (Asp414, Asp415, Asp416 and Glu418 out of the five); [b]equilibrium constant estimated for amino acids embedded in a polypeptide chain (Cantor and Schimmel, 1980)

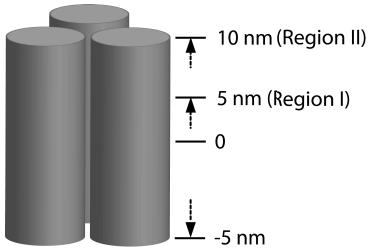

Figure 6.3: *Assignment of charge locations of the selected gp64 regions for the gp64 trimer model defined in Fig. 6.1 and Table 6.1: the origin 0 is the point over the outer lipid layer surface of the rBV envelope; it is assumed that approximately 5 nm of the gp64 trimer is buried into the envelope and that regions I and II have their punctual locations (for simplicity) at 5 and 10 nm from the envelope.*

at condensed regions (1/0.24) before viral budding. Under this assumption the number of gp64 trimers becomes approximately 96 *per* rBV particle whose effective area (apex surface) is 0.024 μm^2 out of the total surface area of 0.097 μm^2. This number of trimers is in good agreement with data from other enveloped viruses: e.g. γ-retroviruses contain approximately 100 trimers *per* retrovirus particle, a result from a cryo-electron tomography study (Forster et al., 2005).

With the described physicochemical data, Eq. 6.13 can then be used to quantify the contribution of gp64 for the average potential Φ_v.

Viral envelope potential

The baculovirus envelope is derived from the insect cell membrane by budding. An extensive biochemical analysis of the AcMNPV has been performed providing the lipid composition of the budded baculovirus envelope (Braunagel and Summers, 1994): 62.5±9.2 % in

acidic lipids (50.2±7.7 % phosphatidylserine (PS) + 12.3±1.4 % phosphatidylinositol (PI)) and 37.5±13.8 % in zwitterionic lipids (5.9±3.9 % lysophosphatidylcholine + 13.2±2.2 % sphingomyelin + 10.7±1.8 % phosphatidylcholine + 7.6±6.0 % phosphatidylethanolamine). Nevertheless, there is no additional information regarding the positioning of the acidic lipids on the lipid bilayer of the baculoviruses. The literature is convergent in that negatively charged lipids, e.g. PS, are typically located on the inner leaflet of biological lipid bilayers (plasma membranes (Yeung et al., 2008) and HIV envelopes (Brugger et al., 2006) although differing in overall composition) and that this lipid orientation is markedly linked with biological functions such as the interactive role with cytosolic proteins and/or formation of endosomes or liposomes (Yeung et al., 2008). Moreover, in the case of HIV, consistent evidence holds lipid rafts as precursors of the viral envelope (Brugger et al., 2006); however, it is still not clear as to how universal this would be (Brugger et al., 2006). Therefore, with the limited structural information available a simplified approach will use here where the expected overall negative charge is assumed to be due to the presence of the acidic lipids spread mostly over the inner lipid leaflet.

The calculation of the electrostatic potential of lipid bilayers has been addressed in the literature using either the non-linear or linear version of the Poisson-Boltzmann equation (Arakelian et al., 1993; Peitzsch et al., 1995). Following the purpose of this work and in line with the rationale above, we will assume that the inner side of the lipid bilayer is composed exclusively of negatively charged lipids (PS and PI altogether) and the outer side is composed of 25 % negative lipids and 75 % neutral lipids according to the remaining lipid composition. The effect of the unknown insect cell-derived membrane proteins and gp64 or cholesterol are assumed to be negligible to the overall electrostatic potential of the envelope *per se*. Furthermore, it has been shown that the potential on the outer lipid leaflet suffers a weak impact regardless of the potential sensed in the inner leaflet (Peitzsch et al., 1995; Arakelian et al., 1993); hence, the contribution to Φ_v in Eq. 6.13 is calculated depending only on the number of negative charges smeared uniformly over the outer envelope surface.

Viral capsid potential

To account for the viral capsid contribution to the overall potential the same strategy described in the gp64 trimers section is used to the major capsid protein, vp39. Only in this case, there is no detailed structural data specifically indicating the exposed amino acid residues in the vp39 protein; little knowledge is also available on the structural assembly of the capsid rather than that there is a number of other proteins in a much lower proportion

(Braunagel and Summers, 1994). As such, we consider the balance of the total number of charged residues of the vp39 polypeptide and take the resulting charge scattered uniformly over the surface of the capsid (Asp # + Glu # = 37 and Arg # + Lys # = 35 resulting in an excess of two negatively charged residues) (Thiem and Miller, 1989).

Viral dsDNA potential

As done by others (Schaldach et al., 2006), the viral dsDNA is assumed in this formalism as a cylindrical continuum having its negative charge density σ_{DNA} (number of base pairs *per* cylindrical volume) divided into volume elements $dq_{\mathrm{DNA}} \approx \sigma_{\mathrm{DNA}} \Delta V$, where ΔV is a specified finite volume considered for the calculation.

6.2 Materials and methods

6.2.1 Cell culture, rBV stock propagation and production

Sf9 insect cells (ECACC #89070101, UK) were routinely grown in Gibco$^{\mathrm{TM}}$ Sf-900 II SFM (serum-free) culture medium (Invitrogen, Paisley, UK) using spinner (stirred at 150 rpm in a magnetic stirrer) or Erlenmeyer vessels (shaken at 110 rpm in an orbital shaker) at 27 °C. Cell concentration and viability were routinely assessed by haemocytometer (Brand, Wertheim, Germany) with cell viability evaluated by 0.4 % trypan blue exclusion dye (Merck, Darmstadt, Germany) in phosphate-buffered saline.

The vector used, rBV-green fluorescent protein (GFP), encodes for the baculovirus major structural capsid protein, vp39, containing on its N-terminal a GFP protein reporter (Kukkonen et al., 2003). Stock aliquots of rBV-GFP were produced in Sf9 cells grown in a 25 L working volume wavebag bioreactor (Wave Europe, Cork, Ireland) using Sf-900 II medium. Sf9 cells were infected at a viable cell concentration at infection of $1 - 2 \times 10^6$ cells.mL^{-1} using an MOI of 0.1 pfu.cell^{-1}. Cell viability and cell infection were monitored for five days post infection. Quantification of the infected cells during the process was done by flow cytometry assessing GFP-expressing cell populations using a CyFlow$^{\mathrm{TM}}$ Space flow cytometer system (Partec, Münster, Germany). Data analysis was done using the manufacturer's acquisition software FlowMax$^{\mathrm{TM}}$ (Partec). The rBV production bulk was harvested when the cell viability reached values of 50 %. Production bulks were clarified as described elsewhere (Vicente et al., 2009).

6.2.2 Purification of rBV_i, $rBV_{e.c.}$, rBV_{gp64^-} and rBV_{env^-}

Infective baculovirus particles (rBV_i), the target product, were purified by ultracentrifugation based on sucrose density gradients (Airenne et al., 2000) yielding standard rBV_i stocks. Briefly, primary clarification and concentration was conducted by depth-filtration and tangential flow filtration using conditions recently described (Vicente et al., 2009). 3-μm retention Sartopure PP2 filter capsules followed by 0.65-μm retention Sartopure PP2 filter capsules were operated in series. Tangential flow filtration was run on an ÄKTAcross-flow system controlled by the UNICORN^{TM} software (all GE Healthcare, Uppsala, Sweden) with a 200 cm^2 Hydrosart^{TM} membrane with 100 kDa nominal molecular weight cut-off (MWCO) (Sartorius Stedim Biotech) at 35 $mL.min^{-1}$ retentate flow rate and a transmembrane pressure of 1.2 bar; buffer exchange to D-PBS was conducted by continuous diafiltration as described elsewhere (Vicente et al., 2009).

rBV concentrated stocks were transferred into ultracentrifuge tubes on top of two discrete sucrose density layers: 8 mL of 50 % (w/v) and 6 mL of 20 % (w/v) sucrose in D-PBS (bottom) sucrose in D-PBS; the tubes were centrifuged at 100 000 g for 1 h at 4 °C. The virus bands were pooled resuspended into 35 mL of ice-cold D-PBS, transferred into ultracentrifuge tubes containing 3 mL of 25 % (w/v) sucrose in D-PBS and centrifuged as above. The concentrated virus buffer was exchanged to D-PBS using a prepacked HiPrep^{TM} 26/10 desalting column coupled to an ÄKTAexplorer system (all GE Healthcare, Uppsala, Sweden). Sterile microfiltration of final material was performed using Acrodisc^{TM} Syringe Filters with Supor^{TM} PES membrane (Pall, New York, USA) before storage at 4 °C in the dark.

Concerning the CsCl gradient method, a similar protocol was followed (described for sucrose gradient). Briefly, the first ultracentrifugation was made with two discontinuous CsCl layers: 8 mL of 34.0 % (w/v) CsCl in D-PBS (1.23 $g.mL^{-1}$, $\eta = 1.3572$) and 6 mL of 19.3 % (w/v) CsCl in D-PBS (1.11 $g.mL^{-1}$, $\eta = 1.3455$); the second ultracentrifugation resolved a continuous CsCl self-gradient using 20 mL of 27.7 % (w/v) CsCl in D-PBS (1.17 $g.mL^{-1}$, $\eta = 1.3514$).

Purified rBV_i preparations were subjected to enzymatic digestion using subtilisin (Sigma-Aldrich, Steinheim, Germany) to produce rBV_{gp64^-} or lipid removal using Triton X-100 (Sigma) to produce rBV_{env^-}. Concentrated subtilisin stock was added to the purified particles in a final subtilisin concentration of 1 $mg.mL^{-1}$. The incubation was carried out for 2 h at 37 °C, after which 5 μg/mL of PMSF (Sigma) was added to suppress the protease; the material was stored at 4 °C in the dark until use. Lipid removal of the rBV particles

was performed by addition of a concentrated stock of 20 % Triton X-100 to achieve final concentration of 0.5 % (v/v), followed by incubation of the samples at 37 °C for 30 min.

The number of genome containing particles was quantified by real-time PCR (qPCR) following the protocol in Vicente *et al.* (Vicente et al., 2009). Viral DNA was extracted and purified using the High Pure Viral Nucleic Acid Kit (Roche Diagnostics, Mannheim, Germany) using the manufacturer instructions. Infective virus titers (IP) were determined with a flow cytometer-based assay (for rBVs-GFP) as developed by Kärkkäinen *et al.* (Karkkainen et al., 2009). Briefly, 500 μL of Sf9 cell suspension at 1.5×10^6 cells.mL^{-1}, seeded into 2.2 mL 96-well plates (ABgene Limited, UK), were infected with 500 μL of serial rBV sample dilutions. After incubating the plates at 27 °C for approximately 18 h in a shake flask orbital shaker at 420 rpm, cell suspensions were directly submitted to flow cytometer analysis using a 96-well plate autosampler (Partec) serially feeding each sample to the flow cytometer for GFP-expressing cell population assessment (Karkkainen et al., 2009). The maximum GFP-expressing cell population percentage (corresponding to a non-diluted viral sample) was used as a normalization factor for reliable titer calculation (Mulvania et al., 2004; Karkkainen et al., 2009).

Cholesterol content of the samples was measured using the Amplex^{TM} Red cholesterol assay kit (Molecular Probes, Eugene OR, USA) and DNA was measured using the Quant-iT^{TM} DNA assay kit (Molecular Probes).

6.2.3 Dynamic light scattering analysis

Hydrodynamic size estimations of rBV particles were obtained by dynamic light scattering (DLS) using a Zetasizer Nano-ZS Series ZEN3600 equipped with a 633 nm He-Ne laser (Malvern, Worcestershire, UK). Viral samples were diluted 25– to 60–fold in D-PBS; size measurements were performed in polystyrene cuvettes. Bovine serum albumin (BSA) (Merck) diluted in D-PBS was used as a control experiment. The rendered experimental correlation functions from DLS were analyzed by the CONTIN method to obtain distributions of decay rate profiles which provided distributions of apparent diffusion coefficient and, consequently, of the apparent hydrodynamic diameter (through the Stokes-Einstein equation). Replicates with over 20 % deviation were neglected. Before data acquisition, the instrument software automatically optimizes operational conditions such as signal attenuation, focal distance and number of scans.

ζ potential profiles at different pH were determined after measuring the electrophoretic mobility of the viral particles and application of the Smoluchowski approximation of the

Henry equation (Hiemenz and Rajagopalan, 1997). Electro-osmosis is avoided by application of a serial slow field reversal and a fast field reversal (phase analysis) allowing for the detection of very low electroforetic mobility of the scattering particles. Measurements were conducted in 10×10 mm polystyrene cuvettes using a dip cell (Malvern) at 25 °C.

6.2.4 Modeling calculations

The estimation of the EDL potential, ϕ, specific of the different rBV species, ϕ_v, at given ionic strength and pH were calculated using Microsoft^{TM} Excel (Microsoft, Redmond WA, USA). To account for the three different sets of m points defined as described in the Introduction section —apex, cylindric and base surface m points—, the summations expressed in Eq. 6.13 were computed using a macro written in Excel to estimate Φ and further incorporated in Eq. 6.12 to calculate ϕ at a chosen δ. To determine the interaction energy between the different rBV species and the putative flat plate, the integrals expressed in Eqs. 6.2-6.6 were computed in Mathematica^{TM} (Wolfram Research, Oxfordshire, UK) using the ϕ values obtained and assuming a constant 25 mV potential for ϕ_p.

6.3 Results and discussion

6.3.1 EDL potential

As mentioned (see Eq. 6.13), three m points sets were assumed to establish the summation of the four distinct n charges (the gp64 two regions, n_1; the envelope, n_2; the capsid n_3; and the DNA, n_4): m_1, a point over the apex surface; m_2, a point over the cylindrical rod surface; and, m_3, a point over the base surface. After fixing these points, the different r_{mn} lengths were computed using the geometric features illustrated (Fig. 6.1) and characteristic dimensions (Table 6.1). DLS was used to perform hydrodynamic size measurements of the different particles studied. These measurements indicated that particle aggregation did not occur (>600-800 nm) while providing a close agreement between the described characteristics (Table 6.1) and experimental results: for rBV_i, a bimodal distribution was observed at 110 ± 20 nm $\times$ 300 ± 100 nm; for rBV_{env^-}, the first peak of the distribution was shifted to 70 ± 20 nm $\times$ 300 ± 100 nm (data not shown). Unfortunately, one does not have sufficient accuracy with this technique to distinguish rBV_i from rBV_{gp64^-} or $rBV_{e.c.}$.

For simplicity of calculation, symmetry elements were assigned for the three regions: a 135/180 circle slice of the apex region (passing through the axis) defining characteristic n_i points within that slice (producing the whole apex surface by a 180° rotation); a line

of length L on the rod surface for n_i points within that region (producing the whole rod surface by a 360º rotation); and a semi-circle slice of the base region for n_i points in the base surface (producing the whole base surface by a 180º rotation).

To account for the pH impact on the charged amino acid residues or COOH groups of the negatively charged lipids, the charge ξ_i of a certain species i was calculated using:

$$\xi_i = \xi_{i,0} + \frac{10^{-(\text{pH-pK}_a)}}{1 + 10^{-(\text{pH-pK}_a)}} \tag{6.14}$$

where $\xi_{i,0}$ is the charge of the species at $\text{pH} > \text{pK}_a$.

Fig. 6.4a shows the behavior of the potential Φ_v calculated at a distance $\delta = \kappa^{-1}$ providing an estimation of the ζ potential. It is clear that using the amino-acid composition of the gp64 trimers and vp39 as theoretically proposed in the previous section, the simulated ζ potential profiles mispredict the order of magnitude and point of zero charge experimentally obtained by DLS (see Fig. 6.4a). Indeed, by trial-and-error, it was observed that including in the calculation more arginine and lysine residues in the region I of gp64 belonging to neighboring regions, the fitting considerably improved, particularly at low pH values. Hence, additional candidate external residues responsible for the interaction are proposed; the final result is illustrated in Fig. 6.4b showing a reasonable agreement between this prediction and the overall experimental data obtained. This fine-tuning process allowed to use more reliable EDL potential data permitting further interaction energy analyses.

By examining Fig. 6.4b, the simulated potential curves for rBV_i and $\text{rBV}_\text{e.c.}$ overlap indicating that the contribution of the DNA inside the enveloped particle is negligible for the overall potential of the particle. As only short-range electric double layer-type interactions are being addressed, it is expectable that the effect of DNA charges are no longer effectively sensed at the surface of the particle. Such observation concurs with a previous report showing that the RNA of a non-enveloped virus (Norwalk virus) is ruled out by compensating ions with the used ionic strengths due to the thickness of the viral coat (Schaldach et al., 2006). The data obtained by DLS for $\text{rBV}_\text{e.c.}$ shows a different behavior compared to the simulated curve especially in what concerns the point of zero charge, although this may be due to the technical difficulty in obtaining quality data at values of ζ potential close to zero using this technique.

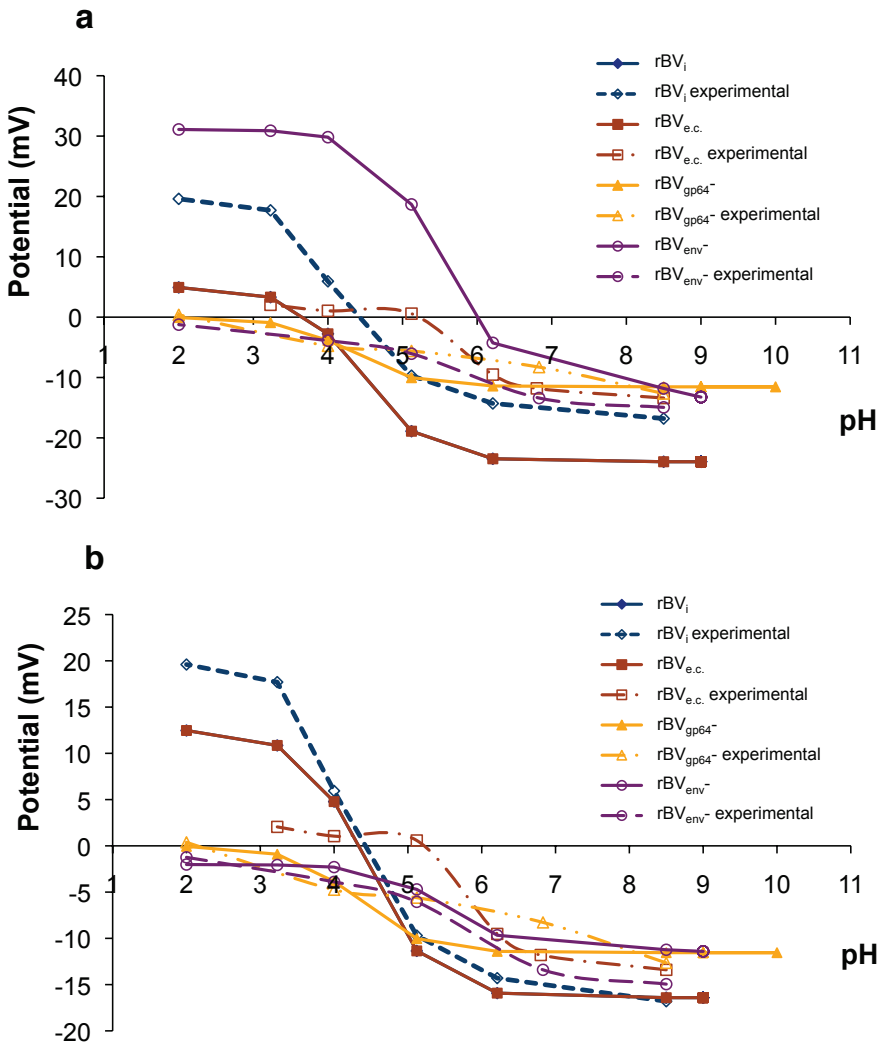

Figure 6.4: *Comparison between simulated mean particle potential Φ_v based on the model implemented at a distance $\delta = \kappa^{-1}$ and experimental ζ potential measurements by DLS at a fixed ionic strength, $I = 25mM$: (a) potential calculated using the amino-acid information shown in the Materials and methods section; (b) potential calculated altering the positive amino-acid composition of the gp64 region II (see Fig. 6.3) (Arg # = 7 and Lys # = 5) and considering only a fraction of the constitutive vp39 amino-acids (Asp+Glu # = 8; Arg # = 3; Lys # = 3).*

6.3.2 Interaction energy

Interaction energies were calculated assuming a putative DEAE ion-exchange surface whose positive constant potential is normalized to 25 mV and adjusted according to the characteristic titration curve of DEAE as a function of pH. A reference 2 nm distance, h separating the particle and the surface was assumed in the calculations as done elsewhere (Schaldach et al., 2006). These simplifications were taken so that one could tackle the electrostatic behavior of these very complex biologics in a more expedite way. The approximations and assumptions made upon the formulation of the model recombinant baculovirus particles studied do bring themselves uncertainty; thus, this simplified model should be still instructive in pinpointing the best selectivity regions in terms of ion-exchange processing. The constant potential values were estimated based on the adjusting process shown in the preceding section, using the conditions set for Fig. 6.4b. The effect of ionic strength, impacting the Debye length of the particle, is shown in Fig. 6.5 at different orientations. When the baculovirus particle apex is facing the charged surface, i.e., with $\alpha = 0$, the free energy of interaction tends to a negative maximum, indicating that the contribution of the gp64 glycoprotein trimers is prominent to the overall net negative surface charge; at the opposite orientation, i.e., with $\alpha = \pi$, only the envelope surface of the tip of the particle has a significant contribution to the overall interaction energy, which is considerably lower in absolute terms than that with $\alpha = 0$. Fig. 6.6 shows a perspective of the influence of pH and ionic strength on the interaction energy at the three key orientations; one can observe that at $\alpha = \pi$, the order of magnitude of the interaction energy is strikingly reduced in comparison to the other two orientations. Based on this deterministic analysis, the thermodynamically most favorable positioning of the baculovirus particle undergoing an electrostatic interaction with a surface of opposite charge is at $\alpha = 0$. Nonetheless, in a chromatographic matrix, the three-dimensionality and flux of material inside the stationary phase may cause a distribution of interaction positions rather than a specific orientation. Moreover, as shown in Fig. 6.5, the interaction energy is still highly negative at the flat position ($\alpha = \pi/2$) suggesting a favorable interaction; this can be observed in Figs. 6.6a and b; the shape of the diagrams is very similar.

To compare the electrokinetic behavior of the desired product, $\mathrm{rBV_i}$, and the considered product-derived impurities, we defined a segregation coefficient, s, as

$$s = \begin{cases} \log_{10}\left(\frac{U^{\mathrm{rBV_{imp.}}}}{U^{\mathrm{rBV_i}}}\right) & \text{for} \quad \frac{U^{\mathrm{rBV_{imp.}}}}{U^{\mathrm{rBV_i}}} > 0 \\ -2 & \text{for} \quad \frac{U^{\mathrm{rBV_{imp.}}}}{U^{\mathrm{rBV_i}}} < 0 \end{cases}, \tag{6.15}$$

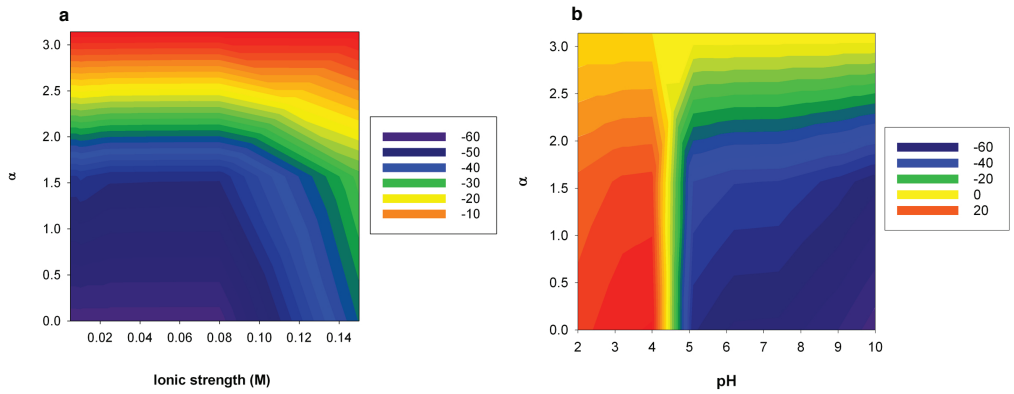

Figure 6.5: *rBV_i particle – putative DEAE surface interaction energy calculated using the trained model implemented (see Text) at the following conditions: (a) varying ionic strength and particle orientation (α angle) at fixed pH=7.4; (b) varying pH and particle orientation (α angle) at fixed $I = 25$ mM.*

where $U^{\mathrm{rBV_{imp.}}}$ is the closest impurity interaction energy to the $\mathrm{rBV_i}$ interaction energy, $U^{\mathrm{rBV_i}}$. As shown in Eq. 6.15, when the two interaction energies have opposite signals, for simplicity of representation $U^{\mathrm{rBV_{imp.}}}/U^{\mathrm{rBV_i}}$ is computed by 10^{-2}, which means that the impurity and the desired product are completely segregated based on their interaction energies, i.e., only one of them interacts favorably with the ion-exchange surface. Figs. 6.7a and b allows to detect the windows of more pronounced interaction differences therefore predicting the zones of better selectivity as far as a bind-elute anion-exchange phenomenon is concerned. As seen before, the $\mathrm{rBV_{e.c.}}$ impurity has the same interaction energy based on the model used herein, hence this species is not included in this assessment.

Moreover, this segregation coefficient can be compared to a selectivity based on the chromatographic retention factors using Eq. 6.11, which relates directly the EDL contribution to adsorption with a hypothetical DEAE ion-exchange bind-elute chromatographic process. Figs. 6.7c and d show analogous plots to Figs. 6.7a and b, respectively. Both segregation and selectivity factors calculated seem to follow the same trend, however, the selectivity factor does not seem to be as sensitive for pH > 6.5. From our experience in processing these biological particles, this insensitivity is unrealistic which could be due to the fact that only electrostatics are taken into consideration as shown in the simplifications considered (see Introduction section); size-exclusion, chromatographic matrix properties and ligand orientation/density or repulsion effects may play a role as well. At the two favorable orientations, $\alpha = 0$ and $\alpha = \pi/2$, when $\mathrm{rBV_i}$ is expected to bind to the ion-exchange surface, it can be seen in Fig. 6.7a and b the regions where $s \to 0$, meaning that the closest impurity in terms of interaction energy should have the same type of behavior

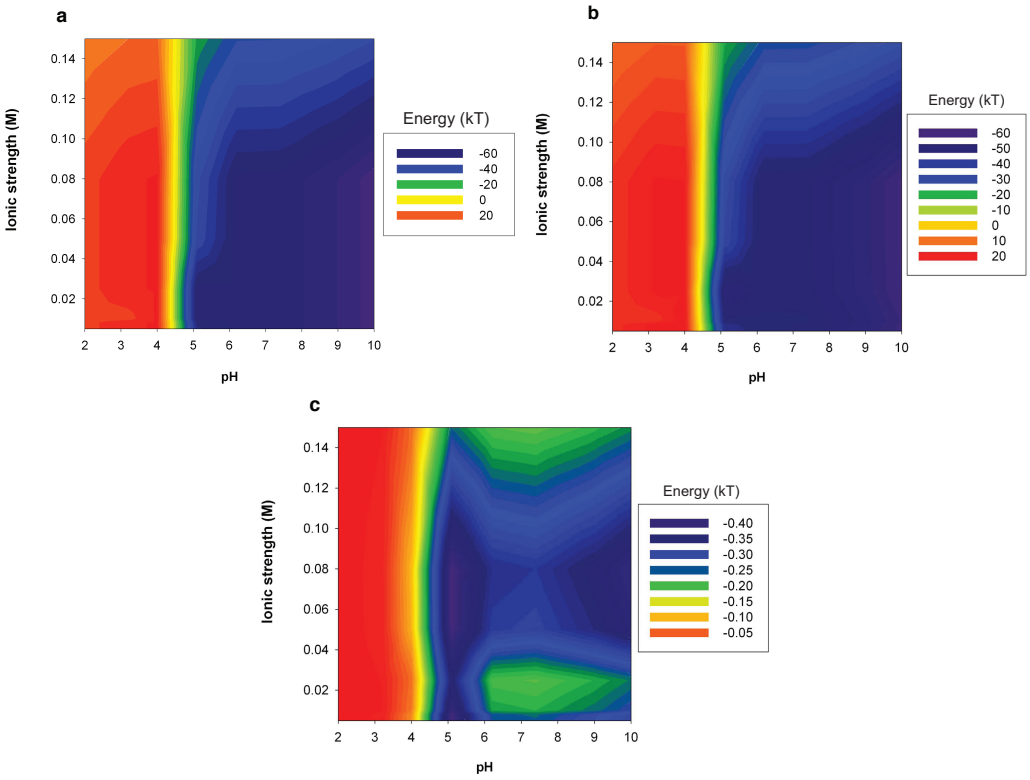

Figure 6.6: *Ionic strength and pH effect over the rBV_i particle – putative DEAE surface interaction energy calculated using the trained model implemented (see Text) at fixed (a) $\alpha = 0$; (b) $\alpha = \pi/2$; and (c) $\alpha = \pi$ particle orientations.*

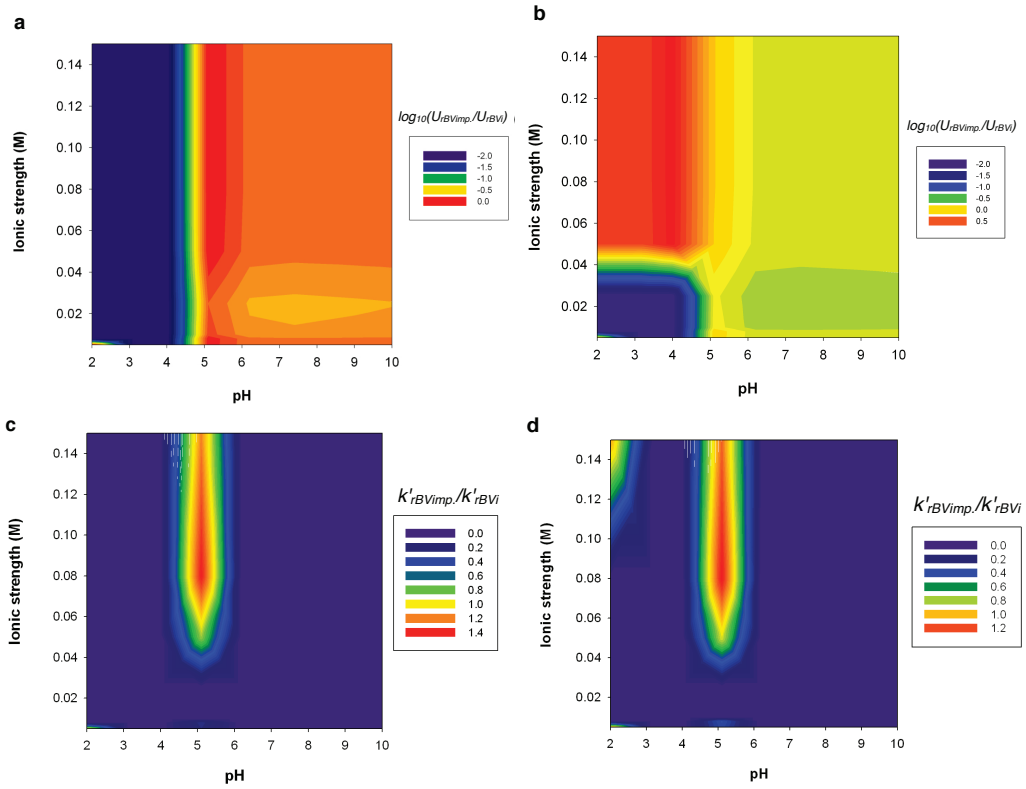

Figure 6.7: *Effect of particle orientation, ionic strength and pH on the logarithm of the ratio rBV_i/closest product-related impurity interaction energy and on the selectivity factor based on chromatographic retention (see Text): (a) and (c) $\alpha = 0$; (b) and (d) $\alpha = \pi/2$; $rBV_{e.c.}$ particles are not considered in this analysis.*

in an ion-exchange process, thus compromising the selectivity. This is predicted to occur for pH within the range of 4.7–6, irrespective of the ionic strength used. The region of pH within 6.5–9, and I within 0.01–0.05 M seems to be the best working region where $s < 0$ and $k'_{\mathrm{rBV_{imp.}}}/k'_{\mathrm{rBV_i}} \to 0$, indicating that the $\mathrm{rBV_i}$ particles present a higher predicted interaction energy as compared to all the product-derived impurities. Regardless of particle orientation, regions of complete segregation, $s = -2$ (opposite signal values) or very low $k'_{\mathrm{rBV_{imp.}}}/k'_{\mathrm{rBV_i}}$, can be detected at pH < 4.5; nevertheless, these conditions are impractical due to gp64 stability issues at pH values lower than 6 (Monsma et al., 1996). Overall, this information based on electrokinetic behavior can be used to narrow the experimentation space on a design of experiments approach for an anion-exchange bind-elute process optimization task.

6.4 Concluding remarks

This paper reports on the use of electrokinetic fundamentals as a means to understand/measure the ion-exchange-type of interactions undergoing between baculovirus vectors (and baculovirus-derived impurities) and a putative DEAE surface. Using ζ potential measurements through DLS, a structural model for the particles (product and impurities) was proposed and fine tuned based on the fundamental biological components and calculated the electrostatic potential and corresponding free interaction energy defined between the whole virus particle and the charged surface at a chosen distance. In the context of ion-exchange purification processes for the recovery of infective virus particle from damaged baculovirus particles, the impact of ionic strength and pH on the overall interaction energy have been addressed.

This rationale permitted to study the selectivity issue by overlaying the interaction behavior of the studied species; a segregation coefficient and a chromatography retention-based selectivity were used to this purpose to predict the best window of operation in a bind-elute anion-exchange chromatography process. Such information is critical for a more rational and cost-effective development of the ion-exchange process which is now underway. Overall, the gp64 trimers covering the head of the baculovirus particles are expected to be highly determinant to the overall charge of the particle surface while the presence of dsDNA does not significantly influence the behavior of the enveloped structure. Indeed, the infective particles are expected to be more negatively charged than their related impurities within these conditions. This study contributes with guidelines to help decrease the ratio of total particles to infective particles using an anion-exchange chromatographic step.

Acknowledgements

We thank Dr. Kari Airenne (University of Kuopio, Kuopio, Finland) for providing the recombinant baculoviruses used in this work. We want also to thank Dr. Pedro Cruz for enlightening discussions, Dr. António Lopes for support on dynamic light scattering and Ana Rodrigues for assistance in the cholesterol assay. We acknowledge funding from the European Commission (Baculogenes, LSHB-2006-037541 and Clinigene—Network of Excellence, LSHB-2006-018933) and Portuguese *Fundação para a Ciência e a Tecnologia* (PTDC/EQU-EQU/71645/2006 and SFRH/BD/31257/2006).

References

Gene therapy clinical trials worldwide. charts and tables, vectors. 2008.

Airenne KJ, Hiltunen MO, Turunen MP, Turunen AM, Laitinen OH, Kulomaa MS, et al. Baculovirus-mediated periadventitial gene transfer to rabbit carotid artery. Gene Ther 2000;7:1499–504.

Airenne KJ, Mähönen AJ, Laitinen OH, Ylä-Herttuala S. Baculovirus-mediated gene transfer: An emerging universal concept. In NS Templeton, ed., Gene and Cell Therapy: Therapeutic Mechanisms and Strategies. CRC Press, Boca Raton, 3rd ed., 2009.

Arakelian V, Walther D, Donath E. Electric potential distributions around discrete charges in a dielectric membrane-electrolyte. Colloid Polym Sci 1993;270:268–276.

Beaton CD, Filshie BK. Comparative ultrastructural studies of insect granulosis and nuclear polyhedrosis viruses. J Gen Virol 1976;31:151–61.

Bhattacharjee S, Elimelech M. Surface element integration: A novel technique for evaluation of dlvo interaction between a particle and a flat plate. J Colloid Interface Sci 1997;193:273–285.

Braunagel SC, Summers MD. Autographa californica nuclear polyhedrosis virus, pdv, and ecv viral envelopes and nucleocapsids: Structural proteins, antigens, lipid and fatty acid profiles. Virology 1994; 202:315–328.

Brugger B, Glass B, Haberkant P, Leibrecht I, Wieland FT, Krausslich HG. The hiv lipidome: a raft with an unusual composition. Proc Natl Acad Sci U S A 2006;103:2641–6.

Cantor C, Schimmel P. Biophysical Chemistry, Part I: The Conformation of Biological Macromolecules. New York, 1980.

Chuang CK, Sung LY, Hwang SM, Lo WH, Chen HC, Hu YC. Baculovirus as a new gene delivery vector for stem cell engineering and bone tissue engineering. Gene Ther 2007;14:1417–24.

Cockrell AS, Kafri T. Gene delivery by lentivirus vectors. Mol Biotechnol 2007;36:184–204.

Combet C, Blanchet C, Geourjon C, Deléage G. Nps@: Network protein sequence analysis. Trends Biochem Sci 2000;25:147–150.

Forster F, Medalia O, Zauberman N, Baumeister W, Fass D. Retrovirus envelope protein complex structure in situ studied by cryo-electron tomography. Proc Natl Acad Sci U S A 2005;102:4729–34.

Fraser MJ. Ultrastructural observations of virion maturation in autographa californica nuclear polyhedrosis virus infected spodoptera frugiperda cell cultures. J Ultrastruct Mol Struct Res 1986;95:189–195.

Gotoh T, Fukuhara M, Kikuchi KI. Mathematical model for change in diameter distribution of baculovirus-infected sf-9 insect cells. Biochem Eng J 2008;40:379–386.

Gottschalk U. Bioseparation in antibody manufacturing: The good, the bad and the ugly. Biotechnol Prog 2008;24:496–503.

Hiemenz PC. Electrophoresis and Other Electrokinetic Phenomena. Marcel Dekker, New York, 1986.

Hiemenz PC, Rajagopalan R. The Electrical Double Layer and Double-Layer Interactions. Marcel Dekker, New York, 1997.

Hofmann C, Sandig V, Jennings G, Rudolph M, Schlag P, Strauss M. Efficient gene transfer into human hepatocytes by baculovirus vectors. Proc Natl Acad Sci U S A 1995;92:10099–10103.

Hogg R, Healy TW, Fuerstenau DW. Mutual coagulation of colloidal dispersions. Trans Faraday Soc 1966; 62:1638–1651.

Hu YC. Baculoviral vectors for gene delivery: a review. Curr Gene Ther 2008;8:54–65.

Kadlec J, Loureiro S, Abrescia NG, Stuart DI, Jones IM. The postfusion structure of baculovirus gp64 supports a unified view of viral fusion machines. Nat Struct Mol Biol 2008;15:1024–30.

Karkkainen HR, Lesch HP, Maatta AI, Toivanen PI, Mahonen AJ, Roschier MM, et al. A 96-well format for a high-throughput baculovirus generation, fast titering and recombinant protein production in insect and mammalian cells. BMC Res Notes 2009;2:63.

King L, Possee R. The baculovirus expression vector system: a laboratory guide. Chapman and Hall, London, 1992.

Kost T, Condreay J, Jarvis D. Baculovirus as versatile vectors for protein expression in insect and mammalian cells. Nat Biotechnol 2005;23:567–75.

Kukkonen SP, Airenne KJ, Marjomaki V, Laitinen OH, Lehtolainen P, Kankaanpaa P, et al. Baculovirus capsid display: a novel tool for transduction imaging. Mol Ther 2003;8:853–62.

Loveland JP, Ryan JN, Amy GL, Harvey RW. The reversibility of virus attachment to mineral surfaces. Colloid Surf A: Physicochem Eng Asp 1996;107:205–221.

Merten OW, Geny-Fiamma C, Douar AM. Current issues in adeno-associated viral vector production. Gene Ther 2005;12:S51–61.

Monsma SA, Oomens AG, Blissard GW. The gp64 envelope fusion protein is an essential baculovirus protein required for cell-to-cell transmission of infection. J Virol 1996;70:4607–16.

Mulvania T, Hayes B, Hedin D. A flow cytometric assay for rapid, accurate determination of baculovirus titers. Bioprocess J 2004;pp. 47–53.

Okada T. Interpretation of ion-exchange chromatographic retention based on an electrical double-layer model. Anal Chem 1998;70:1692–1700.

Okada T. Interpretation of chromatographic behavior of ions based on the electric double-layer theory. J Chromatogr A 1999;850:3 – 8.

O'Reilly D, Miller L, Verne A. Baculovirus Expression Vectors: A Laboratory Manual. Freeman, New York, 1994.

Overbeek JTG. The role of energy and entropy in the electrical double layer. Colloid Surface 1990;51:61–75.

Palomares L, Pedroza R, Ramirez O. Cell size as a tool to predict the production of recombinant protein by the insect-cell baculovirus expression system. Biotechnol Lett 2001;23:359–364.

Peitzsch R, Eisenberg M, Sharp K, McLaughlin S. Calculations of the electrostatic potential adjacent to model phospholipid bilayers. Biophys J 1995;68:729–738.

Peixoto C, Ferreira TB, Sousa MFQ, Carrondo MJT, Alves PM. Towards purification of adenoviral vectors based on membrane technology. Biotechnol Prog 2008;24:1290–1296.

Pujar NS, Zydney AL. Electrostatic effects on protein partitioning in size-exclusion chromatography and membrane ultrafiltration. J Chromatogr A 1998;796:229–38.

Rodrigues T, Alves A, Lopes A, Carrondo MJ, Alves PM, Cruz PE. Removal of envelope protein-free retroviral vectors by anion-exchange chromatography to improve product quality. J Sep Sci 2008;31:3509–18.

Rodrigues T, Carrondo MJT, Alves PM, Cruz PE. Purification of retroviral vectors for clinical application: Biological implications and technological challenges. J Biotechnol 2007;127:520–541.

Schaldach CM, Bourcier WL, Paul PH, Wilson WD. Electrostatic potentials and fields in the vicinity of engineered nanostructures. J Colloid Interface Sci 2004;275:601–611.

Schaldach CM, Bourcier WL, Shaw HF, Viani BE, Wilson WD. The influence of ionic strength on the interaction of viruses with charged surfaces under environmental conditions. J Colloid Interface Sci 2006;294:1–10.

Schmitz KS. Pairwise "gibbsian" free energy and screened coulombic interactions. Langmuir 1996;12:3828–3843.

Staahlberg J. Electrostatic retention model for ion-exchange chromatography. Anal Chem 1994;66:440–449.

Thiem S, Miller L. Identification, sequence, and transcriptional mapping of the major capsid protein gene of the baculovirus autographa californica nuclear polyhedrosis virus. J Virol 1989;63:2008–2018.

Urabe M, Xin K, Obara Y, Nakakura T, Mizukami H, Kume A, et al. Removal of empty capsids from type 1 adeno-associated virus vector stocks by anion-exchange chromatography potentiates transgene expression. Mol Ther 2006;13:823–828.

Vicente T, Peixoto C, Carrondo MJT, Alves PM. Purification of recombinant baculoviruses for gene therapy using membrane processes. Gene Ther 2009;16:766–775.

Vicente T, Sousa MFQ, Peixoto C, Mota JPB, Alves PM, Carrondo MJT. Anion-exchange membrane chromatography for purification of rotavirus-like particles. J Membr Sci 2008;311:270–283.

Yeung T, Gilbert GE, Shi J, Silvius J, Kapus A, Grinstein S. Membrane phosphatidylserine regulates surface charge and protein localization. Science 2008;319:210–3.

Yoon BJ, Lenhoff AM. Computation of the electrostatic interaction energy between a protein and a charged surface. J Phys Chem 1992;96:3130–3134.

Chapter 7

IMPACT OF LIGAND DENSITY ON THE OPTIMIZATION OF ION-EXCHANGE MEMBRANE CHROMATOGRAPHY FOR VIRAL VECTOR PURIFICATION

Adapted from:

Vicente T, Fáber R, Alves PM, Carrondo MJT, Mota JPB. Impact of ligand density on the optimization of ion-exchange membrane chromatography for viral vector purification. In final preparation.

Abstract

The effect of ligand density on anion-exchange membrane chromatography (AEXmc) for the purification of recombinant baculoviruses (rBVs), potential viral vectors in clinical applications, is studied by surface plasmon resonance on customized AEX surfaces and gradient elution experiments on Sartobind D membrane prototypes with different diethylamine ligand densities, complemented by dynamic light scattering analysis for estimation of the hydrodynamic particle size of the various biologicals. A chromatographic-column model based on the steric mass action model of ion exchange is employed to analyze the gradient-elution AEXmc experiments, extrapolate the results to other operating conditions, and provide directions for process improvement. Although counterintuitively, the experimental evidence provided in this paper shows that the lowering of ligand density is beneficial for rBV purification by AEXmc in bind-and-elute mode, because it decreases the residual concentrations of host cell protein, dsDNA, and non-infective rBVs in the eluted product cut, and increases the overall yield by roughly 20% over current standard values. Overall, we present a case study on how rational design can streamline downstream process development.

Contents

7.1 Introduction

The development of scalable processes has been identified as critical for the generation of recombinant viral vectors for clinical applications (Wu and Ataai, 2000). The increasing number of pre- and clinical trials urges for larger amounts of highly pure (often challenging, labile) biological material (Rodrigues et al., 2007; :20, 2009). Still, many downstream processing teams in the industry and academia frequently resort to ultracentrifugation-based purification steps to generate their viral stocks; these are typically costly, non-cGMP amenable and not easily scalable. To circumvent this, ion-exchange (IEX) chromatography, which is scalable and cGMP compliant, is becoming the process of choice for the recovery of not only recombinant proteins or vaccines, but also viral vectors (Peixoto et al., 2008; Vicente et al., 2008, 2009; Opitz et al., 2007; Rodrigues et al., 2006; Okada et al., 2009). The issue then is to find an efficient means for the optimization of this preferred process.

Charge-dependent unit operations rely on the evaluation of key operating parameters, such as ionic strength and pH of the suspension buffer. These procedures tend to become

highly costly when a high added-value product is recovered from a complex preparation, such as an animal-cell-derived bioreaction bulk. In order to save time and reduce costs, scaled-down models are often used as economic and convenient tools for early stage process development (Coffman et al., 2008; Rege et al., 2006; Wensel et al., 2008). For example, we have recently employed surface plasmon resonance (SPR) as a scaled-down chromatographic tool to measure the adsorption equilibria and kinetics of complex biologicals on a micrometric surface functionalized with ion-exchange ligands, mimicking an ion-exchange matrix (Vicente et al., 2010b,a). Additionally, it has been shown that dynamic light scattering (DLS) provides useful information for selecting the correct operating window when a bind-and-elute chromatographic process is envisaged (Vicente et al., 2010c). To complement these analytical tools, good modeling tools are also required for a more sound design of the actual purification process. For instance, the steric mass action model of ion exchange (Brooks and Cramer, 1992) has been employed in concert with a standard chromatographic-column model to simulate and predict with reasonable accuracy VLP binding and elution in anion-exchange membrane chromatography (AEXmc) (Vicente et al., 2008).

Membrane chromatography matrices have important advantages over resin-based matrices (Teeters et al., 2002), e.g.: (i) convection is the prevailing mass transport mechanism in membrane adsorbers with nearly no diffusion limitation, which improves the chromatographic kinetics and imposes less constraints on the flow rates; (ii) the ligands bound to the membrane surface are accessible to very large biologicals (e.g., virus particles) with small diffusivities, which are excluded from the intra-bead pores of a typical resin bead; (iii) membrane chromatography is easy to scale-up because of the significant level of flexibility in flow rate selection; (iv) because membrane chromatography capsules are designed for disposable operation, they are simple to use without the need for cleaning, sterilization and validation. These advantages led to a number of reported application studies on vaccine/viral vector purification by membrane chromatography operated in a bind-and-elute mode (Vicente et al., 2008, 2009; Wu et al., 2007; Kutner et al., 2009).

The purification of recombinant baculoviruses (rBVs) is a challenging case study; these viral vectors hold potential in human gene therapy or vaccination due to important (and alternative) advantages over other more studied vectors as adeno- or retroviruses (Kost et al., 2005; Airenne et al., 2009). An integrated strategy for rBV purification that is fully based on scalable and cGMP compatible downstream processing steps has been reported (Vicente et al., 2009). However, there is still room for improvement especially at the capture step using AEXmc. It is not difficult to anticipate that a sensible selection of binding

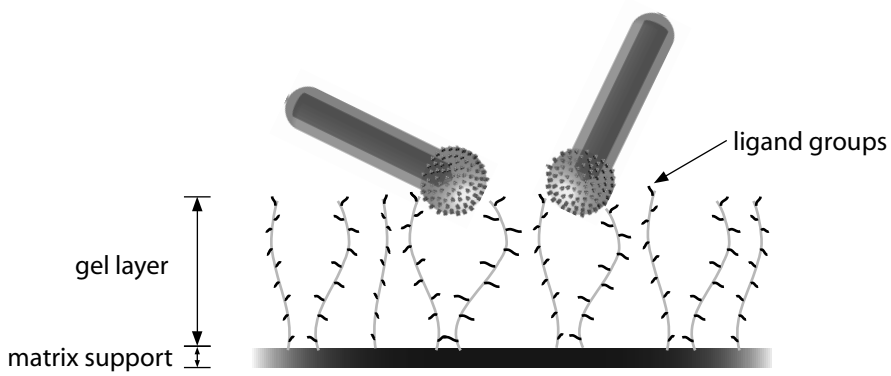

Figure 7.1: *Schematic representation of ligand density exclusion effect for large particles within the gel layer of a cut of Sartobind D membrane adsorber cellulose matrix (Tatárová et al., 2009). Here, rod-shaped baculovirus particles (120-350 nm) (Vicente et al., 2009) are used as an illustrative example of the inability of a large particle to have to access to the ligand groups within the depth of the gel layer.*

conditions (pH and ionic strength) should result in process performance improvements. Here we shall demonstrate that scaled-down analytical tools, such as SPR, are useful helpers in this task.

A recent study shows that an exclusion effect occurs for very large molecules, with over 100 nm, when approaching the ligand sites functionalized within the gel layer covering a commercially available membrane adsorber matrix backbone (Tatárová et al., 2009). This effect is illustrated in the schematic of Fig. 7.1. We hypothesize that an excess in ligand binding sites may be counterproductive for virus purification, because the excess sites will favor the adsorption of process-derived impurities, such as host cell protein (HCP), host cell dsDNA, and/or other smaller biologicals, over the virus particles themselves. Therefore, the use of lower ligand densities than those found in commercially available membrane units may yield improved purity without sacrificing the capacity of the binding step (for the virus particle).

In the present work the effect of varying the ligand density on AEXmc using SPR-sensor surfaces derivatized with diethylaminoethyl cellulose (DEAE) and Sartobind D membrane prototypes grafted with similar diethylamine functional groups was studied. The hydrodynamic particle sizes of the various biologicals were determined by dynamic light scattering analysis. To validate the results, a design of experiments (DoE)-based approach was devised to address the influence of ligand density, loading salt concentration, and elution gradient length on the rBV purification by AEXmc. The steric mass action (SMA) model of ion exchange is employed in concert with a chromatographic-column model to predict

the performances of the capture and elution steps and to provide directions for process improvement.

We provide evidence that the sensible reduction of ligand density to a level below those of current commercial chromatographic membranes improves purity and quality of the final eluted product fraction. In the present case, a rational optimization of the anion-exchange chromatography step leads to improved yields as high as 85%, which is an improvement of 20% over the currently reported state-of-the-art values of around 65%. This work constitutes a proof of concept on how the leverage of fundamental strategies can be implemented to streamline downstream process development for complex biologicals.

7.2 Materials and methods

7.2.1 Cell culture and recombinant virus production

Sf9 insect cells (ECACC #89070101, UK) were routinely grown in Gibco^{TM} Sf-900 II SFM (serum-free) culture medium (Invitrogen, Paisley, UK) using spinner (stirred at 150 rpm in a magnetic stirrer) or Erlenmeyer vessels (shaken at 110 rpm in an orbital shaker). Cell concentration and viability were assessed by haemocytometer (Brand, Wertheim, Germany) with cell viability evaluated by 0.4% trypan blue exclusion dye (Merck, Darmstadt, Germany) in phosphate-buffered saline. The vector used, rBV-green fluorescent protein (GFP), encodes for the baculovirus major structural capsid protein, vp39, containing on its *N*-terminal a GFP protein reporter (Kukkonen et al., 2003). Stock aliquots of rBV-GFP were produced in Sf9 cells grown in a 25 liter working volume wavebag bioreactor (Wave Europe, Cork, Ireland) using Sf-900 II medium. Sf9 cells were infected at a viable cell concentration of 1–2$\times 10^6$ cells.mL^{-1}, using a multiplicity of infection (MOI) of 0.1 pfu.cell^{-1}. Cell viability and cell infection were monitored for five days post infection. Quantification of the infected cells during the process was done by flow cytometry assessing GFP-expressing cell populations using a CyFlow^{TM} space-flow cytometer system (Partec, Münster, Germany). The rBV production bulk was harvested when the cell viability reached values of 50%.

Replication-defective adenoviruses type 5 (Ad5) were produced in 293 cells (ATCC–CRL–1573) adapted to suspension and grown in CD293 supplemented with 4 mM of glutamine (all from Invitrogen, Paisley, UK) in a humidified atmosphere of 8% CO2 at 37°C. Ad5 production was performed in a 5-L bioreactor (Sartorius, B. Braun, Germany). The dissolved oxygen and pH were controlled at 80% of air saturation and 7.2, respectively.

Infections were performed using an MOI of 10 and the Ad5 bulk was harvested at 72 hours post-infection. Standard Ad5 stocks were purified using CsCl-based ultracentrifugation density gradient as described elsewhere (Kanegae et al., 1994).

7.2.2 Purification of standard baculovirus stocks

Infective baculovirus particles, the target product, were isolated by ultracentrifugation based on sucrose density gradients (Airenne et al., 2000). Clarification and concentration were conducted using depth-filtration and tangential flow filtration described elsewhere (Vicente et al., 2009). Briefly, 3 μm retention Sartopure PP2 filter capsules, followed by 0.65 μm retention Sartopure PP2 filter capsules, were operated in series. Tangential flow filtration was run on an ÄKTAcrossflow^{TM} system controlled by the UNICORN^{TM} software (all GE Healthcare, Uppsala, Sweden) with a 200 cm^2 Hydrosart^{TM} membrane with 100 kDa nominal molecular weight cut-off (MWCO) (Sartorius Stedim Biotech) at 35 mL/min retentate flow rate and a transmembrane pressure of 1.2 bar; buffer exchange to D-PBS was accomplished by continuous diafiltration. rBV concentrated stocks were transferred into ultracentrifuge tubes on top of two discrete sucrose density layers: 8 mL of 50% (w/v) and 6 mL of 20% (w/v) sucrose in D-PBS (bottom); the tubes were centrifuged at 100,000 g and 4°C for 1 h. The virus bands were pooled, resuspended into 35 mL of ice-cold D-PBS, transferred into ultracentrifuge tubes containing 3 mL of 25% (w/v) sucrose in D-PBS, and centrifuged as above. The concentrated virus buffer was exchanged to 10 mM phosphate buffer pH 7.2 with 10 mM NaCl using a prepacked HiPrep^{TM} 26/10 desalting column coupled to an ÄKTAexplorer100 system (all GE Healthcare). Sterile microfiltration of final material was performed using Acrodisc^{TM} Syringe Filters with Supor^{TM} PES membrane (Pall, New York, USA) before storage at 4°C in the dark.

7.2.3 Main process-derived impurities

Reference biologicals have been used to study their behavior in binary mixtures with rBV in the SPR-based studies. DNA was obtained from an Sf9 insect cell culture after DNA extraction using the High Pure PCR template Acid Kit (Roche Diagnostics, Mannheim, Germany). Bovine serum albumin (BSA) is of analytical grade (> 98% electrophoresis purity) purchased from Merck KGaA (Darmstadt, Germany). All solutes were conditioned in 10 mM phosphate buffer at pH 7.2 with a given NaCl concentration.

7.2.4 Dynamic light scattering analysis

Hydrodynamic size estimations of sample particles were obtained by dynamic light scattering (DLS) using a Zetasizer Nano-ZS Series ZEN3600 equipped with a 633 nm He-Ne laser (Malvern, Worcestershire, UK). Viral samples were diluted 25- to 60-fold in D-PBS; size measurements were performed in polystyrene cuvettes. Bovine serum albumin (BSA) (Merck, Darmstadt, Germany) diluted in D-PBS was used as a control experiment. The rendered experimental correlation functions from DLS were analyzed by the CONTIN method to obtain distributions of decay rate profiles which provided distributions of apparent diffusion coefficient and, consequently, of the apparent hydrodynamic diameter (through the Stokes-Einstein equation). Replicates with over 20% deviation were neglected. Before data acquisition, the instrument software automatically optimizes operational conditions such as signal attenuation, focal distance and number of scans.

7.2.5 Surface plasmon resonance

Sensor surface preparation

In order to address prospectively the impact of DEAE ligand density on the adsorption of baculoviruses and major process-related impurities, three different DEAE ligand density sensor chips were produced: an 11-mercaptoundecanoid acid (MUA)-DEAE sensor chip, a CM3-DEAE sensor chip, and a CM5-DEAE sensor chip. These sensor chips were customized as follows.

For MUA-DEAE, DEAE ligands were covalently immobilized to a self-assembled monolayer (SAM) previously coupled on a gold sensor chip (Biacore/GE Healthcare, Uppsala, Sweden) surface according to protocols described in the literature (Roper and Nakra, 2006; Vicente et al., 2010b). MUA (NanoThinks^{TM} ACID11 solution from Sigma-Aldrich, München, Germany) was used as thiolate for SAM preparation. The refractive index (RI) was monitored throughout the MUA-SAM immobilization procedure with a Leica AR200 digital hand-held refractometer (Leica Microsystems, Wetzlar, Germany). Briefly, the gold sensor chip surface was first equilibrated with ultra-pure, deionized water at 18.2 M$\Omega \cdot$cm. The surface was sanitized with 0.1 M NaOH and 1% Triton^{TM} X-100 (Sigma-Aldrich) and then re-equilibrated in 10 mM 4-Morpholineethanesulfonic acid (MES) (Sigma) buffer at pH 5.0. Ethanol was then used to washout the buffer and the surface was exposed directly to the NanoThinks ACID11 solution (5 mM MUA in ethanol) and left overnight in a closed compartment inside a laminar flow bench. The freshly formed SAM of MUA was rinsed

with ethanol and re-equilibrated with the 10 mM MES buffer previously used until the refractive index stabilized.

For CM3-DEAE and CM5-DEAE, DEAE ligands were covalently immobilized to either a CM3 sensor chip or a CM5 sensor chip (all Biacore/GE Healthcare), which contains a dextran extension layer of 30 nm (Kyprianou et al., 2009) or 100 nm (Yu et al., 2004; Wofsy and Goldstein, 2002), respectively, over the sensor surface with available carboxyl groups for coupling chemistry.

Each of the three different density sensors –MUA-DEAE, CM3-DEAE and CM5-DEAE– were docked in the SPR system, a Biacore^{TM} 2000 (Biacore/GE Healthcare), for 2-diethylaminoethylamine (DEAEA) (99% purity grade from Sigma-Aldrich) immobilization using amide coupling chemistry. MES buffer was used as running buffer for the duration of the immobilization procedure. Freshly prepared solutions of 0.4 M 1-ethyl-3-(3-dimethylaminopropyl)carbodiimide hydrochloride (EDC) and 1.0 M N-hydroxysuccinimide (NHS) (amine coupling kit from Biacore/GE Healthcare) in water were mixed 1:1 and injected in a pulse of 200 μL at 20 μL/min to activate the terminal carboxyl group for amide bond formation. 1.0 M DEAEA in MES running buffer was added in serial 100 μL pulses at 20 μL/min until the SPR signal stabilized.

SPR experiments

All SPR experiments were performed on a Biacore 2000 system at 25°C. Product (rBVs) and main process-related impurities (dsDNA and model BSA) were diluted to a given concentration (c_{B}) in 10 mM phosphate buffer at pH 7.2 with the specified NaCl concentration (c_0). All buffers were prepared sterile and degassed prior to use in the equipment.

The experiments were performed at constant flow rate of running buffer (with a salt concentration $c_{0,\mathrm{ref}}$) and sample injection of 100 μL/min. Each run consisted of the following sequence of steps: (i) equilibration of the flow cell with running buffer; (ii) injection of 100 μL of analyte solution or binary mixture of analytes at ($c_0 = c_{0,\mathrm{ref}}, c_{\mathrm{B}}$); and (iii) desorption and equilibration with running buffer ($c_0 = c_{0,\mathrm{ref}}$,$c_{\mathrm{B}} = 0$). Before starting a new cycle, the flow cell was subjected to an aggressive desorption step using 100 μL of 1.5 M NaCl in 10 mM phosphate buffer at pH 7.2, and then cleaned/sanitized with 100 μL of 0.1 M NaOH for complete sanitization of the surface.

DEAE ligands and SAMs have been shown to be fully resistant to pulses of NaOH (or HCl) up to 1 M (Knoll et al., 1998). The baseline stability was controlled throughout the course of each experiment.

SPR data analysis

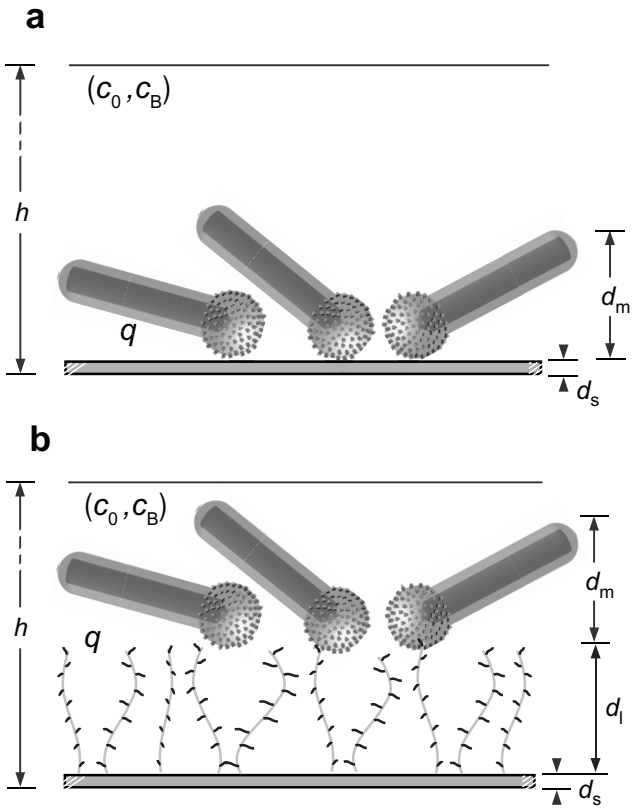

Figure 7.2: *Schematic of rBV adsorption onto a surface film of thickness d_s in the Biacore sensor chip flow cell. (a) represents monolayer adsorption onto MUA-DEAE, i.e., without dextran layer extension; (b) represents adsorption onto CM3-DEAE or CM5-DEAE, with a dextran layer, d_l. It is assumed that rBVs cannot diffuse into the dextran layer, contrary to what happens freely for an adsorbing protein model, BSA. The bulk aqueous solution has salt concentration c_0 and rBV concentration c_B; $h = 0.05$ mm is the height of the Biacore flow cell; d_m is the thickness of the adsorbed monolayer, q is the surface concentration of adsorbed rBV, and d_p is the effective penetration depth of the evanescent electromagnetic field; for the case of the Biacore 2000 machine, $d_p \approx 150$ nm.*

The underlying probing mechanism of the Biacore machine for a MUA-DEAE ion-exchange surface system has been recently reviewed, and explicit formulae for deconvoluting SPR data into adsorbate biological concentration, c_m, bulk adsorptive concentration, c_B, and salt concentration, c_0, have been derived (Vicente et al., 2010b,a).

For solute monolayer adsorption (i.e., on a MUA-DEAE), and assuming a constant pH, the SPR signal shift, ΔR, obtained as response to a typical ion-exchange adsorption

Table 7.1: *Characteristic features of rBVs and BSA as model protein impurity.*

Biological	Structure
rBV	Rod-shaped virus particle $d_{\mathrm{m}} = 120 - 350$ nm
BSA	Protein with diameter $d_{\mathrm{m}} = 5.4$ nm

process on the sensor surface is given by (Vicente et al., 2010b,a)

$$\Delta R = (m_{\mathrm{B}} - m_0 c_0 v_{\mathrm{B}}) \left[c_{\mathrm{m}} + \phi_{\mathrm{m}}(c_{\mathrm{B}} - c_{\mathrm{m}})\right] + m_0(c_0 - c_{0,\mathrm{ref}}), \tag{7.1}$$

where m_0 and m_{B} are the calibration constants associated with the SPR response to changes in c_0 and c_{B}, respectively; v_{B}, the molar volume of the adsorbed solute; c_{m}, the solute concentration in the volume of the adsorbed layer; $\phi_{\mathrm{m}} = \exp(-d_{\mathrm{m}}/d_{\mathrm{p}})$ where d_{m} is the thickness of the adsorbed layer and d_{p} the characteristic penetration depth of the evanescent electromagnetic field (Fig. 7.2); and $c_{0,\mathrm{ref}}$, the salt concentration in the buffer solution used to equilibrate the flow cell and to define the baseline of the SPR's signal. The adsorbed concentration, c_{m}, can be converted into a surface concentration through the trivial formula $q = d_{\mathrm{m}} c_{\mathrm{m}}$.

For the general case, when there is a dextran layer of height d_{l}, Eq. 7.1 remains valid, however, the thickness d_{m} becomes the specific d_{l} for the case of small biomolecules as the model BSA protein, of the dextran layer (30 nm or 100 nm, for CM3 or CM5 sensor chip, respectively). For the case of large particles, hindered by the dense dextran layer which mimics the gel layer present in a membrane adsorber (Tatárová et al., 2009), d_{m} is assumed to be 120 nm (Table 7.1).

Solving Eq. 7.1 for c_{m} gives

$$c_{\mathrm{m}} = \frac{\Delta R - m_0(c_0 - c_{0,\mathrm{ref}})}{(1 - \phi_{\mathrm{m}})(m_{\mathrm{B}} - m_0 c_0 v_{\mathrm{B}})} - \frac{\phi_{\mathrm{m}}}{1 - \phi_{\mathrm{m}}} c_{\mathrm{B}}. \tag{7.2}$$

7.2.6 Anion-exchange membrane chromatography

AEXmc experiments

Sartobind D membrane prototypes with different diethylamine ligand densities were manufactured by Sartorius-Stedim Biotech (Göttingen, Germany) (see Table 7.2 for details). Each prototype was assembled as stack of three layers with 5 cm^2/layer mounted in a membrane disc holder, and then connected to an ÄKTAexplorer100 system coupled with the UNICORN software. Concentrated virus bulks previously prepared by the method

Table 7.2: *Characteristics of Sartobind D membrane prototypes used in this study.*

Charge density (μmol.cm^{-2})	% charge density (%)	10% DBC* (mg.cm^{-2})	Λ[a] (mM)
2.2	36.1	0.32	81
5.0	82.0	0.58	185
6.1	100.0[b]	0.98	226

[a]Λ stands for ligand binding capacity; [b]reference ligand density; *stands for dynamic binding capacity of BSA model protein

described elsewhere (Vicente et al., 2009), using 10 mM phosphate buffer pH 7.2 (optimal pH for rBV binding (Vicente et al., 2010c)) with a given NaCl concentration (buffer A) as diafiltration buffer, were subjected to AEXmc experiments. These runs were carried out using the following systematic procedure: (i) loading of concentrated virus bulk into the membrane at a flow rate of 5 mL/min; (ii) washing out of weakly- or non-adsorbing biological solutes from the membrane with 2 MVs of buffer A; (iii) gradient elution with a specified length (in MVs) by the admixture of buffer A and buffer A containing 1.5 M NaCl (buffer B).

Between each run, the membrane adsorber was regenerated with buffer B, sanitized with a pulse of 0.5 M NaOH, and equilibrated with buffer A supplemented with a given NaCl concentration. Fractions were collected for analysis throughout the course of each run. The chromatographic runs were performed at room temperature.

The same sort of experiments, but with diluted injections of each biological, were carried out to estimate the relevant SMA parameters for the IEX interactions of the baculovirus and main impurities with the membrane ligands, namely K_i and ν_i (these are discussed below in section 7.2.6). Pulses of 1×10^6 pfu of rBVs obtained from standard purification procedure and 0.5 mg of BSA and dsDNA were used for these runs.

AEXmc process modeling

In this section a brief description of the implementation of a SMA model for interpreting the IEX adsorption interactions of the baculovirus system with the membrane ligands is provided. The SMA model has been widely used for the understanding of ion-exchange processes (Brooks and Cramer, 1992; Shi et al., 2005; Karlsson et al., 2004). We use previous work on a virus-like particle system (Vicente et al., 2008) as a basis to address the AEXmc step for the purification of baculoviruses.

The SMA model defines three parameters—the characteristic charge, ν_i, the steric factor, σ_i, and the equilibrium constant, K_i—that determine the adsorption process as a stoichiometric exchange reaction of each solute with a certain number of adsorbed counte-

rions (Brooks and Cramer, 1992):

$$c_i + \nu_i q_0 \rightleftarrows q_i + \nu_i c_0 \qquad i = 1, ..., N_c, \tag{7.3}$$

where c_i and q_i are concentration of the biological i in the mobile and in the stationary phase, respectively, c_0 is the concentration of the salt in the mobile phase and q_0 is the concentration of bound salt available for exchange. The inherent equilibrium constant, K_i, is

$$K_i = \frac{q_i}{c_i}\left(\frac{c_0}{q_0}\right)^{\nu_i} \qquad i = 1, ..., N_c. \tag{7.4}$$

Some salt counterions are assumed to be sterically hindered by each biological i on the adsorptive surface; the concentration of the "blocked" salt counterions, q_0^*, is given by

$$q_0^* = \sum_{i=1}^{N_c} \sigma_i q_i \qquad i = 1, ..., N_c. \tag{7.5}$$

The condition of electroneutrality requires that

$$\Lambda = q_0 + \sum_{i=1}^{N_c} (\nu_i + \sigma_i) q_i, \tag{7.6}$$

where Λ is the capacity of the membrane.

The dynamics of the membrane adsorber, which is assumed to behave as a chromatographic column (with geometric parameters listed in Table 7.2), is described by an equilibrium dispersed plug-flow model (Guiochon et al., 1994). The differential material balance for component i can be written as

$$\frac{\partial c_i}{\partial \theta} + \frac{1-\epsilon}{\epsilon}\frac{\partial q_i}{\partial \theta} = \frac{1}{Pe}\frac{\partial^2 c_i}{\partial x^2} - \frac{\partial c_i}{\partial x} \qquad (0 < x < 1), \tag{7.7}$$

with boundary conditions

$$\begin{aligned} c_i - \frac{1}{Pe}\frac{\partial c_i}{\partial x} &= c_i^{in} \qquad \text{for } x = 0, \\ \frac{\partial c_i}{\partial x} &= 0 \qquad \text{for } x = 1, \end{aligned} \tag{7.8}$$

where ϵ is the void fraction, $x = z/L$ is the dimensionless axial position in the adsorber (z is the axial position within the thickness L of the stack of membrane sheets), $\theta = t/\tau$ is the dimensionless temporal coordinate ($\tau = L/u$ is the reference time with u the

interstitial linear velocity), Pe is the Péclet number for axial dispersion, and c_i^{in} is the inlet concentration. Initially, the membrane adsorber is solute-free and equilibrated with salt solution with concentration c_0^0; in this case the initial conditions are

$$\begin{aligned} c_0(0,x) &= c_0^0, \quad q_0(0,x) = \Lambda \\ c_i(0,x) &= 0, \quad q_i(0,x) = 0, \qquad i = 1, ..., N_c. \end{aligned} \tag{7.9}$$

For a bind-end-elute experiment, where the desorption is carried out by linear-gradient elution, the following boundary conditions apply:

$$\begin{aligned} c_0(\theta,0) &= \begin{cases} c_0^0, & \theta < \theta_F \\ c_0^0 + G(\theta - \theta_F), & \theta \geqslant \theta_F \end{cases} \\ c_i(\theta,0) &= \begin{cases} c_i^F, & \theta < \theta_F \\ 0, & \theta \geqslant \theta_F \end{cases} \end{aligned} \tag{7.10}$$

where θ_F is the dimensionless duration of the feed pulse, c_i^F is the feed concentration, and G is the gradient slope. The equations are numerically solved using gPROMS (Process Systems Enterprise, London, United Kingdom) as described elsewhere (Vicente et al., 2008). The characteristic charge, ν_i, the equilibrium constant, K_i, and the steric factor, σ_i are unknown parameters. The Péclet number is expected to be high, as we are using a system with good mass-transfer characteristics operated at reasonable flow rates; therefore, dispersion should not be significantly altered within the operating velocity window.

Under diluted material concentrations ($\Sigma_{i=1}^{N_c} c_i \to 0$), the adsorption isotherms are simplified to the linear form of Henry's law:

$$q_0 \to \Lambda, \qquad q_i \to K_i \left(\frac{\Lambda}{c_0}\right)^{\nu_i} c_i \qquad i = 1, ..., N_c. \tag{7.11}$$

The partition coefficient retains the nonlinear dependence on salt concentration but the steric factor becomes redundant. For the case of linear gradient chromatography, the retention time, θ^*, of an infinitely diluted peak can be predicted using the following expression (Gallant et al., 1996):

$$\theta^* = 1 + \frac{\left[\gamma_i G + (c_0^0)^{\nu_i+1}\right]^{1/(\nu_i+1)} - c_0^0}{G}, \qquad \gamma_i = (\nu_i + 1)\frac{1-\epsilon}{\epsilon} K_i \Lambda^{\nu_i} \tag{7.12}$$

Values of K_i and ν_i can be determined by fitting Eq. 7.12 to the retention times of several chromatographic runs at different gradient slopes, G, and different initial salt concentrations, c_0^0.

7.2.7 Analyticals

The number of genome containing particles was quantified by real-time PCR (qPCR) following the protocol described elsewhere (Vicente et al., 2009). Infective virus titers (IP) were determined with a flow cytometer-based assay (Vicente et al., 2009; Karkkainen et al., 2009). Protein profiling of samples collected after each of the purification steps were performed using NuPAGE Novex 4-12% Bis-Tris pre-cast polyacrilamide gels (Invitrogen, Paisley, UK) using standard running conditions. Visual detection was carried out using SimplyBlue Safe Stain (Invitrogen). Protein transfer onto nitrocellulose membrane was done with a semi-dry transfer unit (GE Healthcare); immunochemical detection of baculovirus main envelope glycoprotein, gp64, was carried out using a commercially available mouse monoclonal antibody (mAb) against gp64, AcV5 clone, affinity purified (1:2000 dilution) (eBioscience, San Diego, CA, USA) followed by incubation with an alkaline phosphatase conjugated anti-mouse IgG antibody (1:5000 dilution) (Sigma-Aldrich, München, Germany) and developed using 1-step NBT/BCIP (Pierce, Rockford, USA). SDS-PAGE and Western Blot band profiles were analyzed by ImageJ software (NIH, USA) using an available add-in designed for gel band densitometry quantification and normalization. The quantification of total dsDNA content in solution throughout processing was performed using the PicoGreen dsDNA Assay kit (Invitrogen, Paisley, UK) in 96-well plates according to the manufacturer's instructions. Total protein content of samples was determined using the BCA protein assay kit (96-well plate protocol) from Pierce following the manufacturer's protocol.

7.3 Results and discussion

7.3.1 Impact of ligand density on the adsorption capacity of DEAE-modified surfaces

The impact of DEAE ligand density on the overall capacities for either rBVs or BSA (the latter used here as a host-cell protein model) was first studied by surface plasmon resonance using the previously reported protocol (Vicente et al., 2010b,a), but with three different

derivatized surfaces rather than just a single one. The three new sensor chips employed here were customized to expose different ligand densities: a self-assembled monolayer on a bare gold sensor surface, MUA-DEAE; a 30 nm long dextran layer chip, CM3-DEAE (Kyprianou et al., 2009); and a 100 nm long dextran layer chip, CM5-DEAE (Yu et al., 2004; Wofsy and Goldstein, 2002). All three chips were covalently immobilized with DEAE ligands.

Using this approach we were able to prepare three anion-exchange sensor chip surfaces with different ligand densities; furthermore, the use of a dextran layer mimics well the gel layer from a commercially available Sartobind D membrane adsorber (Tatárová et al., 2009). Analysis of adsorption of rBV and BSA (as a control) was performed on the three surfaces to assess the impact of DEAE ligand density.

As shown in Fig. 7.3a, the decrease in ligand density has a clearer impact on BSA adsorption than on rBV. Indeed, the BSA overall adsorption capacity dramatically decreases to approximately 20% of the highest reference ligand density surface. However, for rBV, a decrease to approximately 60% is obtained, indicating that ligand density is playing a less important role for equally efficient viral particle adsorption. The maintenance of the adsorbed rBV concentration at high levels regardless of ligand density is indicative that these particles (of over 90-120 nm in diameter and 350 nm in length) remain outside the inner dextran layer ligand sites which are only freely accessible to smaller biomolecules like BSA. The same type of phenomenon is anticipated to occur in a membrane adsorber with decreased ligand densities.

In order to support these exploratory experiments, similar tests were performed with another important viral vector in clinical applications: human adenovirus type 5, a non-enveloped virus with an equivalent particle diameter of approximately 90-100 nm (Trilisky and Lenhoff, 2007). Even with a smaller overall size compared to rBV, the maximum adsorption of these particles is not affected by the decrease in ligand density (Fig. 7.3b). Thus, reduced ligand densities seem to improve selectivity for virus as less contaminating protein is being adsorbed under lower ligand densities.

The results obtained from these SPR experiments justified the production of prototypes Sartobind D membranes with lower ligand densities for testing this hypothesis.

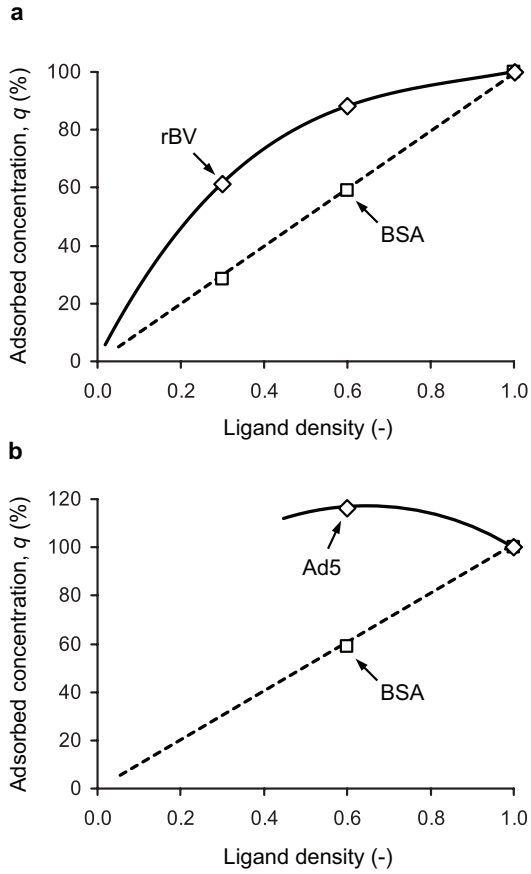

Figure 7.3: *Comparison between adsorption concentration obtained under equal adsorption conditions (same ionic strength) on surfaces with different DEAE ligand densities: respectively, a) rBV particles, and, b) Ad5 particles compared to BSA total adsorption versus ligand density on SPR sensor chip; each isolated biological was injected over previously sanitized sensor surfaces at* $c_0 = 0.010$ *M at a constant pH=7; ligand fraction = 1 is defined as the highest DEAE density (in this work, CM5 sensor chip derivatized with DEAE); 100% total adsorbed concentration stands for the value obtained for CM5 sensor chip derivatized with DEAE;* d_m *=100 nm for Ad5 particles, a value from hydrodynamic size measurements via DLS; the lines serve as guide.*

7.3.2 AEXmc experiments with Sartobind D membrane prototypes

Impact of ligand density, salt equilibration, and elution gradient length on process performance

Sartobind D membrane adsorber sheets with different ligand densities were used as membrane prototype layers for studying the impact of ligand density on process performance (Table 7.2). The prototype units were assembled by stacking 3 layers, with a summed total area of 15 cm^2 equal to total membrane area of the commercially available Sarto-

bind D MA15 units from Sartorius-Stedim Biotech. A DoE-type of experimental design was devised to evaluate the impact of ligand density, salt equilibration of the rBV bulk feedstock (by means of adjusting the buffer salt concentration upon the previous diafiltration process), and linear elution gradient length.

Table 7.3 summarizes the results obtained for the systematic testing of the Sartobind D membrane prototypes. Four process performance indicators are assessed for the evaluation of the sets of experiments derived from the permutation of the three operating conditions. These results refer to the analysis of the peak pools obtained in each of the experiments.

Although some variability is observed, the active, infective rBV yields are highest at the lowest ligand density. Compared to the current purification strategy based on commercial Sartobind D membranes (Vicente et al., 2009), an increase of over 20% in infective particles is achieved with the lowest membrane ligand density tested here. The quality of the rBV pools are also improved, which should be directly related to the increase of infective titer obtained, but might also be due to the fact that some of the damaged rBV particles (product-derived impurities) have either flown through the membrane during the loading step or, being weakly adsorbed, eluted during the washing step before the actual linear gradient elution; as a consequence, the TP/IP was decreased from 18 to 5.

With regards to the process-derived impurities, the decrease in ligand density has a clear impact on the host cell derived dsDNA content; this impurity concentration is lowest at the lowest ligand density (Table 7.3). The total protein content is also lowest at the two lower ligand density membranes and lower at higher salt equilibration concentration (Table 7.3).

Overall, these results show the expected trend: improved product purity and yield as an outcome of decreased membrane ligand density. This suggests that for this rBV system the deprivation of some of available ligand sites affects primarily the binding of process-derived impurities (total protein and dsDNA) and, to a smaller extent, also the product-derived impurities (damaged rBV particles). The tested range of salt equilibration concentration does not show a significant impact on the process indicators; however, in some cases (as for total protein) an increase in the salt concentration confers an increase in purity. The gradient lengths seemed of no significance here possibly due to the short range chosen, not sufficient to improve peak resolution. This gradient effect is addressed in more detail in the following section using the implemented SMA model predicting tool.

Table 7.3: *DoE-based approach results on ligand density, salt equilibration and gradient length operating conditions impact on binding and elution of rBVs.*

Ligand density (μmol.cm^{-2})	Salt equilibration (mM)	Gradient length (MV)	Recovery yield, IP[a] (%)	TP[b]/IP	dsDNA (ng.(10^8 IP)$^{-1}$)	Total protein (mg.(10^8 IP)$^{-1}$)
2.2	30	40	73	4	5	61
2.2	30	40	47*	6*	15*	121*
2.2	30	40	82	4	8	35
2.2	45	120	73	4	9	66
2.2	60	40	83	5	7	37
2.2	60	120	75	5	7	31
5.0	50	40	70	6	8	55
5.0	50	80	64	6	4	35
5.0	50	80	56	9	14	51
5.0	50	120	59	8	8	45
6.1	30	40	52	24	120	101
6.1	30	120	28	11	168	231
6.1	60	40	59	2	105	101
6.1	60	120	50	6	143	151

[a]infective particle; [b]total particle; TP/IP ratio provides a means for estimating virus quality; *denotes an outlier experiment.

Table 7.4: *SMA parameters used for AEXmc process simulation.*

ϵ^{a}	0.62
Salt equilibration (mM)	40
Pe^{b}	7880
(ν_0, K_0)	$(1, 1)$
(ν_1, K_1)	$(4.3, 6.0 \times 10)$
(ν_2, K_2)	$(4.7, 6.7 \times 10^3)$
(ν_3, K_3)	$(4.8, 6.8 \times 10^4)$
(ν_4, K_4)	$(5.1, 8.0 \times 10^2)$
(ν_5, K_5)	$(2.6, 8.0)$
(ν_6, K_6)	$(1, 0)$

[a]obtained through estimation of membrane void volume; [b](Vicente et al., 2008); in this table the indexes 0, 1, 2, 3, 4, 5, and 6 correspond, respectively, to salt, rBV 1st peak, rBV 2nd peak, rBV 3rd peak, dsDNA, HCP, and non-adsorbing material.

SMA modeling and recommendations

In this section, the implementation of our previously used SMA-based model for AEXmc process interpretation and prediction (Vicente et al., 2008) is presented. The first step was to estimate the key model parameters described in the Materials and methods section. Table 7.4 summarizes the used parameters for process simulations. The total porosity, ϵ, was estimated by injecting a salt pulse on the ÄKTA system with and without the membrane unit mounted; the membrane void volume is obtained by difference. As we have observed in our experimental chromatograms of rBV preparations the elution of three peaks with different retention times (or volumes), we assume the whole sum of the three rBV peaks to be the final product, as all three contain active (infective) viral particles, although not in the same proportion. The last peak to elute was observed to be somewhat more infective (data not shown), suggesting that the rBVs eluting earlier may either adsorb at a different position or may contain an altered envelope (deprived of a fraction of the gp64 glycoproteins). This result was confirmed by qPCR (data not shown). The remaining components constitute the two major process derived impurities, dsDNA and HCP. Simulations of the chromatograms obtained could then be rendered using the gPROMS software tool.

Figure 7.4 shows the simulations performed after parameter estimation, identification of the different component peaks and comparison with experimental chromatograms. Overall, there is a good prediction of the rendered chromatograms agreeing well with the experimental runs. This reinforces the applicability of the SMA model to this viral vector system, similarly to what was observed before for a VLP system (Vicente et al., 2008).

One can now hypothesize that the lowest membrane prototype ligand density tested in this work, 2.2 μmol.cm^{-2}, does not significantly limit the adsorption of rBV particles, because their large size ($>$ 100 nm) prevents them from having access to the ligands within

the depth of the hydrogel layer (Tatárová et al., 2009). If this were the case, one can assume that when the total adsorption capacity, Λ, is increased, only the smaller biomolecules—HCP and host cell dsDNA—should experience an increase in total adsorption and thereby an increase in the released peak intensity upon elution using the linear salt gradient. This can be confirmed with the SMA formalism implemented in this work: using the described model and membrane characteristics, simulations can be performed for the different Λ values corresponding to the prototype membranes used.

Figure 7.4 compares the experimental and simulated chromatograms of the AEXmc process at different Λ values. From the simulated chromatograms it is possible to estimate when the rBVs are expected to elute (see Figs. 7.4b, d and f). Additionally, the peaks of the process-derived impurities are seen to be partially co-eluting with the rBVs. This is in agreement with the fact that HCP and dsDNA are still present in the viral peaks samples obtained (Table 7.3).

If Λ is varied, the simulated chromatograms still predict well the retention volume of the different material peaks. However, if the amount of HCP and dsDNA that was obtained in the flowthrough and peak pools and the peak concentration of the rBVs are taken into account, one concludes that the decrease in ligand density results mostly in the decrease of the process-derived impurities peaks. In fact, the AEXmc simulations show good agreement with the results shown in Table 7.3.

These results provide evidence that the model is capable of explaining the possible accessibility issue of large particles to the available ligand sites. It is worth noting, however, that the simulations assume that the large particles are not hindered by the overloading of the other process-derived impurities. Such effect has to be studied in more detail to assess how much of the ligands are effectively available at the exposed hydrogel layer over the membrane cellulosic backbone.

Looking at the elution profiles obtained with the chosen linear salt gradients (typical lengths used in preparative ion-exchange chromatography), it is clear that the process resolution is unsatisfactory. Resolution of eluted peaks can be increased either by extending the linear salt gradient length or by increasing the amount of stationary phase.

Figure 7.5b shows an extension of the linear salt gradient predicted by the SMA model. Comparing this figure with the original chromatogram in Fig. 7.5a, it is seen that in Fig. 7.5b there is a better separation of the eluted peaks; however, they also elute more dispersedly. Moreover, a too extended linear salt gradient can be an unacceptable option as it reduces the benefits of using membrane adsorbers: buffer consumption is dramatically

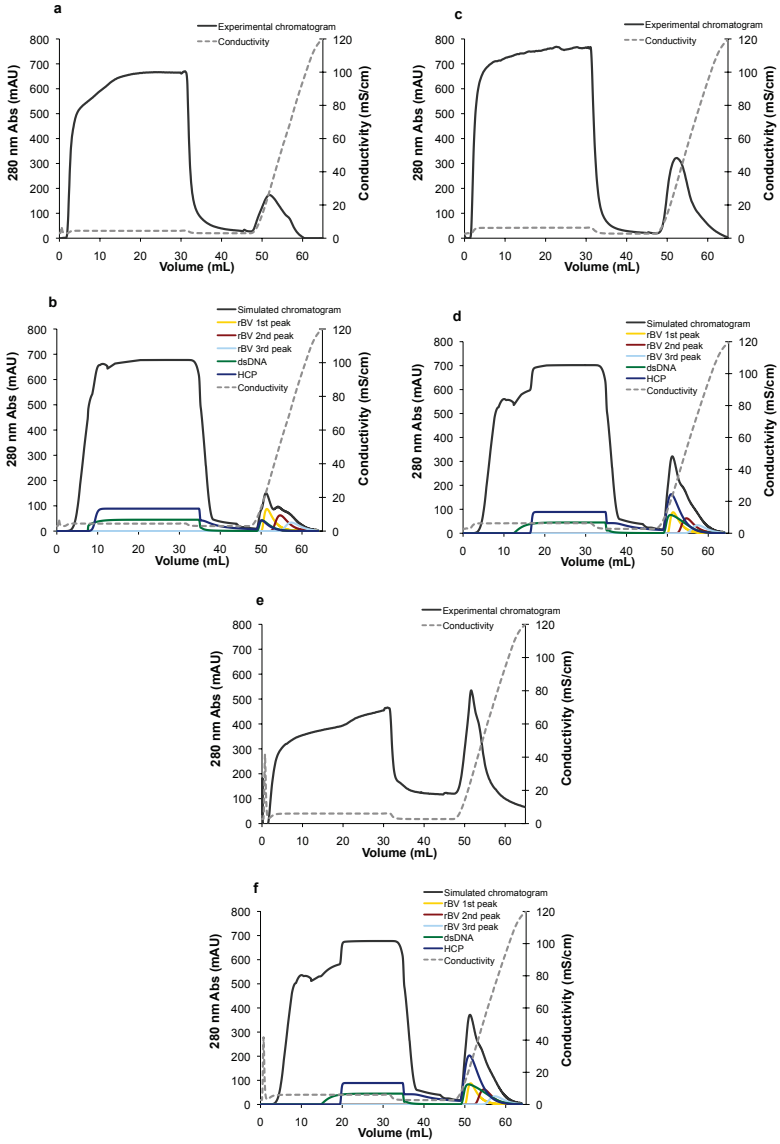

Figure 7.4: *Effect of ligand density, i.e., total adsorption capacity, Λ, on AEXmc elution peaks and comparison with simulated chromatograms. Experimental runs: $\Lambda = 81$ mM (a), 185 mM (c), 226 mM (e); the corresponding simulated chromatograms are, respectively, (b), (d), and (f), in which "simulated chromatogram" stands for the sum of all component curves. The flow rate in all experiments is 5 mL/min.*

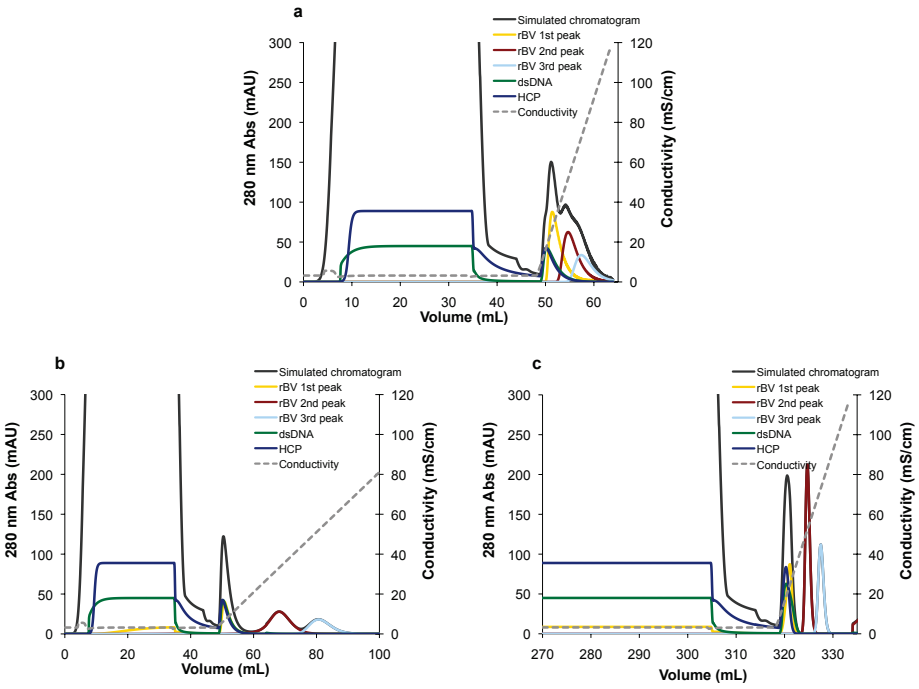

Figure 7.5: *AEXmc process resolution improvement assessment via SMA model simulations using the membrane with lowest ligand density, Λ=81 mM: a) represents the original AEXmc process; b) and c) show, respectively, the elution profile prediction when increasing the gradient length 5-fold (flow rate is maintained at 5 mL.min^{-1}), and, when increasing 10-fold the membrane bed height with concomitant 10-fold load scale-up (flow rate is maintained at 5 mL.min^{-1} except at the membrane loading step, increased to 50 mL.min^{-1}).*

increased and productivity may be decreased by too extended duration of the AEXmc process. Alternatively, resolution can be improved by using a membrane matrix with a taller stack of membrane layers (increased amount of stationary phase); for instance, if the height of the membrane is increased 10-fold while maintaining the membrane unit diameter, even if scaling-up the load by 10-fold, the resolution is enhanced as observed in Fig. 7.5c in comparison to the original membrane in Fig. 7.5a.

7.4 Conclusions

This paper evaluated the ligand density effect on an anion-exchange membrane chromatography process for the purification of recombinant baculoviruses, potential biopharmaceuticals in clinical applications. A previously implemented scale-down strategy based on surface-plasmon resonance to address DEAE ligand density was used. Exploratory results combined with previous knowledge indicating inaccessibility of large particles to some of

the ligand sites in the hydrogel layer covering the cellulose backbone of the membrane matrix led to the development of membrane prototypes with different ligand densities. Both SPR-derived and membrane chromatography-derived results suggest that lower ligand density is beneficial for rBV particle purification, increasing the overall yields by over 20%, improving the removal of process-derived impurities and increasing product quality as measured by the decreased TP/IP ratio. A theoretical model based on the steric mass action formalism, served as a useful predicting tool to determine how conditions can be altered to further improve process resolution/selectivity ultimately enhancing final product purity and recovery yield. A patent has been filed to support the use of these knowledge-based strategies to improve membrane design and faster process optimization.

Acknowledgements

We thank Dr. Kari Airenne (University of Eastern Finland, Kuopio, Finland) for providing the recombinant baculoviruses used in this work. We want also to thank David Tomaz and Rimenys Carvalho for analytical support and Ana Silva for purified Ad5 material. We acknowledge funding from the European Commission (Baculogenes, LSHB-2006-037541 and Clinigene – Network of Excellence, LSHB-2006-018933) and the Portuguese *Fundação para a Ciência e a Tecnologia* (PTDC/EQU-EQU/71645/2006 and SFRH/BD/31257/2006).

References

Gene therapy clinical trials worldwide. charts and tables, vectors. J Gene Med 2009.

Airenne KJ, Hiltunen MO, Turunen MP, Turunen AM, Laitinen OH, Kulomaa MS, et al. Baculovirus-mediated periadventitial gene transfer to rabbit carotid artery. Gene Ther 2000;7:1499–504.

Airenne KJ, Mähönen AJ, Laitinen OH, Ylä-Herttuala S. Baculovirus-mediated gene transfer: An emerging universal concept. In NS Templeton, ed., Gene and Cell Therapy: Therapeutic Mechanisms and Strategies. CRC Press, Boca Raton, 3rd ed., 2009.

Brooks CA, Cramer SM. Steric mass-action ion exchange: Displacement profiles and induced salt gradients. AIChE J 1992;38:1969–1978.

Coffman JL, Kramarczyk JF, Kelley BD. High-throughput screening of chromatographic separations: I. method development and column modeling. Biotechnol Bioeng 2008;100:605–618.

Gallant SR, Vunnum S, Cramer SM. Optimization of preparative ion-exchange chromatography of proteins: linear gradient separations. J Chromatogr A 1996;725:295–314.

Guiochon G, Golshan-Shirazi S, Katti A. Fundamentals of Preparative and Nonlinear Chromatography. Academic Press, Boston, MA, 1994.

Kanegae Y, Makimura M, Saito I. A simple and efficient method for purification of infectious recombinant adenovirus. Jpn J Med Sci Biol 1994;47:157–66.

Karkkainen HR, Lesch HP, Maatta AI, Toivanen PI, Mahonen AJ, Roschier MM, et al. A 96-well format for a high-throughput baculovirus generation, fast titering and recombinant protein production in insect and mammalian cells. BMC Res Notes 2009;2:63.

Karlsson D, Jakobsson N, Brink KJ, Axelsson A, Nilsson B. Methodologies for model calibration to assist the design of a preparative ion-exchange step for antibody purification. J Chromatogr A 2004;1033:71–82.

Knoll W, Schmitt FJ, Klein C, Guder HJ, Liley M, Spinke J. Universal binding film. US Patent 5763191 1998.

Kost T, Condreay J, Jarvis D. Baculovirus as versatile vectors for protein expression in insect and mammalian cells. Nat Biotechnol 2005;23:567–75.

Kukkonen SP, Airenne KJ, Marjomaki V, Laitinen OH, Lehtolainen P, Kankaanpaa P, et al. Baculovirus capsid display: a novel tool for transduction imaging. Mol Ther 2003;8:853–62.

Kutner RH, Puthli S, Marino MP, Reiser J. Simplified production and concentration of hiv-1-based lentiviral vectors using hyperflask vessels and anion exchange membrane chromatography. BMC Biotechnol 2009;9:10.

Kyprianou D, Guerreiro AR, Chianella I, Piletska EV, Fowler SA, Karim K, et al. New reactive polymer for protein immobilisation on sensor surfaces. Biosens Bioelectron 2009;24:1365–1371.

Okada T, Nonaka-Sarukawa M, Uchibori R, Kinoshita K, Hayashita-Kinoh H, Nitahara-Kasahara Y, et al. Scalable purification of adeno-associated virus serotype 1 (aav1) and aav8 vectors, using dual ion-exchange adsorptive membranes. Hum Gene Ther 2009;20:1013–21.

Opitz L, Salaklang J, Buttner H, Reichl U, Wolff MW. Lectin-affinity chromatography for downstream processing of mdck cell culture derived human influenza a viruses. Vaccine 2007;25:939–947.

Peixoto C, Ferreira TB, Sousa MFQ, Carrondo MJT, Alves PM. Towards purification of adenoviral vectors based on membrane technology. Biotechnol Prog 2008;24:1290–1296.

Rege K, Pepsin M, Falcon B, Steele L, Heng M. High-throughput process development for recombinant protein purification. Biotechnol Bioeng 2006;93:618–30.

Rodrigues T, Carrondo MJT, Alves PM, Cruz PE. Purification of retroviral vectors for clinical application: Biological implications and technological challenges. J Biotechnol 2007;127:520–541.

Rodrigues T, Carvalho A, Roldao A, Carrondo MJT, Alves PM, Cruz PE. Screening anion-exchange chromatographic matrices for isolation of onco-retroviral vectors. J Chromatogr B 2006;837:59–68.

Roper DK, Nakra S. Adenovirus type 5 intrinsic adsorption rates measured by surface plasmon resonance. Anal Biochem 2006;348:75–83.

Shi Q, Zhou Y, Sun Y. Influence of ph and ionic strength on the steric mass-action model parameters around the isoelectric point of protein. Biotechnol Prog 2005;21:516–23.

Tatárová I, Fáber R, Denoyel R, Polakovic M. Characterization of pore structure of a strong anion-exchange membrane adsorbent under different buffer and salt concentration conditions. J Chromatogr A 2009; 1216:941–947.

Teeters MA, Root TW, Lightfoot EN. Performance and scale-up of adsorptive membrane chromatography. J Chromatogr A 2002;944:129–139.

Trilisky EI, Lenhoff AM. Sorption processes in ion-exchange chromatography of viruses. J Chromatogr A 2007;1142:2–12.

Vicente T, Mota JPB, Peixoto C, Alves PM, Carrondo MJT. Analysis of adsorption of a baculovirus bioreaction bulk on an ion-exchange surface by surface plasmon resonance. J Biotechnol 2010a;148:171–181.

Vicente T, Mota JPB, Peixoto C, Alves PM, Carrondo MJT. Modeling protein binding and elution over a chromatographic surface probed by surface plasmon resonance. J Chromatogr A 2010b;1217:2032–2041.

Vicente T, Peixoto C, Alves PM, Carrondo MJT. Modeling electrostatic interactions of baculovirus vectors for ion-exchange process development. J Chromatogr A 2010c;1217:3754–3764.

Vicente T, Peixoto C, Carrondo MJT, Alves PM. Purification of recombinant baculoviruses for gene therapy using membrane processes. Gene Ther 2009;16:766–775.

Vicente T, Sousa MFQ, Peixoto C, Mota JPB, Alves PM, Carrondo MJT. Anion-exchange membrane chromatography for purification of rotavirus-like particles. J Membr Sci 2008;311:270–283.

Wensel DL, Kelley BD, Coffman JL. High-throughput screening of chromatographic separations: Iii. monoclonal antibodies on ceramic hydroxyapatite. Biotechnol Bioeng 2008;100:839–854.

Wofsy C, Goldstein B. Effective rate models for receptors distributed in a layer above a surface: application to cells and biacore. Biophys J 2002;82:1743–1755.

Wu C, Soh KY, Wang S. Ion-exchange membrane chromatography method for rapid and efficient purification of recombinant baculovirus and baculovirus gp64 protein. Hum Gene Ther 2007;18:665–72.

Wu N, Ataai MM. Production of viral vectors for gene therapy applications. Curr Opin Biotechnol 2000; 11:205–8.

Yu F, Persson B, Löfås S, Knoll W. Attomolar sensitivity in bioassays based on surface plasmon fluorescence spectroscopy. J Am Chem Soc 2004;126:8902–8903.

Part III

Overview

Chapter 8

DISCUSSION AND CONCLUSIONS

Contents

8.1 Discussion

Innovative advanced therapies are emerging; gene therapy and novel vaccines are becoming increasingly relevant for the treatment of prominent human diseases. Complex biopharmaceuticals, like the VLPs from Rotavirus and baculovirus vectors studied in this dissertation, are examples of relevant biologicals holding a number of advantages and with very encouraging results in pre-clinical trials. However, as for any pharmaceutical product, efficient, scalable, cost-effective manufacturing processes capable of generating material to support clinical trials are required. This currently constitutes a great challenge in an investigational new drug (IND) product lifecycle.

Although very important advances have taken place in the last decade, the development of economic and highly efficient downstream processes is still quite incipient. The work presented in this thesis aimed at building sound tools for a more rational understanding of the downstream processing of enveloped viruses, in particular baculoviruses.

The focus has been directed to one of the most relevant purification steps: ion-exchange (IEX) chromatography. Due to its very appealing advantages, which include scalability, robustness, cost-effectiveness, and high resolution power, we have attempted to better understand the physicochemical phenomena involved in the product-matrix interaction in order to more efficiently design the chromatographic processes.

8.1.1 Improved tools for process design

Understanding the ion-exchange chromatography step

The work carried out during this thesis gave rise to:

(i) A mathematical model of IEX membrane cromatography based on a thermodynamic formulation of the multicomponent adsorption equilibrium, which uses the steric mass action (SMA) model for predicting the IEX process (Chapters 2 and 7, Vicente et al. (2008, 2010a));

(ii) A scale-down analytical tool based on surface plasmon resonance (SPR), which works as a planar micrometric chromatographic adsorber, for measuring adsorption equilibrium and kinetics, supported by the required theory and modeling tools that explain in detail the binding and elution mechanisms (Chapters 4 and 5, Vicente et al. (2010b,c));

(iii) A theoretical analysis, supported on dynamic light scattering (DLS) experiments, of the impact of the electrostatics of the different viral components and their implication on the overall electrokinetic potential of the infective virus (Chapter 6, Vicente et al. (2010d)); the combination of these fundamental tools created a good knowledge basis to study a complex bioproduct—an enveloped virus, the baculovirus—and allowed to improve a critical purification step—IEX chromatography.

The IEX chromatography step, implemented under the configuration of a membrane adsorber, could be simulated appropriately using the developed models. Successfully predicting the product peak elution using this model allowed to estimate the relevant process parameters. Furthermore, knowledge from the SPR- and DLS-based experiments was employed in the early-stages of process development for identifying an optimum range of operating conditions, namely ionic strength and pH, for process optimization at-scale. In Chapter 7, useful recommendations for process and matrix improvement could be made by performing chromatographic simulations; the effects of flow rate, elution gradient velocity, and feedstock loads were studied in order to determine possible matrix alterations yielding better resolution. Overall, the following outcomes were achieved:

- Baculovirus characterization with regards to infectivity, i.e., infective *versus* non-infective baculovirus particles; the impact of envelope and glycoprotein on IEX adsorption and elution was studied in Chapters 5 and 6;

- Baculovirus binding orientation: non-spherical nature and heterogeneity of the rod-shaped baculovirus particles dictated a distribution of the thermodynamically most favored interaction orientations (Chapter 6);

- Baculovirus *versus* process-related impurities: a comparison based on adsorption

isotherms of the isolated components could be obtained (Chapter 5).

This type of *in silico* tools facilitate bridging of efforts from bioseparation scientists and manufacturers of purification materials. Using these tools, novel prototype matrices can be designed and evaluated much more rapidly using minute amounts of biological material. The determination of the adsorption isotherms of the critical players in this system over a broad range of equilibrium conditions in a scaled-down system permits to setup advanced process design strategies for this IEX process.

In principle, continuous or semi-continuous, multicolumn processes, like the ones being developed in the mAb field based on the simulated moving bed (SMB) concept (Müller-Späth et al., 2008, 2010), can be conveniently and cost-effectively designed with the analytical techniques proposed in this thesis. Multicolumn or multi-unit processes (where by 'unit' we mean any suitable adsorbent matrix) present great advantages over single-column solvent-gradient batch chromatography, with or without recycle, but are more difficult to design (Rodrigues et al., 2010) and require knowledge about the adsorption equilibrium of the competing solutes. This information is the basis for the design or optimization of any chromatographic process governed by the thermodynamics of adsorption; this is the case of IEX chromatography. Mass transfer and axial dispersion influence the composition fronts in the chromatographic matrix, by smearing the concentration profiles, but do not change their stoichiometric positions when the process is not limited by the adsorption kinetics. Moreover, convection is known to be the prevailing mass transport mechanism in membrane adsorbers where there are nearly no diffusion limitations. If the adsorption isotherms are known, suitable operating conditions can be determined through the application of design rules, such as those developed for SMB chromatography, or by computer-aided optimization (Araújo et al., 2010). We propose the use of scaled-down models of IEX stationary phases and others, such as those employed in our SPR experiments, for the preliminary design of the multicolumn solvent-gradient chromatographic processes that are now emerging for the separation of complex biomixtures.

Fig. 8.1 illustrates the design and optimization of an IEX process: (i) we start by gathering fundamental data using cost-effective strategies as the ones developed during this thesis; (ii) this information is then used to design an optimized IEX process operated in batch mode; (iii) but we can envisage its ultimate use on the design of a more sophisticated continuous (or semi-continuous) IEX process, granting high productivity, recovery yield, purity and process consistency.

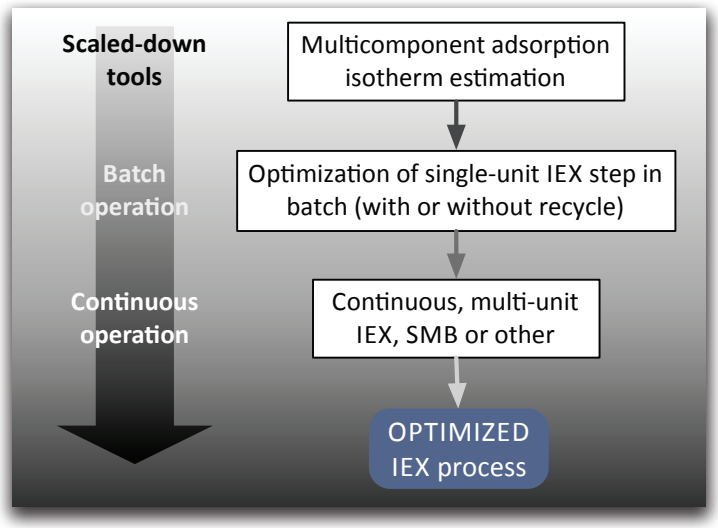

Figure 8.1: *From batch to continuous IEX process development. The present thesis focused its attention on the first and part of the second stage.*

To do this optimization, targets and constraints need to be clearly defined. The following premises can be used in an *in silico* process optimization routine:

- Constraint one: minimum purification factor – cutting the peaks at a maximum "peak overlapping": the process-derived impurities (host cell protein (HCP) and host cell DNA (HC DNA)) in the final product peak must be below a certain threshold value;
- Constraint two: minimum total particle/infective particle (TP/IP) ratio at final product peak due to likely product and product-related "peak overlapping";
- Constraint three: minimum concentration factor – linear flow velocity or flow rate in a *per* day and *per* batch volume: an efficient purification step time and productivity has to be reached.
- Objective one: maximum throughput/productivity – assess how, by changing one (or more) operating conditions, the process can be run faster yielding the desired performance indicators;
- Objective two: maximum product titer (potency) – assess how, by changing one (or more) operating conditions, the process can yield a higher product titer, whilst preventing product aggregation.

It should be emphasized that the above constraints and objectives are closely interrelated, which means that the best compromise has to be obtained in order to optimize

the whole process. These type of interrelations can be assessed by a DoE approach. For instance, if the concentration factor attained is too high (objective two), the impurities co-eluting in the product fraction peak might also exceed the acceptable concentration limit: this may turn out to be critical in the case of HC DNA or HCP (constraint one). Also, if a too extended linear elution gradient is necessary to permit an acceptable TP/IP (constraint two), it may result in a very low throughput and probably in a low titer (objectives one and two). Therefore, such hurdles inherent to this complex biological system may oblige to add extra rules in order the find the best solution for the optimization problem.

The importance of a good DSP backbone

The overall strategy outlined in Fig. 8.2 summarizes the rationale in this thesis. The first efforts were based primarily on a pragmatic and preliminary sensible selection of the best technologies and matrices available in the market. This constitutes the essence of the work presented in Chapter 3, where an industrially relevant DSP strategy is proposed (Vicente et al., 2009a). From that point on, process development could be performed in a much more solid way. Such an integrated view of the process optimization was successful in improving the overall DSP, capable of delivering the final material within the required QC specifications.

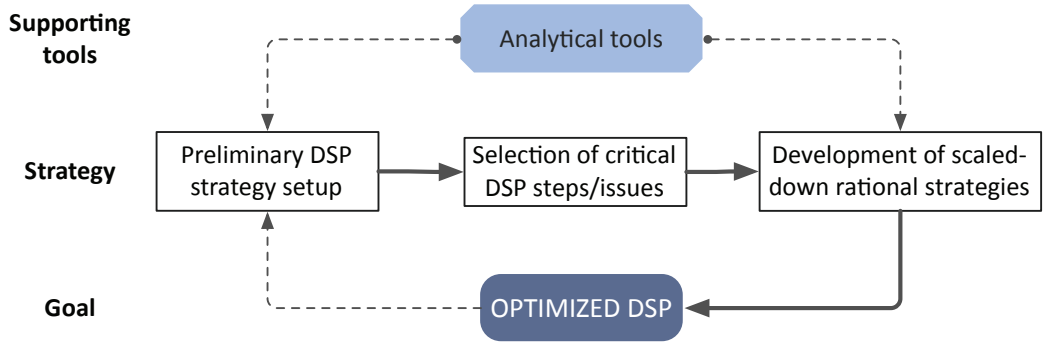

Figure 8.2: *Schematic representation of the rationale used in the thesis for improved process design and optimization.*

As shown in Chapters 2 and 3, gathering the best empirical/heuristics information about the current state-of-the-art technologies for the purification of complex biopharmaceuticals was shown to be critical. The use of membrane processes for early clarification/recovery and concentration/purification, studied in Chapters 2 and 3, indicates how disposable processes can be implemented with very good yields and throughputs. Even though centrifugation is still the gold standard in industry for cell debris removal, the type

of flexibility these new technologies bring in terms of upfront investment and cGMP ease of operation is highly attractive (Peixoto et al., 2008; Gottschalk, 2008; Vicente et al., 2009a,b). Especially when a complex biological tends to be highly labile, the higher the throughput that can be obtained using mild conditions the better. Depth-filtration and tangential flow filtration (TFF) both have been shown to be best for this enveloped virus system (Vicente et al., 2009a) but also for non-enveloped viruses (Peixoto et al., 2008), outperforming other alternatives at the upfront clarification and concentration stages.

Moreover, these technologies are now available from various disposable equipment manufacturers saving validation labor and costs. As emphasized in the introduction chapter, it is anticipated that monoliths will be added to these "new" generation matrices, together with membrane adsorbers, for the purification of large biopharmaceuticals as viral particles (Jungbauer and Hahn, 2008; Trilisky and Lenhoff, 2009).

8.1.2 The leverage of fundamental knowledge in process development

Chapter 7 provides a proof of concept where the usage of the proposed scaled-down approaches streamlined a DoE-type of approach (Vicente et al., 2010a). The suitable pH and ionic strength of the equilibration buffer could be determined from the modeling tool based on ζ-potential (Vicente et al., 2010d) and the information gathered during preliminary SPR data modeled as an IEX chromatography tool (Vicente et al., 2010b). Ligand density, a major parameter in any chromatographic matrix, was assessed by expedite means: counter-intuitively, too high ligand density seems not to be conducive to improved capture of virus particles as it mainly contributes to increasing impurity binding and thus contamination of the product peaks. Therefore, lower than maximum ligand densities improved recovery yields whilst also increasing product quality (by decreasing TP/IP) and decreasing the content in process-related impurities (HCP and HC DNA).

However, there is still much more to be known in terms of accessibility of these large biological particles to the ligand sites placed within the hydrogel of the membrane adsorber (Tatárová et al., 2009). Only smaller (and simpler) biomolecules as proteins seem to have full access to the ligand sites. It is perhaps due to this fact that, using our SMA model implementation (in Chapters 2 and 7, Vicente et al. (2008, 2010a)), the characteristic charges, ν_i, found for the viral particles studied, where quite comparable to the values found for protein molecules (Ladiwala et al., 2005). Most likely, only a very small fraction of the viral particle surface is effectively participating in the interaction with the ion-exchange

matrix; further research in this topic is thus needed to assess whether the capacity of these porous matrices to bind these biological particles can still be increased.

8.1.3 Putting targets into perspective: did we do the job?

A clear identification of the goals of the purification design must be set from the very beginning. For instance, the level of HC DNA must be below 10 ng/dose. As shown in Chapter 2, the purified RLP product contained a final dsDNA concentration in the range of 2-20 ng/dose, assuming that the VLP dosage may be up to 10-20 μg, although doses as low as 1 μg are possible, as seen for an influenza VLP (Galarza et al., 2005). As for protein impurities it is still challenging to find highly accurate methods to clearly identify VLP-derived protein from the host cell-derived protein; immunoblotting and ELISA combined with SDS-PAGE provides an indication, but the accuracy is still low. Nonetheless, it could be observed that the employed DSP resulted in HCP purity over 98% (Vicente et al., 2008).

Similarly, for the baculovirus system, very good reduction of both impurities resulted in over 98% of final product purity (Vicente et al., 2009a). However, as discussed in Chapter 3, the amount of impurities depends on the dose required to attain a certain biological response. In special cases, where the final formulation and/or application requires very high doses (Airenne et al., 2009), virus titers above 10^{10} pfu/mL may be needed, requiring larger concentration factors than usual in DSP. This may prove challenging as aggregation might start to be an issue decreasing the potency of the final, purified vectors (Barsoum, 1999). At the same time, the other impurities, non-infective viral particles, HCP and HC DNA may also get co-concentrated. Although engineering improvement is still feasible, efforts directed towards enhanced molecular biology for these products are also needed: e.g., one of the issues to overcome in the case of baculovirus, often requiring too high virus titers for efficient gene transfer, is to create virus surface modifications evading the complement system upon virus transduction (Airenne et al., 2009). Thus, extra hurdles still lie ahead for which the tools developed herein may facilitate progress.

8.2 Conclusions and perspectives

Rational optimization of downstream processes for complex biopharmaceuticals, as virus particles or VLPs, is in its infancy, this thesis contributing to such efforts. It could be shown that knowledgeable approaches improve optimization reducing its time and costs. A step towards a concept that is now familiar in the biopharmaceutical industry—Quality

by Design (QbD)—has been taken, improving early stage screening strategies based on DoE and/or HTS.

Studies focusing on the orientation and placement of the specific binding sites of proteins have been published recently (Dismer and Hubbuch, 2010; Dismer et al., 2008; Dismer and Hubbuch, 2007); combining such molecular-based knowledge with the thermodynamic data obtained using the electrokinetic model presented in Chapter 6 (Vicente et al., 2010d) and a refined three-dimensional structure resolution of the hydrogel layer present in a membrane adsorber matrix could push rational design forward.

Furthermore, the SPR-based tools open up new perspectives of possible investigation, for example, modified sensor chips harboring the desired ligand chemistry produced by chromatographic manufacturers themselves. Such sensor chips will be able to mimic much more closely a real-world chromatographic matrix, including mass transfer issues in a three-dimensional environment, allowing to focus into the adsorption and desorption of the different components of these complex systems. The SPR-based methodology developed in this thesis was intended, as a first step, to make a broad comparison, providing a means to evaluate how, by changing critical operating conditions, the best resolution and yield could be obtained. This was more important at a preliminary stage than calculating very accurately the adsorption of each component, either the product (the virus particle) or the impurities present in the bulk. A next step performing multi-component analysis using enhanced sensor chips shall provide a closer picture of the actual IEX process. Evaluating simultaneously the binding of the virus particles and HCP (or other impurities) may provide further insights regarding the impact of ligand density and/or ligand approachability. We expect that monoliths, showing excellent results for large particle purification, shall also greatly benefit from these studies; indeed, these matrices use very similar principles to membranes but allowing enhanced resolution.

The ultimate objective for the future would be to be able to design continuous IEX processes like the advanced strategies based on simulated moving bed (SMB) being developed for mAbs. Continuous processes are standard in chemical engineering processes, but the biopharmaceutical industry is clearly not there yet.

Although this thesis focused on IEX, the same rationale can be used to improve other interaction-based purification processes, e.g., affinity. It should be emphasized that affinity chromatography can also become a cost-effective option at the large scale when justified by outstanding gains in concentration and purity during DSP. This has been the case in mAb purification using Protein A affinity chromatography. SPR methodologies as the one

developed in this study can also be easily adapted to help improve such processes.

In conclusion, this dissertation has enlarged the rational toolbox by developing methodologies to unravel some of the many issues of complex biopharmaceuticals. As shown herein for IEX chromatography, working out the underlying mechanisms and understanding the product has proved to be key for a better control and better design of the process. Likewise, we anticipate that the type of tools created here shall be extremely helpful to tackle other biological systems, either enveloped virus or simpler particles as non-enveloped viruses or VLPs, as well as other chromatographic processes.

References

Airenne KJ, Mähönen AJ, Laitinen OH, Ylä-Herttuala S. Baculovirus-mediated gene transfer: An emerging universal concept. In NS Templeton, ed., Gene and Cell Therapy: Therapeutic Mechanisms and Strategies. CRC Press, Boca Raton, 3rd ed., 2009.

Araújo JMM, Rodrigues RCR, Eusébio MFJ, Mota JPB. Chiral separation by two-column, semi-continuous, open-loop simulated moving-bed chromatography. J Chromatogr A 2010;1217:5407–5419.

Barsoum J. Concentration of recombinant baculovirus by cation-exchange chromatography. Biotechniques 1999;26:834–6, 838, 840.

Dismer F, Hubbuch J. A novel approach to characterize the binding orientation of lysozyme on ion-exchange resins. J Chromatogr A 2007;1149:312–320.

Dismer F, Hubbuch J. 3d structure-based protein retention prediction for ion-exchange chromatography. J Chromatogr A 2010;1217:1343–1353.

Dismer F, Petzold M, Hubbuch J. Effects of ionic strength and mobile phase ph on the binding orientation of lysozyme on different ion-exchange adsorbents. J Chromatogr A 2008;1194:11–21.

Galarza JM, Latham T, Cupo A. Virus-like particle (vlp) vaccine conferred complete protection against a lethal influenza virus challenge. Viral Immunol 2005;18:244–51.

Gottschalk U. Bioseparation in antibody manufacturing: The good, the bad and the ugly. Biotechnol Prog 2008;24:496–503.

Jungbauer A, Hahn R. Polymethacrylate monoliths for preparative and industrial separation of biomolecular assemblies. J Chromatogr A 2008;1184:62–79.

Ladiwala A, Rege K, Breneman CM, Cramer SM. A priori prediction of adsorption isotherm parameters and chromatographic behavior in ion-exchange systems. Proc Natl Acad Sci U S A 2005;102:11710–5.

Müller-Späth T, Aumann L, Melter L, Ströhlein G, Morbidelli M. Chromatographic separation of three monoclonal antibody variants using multicolumn countercurrent solvent gradient purification (mcsgp). Biotechnol Bioeng 2008;100:1166–77.

Müller-Späth T, Krättlia M, Aumann L, Ströhlein G, Morbidelli M. Increasing the activity of monoclonal antibody therapeutics by continuous chromatography (mcsgp). Biotechnol Bioeng 2010;in press.

Peixoto C, Ferreira TB, Sousa MFQ, Carrondo MJT, Alves PM. Towards purification of adenoviral vectors based on membrane technology. Biotechnol Prog 2008;24:1290–1296.

Rodrigues RCR, Silva RJS, Mota JPB. Streamlined, two-column, simulated countercurrent chromatography for binary separation. J Chromatogr A 2010;1217:3382–91.

Tatárová I, Fáber R, Denoyel R, Polakovic M. Characterization of pore structure of a strong anion-exchange membrane adsorbent under different buffer and salt concentration conditions. J Chromatogr A 2009; 1216:941–947.

Trilisky EI, Lenhoff AM. Flow-dependent entrapment of large bioparticles in porous process media. Biotechnol Bioeng 2009;104:127–33.

Vicente T, Faber R, Mota JPB, Alves PM, Carrondo MJT. Impact of ligand density on the optimization of ion-exchange membrane chromatography for viral vector purification 2010a;in final preparation.

Vicente T, Mota JPB, Peixoto C, Alves PM, Carrondo MJT. Analysis of adsorption of a baculovirus bioreaction bulk on an ion-exchange surface by surface plasmon resonance. J Biotechnol 2010b;148:171–181.

Vicente T, Mota JPB, Peixoto C, Alves PM, Carrondo MJT. Modeling protein binding and elution over a chromatographic surface probed by surface plasmon resonance. J Chromatogr A 2010c;1217:2032–2041.

Vicente T, Peixoto C, Alves PM, Carrondo MJT. Modeling electrostatic interactions of baculovirus vectors for ion-exchange process development. J Chromatogr A 2010d;1217:3754–3764.

Vicente T, Peixoto C, Carrondo MJT, Alves PM. Purification of recombinant baculoviruses for gene therapy using membrane processes. Gene Ther 2009a;16:766–775.

Vicente T, Peixoto C, Carrondo MJT, Alves PM. Virus production for clinical gene therapy. Methods Mol Biol 2009b;542:447–470.

Vicente T, Sousa MFQ, Peixoto C, Mota JPB, Alves PM, Carrondo MJT. Anion-exchange membrane chromatography for purification of rotavirus-like particles. J Membr Sci 2008;311:270–283.